eman ta zabal zazu

Universidad del País Vasco

Euskal Herriko Unibertsitatea

ASSESSING THE HYDROGICAL RESPONSE FROM AN ENSEMBLE OF CLIMATE PROJECTIONS IN THE TRANSITION ZONE OF THE ATLANTIC REGION (BAY OF BISCAY)

Evaluation of SWAT model performance in small and forested catchments

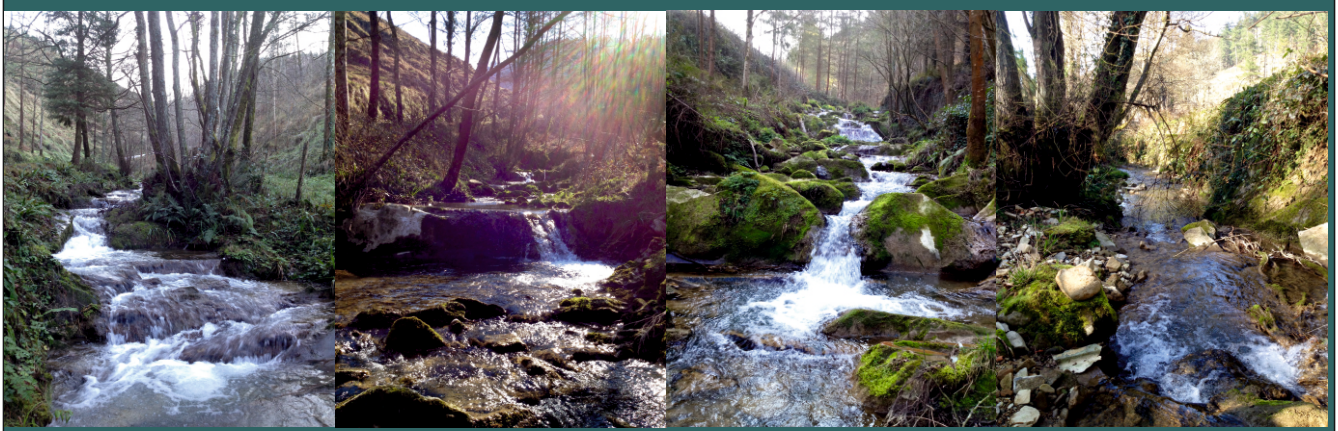

Doctoral Thesis

MAITE MEAURIO ARRATE

Doktorego-tesiaren txostena

Leioa ,2017

eman ta zabal zazu

Universidad del País Vasco
Euskal Herriko Unibertsitatea

Maite Meaurio Arrate

Euskal Herriko Unibertsitateak (UPV/EHU) Zientzietan Doktore titulua eskuratzeko ondorengo tesia aurkezten du:

Assessing the hydrological response from an ensemble of climate projections in the transition zone of the Atlantic region (Bay of Biscay).

Evaluation of SWAT model performance in small and forested catchments.

Zuzendariak:

Iñaki Antiguedad Auzmendi

Hidrogeologian Katedraduna

Geodinamika Saila

Zientzia eta Teknologia Fakultate (UPV/EHU)

Ane Zabaleta Lopetegi

Ikertzaile Doktorea

Geodinamika Saila

Zientzia eta Teknologia Fakultate (UPV/EHU)

Eskerrak emanez…

Hidrologia eta Ingurumen taldean lanean hasi nintzenetik hona, hainbat lekutatik pasatu naiz eta beti jende zoragarria aurkitzeko zortea izan dut. Hurrengo lerroetan pertsona eta baita erakunde horiei eskerrak eman nahi dizkiet, prozesu guzti honetan, era batetara edo bestera lagundu nautelako.

Lehenik eta behin Euskal Herriko Unibertsitateari (UPV/EHU) aurre-doktorego beka baten bitartez finantzazioa eman izana eskertu nahiko nioke eta Talde Kontsolidatuei (Eusko Jaurlaritza IT 598-13 eta 1029-16).

Gainera tesi honen parte bat IHOBEk emandako KLIMATEK laguntzen esparruan egin da, ikerketa talde guztiz desberdinek amankomuneko norabide batean lan egin izana polita izan da. Eta azkenik erronka berriak, AGUAMOD proiektuan lan eskala aldatuko dugu, eta guretzat berriak diren ikerketa bideak zabaldu.

Eta orain bai, eskerrik asko tesi zuzendariei zuen pazientzia eta laguntzagatik. Eskerrik asko Iñaki hidrologiaren taldean lanean hasteko aukera eman izanagatik, eta baita ere urte guzti hauetan zurekin ikasi dudan guztiagatik. Etorkizunean ere horrenbeste beste ikasiko banu, pozik!. Eta Ane, zer esan, eskerrik asko emandako laguntza guztiagatik, ez da izan gutxi!, aholkuengatik eta irakatsitakogatik. Zorte handia izan da zuekin lan egitea.

También me gustaría agradecer a Jose Miguel y Sabine su orientación y el apoyo que me han dado durante todo este tiempo. And thank you very much Srini for giving me the opportunity to stay in Agrilife. And thank you for your availability and all you help. Muchas gracias también a Estilita por apoyarme desde el principio y por hacerme un hueco en el laboratorio.

Eskerrak baita ere taldeko kideei. Eskerrik asko Jesus hainbat eta hainbatetan eman didazun laguntzagatik. Y muchas gracias Tomas por todas esas ideas que nos das y que nos dan siempre visión nueva. Gracias también a Laura por

la energía y la positividad que desprendes eta Isabel eskerrik asko horrenbeste arduratzen zarelako. Eta noski, faltan botatzen ditudan horiei: Mirentxu, Itsasne, Barbara, Ane, Imanol. Gutxitan egoten gara baina ze gustura egoten naizen geratzen garenean.

San Mameseko joan naizen guztietan laguntzeko prest dagoen jendea topatu dut eta hori eskertzekoa da. Eskerrak Borja, Jon, Mirentxu, Melissa, y a los “nuevos” Jessica y Juan Luis.

Lurzoruen inguruan egindako lanarekin Neikerreko Nahia eta Anderri ere eskertu nahi nieke emandako laguntza. Eta Garikoitz, zu bai langilea! Eskerrik asko.

Mile esker falimiari eta lagunei, zuek zarie benetan zoriontsu eiten nabenak. Aitxe, ama, eskerrak beti nigan eduki dozuen konfidantzagatik eta Beñat, eskerrak bai momentu txarretan bai onetan nire ondoan egotiegatzik. Holako jentiegaz nire inguruen zer gehiau eskatu leike da!

ABSTRACT

The climate changes projected for the 21st century will have consequences on the hydrological systems of catchments. These changes, and their consequences, are most uncertain in the transition zones. The study area of this Thesis, in the Bay of Biscay, is located in the transition zone of the European Atlantic region where hydrological impact of climate change was scarcely studied. To evaluate these impacts the climate projections derived from an ensemble of General Circulation Models (GCMs), downscaling methods (regional and statistical) and emission scenarios or Regional Concentration Pathways (RCPs) were used. The results show the high uncertainty of future sediment yield projections. Regarding the hydrological projections, the discharge would decrease seasonally and annually, being these decreases higher when the century draws on. Winter will be the less affected season, whereas summer seems to be extended as autumn is expected to experience the higher discharge decrease. These results are in line with those predicted for the Atlantic region (France and the Iberian Peninsula). Trends for high, mean and low flows were also analysed: the most significant trend shows an increase in the duration (days) of low flows. These results, highlighted the need to understand better the lower part of the hydrograph, where the related uncertainties are high and where the land use can play and important role. From an environmental point of view, and considering the need to meet the objectives established by the Water Framework Directive (WFD), this would be a drawback for the future planning on water management. Uncertainties are inherent to the evaluation of climate change impacts on hydrological systems, but even more in transition zones, for this reason it is necessary to continue with this type of research works in more catchments of the Atlantic region (Bay of Biscay).

INDEX

INDEX OF FIGURES

INDEX OF TABLES

1.

INTRODUCTION

1. INTRODUCTION

1.1 IMPACTOS DEL CAMBIO CLIMÁTICO EN LOS RECURSOS HÍDRICOS

Durante el Cuaternario se han alternado periodos secos y húmedos, sin embargo, la intensidad y la frecuencia de los cambios recientes no tienen precedentes, al menos desde comienzos del Holoceno (Mann et al., 1998; Barnett et al., 2001). Además, se considera que desde 1950 hasta la actualidad estos cambios han sido más bruscos que en los últimos decenios o milenios, de forma que se puede afirmar que el calentamiento del sistema climático es inequívoco (IPCC, 2007, 2013).

Ante las evidencias del calentamiento del sistema climático, en 1994 entró en vigor la Convención Marco de las Naciones Unidas sobre el Cambio Climático (Unite Nations Framework Convention on Climate Change, UNFCCC). Hoy en día está compuesto por 192 países y su objetivo principal es impedir la interferencia “peligrosa” del ser humano en el sistema climático. La creación del

UNFCCC fue el primer paso para que la sociedad y los dirigentes de distintas naciones tomaran conciencia de los efectos que el calentamiento global puede causar. Las bases científico-técnicas para la UNFCCC son establecidas por el Panel Intergubernamental de Cambio Climático (IPCC) que hasta la fecha ha emitido 5 informes de evaluación (AR); AR1 en 1990 (IPCC, 1990), AR2 en 1996 (IPCC, 1996), AR3 en 2001 (IPCC, 2001), AR4 en 2007 (IPCC, 2007) y AR5 en 2013-2014 (IPCC, 2013).

El IPCC define el "cambio climático" como un cambio en el clima que es posible identificar mediante análisis estadísticos u otras técnicas, y que es prolongado en el tiempo (décadas a millones de años), sin que sea relevante su origen (antropogénico o natural). Sin embargo, el UNFCCC define el cambio climático como una variación en el clima provocada de forma directa o indirecta por la actividad humana. Para nombrar las alteraciones naturales que modifican la atmósfera este organismo utiliza el término "variabilidad climática". Por otro lado, el término "cambio global" se entiende como el conjunto de cambios ambientales que afectan al sistema terrestre y que son originados por la actividad humana (Duarte et al., 2006).

1.1.1 Evidencias de cambio en el clima durante el siglo XX

Las variaciones de temperatura son uno de los cambios más evidentes y fácilmente medibles del actual cambio climático, pero la humedad atmosférica, la precipitación y la circulación atmosférica también están sujetos a modificaciones, ya que todo el sistema se ve afectado. En conjunto, estos efectos alteran el ciclo hidrológico, afectando especialmente a las características de la precipitación y a los eventos extremos (Trenberth et al., 2003).

Se estima que desde 1861 la temperatura media global ha aumentado en 0.6 ± 0.2 °C (IPCC, 2007, 2013) y ha sido el mayor incremento registrado en los últimos 1000 años (Yue et al., 2012). Pero este calentamiento no ha sido constante ni geográficamente homogéneo. Desde que se registra la temperatura, las últimas tres décadas han sido consecutivamente las más calurosas siendo la década del 2000 la más calurosa (IPCC, 2013).

El hemisferio norte es el que sufre mayor calentamiento; desde 1900 en Europa el incremento ha sido de 0.9 °C, mientras que a escala global ha sido de 0.72 °C. Además, en Europa el aumento de las temperaturas no ocurre de forma homogénea durante el año, sino que es mayor en los meses de verano y primavera (de Castro et al., 2005; EEA, 2008). Respecto a la península ibérica, en el periodo comprendido entre 1975 y 2005 se estima que el incremento de temperatura fue de 0.5 °C por década, un 50 % superior a la media continental en el hemisferio norte. Además, al igual que a escala continental, en la península los meses más castigados son los de verano y primavera (Pérez & Boscolo, 2010). En cuanto al norte de la península ibérica, Brunet et al. (2007) estimaron que en el periodo comprendido entre 1901 y 2005 el incremento de temperatura en la zona cantábrica fue de 0.13 °C por década, mientras que entre 1975 y 2005 fue de 0.51 °C por década. Sáenz et al. (2001), en un estudio realizado con datos de estaciones de la vertiente cantábrica registrados entre 1950 y 1996, mostraron incrementos de temperatura en invierno de 0.2 a 0.3 °C por década.

Los cambios en la distribución espacial, la frecuencia y la intensidad de la precipitación, hacen que sea complicado encontrar una señal antropogénica en las series de precipitación. Además, su naturaleza variable dificulta la existencia de tendencias (Chust et al., 2011), al menos a corto plazo. Los cambios producidos en el ciclo hidrológico debido al aumento de la temperatura son visibles; se ha comprobado que desde 1901 la precipitación en el hemisferio norte ha aumentado (IPCC, 2014). Las tendencias de precipitación anual en Europa (1900-2000) muestran un contraste importante entre el norte (10-40 % más húmedo) y el sur (20 % más seco). Respecto a acontecimientos extremos, durante el siglo XX aumentaron considerablemente las lluvias intensas (entre 4 y 8 %) en el norte de Europa (Mokhov et al., 2005; Khon et al., 2007). En la península ibérica, con excepción de las zonas más meridionales donde existen tendencias generalizadas de descenso de la precipitación (De Luis et al., 2009; Jacobeit, 2000; Rodrigo & Trigo, 2007; López–Moreno et al., 2010), el cómputo total anual general no mostró cambios significativos durante el siglo XX (de Castro et al., 2005). Esto ocurre porque en la península ibérica la distribución espacial de la precipitación es heterogénea y además existen fuertes contrastes

estacionales (García-Ruiz et al., 2011). Así, las áreas expuestas a condiciones atlánticas tienden a mostrar valores constantes de precipitación anual (Jacobeit, 2000; Lopez-Bustins et al., 2008), aunque en el noroeste de la península se han observado tendencias de aumento (García-Ruiz et al., 2011). Durante la última mitad del siglo pasado se observaron descensos en la zona cantábrica (ej. Serrano et al., 1999, Mosmann et al., 2004), sin embargo, esto no ocurrió en el País Vasco donde entre 1961 y 2000 no se observaron descensos importantes (-1 ± 3 % por década) (Moncho et al., 2009). Estos resultados son consistentes con un análisis similar llevado a cabo por Trigo et al. (2008).

1.1.2 Evidencias de cambio en el régimen de caudales durante el siglo XX

Los cambios en temperatura y precipitación mencionados con anterioridad generan impactos en los recursos hídricos alterando su cantidad, calidad y distribución temporal (MOPTMA, 1995; IPCC, 2007; UNESCO, 2011). Estos efectos ya se han observado en numerosos estudios realizados en cuencas de todo el mundo con caudales registrados durante el siglo XX.

A nivel mundial Svensson et al. (2005) no encontraron patrones claros en la magnitud de las crecidas, sin embargo, sí observaron un incremento significativo de caudales bajos. El estudio llevado a cabo por Stahl et al. (2010) en 441 cuencas europeas mostró un patrón generalizado de tendencias negativas en caudales medios mensuales en el sur y el este del continente. Estos resultados coinciden con los de Milly et al. (2005). Ambos estudios muestran la existencia de cambios estacionales, con descensos del caudal en los meses de verano e incremento en los meses de invierno. En investigaciones nacionales y regionales del norte de Europa (Birsan et al., 2005; Wilson et al., 2010) llegaron a conclusiones similares. Giuntoli et al. (2013) encontraron una distribución geográfica al estudiar la severidad de los caudales bajos en Francia; del centro al sur del país la severidad aumentaba y cuanto más al sur ésta era más evidente. En cuanto a la península ibérica, son numerosos los estudios que muestran tendencias negativas en caudales medios anuales (ej. Stahl et al., 2010; Lorenzo-Lacruz et al., 2012; Martínez-Fernández et al., 2013; Mediero et al., 2015). Estas tendencias se observan incluso en zonas montañosas como los Pirineos (García-

Ruiz et al., 2001; López-Moreno et al., 2008) en donde a causa del descenso del volumen de glaciares, existe una pérdida generalizada de caudales pico en primavera (Morán-Tejeda et al., 2010). Prieto (1996) analizó un número importante de ríos españoles y llegó a la conclusión de que la pérdida del recurso hídrico durante el siglo XX había sido de un 34 %. Gallart & Llorens (2001) estimaron esta pérdida en un 60 % en el Duero, Ebro y en el Tajo. Los caudales bajos también han ido descendiendo durante el siglo XX (Coch & Mediero, 2015), algo que puede ser debido al descenso de los días de lluvia en verano y primavera (Gallego et al., 2011) o a la tendencia generalizada de incremento de la temperatura media en todas las estaciones (Del Río et al., 2011). Si nos centramos en la vertiente atlántica del centro-norte de la península, en la cuenca del río Duero también se observan descensos en la media total anual del caudal y en los caudales pico (Machín et al., 2005; Nunes, 2007; Ceballos-Barbancho et al., 2008; Morán-Tejeda et al., 2011; Morán-Tejeda et al., 2012) debidos a un descenso en la precipitación en invierno (Morán-Tejeda et al., 2011). Además, estas tendencias negativas en el caudal, son de mayor significancia en invierno y primavera (Morán-Tejeda et al., 2011), algo que también ocurre a nivel peninsular (Lorenzo-Lacruz et al., 2012). En cuencas de la vertiente cantábrica también existe una tendencia negativa significativa (Coch & Mediero, 2015) que indica un descenso de los caudales. En el País Vasco, en un estudio llevado a cabo por Zabaleta et al. (2012) y Zabaleta & Antiguedad (2012), en 42 cuencas de la vertiente cantábrica y mediterránea se observó una tendencia al aumento de la duración de los periodos de caudales bajos en verano y otoño y al aumento de caudales altos en primavera e invierno (entre 1973 y 2007). En el mismo estudio también se constató la existencia de un desplazamiento en los caudales altos, de invierno a primavera. Este hecho puede estar relacionado con los resultados de De Luis et al. (2010) que muestran un movimiento en las estaciones de mayor precipitación en la zona cantábrica de otoño-invierno (1946-1975) a invierno-primavera (1976-2005). El incremento de caudales altos y el descenso de caudales bajos genera una mayor amplitud del hidrograma, que puede derivar en que los episodios extremos sean de mayor magnitud y además estos podrán ocurrir con mayor frecuencia.

1.1.3 Posibles impactos del cambio climático en los recursos hídricos

Los cambios producidos en los recursos hídricos como consecuencia del cambio climático, afectarán a diversos campos como los ecosistemas, los recursos naturales, los sectores productivos y la salud pública (UNESCO, 2011). Entre otros factores, la temperatura, la precipitación y la humedad del suelo afectan a los recursos hídricos. La temperatura influye en la generación y el estado de la precipitación, la evaporación y la evapotranspiración. En la generación de escorrentía es importante considerar cuándo llueve y con qué intensidad, duración y frecuencia lo hace. El cambio climático puede afectar a la distribución temporal de la precipitación, que a su vez influye en el régimen de crecidas y en la capacidad de regulación de los ríos (Iglesias et al., 2005) y, por lo tanto, en la disponibilidad de agua (Arnell, 2011). Por lo tanto, la distribución tempral de la precipitación y la temperatura, en muchas ocasiones, tiene mayor impacto en los recursos hídricos que los propios valores climáticos.

El ciclo hidrológico está además fuertemente influenciado por el uso del suelo, puesto que la vegetación afecta de forma directa a procesos hidrológicos como la infiltración, intercepción, evapotranspiración y generación de escorrentía (Cosandey et al., 2005; Foley et al., 2005). Además, también afecta a la generación de sedimentos debido a la erosión del suelo. Las superficies forestales, por ejemplo, pueden contribuir a aumentar la tasa de infiltración y evapotranspiración, generar menor escorrentía y consecuentemente disminuir la carga de sedimento. De esta forma, pueden amortiguar algunos de los efectos de los peligros relacionados con el agua, en particular las pequeñas y medianas inundaciones, y además durante los periodos secos el suministro de agua suele ser más constante (Ilstedt et al., 2007; Bredemeier, 2011) aunque puede que la cantidad sea algo menor. Por lo tanto, al estudiar los posibles efectos del cambio climático en los recursos hídricos, es importante tener en cuenta el uso del suelo y sus cambios, ya sean derivados de la propia adaptación de la vegetación al cambio climático o de las decisiones de origen antrópico (Garmendia et al., 2012). Esto puede resultar complicado, por un lado, porque los usos en suelos agrícolas o forestales están sujetos a factores socio-económicos que son difíciles de predecir. Por otro lado, la cantidad de agua disponible para las plantas en

muchos casos será menor y esto afectará a su crecimiento, desarrollo (Vicente-Serrano et al., 2013) y distribución fenológica. Por tanto, los ciclos de florecimiento, polinización y maduración de los frutos se verán afectados (Giannakopoulos et al., 2009). Estos cambios fenológicos pueden conducir a que cambien las especies y variedades de cultivo, las técnicas agronómicas y el calendario de cultivos. Además, los cambios hidrológicos afectan al desarrollo del arbolado, a las especies forestales (Serra-Diaz et al., 2012), y a las funciones de los ecosistemas que pueden derivar en menor diversidad y, por tanto, en un declive de los bosques (Sarris et al., 2007) que además se verán afectados por un mayor riesgo de incendios (Moriondo et al., 2006).

Se prevé que la frecuencia y la severidad de las sequías aumentará de forma significativa en el sur y el sudeste de Europa (Lehner et al., 2006; Forzieri et al., 2014). Por lo tanto, se estima que la disponibilidad de agua superficial y subterranea disminuirá y aumentarán las olas de calor, las lluvias intensas, las inundaciones y los incendios (Kovats & Valentini, 2014). Si las predicciones se cumplen, el agua será relativamente escasa durante la mayor parte del año, mientras que en momentos puntuales las inundaciones podrán causar daños materiales y humanos. Resulta un problema añadido que la mayor parte de las infraestructuras diseñadas durante el siglo XX se construyeron pensando en condiciones climáticas e hídricas estables a lo largo del tiempo.

Existen numerosas incertidumbres acerca de cómo el cambio climático afectará a la cantidad y a la calidad de los recursos hídricos, a los regímenes fluviales y a la gestión del agua ante las nuevas condiciones (García-Ruiz et al., 2011). Desde un punto de vista ecológico, la reducción del caudal puede provocar que los periodos con caudal menor al llamado “caudal ecológico” puedan prolongarse, afectando la calidad medioambiental de las masas de agua (IPCC, 2008). Para hacer frente a estos problemas es necesario prestar especial atención a las zonas de montaña, ya que son las mayores fuentes de agua (Beniston, 2003). Sin embargo, son zonas sometidas a numerosos impactos antropogénicos como deforestaciones a causa de la sobreexplotación y los incendios o reforestaciones a causa del abandono de zonas de cultivo, entre otros. Por otro lado, en numerosas zonas del Planeta la precipitación ha

aumentado durante las últimas décadas (IPCC, 2007). Un clima más cálido trae consigo una mayor evaporación del agua superficial, el contenido de humedad atmosférica es más alto y, por lo tanto, en algunas regiones se genera más lluvia. Como resultado, los eventos extremos de precipitación podrían aumentar considerablemente, concentrándose la precipitación en algunas estaciones del año con mayor frecuencia e intensidad, por lo que la cantidad y la magnitud de avenidas aumentará en el futuro (Allen & Ingram, 2002; IPCC, 2007; Dankers & Feyen, 2009). Este aumento de la precipitación se proyecta fundamentalmente en latitudes medias y altas (Meehl et al., 2007), como el norte europeo o algunos sectores del Pirineo (Beguería et al., 2003; Morán-Tejeda et al., 2010) donde, a causa del incremento de temperatura, en la actualidad el deshielo coincide con épocas de mayor precipitación (De Luis et al., 2010). Sin embargo, el aumento de intensidad de lluvia puede ocurrir también en zonas en las que en promedio el clima es más seco, de manera que los eventos de precipitación se pueden volver más esporádicos e intensos (Christensen & Christensen, 2004).

En un estudio llevado a cabo por Alfieri et al. (2015) se estima que en la actualidad 216000 personas se ven afectadas por las inundaciones cada año en Europa. Económicamente esto supone unos 5.3 B€. Para finales de siglo se considera que solamente debido al cambio climático el impacto socio-económico de las inundaciones en Europa aumentará un 220 % afectando a unas 950000 personas. Teniendo en cuenta que las avenidas pueden ser catastróficas y predecibles solo con unos pocos días u horas de antelación, la coordinación internacional es fundamental para preparar y poner en marcha, previamente, planes de mitigación y adaptación.

Tal y como se ha mencionado en este apartado el cambio climático afecta de forma significativa a caudales extremos. Tanto desde el punto de vista socio-económico, como humano y medioambiental es importante prever las posibles variaciones de estos caudales extremos para que sea posible hacer planes de adaptación y tomar las medidas oportunas en cada caso. Por ello, cuando se realizan estudios hidrológicos a futuro, además de estudiar los caudales medios, es esencial estudiar los extremos.

1.1.4 Metodología para la obtención de proyecciones climáticas e hidrológicas. Incertidumbres asociadas al proceso

Los principales pasos para evaluar los impactos del cambio climático sobre los recursos hídricos se pueden resumir de la siguiente manera (Fig. 1.1):

1. Construir escenarios de emisión de gases de efecto invernadero y/o trayectorias de concentración representativa (Representative Concentration Pathways; RCPs) que se basan en el forzamiento radiativo proyectado para el 2100.
2. Modelizar el clima con Modelos Generales de Circulación (General Circulation Models GCM) utilizando como forzamiento los escenarios de emisión o RCPs definidos en el paso anterior.
3. Hacer la regionalización o downscaling de las proyecciones climáticas obtenidas a partir de los GCMs que puede ser dinámico (Regional Circulation Models; RCM) y/o estadístico.
4. Introducir las variables climáticas regionalizadas en modelos hidrológicos con el fin de obtener caudales futuros.

Cada uno de estos pasos conlleva incertidumbres que se propagan durante los pasos sucesivos, desde aquellas asociadas a la posible evolución socio-económica, hasta las relacionadas con aspectos físicos y matemáticos, pasando por la propia variabilidad y complejidad natural de los procesos modelizados.

A continuación, para poder entender mejor cómo se realizan las proyecciones climáticas e hidrológicas, y cuáles son las fuentes de incertidumbre asociadas, se profundizará en algunos de estos pasos.

ESCENARIOS DE EMISIÓN DE GASES DE EFECTO INVERNADERO Y VÍAS DE CONCENTRACIÓN REPRESENTATIVA

Los escenarios de emisión son representaciones de la evolución futura de sustancias radiativamente activas en la atmósfera, como, por ejemplo, los aerosoles o los gases de efecto invernadero (Fig.1.1 a)). Para poder determinar dicha evolución, han de tenerse en cuenta parámetros socio-económicos, la

evolución de la tecnología, el desarrollo demográfico y otros aspectos que condicionan la generación y emisión de estas sustancias. Son los escenarios de concentraciones obtenidos de los escenarios de emisión los que se introducen en los GCMs (Fig.1.1 a) b)).

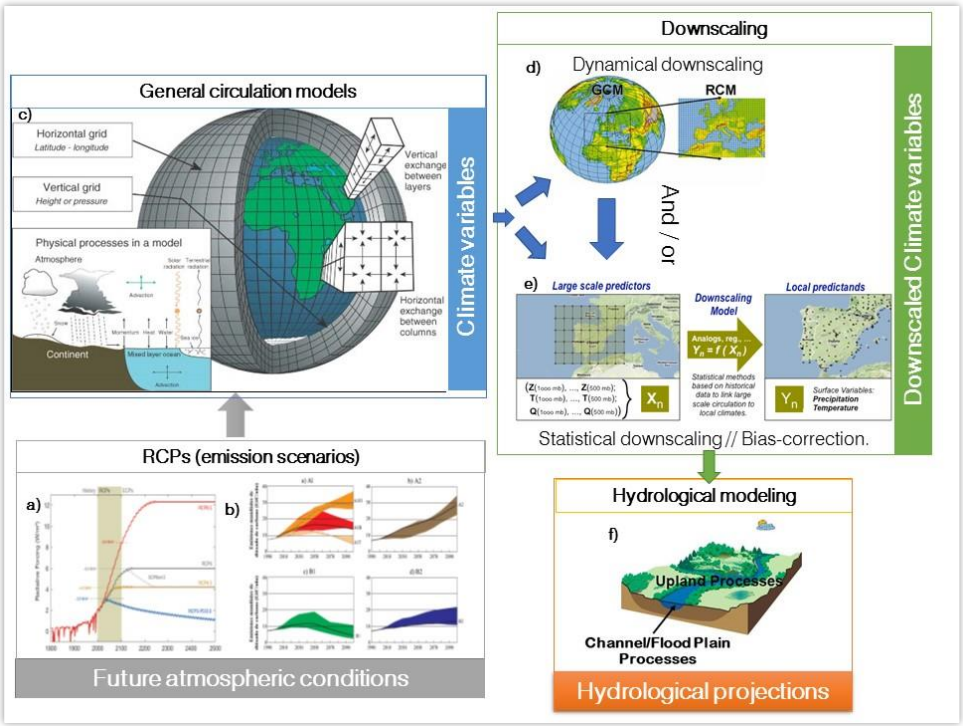

Figura 1.1. *Esquema de los pasos necesarios para realizar proyecciones hidrológicas. a) Meinshausen et al., 2011, b) IPCC2001, c) Edwards, 2010, d) www.wmo.int e) www.meteo.unican.es, f)www.swat.tamu.edu.*

El IPCC es el organismo encargado de generar los escenarios de emisión. En 1990 y 1992 este organismo desarrolló varios escenarios de emisiones a largo plazo (escenarios IS92). Sin embargo, en 1996 se decidió modificar dichos escenarios porque el conocimiento que se tenía sobre las fuerzas que rigen las emisiones, y la metodología, habían cambiado (IPCC, 1996). En el 2000 publicó el Informe Especial sobre Escenarios de Emisiones (Special Report on Emissions Scenarios; IPCC SRES, 2000) donde se establecían los nuevos escenarios de emisión y sus concentraciones. Estos escenarios fueron los que se utilizaron en el 3er informe del IPCC, el AR3 (2001) y consideran distintas hipótesis para estimar la evolución del forzamiento

climático futuro. Dichas hipótesis contemplan factores socio-económicos que en última instancia afectan a las emisiones de gases de efecto invernadero (Fig. 1.2). Se agrupan en cuatro líneas evolutivas:

- Familia evolutiva A1: presupone un crecimiento económico mundial muy rápido, una población mundial que alcanza su valor máximo a mediados del siglo XXI y una rápida introducción de tecnologías nuevas y más eficientes. Se subdivide en tres grupos que reflejan tres direcciones diferentes del desarrollo tecnológico: intensiva en combustibles fósiles (A1F1), energía de origen no fósil (A1T) y equilibrio entre las distintas fuentes (A1B) (Fig. 1.2, a)).
- Familia evolutiva B1: describe un mundo con la misma población que A1, pero con una evolución más rápida de las estructuras económicas hacia una economía de servicios y de la información (Fig. 1.1, c)).
- Familia evolutiva B2: en este caso la población mundial es intermedia y el crecimiento económico también. Se desarrollan soluciones locales para alcanzar la sostenibilidad económica, social y medio ambiental (Fig. 1.2, d)).
- Familia evolutiva A2: un mundo heterogéneo donde el crecimiento de la población es muy fuerte, con un desarrollo económico y tecnológico lento (Fig. 1.2, b)).

A partir de estos escenarios se concretan las concentraciones de emisión que después se introducen en los GCMs (Fig. 1.1). Por lo tanto, se centran en emisiones antropogénicas que no tienen en cuenta los factores de cambio naturales como el forzamiento que pueden provocar los volcanes o las emisiones naturales de CH_4 y N_2O. Por este motivo, el quinto informe del IPCC, el AR5 (2013) optó por contar con nuevos escenarios llamados Vías o Trayectorias de Concentración Representativa (Representative Concentration Pathways; RCPs). Estos se definen por el forzamiento radiativo estimado para el año 2100 en relación a 1750. Este parámetro indica el cambio de flujo neto de energía radiativa hacia la superficie de la Tierra que ocurre por cambios en la composición de la atmósfera, o cambios en el aporte de energía solar. Cuando

su valor es positivo contribuye a que la superficie de la Tierra se caliente, mientras que un valor negativo indica un enfriamiento.

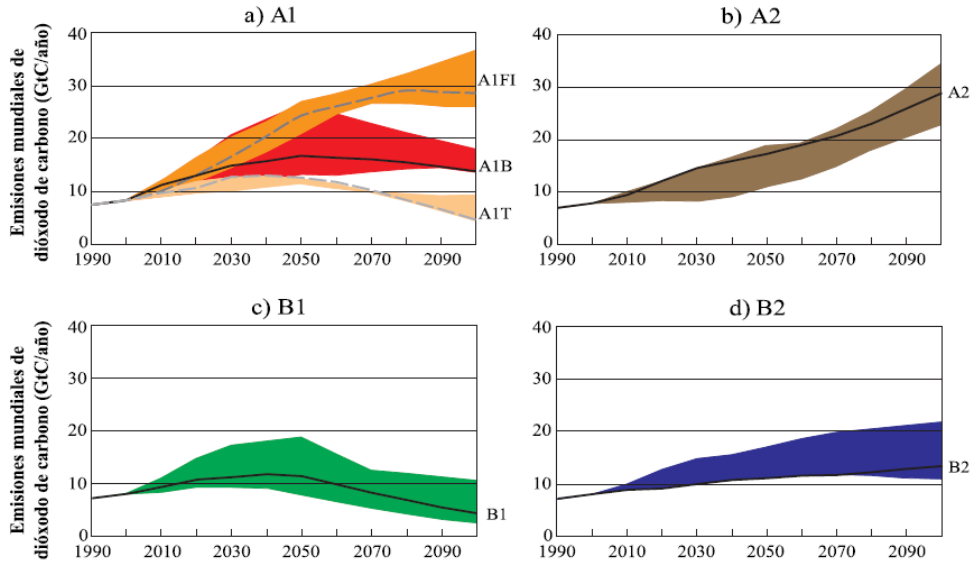

Figura 1.2. *Emisiones anuales totales de CO_2 provenientes de todas las fuentes (energía, industria y cambio de uso del suelo) entre 1990 y 2100 (en gigatoneladas de carbono (GtC año^{-1}). Se ofrece un escenario ilustrativo para cada uno de los grupos de escenarios, incluidos los cuatro de referencia (A1, A2, B1 y B2, en líneas de trazo continuo), y dos escenarios ilustrativos para A1FI y A1T (líneas de trazos) (IPCC, 2001).*

Los RCPs se dividen en cuatro categorías (Fig.1.3):

- RCP2.6: es el escenario de mitigación que estima un forzamiento radiativo muy bajo. Como se puede ver en la figura 1.3 el forzamiento radiativo aumenta hasta algo menos de mitad de siglo para descender hasta 2.6 W m2 (~400 ppm CO2 eq) para 2100.

- RCP4.5: escenario de estabilización con un forzamiento radiativo medio de 4.5 W m2 (~650 ppm CO2 eq) que se mantiene constante en este valor aproximadamente desde mitad de siglo en adelante.

- RCP6.0: escenario de estabilización con un forzamiento radiativo medio de 6.0 W m2 (~850 ppm CO2 eq) que se estabiliza poco después del año 2100.

- RCP8.5: escenario con emisiones de gases de efecto invernadero muy altas y por lo tanto forzamiento radiativo alto de 8.5 W m2 (~1370 ppm CO2 eq) que incluso sigue aumentado a partir del 2100.

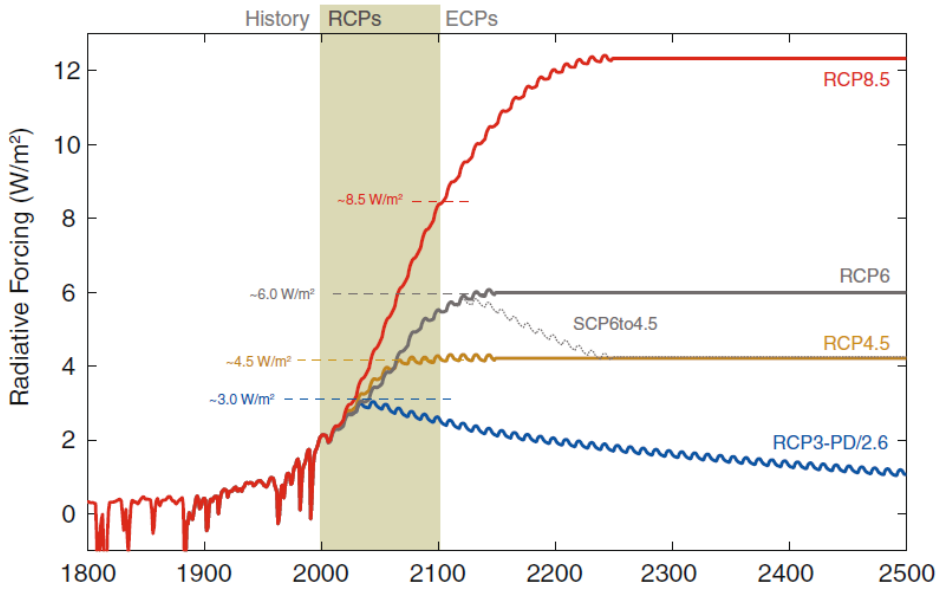

Figura 1.3. *Forzamiento radiativo total (antropogénico y natural) de los RCPs (Meinshausen et al., 2011).*

Los RCPs se obtienen de la combinación de modelos integrados de evaluación, modelos climáticos simples, química atmosférica y modelos del ciclo global del carbono. Según el Coupled Model Intercomparison Project Phase 5 (CMIP5), del que se hablará más adelante, los valores de forzamiento radiativo deben entenderse como meramente indicativos, ya que el forzamiento climático resultante varía según el GCM debido a las características específicas del modelo. Cada RCP proporciona datos espaciales del uso del suelo y especifica las concentraciones de gases de efecto invernadero tanto naturales como antropogénicas hasta 2100. Estos son los datos que se introducen en los GCMs desarrollados por el CMIP5 y que aparecen en el 5º informe del IPCC, el AR5 (2013).

MODELOS GENERALES DE CIRCULACION

Los Modelos Generales de Circulación (General Circulation Models; GCM, también conocidos como Atmosphere Ocean General Circulation Models, AOGCM) son modelos numéricos que representan los procesos físicos de la atmósfera, hidrosfera, criosfera, biosfera y litosfera (Fig. 1.1 b)). Se basan en la resolución de ecuaciones de cada componente del sistema y los intercambios de masa que se producen entre ellos. Actualmente son las herramientas más avanzadas disponibles para simular la respuesta del sistema climático a los gases de efecto invernadero, y las más utilizadas (ej. Zhang et al., 2011; Brunet et al., 2007). En comparación con los modelos climáticos utilizados en meteorología, los GCMs, en combinación con modelos regionales (Regional Climate Models; RCMs), proporcionan estimaciones geográficas y físicas consistentes del cambio climático regional que son necesarias para el análisis de impactos (IPCC, 2013).

Los GCMs representan el clima utilizando una rejilla tridimensional sobre la superficie terrestre que normalmente tiene una resolución horizontal de entre 250 y 600 km. Verticalmente el número de capas que representan la atmósfera es variable. Usualmente sobre la tierra suelen ser entre 10 y 20 capas mientras que sobre los océanos puede haber hasta 30. Estos datos muestran que la resolución espacial de los GCMs es muy pobre, lo que genera dos problemas principales: 1) Existen procesos físicos en la atmósfera que ocurren a escala más reducida, como por ejemplo los que se dan en las nubes, y que no pueden ser modelados de forma adecuada. Para poder realizar simulaciones lo más reales posibles, las propiedades conocidas de estos procesos han de ser promediadas e introducidas en los modelos en forma de parámetros que, por supuesto, serán una fuente de incertidumbre. Además, ocurren numerosos procesos en la atmósfera a menor escala que la simulada por los GCMs, que se retroalimentan, como por ejemplo la generación de vapor de agua, el calentamiento de las nubes y la radiación, la circulación oceánica y el hielo o el albedo de la nieve. Por tanto, simplemente por la forma de considerar los procesos que ocurren a menor escala, ante el mismo forzamiento radiativo cada GCM dará distintas respuestas. 2) Otro problema asociado a la resolución espacial de los GCMs es que sus

resultados son demasiado generales para hacer estudios de impacto. En el caso de los sistemas hídricos el método más usado para evaluar el impacto del clima futuro es introducir los datos obtenidos de los GCMs en modelos hidrológicos (Gosling et al., 2011). Esta es una buena herramienta para el estudio de la relación entre el clima, las actividades humanas y los recursos hídricos (Jothityangkoon et al., 2001, Leavesley, 1994). Sin embargo, debido a su baja resolución espacial si los datos resultados de los GCMs se introducen directamente en modelos hidrológicos, el resultado será pobre y poco fiable (Fowler et al., 2007). Por lo tanto, para poder llevar a cabo estudios de impacto, es necesario obtener datos de mayor resolución. Actualmente esto se consigue mediante técnicas de regionalización o downscaling.

Los GCMs se desarrollan en distintas instituciones de investigación climática como el Instituto Meteorológico Max-Planck (modelos de la serie ECHAM y MPI-ESM) de Hamburgo, el Centro Euro-Mediterráneo del cambio climático (modelos de la serie CMCC), el Hadley Center de la Oficina Meteorológica del Reino Unido (modelos de la serie HadCM) o la institución CSIRO-BOM australiana (modelos de la serie ACCESS), entre otros. La coordinación de los institutos la hace el Working Group on Coupled Modelling (WGCM) que opera bajo el World Climate Research Program (WCRP) (Fig.1.4). En 2008, 20 grupos de modelos climáticos del WGCM acordaron promover una nueva serie de experimentos coordinados. Sus resultados se recogen en la quinta fase del Coupled Model Intercomparison Project (CMIP5) que es el que se ha utilizado para crear el AR5 (IPCC, 2013). Además de generar nuevas series de precipitación, temperatura y otros parámetros climáticos, uno de los principales objetivos del CMIP5 es determinar por qué los modelos climáticos forzados de forma similar tienen resultados tan variados. La mayoría de los modelos del CMIP5 incluyen ciclos interactivos del carbono, por eso también se les llama Modelos del Sistema Terrestre. Debido a que los CMIP5 son bastante recientes, la mayoría de estudios relacionados con el cambio climático se han realizado con modelos de versiones anteriores (Ho et al., 2015).

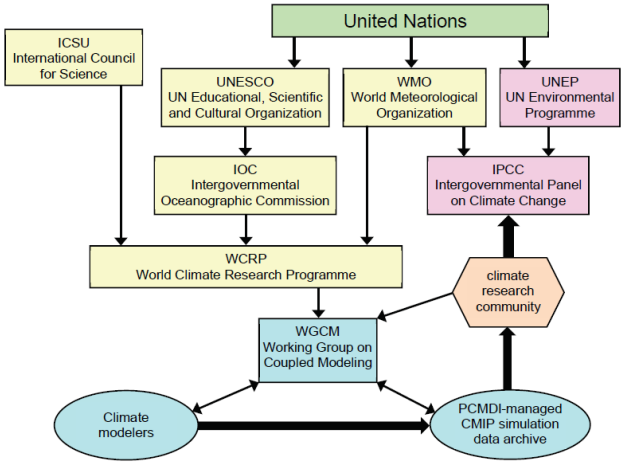

Figura 1.4. *La relación de CMIP5 con las organizaciones establecidas para coordinar las actividades de investigación sobre el clima a nivel internacional y el IPCC, los centros de modelización, y la comunidad de investigación sobre el clima (Taylor et al., 2011).*

Los GCMs no pretenden predecir el clima futuro exacto, y aún menos en un día concreto. Lo que se consigue con estos modelos es conocer la probabilidad relativa de las distintas tendencias climáticas que podría haber a largo plazo, teniendo en cuenta las limitaciones establecidas por las observaciones y la comprensión física disponible en la actualidad (Allen & Ingram, 2002).

DOWNSCALING

La resolución espacial de los resultados u outputs de los GCMs y la de los datos requeridos por los modelos hidrológicos es el mayor obstáculo a la hora de estudiar el impacto del cambio climático en los recursos hídricos (Leavesley, 1994; Hostetler, 1994; Xu, 1999). Por lo tanto, es necesario tratar los datos climáticos para que se puedan ajustar a escalas mucho menores que las de los GCMs. Esto se consigue mediante técnicas de downscaling que pueden ser de dos tipos; dinámicas (regional climate models, RCMs) o estadísticas (Fig. 1.1 d)e)). Los RCMs son modelos matemáticos que trabajan integrados en zonas o mallas de menor resolución que los GCMs y que su condición de contorno es función del tiempo. Esto se consigue interpolando los resultados del GCM para generar condiciones iniciales y de contorno para la zona de mayor resolución (Brunet et al., 2009). Hoy en día la resolución de los RCMs puede ser de pocos

kilómetros, aunque normalmente trabajan entre 10 y 50 km de resolución horizontal. Existen numerosos proyectos que ofrecen downscaling dinámico en Europa. Dos de los proyectos de mayor relevancia, y que ofrecen estos datos regionalizados para la península ibérica, son los proyectos PRUDENCE (Prediction of Regional scenarios and Uncertainties for Defining European Climate change risks and Effects; Christensen, 2005) y ENSEMBLES (Hewitt & Griggs, 2004). Actualmente está en vigor el programa Coordinated Regional Climate Downscaling Experiment (CORDEX) patrocinado por el WCRP. Este programa ofrece un conjunto de modelos climáticos dinámicos y estadísticos considerando los GCMs del CMIP5, y es el primer programa multimodelo que se realiza a escala mundial (abarca casi todas las zonas del planeta). En un principio el intervalo de rejilla utilizado fue de 50 km (inicialmente se centraron en África) pero actualmente, en algunas zonas del planeta, han conseguido reducirlo a 10 km. Para poder realizar el downscaling, el programa CORDEX aprovecha los proyectos regionales existentes, como el proyecto ENSEMBLES en el caso de Europa. En el apartado *2.2 Climate Change Projections* se da más información sobre los proyectos PRUDENCE, ENSEMBLES y CMIP5 y los métodos de downscaling que se utilizan en esta Tesis.

Uno de los mayores problemas que presentan los RCMs es su alto coste computacional (Solman & Nunez, 1999). Por ello, en ocasiones el número de GCMs de los que se hace el downscaling es menor de lo deseado. Además, para aplicaciones prácticas, cuando se trata de la modelización de cuencas pequeñas los resultados de los RCMs en ocasiones no tienen la suficiente precisión espacial (Chen et al., 2011).

Otra opción son las técnicas de donwscaling estadísticas. En la actualidad existe una amplia variedad de métodos de este tipo (Wilby et al., 2004; Haylock et al., 2006). Estas aplican un método estadístico para construir una relación empírica entre variables atmosféricas de gran escala (resultados de los GCMs y en ocasiones de RCMs) (predictor) y las variables locales de superficie (predictando; que en la mayoría de los casos son los datos observados para el periodo de referencia o baseline). A continuación, sobre la base de esa relación empírica, los predictores se utilizan para generar los escenarios climáticos de

alta resolución. Normalmente las variables climáticas suelen ser la precipitación y la temperatura máxima y mínima. Actualmente los modelos estadísticos se basan en datos históricos (predictandos), asumiendo de esta manera que las relaciones establecidas entre predictores y predictandos son invariables frente al cambio climático (Brunet et al., 2009; Chen et al., 2011). Este planteamiento teórico puede ser una fuente importante de incertidumbre debido a que puede omitir procesos físicos importantes que se den en el futuro pero que en las condiciones climáticas actuales no se estén dando.

Los RCMs son capaces de simular la mayor parte de procesos físicos que ocurren en la atmósfera, aunque el clima sea cambiante. Desde este punto de vista su incertidumbre es menor, pero, tal y como se ha mencionado con anterioridad, para muchos estudios de impacto su resolución sigue siendo escasa, por lo que en ocasiones a éstos hay que aplicarles correcciones de sesgo similares a las realizadas en el downscaling estadístico. Estas correcciones también consideran que las condiciones del clima son invariables en el tiempo. Por otro lado, su alto coste computacional hace que sea difícil obtener un gran conjunto de escenarios climáticos regionalizados con técnicas dinámicas, mientras que la principal ventaja del downscaling estadístico es que su coste no es alto y por lo tanto, se puede aplicar a un amplio número de GCMs.

MODELOS HIDROLÓGICOS

Cuando se dispone de datos climáticos futuros de suficiente resolución, éstos se introducen en los modelos hidrológicos (Fig. 1.1). En los últimos años se han publicado numerosos estudios en los que se evalúa la incertidumbre de los modelos hidrológicos y los parámetros asociados a éstos (ej. Arnell, 2011; Coron et al., 2012; Teng et al., 2012; Brigode et al., 2013) y todos ellos indican que la incertidumbre de los GCMs es mucho mayor que la de los modelos hidrológicos. Es evidente que en función de la elección del modelo hidrológico (conceptual o de base física, distribuido o semi-distribuido...) las proyecciones hidrológicas pueden ser distintas. A menudo se considera que los modelos de base física son indispensables para mantener el poder predictivo de los modelos hidrológicos en un clima cambiante (Ludwig et al., 2009). Algunos estudios han

tratado este tema y han utilizado modelos tanto conceptuales como de base física. Los resultados mostraron que la conceptualización de los modelos no era la mayor fuente de variabilidad en las proyecciones hidrológicas (Ducharne et al., 2009, 2011).

En los estudios hidrológicos de cambio climático, los modelos hidrológicos se suelen calibrar para unas condiciones dadas que normalmente corresponden a un clima y uso del suelo conocidos, es decir, a los registrados en los últimos años (Vaze & Teng, 2011). Independientemente de la incertidumbre que puede generar el cambio de uso del suelo o los cambios físicos que puedan darse en las cuencas en el futuro, calibrar el modelo hidrológico en condiciones climáticas actuales puede ser una fuente importante de incertidumbre. Las proyecciones climáticas nos indican que el clima futuro cambiará y parece que los eventos extremos se incrementarán. Por eso, para asegurar la estabilidad de los parámetros en el tiempo es importante asegurar que la calibración del modelo también se ajuste a este tipo de situaciones y no sólo a valores medios (Coron et al., 2012; Brigode et al., 2013).

En el apartado *1.2 Hydrological Models* se profundiza más en los tipos de modelo hidrológico.

INCERTIDUMBRE

La evaluación cuantitativa de las incertidumbres asociadas a las proyecciones hidrológicas futuras es bastante complicada, aunque cualitativamente se reconoce que estas incertidumbres son considerables (Brigode et al., 2013).

Los modelos climáticos son la herramienta más sólida para generar proyecciones de cambio climático consistentes (Forzieri et al., 2014). Sin embargo, son una fuente considerable de incertidumbres debido a una representación incompleta de los procesos físicos. Además, para poder simular estos procesos, los modelos están compuestos por una serie de parámetros que suelen tener valores aproximados (Katz et al., 2002; Déqué et al., 2012). Como ya se ha mencionado, una de las cuestiones fundamentales relacionadas con los GCMs es entender por qué sus resultados, sobre todo los de precipitación,

difieren de forma considerable. Por lo tanto, en los estudios de impacto del cambio climático en los recursos hídricos, la mayor fuente de incertidumbre son los resultados climáticos de los GCMs. (ej. Arnell, 1999; Bergstrom et al., 2001; Nijssen et al., 2001; Chen et al., 2011; Arnell et al., 2011; Teng et al., 2012). Es por este motivo que las proyecciones basadas en un conjunto o ensemble de modelos climáticos proporcionan resultados más sólidos (IPCC, 2007, Stahl et al., 2011; Gudmundsson et al., 2012). Además, de esta forma se puede estimar la incertidumbre asociada a los GCMs (Wilby & Dessai, 2010).

En un estudio de proyecciones hidrológicas futuras, cada uno de los componentes de la cadena de modelado (Fig.1.1) es una fuente potencial de incertidumbre que se propaga dentro de la cadena de modelado (Bosshard et al., 2013). Aunque es bastante evidente que la mayor fuente de incertidumbre son los modelos climáticos, no está tan clara la posición de las otras fuentes de incertidumbre. Por ejemplo, Wilby & Harris (2006) consideraron que el orden de fuentes de incertidumbre, de mayor a menor, es el siguiente; GCMs -> método de downscaling -> estructura del modelo hidrológico -> parámetros del modelo hidrológico -> escenario de emisión, mientras que Chen et al. (2011) consideraron que las mayores fuentes de incertidumbre son los GCMs y las técnicas de downscaling seguidos por los escenarios de emisión, la estructura del modelo hidrológico y por último los parámetros utilizados en la calibración del modelo.

Tal y como se ha podido ver en este apartado, cada componente o paso en el proceso de modelización, desde las proyecciones climáticas hasta el valor de los parámetros del modelo hidrológico, tienen asociada una incertidumbre. Es por ello que, tal y como indica el IPCC (2007, 2013), lo recomendable es utilizar un conjunto o ensemble de GCMs, métodos de downscaling, escenarios de emisión o RCPs… De esta forma, en lugar de dar un único valor es posible dar un rango de probables tendencias.

1.1.5 El País Vasco en el contexto general del cambio climático

Europa es representativa de los cambios ocurridos a escala global como consecuencia del calentamiento del clima (Shorthouse & Arnell, 1999). Existe un

claro contraste entre el norte y el sur del continente. Numerosos estudios realizados en zonas del norte de Europa apuntan a un incremento de precipitación y, como consecuencia, un incremento de caudal (ej. Arnell, 1998; Kiely, 1999; Xu & Halldin, 1997; IPCC, 2001; IPCC, 2007). En el sur la tendencia es inversa, se predice una disminución de la precipitación y, por lo tanto, una disminución del caudal (ej. Mimikou et al., 2000; Ayala-Carcedo & Iglesias, 2000; Ribalaygua et al., 2013, Lespinas et al., 2014, Valverde et al., 2015), acompañada de un aumento en la variabilidad espacio temporal de ambas variables (Ceballos-Barbancho et al., 2008). Por lo tanto, entre el norte y el sur de Europa existe una zona de transición en la que se pasa de un incremento en las predicciones de precipitación y caudal (norte) a un descenso de estas variables (sur). Situar esta zona no resulta fácil puesto que, debido a la baja resolución espacial de los modelos climáticos, en función del modelo su localización es distinta. Por ejemplo, Habets et al. (2013) sitúan esta zona en el norte de Francia, mientras que el IPCC (2007) y Goubanova & Li (2007) la emplazan en el norte de la península ibérica. Por supuesto, las incertidumbres asociadas al cambio climático y sus impactos en la zona de transición son mayores que en otras áreas y es más difícil que las tendencias, tanto climáticas como de caudal, sean marcadas, por ello debería ser una zona a la que se le preste especial atención. Sin embargo, la realidad es que en comparación con otras zonas europeas el número de estudios realizados en esta zona es bastante escaso (tabla 1.1 y 1.2).

El País Vasco, debido a su situación geográfica, no se puede englobar dentro de las áridas condiciones proyectadas para el sur de Europa, pero tampoco parece evidente que como indican las proyecciones para el norte de Europa, sea una zona en la que el caudal vaya a aumentar. Coch & Mediero (2015) se basaron en caudales bajos para identificar distintas zonas en la península iberica. Para ello utilizaron datos recogidos en 60 cuencas entre 1949 y 2009. Este estudio, englobó a la vertiente cantábrica y el centro-oeste de la península ibérica en lo que denominaron “zona o región atlántica”. La región se caracteriza porque la estación más seca es la de verano, mientras que de otoño a primavera llegan sistemas frontales atlánticos que aumentan el caudal. Mediero et al. (2015), en un estudio realizado para identificar las regiones de inundación

de Europa, llegaron a la conclusión de que la región atlántica comprende el oeste-noroeste de la península ibérica, el centro-oeste de Francia, Bélgica, Países Bajos, norte-oeste de Alemania, Dinamarca y el Reino Unido. Analizando los efectos del cambio climático, el IPCC en su 4º informe publicó un mapa de vulnerabilidad de Europa para el siglo XXI (Fig. 1.5).

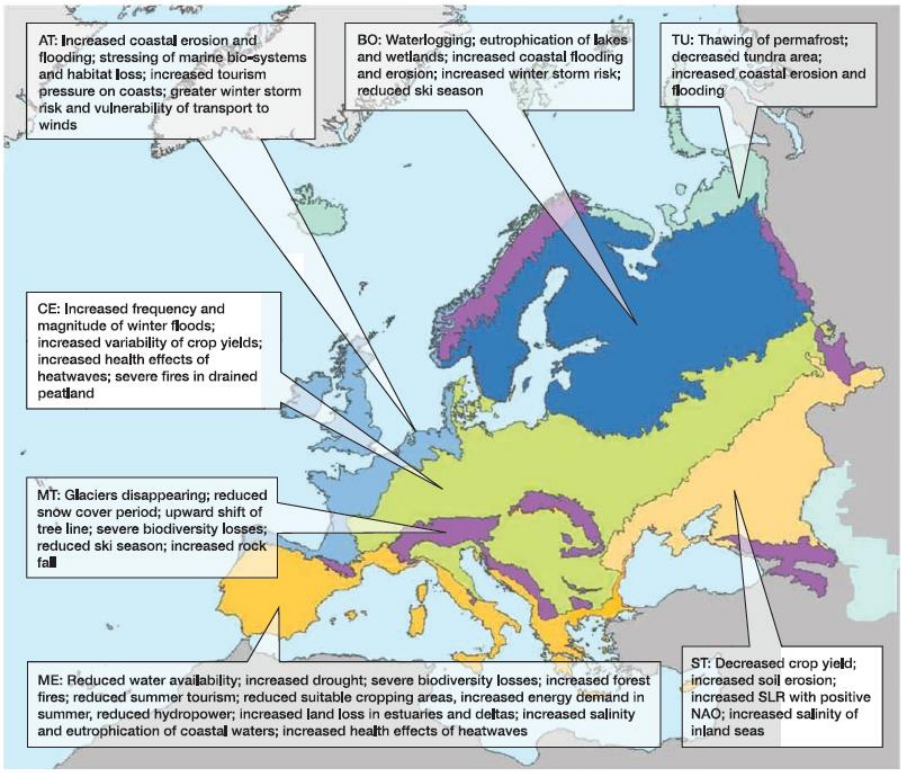

Figure 12.3. *Key vulnerabilities of European systems and sectors to climate change during the 21st century for the main biogeographic regions of Europe (EEA, 2004a): TU: Tundra, pale turquoise. BO: Boreal, dark blue. AT: Atlantic, light blue. CE: Central, green; includes the Pannonian Region. MT: Mountains, purple. ME: Mediterranean, orange; includes the Black Sea region. ST: Steppe, cream. SLR: sea-level rise. NAO: North Atlantic Oscillation. Copyright EEA, Copenhagen. http://www.eea.europa.eu*

Figura 1.5. *Zonas de vulnerabilidad al cambio climático de Europa (IPCC, 2007).*

Según el 4º informe informe del IPCC las zonas incluídas dentro de la denominada región atlántica tienen en común que, entre otras cosas, se prevé que las tormentas de invierno, las inundaciones, y la erosión de la costa aumenten. Las zonas englobadas dentro de la región atlántica coinciden a groso modo con las descritas por Mediero et al. (2015). En cualquier caso, en los tres estudios citados, el País Vasco se sitúa dentro de dicha región además de estar en la zona de transición hidrológica de Europa. Nótese que, en la presente Tesis

doctoral, cuando se mencione la región atlántica se referirá a la descrita por el IPCC y que se puede observar en la figura 1.5.

PROYECCIONES CLIMÁTICAS PARA EL PAÍS VASCO

En función de la fuente consultada, al tratarse de una región compleja que se sitúa en una zona de transición entre distintas tendencias, las previsiones climáticas para el País Vasco pueden variar. Por este motivo, se ha optado por analizar los resultados de los modelos climáticos más recientes (CMIP5) a los que la Agencia Estatal de Meteorología (AEMET) ha realizado dos tipos de downscaling estadístico. Por un lado, han utilizado el método de análogos (AN) (Petisco & Martín, 2006), y, por otro lado, el "statistical downscalign method" (SDSM) que es un tipo de downscalign de regresión lineal (Wilby et al., 2002). En el Apéndice 1 se muestran los resultados del downscaling realizado a 19 GCMs, de precipitación, temperatura máxima y temperatura mínima, anual y estacional, en distintas condiciones de forzamiento radiativo (RCP 4.5, 6.0 y 8.5).

Las proyecciones de precipitación anual para el siglo XXI en el País Vasco muestran tendencias de descenso. Como se puede observar en la figura 1.6 (a, b), a finales de siglo se espera llueva entre un -5% y un -20% menos (considerando los dos métodos de downscaling). También se pueden apreciar las diferencias existentes entre los dos métodos de downscaling. En general, el método AN proyecta mayores descensos de precipitación y su banda de incertidumbre es mayor. Además, también se observan tendencias opuestas en función del método de downscaling. Como se puede ver en la figura el método de downscaling AN proyecta un descenso en precipitaciones intensas (Fig. 1.6, c), mientras que el método SDSM predice un aumento (Fig. 1.6, d). Por lo tanto, aunque parece evidente que la precipitación descenderá, no queda claro qué ocurrirá con las precipitaciones intensas.

En cuanto a los periodos secos, parece que su duración (días) se mantendrá como en la actualidad, y se dará una disminución en el número de días de lluvia (Appendix 1; Fig.A_1 y A_7). Las proyecciones de precipitación estacional para finales de siglo, muestran, además, que los mayores descensos se darán en las estaciones más húmedas; entre -5% y -25% en otoño, entre -5%

y -15% en primavera e invierno y, por último, entre +5% y -15% en verano (Appendix 1: Fig. A_2 y A_8). Las mayores bandas de incertidumbre se registran en invierno.

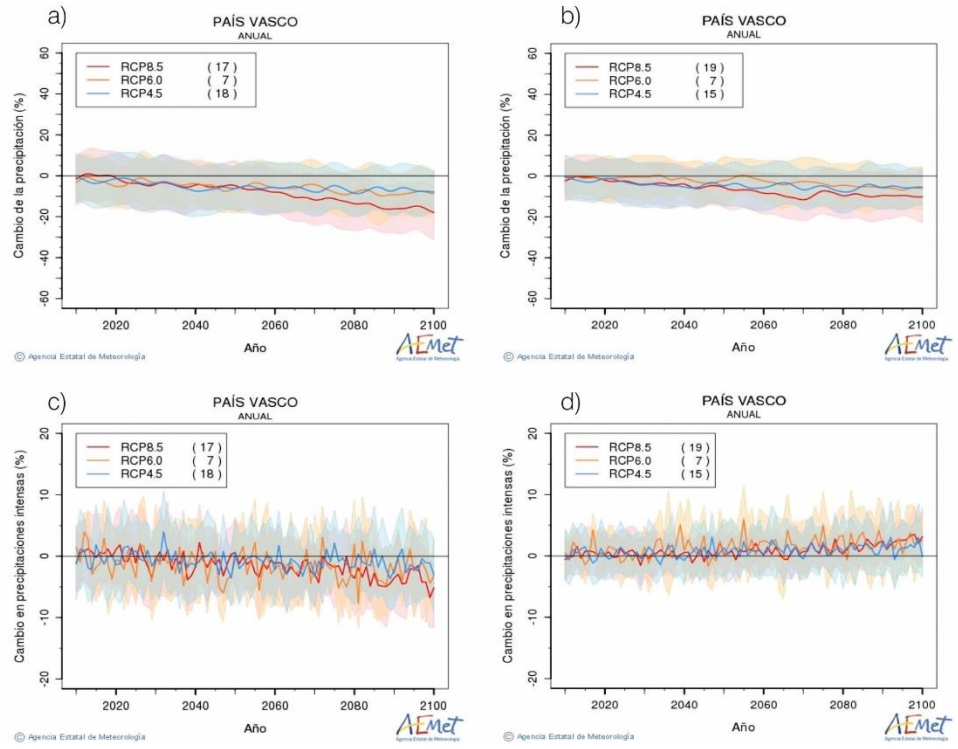

Figura 1.6. *Proyecciones de precipitación anual para el País Vasco (2010-2100). a) muestra el cambio de precipitación respecto al baseline (1960-2000) en % de los GCMs a los que se les ha realizado el downscaling del método AN y b) los del método SDSM. c) muestran el cambio en precipitaciones intensas (%) que projectan los GCMs a los que se les a aplicado el método de downscaling AN, mientras que d) muestran el cambio en precipitaciones intensas (%) que projectan los GCMs a los que se les a aplicado el método de downscaling SDSM. Fuente: www.aemet.es.*

El forzamiento radiativo ejerce influencia directa sobre la temperatura, por tanto, existen diferencias considerables entre los RCPs 4.5 y 6.0 (forzamiento radiativo medio que se mantiene constante de mitad de siglo en adelante Fig. 1.3), que muestran comportamientos similares, en comparación con el RCP 8.5 que predice incrementos de temperatura mucho más considerables. Así, las proyecciones indican que a finales de siglo la temperatura máxima y mínima anual habrán aumentado entre 2 °C (RCP 4.5 y 6.0) y 4 °C (RCP 8.5) (Fig.1.7).

Según las predicciones otoño será la estación en la que mayores aumentos de temperatura se darán (Appendix 1; Fig.A_4 y A_12).

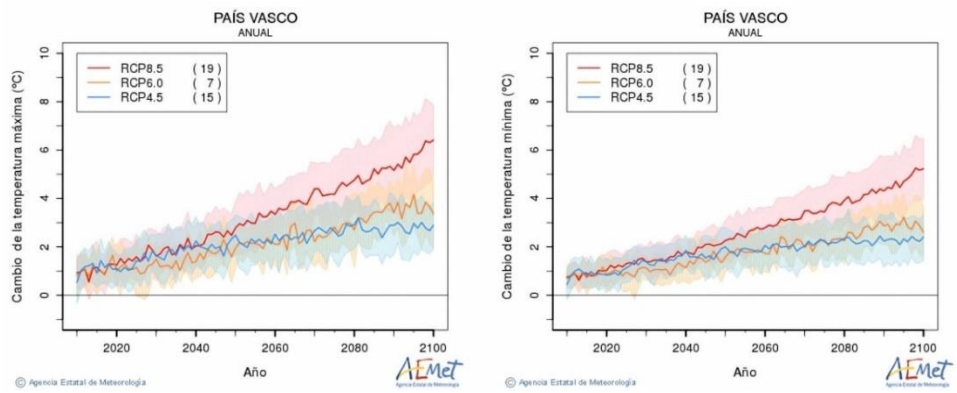

Figura 1.7. *Proyecciones de temperatura máxima anual (izquierda) y mínima (derecha) (2010-2100) (www.aemet.es).*

1.1.6 Impactos del cambio climático sobre los recursos hídricos de la península ibérica

A continuación, se muestra un resumen de los estudios realizados desde el año 2000 en los que se evalúan los impactos del cambio climático en los recursos hídricos. En ocasiones, en estudios a escala regional y/o global, se engloban los resultados de la península ibérica sin discernir entre zona mediterránea y atlántica o entre norte y sur. Es por ello, y también para poder tener una visión más general, que, en esta Tesis doctoral, se muestran los estudios de lo que con anterioridad se ha expuesto como región atlántica y los de la península ibérica, por separado. En los siguientes sub-capítulos se muestran los resultados generales de muchos de los estudios realizados en ambas zonas.

En la tabla 1.1 se muestra un resumen de algunos de los estudios realizados en la península ibérica desde el año 2000. Sus resultados aparecen en % de cambio de caudal respecto al periodo-base, o baseline, que es el periodo con el que se comparan los caudales futuros proyectados. Como se puede observar la metodología (GCMs, métodos de downscaling, escenarios de emisión o RCPs, modelos hidrológicos e incluso años de estudio) entre distintos estudios es diferente por lo que no resulta sencillo realizar comparaciones entre

ellos. Además, los tipos de cuenca analizados y su localización en la península también son diferentes por lo que es posible esperar resultados muy diversos. Sin embargo, esta recopilación ofrece la posibilidad de observar la evolución en las metodologías de estudios de impacto del cambio climático en la hidrología, y también de obtener tendencias generales.

Uno de los primeros estudios que se realizó en la península para estudiar los efectos del cambio climático en los recursos hídricos, fue llevado a cabo por Ayala-Carcedo & Iglesias (1996). Utilizaron el modelo climático del Hadley Centre en las cuencas de mayor tamaña de la península ibérica hasta el horizonte 2060. En el año 2000 el Ministerio de Medioambiente y Obras Publicas publicó El libro blanco del agua en España (*1*, en la tabla 1.1). Entre otras cosas, sus objetivos eran evaluar la situación del agua en España y así poder estimar su evolución para gestionar mejor este recurso. Para ello utilizaron un GCM (UKMO) y un RCM (PROMES), dos modelos hidrológicos y tres escenarios de emisión. El primer escenario contemplaba que para 2030 la temperatura media anual subiría un grado, en el segundo la precipitación anual descendería un 5 % y la temperatura subiría un grado, y en el tercero, la precipitación media anual descendería un 15 % y se daría un aumento extremo de la temperatura (4°C más) respecto al baseline. Debido a que el tercer escenario es muy extremo, en la tabla 1.1 se presentan los resultados de los dos primeros. Además del descenso de los recursos hídricos proyectado para 2030 (descenso respecto al baseline del 5 al 14 %), también se señala al sur de la península y las zonas insulares como las que sufrirán mayor impacto. En 2002 Fernández (*2*, en la tabla 1.1) desarrolló un procedimiento metodológico para estudiar los efectos del cambio climático en los recursos hídricos. Con tal fin, utilizó el modelo hidrológico SIMPA, un modelo distribuido de escala mensual al que introdujo los datos climáticos de modelos regionales (PROMES) en 19 cuencas de la península. Pérez-Martín (2005) (*3*, en la tabla 1.1), utilizó los datos climáticos del mismo RCM para proyectar la evolución hidrológica en la cuenca del río Jucar. La reducción del caudal proyectada en este estudio para finales de siglo es del 40 %, con una distribución geográfica heterogénea. Las áreas del interior serán las más afectadas (reducciones de hasta el 50 %) mientras que las zonas cercanas a la costa

mediterránea muestran menores descensos (25 %). El estudio también analiza las futuras necesidades de agua de regadío, que por el aumento de las temperaturas y el descenso de la precipitación serán mayores.

En 2007 da Cunha et al. (*4*, en la tabla 1.1) publicaron un informe para evaluar el impacto de los efectos del cambio climático en los recursos hídricos de Portugal. El estudio se llevó a cabo en 16 cuencas localizadas de norte a sur del país utilizando los resultados climáticos de un GCM (HadCM3) y un RCM (HadRM2) del Hadley Centre. En la tabla 1.1 se muestra los valores mínimos y máximos de cambio en el caudal respecto al baseline (1960-1990) de todo el país. Por este motivo no es posible apreciar en la tabla el descenso gradual de las proyecciones de caudal, del norte a sur de Portugal. Por otro lado, los resultados obtenidos a partir de ambas proyecciones climáticas, muestran un patrón de incremento del caudal (o mantenimiento) en invierno y un descenso en el resto de estaciones, sobre todo en otoño. Nunes et al. (2008) (*5*, en la tabla 1.1) estudiaron el impacto del cambio climático no solo en los recursos hídricos, sino también en la producción de vegetación y la erosión. Investigaron 18 cuencas del sudeste de Portugal, divididas en dos zonas claramente contrastadas, Alentejo de condiciones semiáridas y Ribatejo, que es una zona húmeda. En este caso, en vez de utilizar resultados climáticos de GCMs o RCMs, los autores establecieron unas condiciones dadas, incrementos de temperatura de hasta 6.4°C, reducción de la precipitación de hasta un 40 % y aumento del CO2 atmosférico de hasta un 100 %. Las variables climáticas fueron simuladas con el modelo hidrológico SWAT. Los principales resultados mostraron que la escorrentía sub-superficial es altamente sensible al cambio climático, que la mayoría de las especies (excluyendo las mediterráneas) muestran una tendencia negativa a la producción de biomasa debido al incremento de temperatura y que la erosión depende del descenso de la escorrentía y la producción de biomasa. Además, los autores también concluyeron que las cuencas húmedas adquirirán propiedades semiáridas como caudales más irregulares.

El CEDEX (2010) (*6*, en la tabla 1.1) realizó un esfuerzo importante para evaluar los efectos del cambio climático en los recursos hídricos de España. En este informe, además de ofrecer cómputos globales, también se analizan

resultados por comunidades autónomas, vertientes… (*6* en la tabla 1.1 y *18* en la tabla 1.2). Los resultados de este informe han sido utilizados por las administraciones. Por ejemplo, son los que ha utilizado la Agencia Vasca del Agua, URA en el Plan Hidrológico del Cantábrico Oriental (URA, 2015). Es un informe muy completo que utiliza 4 modelos generales de circulación del AR3 (IPCC, 2001), 2 métodos de downscaling estadístico, dos modelos regionales de circulación y dos escenarios de emisión (A2, B2). Según los resultados de este informe, parece bastante evidente que el caudal anual de los ríos de España descenderá, y que cuanto más avance el siglo el descenso será mayor. Invierno es la estación que menos se resentirá mientras que los mayores descensos se darán en los meses de primavera y verano. En este caso, el valor que ofrece el CEDEX es una media de los resultados de todas las cuencas analizadas, es decir, que se hace una media con cuencas de influencia atlántica, mediterránea y de los Pirineos.

Rojas et al. (2012) (*7*, en la tabla 1.1) estudiaron el riesgo de inundación con periodos de retorno de 100 años en Europa. Usaron 12 RCMs del proyecto ENSEMBLES y el escenario de emisión A1B. Para finales de siglo, el estudio señala que habrá un incremento (> 40%) en el riesgo de inundación en el Reino Unido, noreste y sudeste de Francia, norte de Italia, en algunas zonas del sudeste de España, los Balcanes y los Cárpatos. El estudio señala que, aunque existe una clara tendencia a la disminución del caudal en la península ibérica, la inundabidad se intensificará puesto que los caudales máximos irán en aumento. Sin embargo, este incremento en los caudales máximos no será homogéneo, cuencas como las de los ríos Ebro, Duero o Tajo no muestran tal aumento. Probablemente esto es debido al descenso de nieve en las zonas de montaña que provocará que sus afluentes tengan menos agua.

Rasilla et al. (2013) (*8*, en la tabla 1.1) analizaron los impactos del cambio climático en los recursos hídricos de la península ibérica utilizando dos GCMs y dos escenarios de emisión (A2 y B2). Aunque los resultados varían en función de la localización de las cuencas y el nivel de calentamiento, como conclusiones más relevantes señalaron que la escorrentía decrecerá, sobre todo en primavera, y verano, y que los caudales pico se desplazarán de primavera a finales de

invierno, sobre todo en áreas de montaña. Este último factor posiblemente esté relacionado con el descenso de caudales pico de primavera descrito por Morán-Tejeda et al. (2010), que ocurre como consecuencia de la reducción gradual de la calidad y duración de las masas de hielo (Rasilla et al., 2013).

Arias (2013) (*9*, en la tabla 1.1) aplicó el modelo hidrológico SWAT en una cuenca agroforestal de A Coruña para estudiar los efectos del cambio climático en la respuesta hidrosedimentaria y la exportación de nitratos. De esta Tesis doctoral se concluye que el caudal descenderá en la cuenca en todas las estaciones del año.

Los estudios mencionados hasta el momento utilizan distintos GCMs, métodos de downscaling y escenarios de emisión. Sin embargo, el modelo hidrológico utilizado en los estudios de cambio climático también es una fuente de incertidumbre. Por este motivo Morán-Tejeda et al. (2015) (*10*, en la tabla 1.10) evaluaron los impactos del cambio climático y los cambios en los usos del suelo en una cuenca del Pirineo, utilizando dos modelos hidrológicos. Los resultados indicaron una disminución del caudal, excepto en invierno, que varía en función del modelo hidrológico utilizado. El mismo año Chirivella et al. (2015) (*11*, en la tabla 1.1), publicaron un estudio centrado en la cuenca del río Júcar. Como conclusiones señalaron que los escenarios regionalizados del projecto ENSEMBLES, por la Agencia Estatal de Meteorología (AEMET), simulaban bien la temperatura, pero tendían a subestimar la precipitación. En cuanto a la distribución espacial, los recursos hídricos que mayor afección sufrirán serán los de las cuencas de cabecera, y otoño e invierno serán los meses que mayores descensos sufrirán. Pascual et al. (2015) (*12*, en la tabla 1.1) centraron su estudio en tres cuencas de tamaño mediano de Cataluña. Las características hídricas de las tres eran distintas puesto que analizaron una cuenca semiárida, otra intermedia y una húmeda. En su estudio concluyeron que en el horizonte 2076-2100 las cuencas húmedas de Cataluña, que actualmente se encuentran en un buen estado hidrológico, serán las que más sufrirán las consecuencias del cambio climático puesto que se proyecta un incremento considerable en el número de días con caudales inferiores al caudal ecológico.

Como se ha mencionado en apartados anteriores, los modelos climáticos han ido evolucionando con el tiempo, de forma que cada vez son capaces de simular más procesos físicos relevantes que ocurren en la atmósfera y que, por tanto, afectan al clima. La última generación de modelos climáticos es la del CMIP5, sin embargo, no son muchos los estudios realizados en la península ibérica con estos modelos. Carvalho-Santos et al. (2015) (*13*, en la tabla 1.1) utilizaron modelos climáticos del CMIP5 y el modelo hidrológico SWAT para estudiar los efectos del cambio del clima y del uso del suelo en la hidrología, la erosión y los nitratos, de una cuenca del norte de Portugal. Utilizaron el RCP 4.5 y sus conclusiones para los horizontes 2021-2040 y 2041-2060 fueron la falta de agua en las estaciones secas y el riesgo de inundación en las húmedas. Por otro lado, Ruelland et al. (2015) (*14*, en la tabla 1.1) estudiaron las incertidumbres relacionadas con los estudios de cambio climático y su impacto en la escorrentía. La investigación se realizó en cuatro cuencas de la zona mediterránea, dos de ellas situadas en la península ibérica. Utilizaron cinco RCMs y sus resultados climáticos se consideraron la primera fuente de incertidumbre. En comparación con los datos observados, los resultados, sobre todo de precipitación, de los RCMs no se ajustaban a los observados. Los resultados hidrológicos mostraron un importante descenso de la escorrentía en primavera, mientras que el resto de estaciones no mostraron tendencias claras. Por último, Fabre et al. (2015) y Grouillet et al. (2015) (*15*, en la tabla 1.1; estudios realizados por los mismos autores) analizaron el estrés hídrico y la demanda de agua de dos cuencas de distintas características, Herault en Francia y Ebro en España. Grouillet et al. (2015) se centraron en la demanda de agua causada por la actividad humana y el cambio climático que habrá en 2050 en ambas cuencas suponiendo un RCP de 8.5. Estos autores concluyeron que las demandas de agua de ambas cuencas incrementarán de forma significativa, de forma que el impacto de las actividades humanas será mayor que el del propio cambio climático. Fabre et al. (2015) estudiaron el estrés hídrico de ambas cuencas en 2050, suponiendo RCPs de 4.5 y 8.5, señalando que los usos de agua proyectados no son sostenibles bajo las condiciones del cambio climático.

Como se puede observar en la tabla 1.1 la metodología utilizada en cada estudio difiere de forma considerable y, además, las características de las cuencas estudiadas son diferentes entre sí. Sin embargo, de los resultados de las investigaciones mencionadas, es posible identificar tendencias. Todos los estudios realizados en la península ibérica coinciden en que el caudal en verano decrecerá. Aunque no esté tan claro, a nivel anual, en otoño y primavera, también parece que el caudal descenderá, mientras que, en invierno, las tendencias son contrapuestas, desde el aumento hasta el descenso. Por lo tanto, la incertidumbre existente en esta estación es considerablemente mayor a la vista de las simulaciones. También parece que las cuencas de cabecera y las cuencas más húmedas serán las que mayor impacto sufrirán (Nunes et al., 2008; Pascual et al., 2015) (tabla 1.1).

	PUBLICATION	LOCATION	CLIMATIC MODEL/PROYECT	HYDROLOGICAL MODEL	BASE LINE	DOWNSCALING	SCENARIO	ANNUAL			AUTUMN			WINTER			SPRING			SUMMER		
								40	70	100	40	70	100	40	70	100	40	70	100	40	70	100
1	**MMA (2000)**	Spain	UKMO PROMES	SIMPA	1940-85	STATSITICAL AND DYNAMICAL	↑1°C	5-14↓														
							↑1°C/↓ 5% pcp															
2	**Fernández (2002)**	19 catchments Spain	UKMO PROMES	SIMPA	1940-85	DYNAMICAL	-	↓ 5-52														
3	**Pérez-Martín (2005)**	Jucar basin (Spain)	PROMES		1960-90	DYNAMICAL	A2/B2			↓40												
4	**Da Cunha et al., 2007**	Portugal	HadCM3	TEMEZ	1960-90		323 ppmv CO_2		↓10-↓30	↓10-↓75		0-↓60	↓20-↓90		0-↓40	0-↓60		↓15-↓60	↓15-↓80		↓20-↓40	↓40-↓80
			HadRM2			DYNAMICAL				↑10-↑30			↓50-↓90			↑10-↑50			↑10-↓50			↓10-↓60
5	**Nunes et al., 2008**	Alentejo and Ribatejo (Portugal centre)	SWAT Weather generator	SWAT	1960-90		300 ppmv CO_2	↓44														
6	**CEDEX 2010**	Spain	IPCC	SIMPA	1961-90	STATSITICAL AND DYNAMICAL	A2	↓8	↓16	↓28	↓8	↓19	↓30	↓3	↓8	↓15	↓14	↓20	↓44	↓24	↓33	↓41
			AR1				B2	↓8	↓11	↓14	↓10	↓9	↓17	↑1	0	↑2	↓13	↓26	↓29	↓27	↓32	↓32
7	**Rojas et al., 2012**	Global: Spain	ENSEMBLES	LISFLOOD	1961-90	DYNAMICAL	A1B			↓42			↓≈20			↓≈10			↓≈40			↓≈60
8	**Rasilla et al 2012**	Iberian Peninsula	HadCM2	1961-90	1961-90	DYNAMICAL	A2			↓10-↓60												
			PCM				B2															
9	**Arias, 2013**	Catchment NW Iberian Peninsula	ENSEMBLES	SWAT	1981-2010		A1B					↓10-↓25	↓10-↓25		↓10-↓30	↓5-↓20		↓10-↓30	↓15-↓35		↓18-↓35	↓15-↓38
10	**Morán-Tejeda et al., 2015**	Aragón River catchment (Spain)	ENSEMBLES	SWAT	1961-90	DYNAMICAL	A1B	↓10-↓13			↓10-↓25			↑9-↑5			↓27-↓31			↓48-↓27		
				RHESS																		
11	**Chirivella et al., 2015**	Júcar basin, (Spain)	ENSEMBLES	PATRICAL	1961-90	DYNAMICAL	A2	↑1-↓9														
							B2															
12	**Pascual et al., 2015**	3 catchments in Catalonia	ECHAM5/MPI-OM	SWAT	1984-2008	DYNAMICAL	A2				↑7-↓9		↓9-↓49	↑7-↓2		↑22-↓30	↓18-↓17		↓15-↓32	↓12-↓25		↓8-↓44
							B1															

	PUBLICATION	LOCATION	CLIMATIC MODEL/PROYECT	HYDROLOGICAL MODEL	BASE LINE	DOWNSCALING	SCENARIO	ANNUAL			AUTUMN			WINTER			SPRING			SUMMER		
								40	70	100	40	70	100	40	70	100	40	70	100	40	70	100
13	**Carvalho-Santos et al., 2015**	Vez River catchment (Portugal)	**CMIP5**	SWAT	1981-2000	STATSITICAL	RCP 4.5	↓6	↓13		0	↓6		↑2	↑3		↓9	↓614		↓17	↓35	
14	**Ruelland et al 2015**	4 mesoscale basins in Mediterranean region	**Med-CORDEX**	GR4j	1986-2005	DYNAMICAL	RCP 8.5											↓2-↓77				
15	**Grouillet et al., 2015 and Fabre et al 2015**	Ebro basin, Spain	**CMIP5**	GR4j	1976-2005	STATSITICAL	RCP 4.5		↑2-↓21			↑17-↓33			↑20-↓17			↑7-↓31			↓4-↓36	
							RCP 8.5															

Tabla 1.1. *Resumen de algunos de los estudios de impacto climático en los recursos hídricos más relevantes realizados en la península ibérica considerando la siguiente información: referencia bibliográfica (Ref.), localización de la(s) cuenca(s) estudiada(s) (location), modelo climático (climatic model), modelo hidrológico (Hydro. Model), baseline, método de downscaling (Down.), y escenario de emisión o RCP (Scen.). "DYNA" se refiere al downscaling dinámico y "STAT" al estadístico. Se presentan los resultados de los estudios en % de cambio de caudal respecto a su baseline, de forma anual y estacional para los años 40, 70 y finales de siglo. * Los resultados de la tabla han sido obtenidos realizando medias a partir de valores gráficos que aparecen en las publicaciones. Ref: 1: MMA, 2000; 2: Fernández, 2002; 3: Pérez-Martín, 2005; 4: da Cunha et al., 2007; 5: Nunes et al., 2008; 6: CEDEX, 2010; 7: Rojas et al., 2012; 8: Rasilla et al., 2013; 9: Arias 2013; 10: Morán-Tejeda et al., 2015; 11: Chirivella et al., 2015; 12: Pascual et al., 2015; 13: Carvalho-Santos et al., 2015; 14: Ruelland et al., 2015; 15: Grouillet et al., 2015 & Fabre et al., 2015.*

1.1.7 Impactos del cambio climático sobre los recursos hídricos de la región atlántica

Son numerosos los estudios realizados en los distintos países que forman la región atlántica definida por el IPCC (2007). A continuación, en la tabla 1.2 se muestra un resumen de estudios llevados a cabo en esta zona. Al igual que en la tabla 1.1 se muestran los aumentos y descensos del caudal en % respecto al periodo-base (baseline) de cada estudio.

En la tabla 1.2 se pueden observar algunas investigaciones recientes realizadas en Bélgica y Holanda. Szêpszô et al. (2014) (*1* en la tabla 1.2) llegaron a la conclusión de que lo más probable es que el caudal de otoño e invierno del río Rhin aumente en las próximas décadas. Tavakoli et al. (2014) (*2* en la tabla 1.2), en un estudio realizado con el fin de evaluar el impacto del cambio climático y del desarrollo de las ciudades en la hidrología de una cuenca de Flandes, llegaron a la conclusión de que los caudales bajos anuales disminuirán y que los más altos aumentarán.

Muchos de los estudios realizados en Gran Bretaña e Irlanda muestran que el caudal en invierno aumentará y descenderá en verano (Diaz-Nieto & Wilby, (2005) (*4* en la tabla 1.2); Fowler & Kilsby, (2007) (*5* en la tabla 1.2); Bastola et al., (2011) (*9* en la tabla 1.2)). Charlton & Arnell (2014) (*11* en la tabla 1.21), en un estudio realizado en seis cuencas de Inglaterra y Escocia, señalaron las importantes diferencias que existen en las proyecciones hidrológicas, en función de las características geológicas de las cuencas y el balance hídrico del baseline de éstas. A pesar de esas diferencias, en general, sus resultados también mostraron aumentos del caudal en invierno y descensos en verano. Por otro lado, no todos los estudios muestran aumentos del caudal en invierno, por ejemplo, Cloke et al. (2010) (*7* en la tabla 1.2), en una cuenca de Inglaterra, prevén un descenso del caudal en todas las estaciones. Diaz-Nieto & Wilby, (2005) (*4* en la tabla 1.2) en un estudio realizado en el río Támesis, indican que los caudales bajos persistirán en otoño, de forma que se alargan en el tiempo, y el aumento de caudal se dará a finales de invierno comienzos de primavera. Para evaluar los recursos hídricos de Gran Bretaña, Prudhomme et al. (2012) (*10* en

la tabla 1.2) realizaron un estudio estacional en el que a mediados de siglo se esperan primaveras con menor caudal (a excepción de Inglaterra central), importantes descensos en verano y descensos en el sur-sudeste en otoño. Los descensos de caudal más importantes previstos para verano (hasta el -80%) ocurrirán en el norte-noroeste. Otros estudios muestran esta área del país como la zona en la que los caudales altos aumentarán más, mientras que en el sur-sudeste, serán los caudales bajos los que aumenten (Arnell, 2004 (*3* en la tabla 1.2); Steele-Dunne et al., 2008 (*6* en la tabla 1.2); Arnell, 2011 (*8* en la tabla 1.2)).

En general, se puede decir que en la región atlántica de Francia se prevé que el caudal medio anual descienda. La estacionalidad de este descenso no queda clara; Ducharne et al. (2010) (*14* en la tabla 1.2) y Chauveau et al. (2013) (*15* en la tabla 1.2) concluyen que el caudal descenderá en todas las estaciones; Habest et al. (2013) (*16* en la tabla 1.2) predicen que el caudal anual descenderá, aunque, el 10 % de las proyecciones (estudio realizado con 147 proyecciones hidrológicas) indica que en invierno puede aumentar; Caballero et al. (2007) (*12* en la tabla 1.2) indican que descenderá en primavera y aumentará en invierno, de forma que el caudal no variará de forma considerable a escala anual, mientras que Boé et al. (2009) (*13* en la tabla 1.2) predicen que el caudal disminuirá en todas las estaciones, aunque las tendencias de descenso son más claras en verano y otoño. En cuanto a la distribución espacial en los estudios realizados, a escala nacional se observa que los mayores descensos se darán en el sudoeste de Francia, es decir, en la cuenca de Adour-Garonne (Caballero et al., 2007 (*12* en la tabla 1.2); Chauveau et al., 2013 (*15* en la tabla 1.2)). Por ejemplo, Boé et al. (2009) (*13* en la tabla 1.2), al estudiar las proyecciones hidrológicas de las cinco mayores cuencas de Francia, indican que la media del descenso anual del caudal será del -20 % (2046-2065). Sin embargo, debido a que la precipitación de invierno disminuirá en mayor medida en el Adour-Garonne, se estima que el descenso del caudal anual en esta cuenca, será del -30 %.

En cuanto a la región atlántica de la península ibérica el estudio llevado a cabo para evaluar los recursos hídricos de Portugal por da Cunha et al. (2007) (*17* en la tabla 1.2) indica que en general los caudales descenderán pero que en algunos casos incluso podrían aumentar en el norte del país. Si comparamos

estos resultados con los que se pueden ver en la tabla 1.1, que corresponden a la media de Portugal (da Cunha et al., 2007 *4* en la tabla 1.1)), se puede decir que en el norte del país los descensos serán menores a excepción del verano donde serán más importantes. Arias (2013) (*19* en la tabla 1.2), prevé que el caudal descenderá en A Coruña en todas las estaciones. En cuanto al estudio realizado por el CEDEX en 2010 (*18* en la tabla 1.2), se puede observar que tanto anualmente como estacionalmente las predicciones indican descensos del caudal en la zona cantábrica. Además, estos descensos son mayores que los proyectados para toda la península (6 en la tabla 1.1). En general, se puede decir que los recursos hídricos anuales en esta zona descenderán y lo harán sobre todo en verano. No está claro lo que ocurrirá en invierno puesto que algunos estudios muestran un pequeño aumento del caudal (da Cunha et al., 2007 (*17* en la tabla 1.2); Carvalho-Santos et al., 2015 (*20* en la tabla 1.2)).

Resumiendo, se podría decir que la mayor parte de las proyecciones indican un aumento en el caudal de invierno en el norte de la región atlántica. En el Reino Unido también se observa esta tendencia, pero los veranos también serán más secos por lo que el caudal medio anual dependerá de cuanto aumente en invierno y cuanto descienda en verano. Los caudales altos, y por lo tanto el riesgo de inundación (Bastola et al., 2011), aumentarán en el noroeste de Gran Bretaña, mientras que los caudales bajos aumentarán en el sudeste. En la región atlántica de Francia las proyecciones muestran que el caudal medio anual descenderá. Los mayores descensos se darán en el sudoeste del país. Por último, en la región atlántica de la península ibérica la tendencia de descenso de caudales anuales se mantiene. La estación que mayor incertidumbre muestra es invierno, puesto que no existen tendencias claras de incremento o descenso del caudal. Por el contrario, en el resto de estaciones el caudal descenderá de forma que las mayores afecciones a los recursos hídricos se registrarán en verano.

REF.	LOCATION	CLIMATIC MODEL	HYDRO. MODEL	BASE LINE	DOWN.	SCEN.	ANNUAL			AUTUMN			WINTER			SPRING			SUMMER		
							40	70	100	40	70	100	40	70	100	40	70	100	40	70	100
1 (a)	Rhine and Upper Danube basins	ECCONET EU FP7 CMIP3	HBV134 COSERO	1961-1990	DYNA.	A1B				↑			↑10 ↓10						0-↓20		
2 (a)	Grote Nete watershed Belgium	CCI-HYDR	WetSpa	1961-1990	STAT.	High, med. & low		↑75pf ↓4.7lf													
3 (b)	Britain	UKCIP02.	-	1960-1990	-	A2	↑10						↑						↓30		
4* (b)	Thames basin, England	UKCIP02. HadRM3H	CATCHMOD	1960-1990	STAT.	A2	↓7	↓8	↓3	↓8	↓22	↓14	↓1	↓5	↑21	↓12	↓1	↓11	↓6	↓6	↓7
						B2	↑21	↓6	↓3	↑10	↓22	↓20	↑11	↑12	↑12	↑3	↓7	-	↑11	↓7	↓3
5* (b)	8 Catchments in the NW England	UKCIP02. HadRM3H	ADM	1960-1990	DYNA.	A2	↓4	↓10	↓16	↓2	↓1	↓1	↑6	↑11	↑15	↓7	↓15	↓25	↓15	↓34	↓54
6* (b)	9 Irish catchments	ECHAM5	HBV-Light	1961-2000	DYNA.	A1B		↑20-↓20			↑20-↓5			↑10-↓40			↑10-↓50			↓20-↓65	
7* (b)	Medway river basin, England	UKCP09 HadRM3	CATCHMOD	1960-1990	DYNA.	A1B				↓5-↓15	↑10-↓20	↑10-↓30	↓10-↓20	↓20-↓30	↓38-↓50	↓5-↓20	↓20-↓35	↓40-↓50	↓5-↓15	↓20-↓30	↓50-↓55
8 (b)	6 catchments in UK	QUEST-GSI CFMIP3	Cat-PDM	1961-1990	STAT.	↑2°C														↑20-↓40	
9* (b)	4 Irish catchments	CMIP3	TOPMODEL NAM HYMOD	-	-	A2 B2	↓3	↓9	↓8	↓1	↑1	↑3	↑1	↓3	↓3	-	↓15	↓13	↓14	↓20	↓19
10 (b)	UK	UKCP09 HadRM3	CERF	1961-1990	DYNA.	A1B					↑60-↓80			↑40-↓20			↓40			↑20-↓80	
11* (b)	6 catchments in England	UKCP09	Cat-PDM	1961-1990	STAT. & DYNA.	B1 A1B A1FI	↑15-↓25	↑15-↓38	↑20-↓40												
12 (c)	Adour-Garonne river basins	CMIP2	SAFRAN-ISBA-MODCOU (SIM)	1985-1995	DYNA.	B2					↓			↑			↓			↓11	
13* (c)	France	CMIP3	SAFRAN-ISBA-MODCOU (SIM)	1971-2000	STAT.			↓20			↓30			↓20			↓30			↓30	
14 (c)	Seine and Somme river basins, France	RExHySS SAFRAN	MODCOU SIM CLSM EROS / GARDENIA GR4J	1970-2000	STAT. & DYNA.			↓28													

REF.	LOCATION	CLIMATIC MODEL	HYDRO. MODEL	BASE LINE	DOWN.	SCEN.	ANNUAL			AUTUMN			WINTER			SPRING			SUMMER		
							40	70	100	40	70	100	40	70	100	40	70	100	40	70	100
15 (c)	France	RExHySS CMIP3	Isba-Modcou GR4J	1961-1990	STAT.	A1B		↓10-↓60			↓			↓			↓			↓	
16* (c)	Seine and Somme river basins, France	RExHySS CMIP3	CLSM EROS GARDENIA GR4 MATHE MODCOU SIM	1971-2000	STAT. & DYNA.	A1B A2		↓20	↓30					0	↓15					↓30	↓40
17* (d)	North Douro, Spain and Portugal	HadCM3 HadRM2	TEMEZ	1960-1990	-	323 ppmv CO_2	↓10	↓20		↓10	↓35		↑20			↓17	↓22		↓30		
					DYNA.				↑20			↓35			↑37						↓65
18 (d)	Cantabrian region	IPCC AR3	SIMPA	1961-1990	STAT. & DYNA.	A2	↓13	↓16	↓29	↓10			↓10			↓12			↓34		
						B2	↓10	↓16	↓17	↓8			↓4			↓11			↓35		
19 (d)	Catchment NW Iberian Peninsula	ENSEMBLES	SWAT	1981-2010	-	A1B					↓10-↓25	↓10-↓25		↓10-↓30	↓5-↓20		↓10-↓30	↓15-↓35		↓18-↓35	↓15-↓38
20* (d)	Vez River catchment (Portugal)	CMIP5	SWAT	1981-2000	STAT.	RCP 4.5	↓6	↓13		0	↓6		↑2	↑3		↓9	↓614		↓17	↓35	

Tabla 1.2 *Resumen de algunos de los estudios más relevantes realizados en la región atlantica considerando la siguiente información: referencia bibliográfica y País en el que se ha realizado el estudio (Ref.), localización de la(s) cuenca(s) estudiada(s) (location), modelo climático (climatic model), modelo hidrológico (Hydro. Model), baseline, método de downscaling (Down.), y escenario de emisión o RCP (Scen.). "DYNA" se refiere al downscaling dinámico y "STAT" al estadístico. "pf" caudal pico y "lf" caudal bajo. Se presentan los resultados de los estudios en % de cambio de caudal respecto a su baseline de forma anual y estacional para los años 40, 70 y finales de siglo. * Los resultados de la tabla han sido obtenidos realizando medias a partir de valores gráficos que aparecen en las publicaciones. Referencia: (a) Bélgica y Países Bajos; (b) Reino Unido; (c) Francia; (d) Península Ibérica; 1: Szêpszô et al., 2014; 2: Tavakoli et al., 2014; 3: Arnell, 2004; 4: Diaz-Nieto & Wilby, 2005; 5: Fowler & Kilsby, 2007; 6: Steele-Dunne et al., 2008; 7: Cloke et a.,l 2010; 8: Arnell, 2011; 9: Bastola et al., 2011; 10: Prudhomme et a.,l 2012; 11: Charlton & Arnell., 2014; 12: Caballero et al., 2007; 13: Boé et al., 2009; 14: Ducharne et al., 2010; 15: Chauveau et al., 2013; 16: Habets et al., 2013; 17: da Cunha et al., 2007; 18: CEDEX, 2010; 19: Arias, 2013; 20: Carvalho-Santos et al., 2015.*

1.2 HYDROLOGICAL MODELS

A model is a simplified representation of the real-world system (Moradkhani & Sorooshian, 2008). Due to the complexity of the natural systems, the models are not able to consider all the processes of real systems and they need to do a series of simplifications and hypotheses, preserving the essential characteristics of the objective of the research (Andreu, 1993). There are different types of models, nevertheless, many of them share structural similarities because their underlying assumptions are the same. To simulate hydrological systems the most extended are the mathematical models. They simulate natural processes of the water flow, sediment, chemical, nutrients and microbial organisms within the catchment, and they quantify the impact of human activities on these processes as well (Singh & Frevert, 2005). Consequently, they can be used to predict the system behaviour or to understand some hydrological processes so that they are nowadays considered an important and necessary tool for water and environment resource management.

The mathematical models change the numerical inputs into numerical outputs using mathematical and logical steps that have a chronological relation. (Jajarmizadeh et al., 2012). Therefore, to study hydrological processes in a natural system it is usual to use a mathematical formulation in a software; a numerical code. The system built by a specific code and a set of parameters and variables is the model (Anderson & Woessner, 1992). Nevertheless, because of the extended use of the word model to refer to the software (numerical code) used to simulate natural processes, in this manuscript it will be used to refer to the construction of the system and to the numerical code.

A model consists of various **parameters** that are considered constant over the time and that characterize the system (e.g. soil texture, hydraulic conductivity, baseflow recession constant…). The values of those parameters are the ones that are changed in the calibration process. The **variables** are quantitative values of the natural phenomena and they can vary over the time and space. The input variables (precipitation, temperature…) are independent data sets to which a series of equations are applied in order to try to represent another

variable. The output variables are obtained calculating the equations that define the processes, some examples are streamflow, sediment load, nutrient… in the output. Finally, the state variables are data sets that represent a situation of the model that affects other state and output variables (soil moisture, surface runoff…) (Epelde, 2015).

Nowadays, the use of hydrological models with different objectives is widespread. Some of its uses are shown below:

- Estimate discharges at ungauged points.
- Estimate discharges in natural systems (or other variable).
- Fill incomplete data series.
- Predict discharge in changing conditions (or other variable).
- Simulate the hydrological processes in a catchment to better understand these processes.
- Test hypotheses and improve knowledge of hydrological systems.

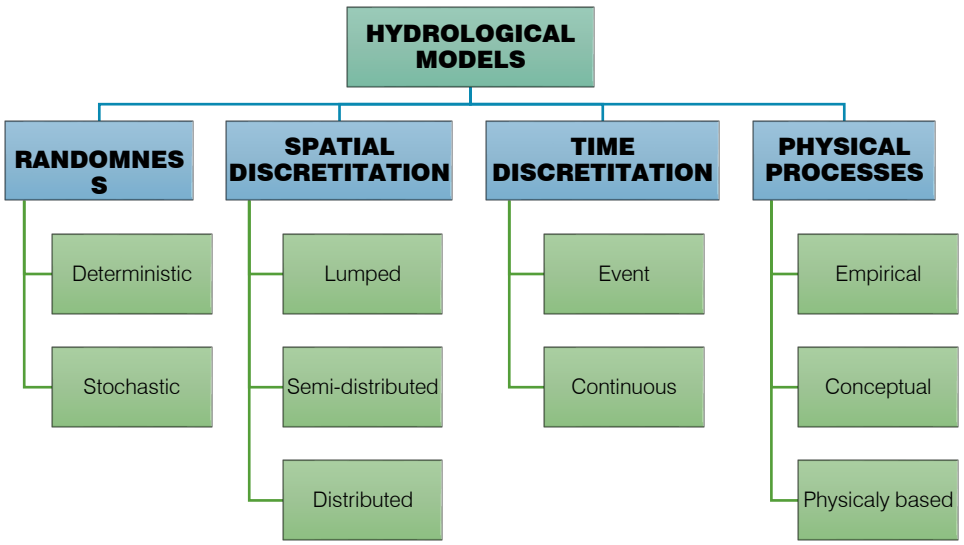

Figure 1.8. *Schematic classification of mathematical models used in hydrological simulation (modified from Epelde, 2015).*

Therefore, there is a wide range of hydrological models that can be classified based on different characteristics. For example, Shaw (1983), Chow et al. (1988), Willems (2000), Wagener et al. (2004), Gosain et al. (2009) … did an effort to classify the hydrological models with different results. However, according to Jajarmizadeh et al. (2012) most hydrological models are not very different from each other because their main differences lie in the operating processes but not in the concepts. In the figure 1.8 it is possible to observe one classification of hydrological models in function of their main characteristics.

In function of the randomness in the modelling of the processes, it is possible to classify the mathematical models in **deterministic** or **stochastic** models. The first, will give the same output for a single set of parameter and input variables, while in the second, for a single set of inputs, the outputs are different because this kind of models possess some inherent randomness. According to the spatial resolution, the models could be lumped, semi-distributed or distributed. **Lumped** models examine the catchment as a single unit generating outputs that do not consider the spatial processes. Usually they need less data and are in general easier to operate. Nevertheless, its range of application is limited and the mean values of the parameters are not representative at catchment level. The **distributed** models divide the catchment into small units (square cells or triangulated irregular network), so that the parameters and all the variable, can vary spatially. They have a high application range but they require a great number of data, usually are more complicated to use than lumped models and they have a high computational cost. The **semi-distributed** models are between lumped and distributed models because they divide the catchment into areas of hydrologic similarity. They have more physically-based structure in compared to the lumped and they require less amount of input data in contrast to the fully distributed models. However, as the distributed models deal with the main physical processes in detail, they can offer a highest degree of accuracy. Nevertheless, they have some nonlinearity, scale, uniqueness and uncertainty problems (Beven, 2001). The temporal discretization of a model distinguishes between **continuous** and single **event** models. One of the most important classifications is the one that describes the physical processes in which the

models operate (Devia et al., 2015). The **empirical** models are also called **metric, data based** or **black box** models because they use mathematical equations to explain the relations between the input and output data instead of the physical processes, therefore this type of models do not consider the hydrological processes that occur in the catchment. They can only be used for the catchment where they were generated because they are valid within the boundary of a given domain. Some examples are the Instantaneous Unit Hidrograph (IUH) (Noorbakhsh et al., 2005) or IHACES (Littlwood & Jakeman, 1994) that are empirical models to show unit hydrographs. The conceptual models are representations of catchment hydrological processes. These models simplify reality assuming that from precipitation to stream release at the outlet it is like a series of interlinked processes and storages (Rahmana & Noury, 2008). Thus, using semi-empirical equations to represent physical elements for the catchment the models consider a number of interconnected storages recharged by precipitation, infiltration, percolation and emptied by evapotranspiration, drainage. In these cases the parameters are not only evaluated from field data but also through calibration, therefore calibration involves curve fitting that sometimes is difficult for physical interpretation. The **conceptual, parametric** or **grey box** models are different from physically-based models because they are not based on physical processes; the conceptual simulate a behaviour system based on perception (Jaharmizadeh et al., 2012). Some conceptual models are Stanford Watershed Model (Crawford & Linsley, 1966), TOPMODEL (Beven & Kirkby, 1979). Finally, the **physically-based**, **mechanistic** or **white box** models, as its very name indicates, are mathematically idealized representations of real physical processes that occur in the hydrological systems (Hapuarachchi et al., 2003). They do not require extensive meteorological or hydrological data for calibration but it is necessary to evaluate a large number of parameters describing the physical characteristic of the catchment. In general, they are complex models and they need human expertise and computational capability. SHE or MIKESHE are physically based models (Aboott et al., 1986).

According to Devia et al. (2015) the best model is the one which give results close to reality with the use of least parameters and model complexity.

However, when choosing a model it is necessary to consider what are the objectives to be achieved and the data available to do that.

1.3 OBJECTIVES

The preliminary **hypothesis** is that the climate change will affect the water resources of the Basque Country, and its impact will not be equal in all the seasons neither for mean and low flows.

Therefore, the main **objective of this Thesis is to make a first sight of the climate change effects on hydrological systems of the Basque Country.** For this purpose, a large number of climate projections have been used to project the hydrological response of 4 catchments of the Basque Country. Furthermore, in this Thesis before doing the hydrological projections the selected hydrological model performance in one of the studied catchments was evaluated.

Thus, the specific objectives of this Thesis are:

- Evaluate the performance of the selected hydrological model to simulate the hydrological processes in small catchments of the Basque Country. This evaluation was made with different points of view:
  - Considering the spatial origin of streamflow.
  - Considering different time steps: daily and hourly.
- Study the hydro-sedimentary impacts of climate change in catchments of the Basque Country:
  - Evaluate the impacts in suspended sediment transport.
  - Evaluate the impacts in different horizons: 2030s, 2060s 2090s, annually, seasonally and monthly.
  - Assess possible trends in high, low and mean discharges.
  - Analyse where are the greatest uncertainties in the methodology used.

1.4 STRUCTURE OF THE MANUSCRIPT

The manuscript is divided in five main chapters:

The FIRST CHAPTER is an introduction where climate change and the steps to evaluate its impacts on hydrological resources are described. In addition, the Basque Country is contextualized in the Iberian Peninsula and in the Atlantic Region. A general description of the prevailing hydrological models is made, and finally, the principal objectives of this Thesis are established.

In the SECOND CHAPTER the methodology used to carry out this Thesis is explained. In this chapter, the selected catchments, the hydrological model used and the climate projections selected and their characteristics are explained. It was establised the methodology 1) to evaluate the climate projections and the hydrological model performance and 2) to analyse the future hydrological projections.

The THIRD CHAPTER is the one that evaluates the performance of the hydrological model Soil and Water Assessment Tool (SWAT). This model was used in a small forested catchment. The evaluation was made to analyse how well the model simulates the spatial origin of the streamflow, and whether it is able to have good results in sub-daily (hourly) time step.

In the FOURTH CHAPTER the evaluation of climate change impact on water resources of the four analysed catchments is made. In one catchment also was evaluated the climate change impact on sediment load. In each case it is exposed the calibration and validation of the hydrological model and the analysis of the effects of climate change in different horizons as well as the trend evaluation for low, high and medium flows.

Finally, the FIFTH CHAPTER includes a general discussion of the methodology and the results, and the most important conclusions obtained in this Thesis. In addition to this, the principal perspective work and the recommendations are also listed.

1.5 REFERENCES

Aboott, M.B., Bathrust, J.C., Cunge, J.A., O´Connell, P.E., Rasmussen, J. 1986. An introduction to the European hydrological system-systeme hydrologique Europeen SHE. 2: Structure of the physically-based distributed modeling system. Journal of Hydrology. 87, 61-77.

Alfieri, L., Feyen, L., Dottori, F., Bianchi, A. 2015. Ensemble flood risk assessment in Europe under high end climate scenarios. Global Environmental Change. 35, 199-212. http://dx.doi.org/10.1016/j.gloenvcha.2015.09.004.

Allen, M.R., Ingram, W.J. 2002. Constraints on future changes in climate and the hydrologic cycle, Nature. 419, 224– 232. http://dxdoi.og/10.1038/ nature01092.

Anderson, M.P., Woessner, W.W. 1992. Applied groundwater modeling. Simulation of flow and advective transport. London, United Kingdom. pp. 381.

Andreu, J. 1993. Análisis de sistemas y modelación en conceptos y métodos para la planificación hidrológica. Ed. Joaquín Andreu (CIMNE), Barcelona, Spain. pp. 391.

Arnell, N.W. 1998. Climate change and water resources in Britain. Climatic Change. 39,83-110.

Arnell, N.W. 1999. The effect of climate change on hydrological regimes in Europe: a continental perspective. Global Environmental Change. 9, 5–23.

Arnell, N.W. 2004. Climate-change impacts on river flows in Britain: The UKCIPO2 scenarios. Water and Environment Journal. 18 2, 112-117. http://dx.doi.org/10.1111/j.1747-6593.2004.tb00507.x.

Arnell, N.W. 2011. Uncertainty in the relationship between climate forcing and hydrological response in UK catchments. Hydrology and Earth System Sciences. 15 (3), 897-912. http://dx.doi.org/10.5194/hess-15-897-2011.

Arnell, N.W., van Vuuren, D.P., Isaac, M. 2011. The implications of climate policy for the impacts of climate change on global water resources. Global Environmental Change. 21 (2), 592–603. http://dx.doi.org/10.1016/j.gloenvcha.2011.01.015.

Arias, R. 2013. Comportamiento hidrosedimentario de una Cuenca agroforestal bajo diferentes condiciones climáticas: importancia para establecer planes de manejo. PhD. Universidad de Coruña.

Ayala-Carcedo, F.J., Iglesias, López A. 1996. Impactos del cambio climático sobre los recursos hídricos, el diseño y la planificación hidrológica en la España peninsular. Tecnoambiente. 64,43-48.

Ayala-Carcedo, F.J., Iglesias, A. 2000. Impactos del posible cambio climático sobre los recursos hídricos, el diseño y la planificación hidrológica en la España peninsular. El Campo De Las Ciencias y Las Artes. 137, 201-222.

Barnett, T.P., Pierce, D.W., Schur, R. 2001. Detection of climate change in the world's oceans. Science. 292, 270–274.

Bastola, S., Murphy, C., Sweeney, J. 2011. The role of hydrological modelling uncertainties in climate change impact assessments of Irish river catchments. Adv.Water Resour. 34, 562-576.

Beguería, S., López-Moreno, J.I., Lorente, A., Seeger, M., García-Ruiz, J.M. 2003. Assessing the effect of climate change and land-use changes on streamflow in the central Spanish Pyrenees. Ambio. 32 (4), 283-286.

Beniston, M. 2003. Climatic change in mountain regions: a review of possible impacts. Climatic Change. 59, 5–31.

Bergstrom, S., Carlsson, B., Gardelin, M., Lindstro, G., Pettersson, A., Rummukainen, M. 2001. Climate change impacts on runoff in Sweden: assessments by global climate models, dynamical downscaling and hydrological modelling. Climate Research. 16, 101–112.

Beven, K.J. 2001. How far can we go in distributed hydrological modeling? Hydrology and Earth System Sciences. 5: 1-12.

Beven, K.J., Kirkby, M.J. 1979. A physically-based, variable contributing area model of basin hydrology. Hydrological Sciences Bulletin, 24, 43-69.

Birsan, M.-V., Molnar, P., Burlando, P., Pfaundler, M. 2005 Streamflow trends in Switzerland. Journal of Hydrology. 314 (1-4), 312–329. http://dx.doi.org/10.1016/j.jhydrol.2005.06.008.

Boé, J., Terray, L., Martin, E., Habets, F. 2009. Projected changes in components of the hydrological cycle in French river basins during the 21st century. Water Resources Research. 45, W08426. http://dx.doi.org.10.1029/2008WR007437.

Bosshard, T., Carambia, M., Goergen, K., Kotlarski, S., Krahe, P., Zappa, M., Schär, C. 2013. Quantifying uncertainty sources in an ensemble of hydrological climate-impact projections. Water Resources Research. 49 (3), 1523–1536.

Bredemeier, M. 2011. Forest climate and water issues in Europe. Ecohydrology. 4(2), 159–167. http://dx.doi.org/101002/eco203.

Brigode, P., Oudin, L., Perrin, C. 2013. Hydrological model parameter instability: A source of additional uncertainty in estimating the hydrological impacts of climate change? Journal of Hydrology. 476 (0), 410-425. http://dx.doi.org/10.1016/j.jhydrol.2012.11.012.

Brunet, B., Casado, M.J., de Castro, M., Galán, P., López, J.A., Martín, J.M., Pastor, A., Petisco, E., Ramos, P., Ribalaygua, J., Rodríguez, E., Sanz, I. Torres, L. 2009. Generacio□n de Escenarios Regionalizados de Cambio Clima□tico para Espan□a. Spanish Meteorological Agency (AEMET).http://www.aemet.es/documentos/es/serviciosclimaticos/cambio_climat/datos_diarios/Informe_Escenarios.pdf. Accessed 5 August 2015.

Brunet, M., Jones, P.D., Sigro, J., Saladie, O., Aguilar, E., Moberg, A., Della-Marta, P.M., Lister, D., Walther, A., Lopez, D. 2007. Temporal and spatial temperature variability and change over Spain during 1850-2005. Journal of Geophysical Research-Atmospheres. 112, D12117. http://dx.doi.org/10.1029/2006JD008249.

Caballero, Y., Voirin-Morel, S., Habets, F., Noilhan, J., LeMoigne, P., Lehenaff, A., Boone, A. 2007. Hydrological sensitivity of the Adour-Garonne river basin to climate change. Water Resources Research. 43, W07448.

Carvalho-Santos, C., Nunes, J.P., Monteiro, A.T., Hein, L., Honrado, J.P. 2015. Assessing the effects of land cover and future climate conditions on the provision of hydrological services in a medium-sized watershed of Portugal. Hydrological Processes, 30 (5), 720-738. http://dx.doi.org/10.1002/hyp.10621.

Ceballos-Barbancho, A., Morán-Tejeda, E., Luengo-Ugidos, M.A., Llorente-Pinto, J.M. 2008. Water resources and environmental change in a Mediterranean environment: the south-west sector of the Duero River basin (Spain). Journal of Hydrology. 351, 126–138.

CEDEX., 2010. Estudio de los impactos del cambio climático en los recursos hídricos y las masas de agua. Ficha 1. Evaluación del impacto del cambio climático en los recursos hídricos en régimen natural. Clave CEDEX 42-407-1-001. Informe técnico para ministerio de Medio Ambiente y Medio Rural y Marino. Madrid, España.

Charlton, M.B., Arnell, N.W. 2014. Assessing the impacts of climate change on river flows in England using the UKCP09 climate change projections. Journal of Hydrology. 519, Part B, 1723-1738. http://dx.doi.org/10.1016/j.jhydrol.2014.09.008.

Chauveau, M., Chazot, S., Perrin, C., Bourgin, P., Sauquet, E., Vidal, J., Rouchy, N., Martin, E., David, J., Norotte, T., Maugis, P., de Lacaze, X. 2013. What will be the impacts of climate change on surface hydrology in France by 2070? La Houille Blanche-Revue Internationale De L´Eau. (4), 5-15. http://dx.doi.org/10.1051/lhb/2013027.

Chen, J., Brissette, F. P., Leconte, R. 2011. Uncertainty of downscaling method in quantifying the impact of climate change on hydrology. Journal of Hydrology. 401(3–4), 190-202. http://dx.doi.org/10.1016/j.jhydrol.2011.02.020.

Chow, V.T., Maidment, D.R., Mays, L.W. 1988. Applied Hydrology. McGraw-Hill, USA.

Chirivella, V., Capilla, J. E., Pérez-Martín, M. A. 2015. Modelling regional impacts of climate change on water resources: The Jucar basin, Spain. Hydrological Sciences Journal. 60 (1), 30-49. http://dx.doi.org/10.1080/02626667.2013.866711.

Christensen, J.H. 2005. Prediction of Regional scenarios and Uncertainties for Defining European Climate change risks and Effects (PRUDENCE). Final Report. URL: http://prudence.dmi.dk/

Christensen, O.B., Christensen, J.H. 2004. Intensification of extreme European summer precipitation in a warmer climate, Global Planet. Change. 44, 107–117, http://dx.doi.org/10.1016/j.gloplacha.2004.06.013.

Chust, G., Borja, A., Caballero, A., Irigoien, X., Sáenz, J., Moncho, R., Marcos, M., Liria, P., Hidalgo, J., Valle, M., Valencia, V. 2011. Climate change impacts on coastal and pelagic environments in the southeastern Bay of Biscay. Climate Research. 48 (2-3), 307-332. http://dx.doi.org/10.3354/cr00914.

Cloke, H. L., Jeffers, C., Wetterhall, F., Byrne, T., Lowe, J., Pappenberger, F. 2010. Climate impacts on river flow: Projections for the medway catchment, UK, with UKCP09 and CATCHMOD. Hydrological Processes. 24 (24), 3476-3489. http://dx.doi.org.10.1002/hyp.7769.

Coch, A., Mediero, L. 2015. Trends in low flows in Spain in the period 1949–2009. Hydrological Sciences Journal, 1-17. http://dx.doi.org//10.1080/02626667.2015.1081202.

Coron, L., Andreassian, V., Perrin, C., Lerat, J., Vaze, J., Bourqui, M., Hendrickx, F. 2012. Crash testing hydrological models in contrasted climate conditions: An experiment on 216 Australian catchments. Water Resources Research. 48, W05552. http://dx.doi.org/10.1029/2011WR011721.

Cosandey, C., Andréassian, V., Martin, C., Didon-Lescot, J.F., Lavabre, J., Folton, N., Mathys, N., Richard, D. 2005. The hydrological impact of the Mediterranean forest: a review of French research. Journal of Hydrology. 301, 235–249.

Crawford, N.H., Linsley, R.K. 1966. Digital simulation in Hydrology. In: Contemporary Hydrology, Wilby, R. (Ed). John Wiley and Sons, England, pp: 157-158.

Dankers, R., Feyen, L. 2009. Flood hazard in Europe in an ensemble of regional climate scenarios. Journal of Geophysical Research. 114. http://dx.doi.org/10.1029/2008jd011523.

da Cunha, L.V., De Oliveira, R.P., Nascimento, J., Ribeiro, L. 2007. Impacts of climate change on water resources: A case-study for Portugal. Water in Celtic Countries: Quantity, Quality and Climate Variability, 310, 37-48.

de Castro, M., Martín-Vide, J., Alonso, S. 2005. El Clima de España: pasado, presente y escenarios de clima para el siglo XXI. En: Moreno, J.M. (Ed.). Evaluación Preliminar de los impactos en España por efecto del cambio climático. Ministerio de Medio Ambiente. pp. 1-64.

de Luis, M., González-Hidalgo, J.C., Longares, L.A., Stepanek, P. 2009. Seasonal precipitation trends in the Mediterranean Iberian Peninsula in second half of 20th century. International Journal of Climatology. 29 (9), 1312–1323.

de Luis, M., Brunetti, M., Carlos Gonzalez-Hidalgo, J., Alberto Longares, L., Martin-Vide, J. 2010. Changes in seasonal precipitation in the Iberian Peninsula during 1946-2005. Global and Planetary Change. 74(1), 27-33. http://dx.doi.org/10.1016/j.gloplacha.2010.06.006.

del Río, S., Herrero, L., Pinto-Comes, C., Penas, A. 2011. Spatial analysis of mean temperature trends in Spain over the period 1961–2006. Global and Planetary Change. 78 (1–2), 65–75. http://dx.doi.org/10.1016/j. gloplacha.2011.05.012.

Déqué, M., Somot, S., Sanchez-Gomez, E., Goodess, C. M., Jacob, D., Lenderink, G., Christensen, O.B. 2012. The spread amongst ENSEMBLES regional scenarios: Regional climate models, driving general circulation models and interannual variability. Climate Dynamics. 38, 951–964.

Devia, G.K., Ganasri, B.P., Dwarakish, G.S. 2015. A Review on Hydrological Models. Aquatic Procedia. 4, 1001-1007. http://dx.doi.org/10.1016/j.aqpro.2015.02.126.

Diaz-Nieto, J., Wilby, R.L. 2005. A comparison of statistical downscaling and climate change factor methods: Impacts on low flows in the river Thames, United Kingdom. Climatic Change. 69 (2), 245-268.

Duarte, C.M., Alonso, S., Benito, G., Montes, C., Pardo, M., Ríos, A.F., Simó, R., Valladares, F. 2006. Cambio global impacto de la actividad humana sobre el sistema Tierra. Consejo Superior de Investigaciones Cientificas.

Ducharne, A., Habets, F., Déqué, M., Evaux, L., Hachour, A., Lepaillier, A., Lepelletier, T., Martin, E., Oudin, L., Pagé, C., Ribstein, P., Sauquet, E., Thiéry, D., Terray, L., Viennot, P., Boé, J., Bourqui, M., Crespi, O., Gascoin, S., Rieu, J. 2009. Impact du changement climatique sur les Ressources en eau et les Extrêmes Hydrologiques dans les bassins de la Seine et la Somme. Rapport final du projet RExHySS, Programme GICC, 62. http://www.sisyphe.upmc.fr/~agnes/ rexhyss/.

Ducharne, A., Habets, F., Page, C., Sauquet, E., Viennot, P., Deque, M., Gascoin, S., Hachour, A., Martin, E., Oudin, L., Terray, L., Thiery, D. 2010. Climate change impacts on water resources and hydrological extremes in northern France. Proceedings of the XVIII International Conference on Computational Methods in Water Resources, 243-250.

Ducharne, A., Sauquet, E., Habets, F., Deque, M., Gascoin, S., Hachour, A., Martin, E., Oudin, L., Page, C., Terray, L., Thiery, D., Viennot, P. 2011. Evolution potentielle du régime des crues de la Seine sous changement climatique. La Houille Blanche. 1, 51–57. http://dx.doi.org/10.1051/lhb/2011006.

EEA (European Environment Agency). 2008. Impacts of Europe's changing climate – 2008 indicator based assessment. EEA Report No 4/2008 European Environment Agency, Copenhagen.

Edwards, P.N. 2010. History of climate modeling. Wires Climate Change, 2 (1), 128-139. http://dx.doi.org/10.1002/wcc.95.

Epelde, A.M. 2015. Modelización de procesos hidrológicos y de contaminación por nitratos mediante dos códigos numéricos (SWAT y MOHID). Cuenca agrícola del río Alegría (País Vasco). PhD Thesis, University of the Basque Country, Leioa.

Fabre, J., Ruelland, D., Dezetter, A., Grouillet, B. 2015. Accounting for hydro-climatic and water use variability in the assessment of past and future water balance at the basin scale. Hydrologic Non-Stationarity and Extrapolating Models to Predict the Future. 371, 43-48.

Fernández, P. 2002. Estudio del impacto del cambio climático sobre los recursos hídricos. Aplicación en 19 cuencas en España. Tesis doctoral. Madrid: Escuela Técnica Superior de Ingenieros de Caminos, Canales y Puertos de Madrid (ETSICCPM), Universidad Politécnica de Madrid (UPM).

Foley, J.A., DeFries, R., Asner, G.P., Barford, C., Bonan, G., Carpenter, S.R., Chapin, F.S., Coe, M.T., Daily, G.C., Gibbs, H.K., Helkowski, J.H., Holloway, T., Howard, E.A., Kucharik, C. J., Monfreda, C., Patz, J.A., Prentice, I.C., Ramankutty, N., Snyder, P.K. 2005. Global consequences of land use. Science. 309, 570–574.

Forzieri, G., Feyen, L., Rojas, R., Flörke, M., Wimmer, F., Bianchi, A. 2014. Ensemble projections of future streamflow droughts in Europe. Hydrology and Earth System Sciences. 18 (1), 85–108.

Fowler, H.J., Kilsby, C.G. 2007. Using regional climate model data to simulate historical and future river flows in northwest England. Climatic Change. 80 (3-4), 337-367. http://dx.doi.org/10.1007/s10584-006-9117-3.

Fowler, H.J., Blenkinsop, S., Tebaldi, C. 2007. Linking climate change modelling to impacts studies: recent advances in downscaling techniques for hydrological modelling. International Journal of Climatology, 27 (12), 1547–1578. http://dx.doi: 10.1002/joc.1556.

Gallart, F., Llorens, P. 2001. Water resources and environmental change in Spain. A key issue for sustainable catchment management. Cuadernos de investigación geográfica. 27, 7-16.

Gallego, M.C., Trigo, R.M., Vaquero, J.M., Brunet, M., Garcia, J.A., Sigro, J., Valente, M.A. 2011. Trends in frequency indices of daily precipitation over the Iberian Peninsula during the last century. Journal of Geophysical Research. 116 (D2), D02109. http://dx.doi.org/10.1029/2010JD014255.

García-Ruiz, J.M., Beguería, S., López Moreno, J.I., Lorente Grima, A., Seeger, M. 2001. Los recursos hídricos superficiales del Pirineo aragonés y su evolución reciente. Geoforma Ediciones. Logroño.

García-Ruiz, J. M., López-Moreno, J. I., Vicente-Serrano, S. M., Lasanta–Martínez, T., Beguería, S. 2011. Mediterranean water resources in a global change scenario. Earth-Science Reviews. 105 (3–4), 121-139. http://dx.doi.org/10.1016/j.earscirev.2011.01.006.

Garmendia, E., Mariel, P., Tamayo, I., Aizpuru, I., Zabaleta, A. 2012. Assessing the effect of alternative land uses in the provision of water resources: Evidence and policy implications from southern Europe. Land Use Policy. 29, 761-770.

Giannakopoulos, C., Le Sager, P., Bindi, M., Moriondo, M., Kostopoulou, E., Goodess, C.M. 2009. Climatic changes and associated impacts in the Mediterranean resulting from a 2 °C global warming. Global and Planetary Change. 68, 209–224. http://dx.doi.org/10.1016/j.gloplacha.2009.06.001.

Giuntoli, I., Renard, B., Vidal, J., Bard, A. 2013. Low flows in France and their relationship to large-scale climate indices. Journal of Hydrology. 482, 105-118.

Gosain, A.K., Mani, A., Dwivedi, C. 2009. Hydrological Modelling-Literature Review. Climawater, Report NO.1.

Gosling, S.N., Taylor, R.G., Arnell, N.W., Todd, M.C. 2011. A comparative analysis of projected impacts of climate change on river runoff from global and catchment-scale hydrological models. Hydrology and Earth System Sciences. 15, 279-294. http://dx.doi.org/10.5194/hess-15-279-2011.

Goubanova, K., Li, L. 2007. Extremes in temperature and precipitation around the Mediterranean basin in an ensemble of future climate scenario simulations. Global and Planetary Change. 57:27–42.

Grouillet, B., Fabre, J., Ruelland, D., Dezetter, A. 2015. Historical reconstruction and 2050 projections of water demand under anthropogenic and climate changes in two contrasted Mediterranean catchments. Journal of Hydrology. 522, 684-696.

Gudmundsson, L., Tallaksen, L.M., Stahl, K.., Clark, D.B., Dumont, E., Hagemann, S., Bertrand, N., Gerten, D., Heinke, J., Hanasaki, N., Voss, F., Koirala, S. 2012. Comparing large-scale hydrological model simulations to observed runoff percentiles in Europe.Journal of Hydrometeorology. 13, 604–620.

Habets, F., Boe, J., Deque, M., Ducharne, A., Gascoin, S., Hachour, A., Martin, E., Page, C., Sauquet, E., Terray, L., Thiery, D., Oudin, L., Viennot, P. 2013. Impact of climate change on the hydrogeology of two basins in northern France. Climatic Change. 121(4), 771-785. http://dx.doi.org/10.1007/s10584-013-0934-x.

Hapuarachchi, H.A.P., Zhijia, L., Flugel, A.W. 2003. Application of models with different types of modelling methodologies for river flow forecasting. Proceedings of the Symposium on Weather Radar Information and Distributed Hydrological Modeling, July 2003, IAHS, Sapporo.

Haylock, M.R., Cawley, G.C., Harpham, C., Wilby, R.L., Goodess, C.M. 2006. Downscaling heavy precipitation over the United Kingdom: A comparison of dynamical and statistical methods and their future scenarios. International Journal of Climatology. 26 (10), 1397-1415. http://dx.doi.org/10.1002/joc.1318.

Hewitt, C.D., Griggs, D.J. 2004. Ensembles-based Predictions of Climate Changes and their Impacts. Eos. 85: 566.

Ho, J. T., Thompson, J. R., Brierley, C. 2015. Projections of hydrology in the Tocantins Araguaia basin, Brazil: Uncertainty assessment using the CMIP5 ensemble. Hydrological Sciences Journal. 1-17. http://dx.doiorg/10.1080/02626667.2015.1057513.

Hostetler, S.W. 1994. Hydrologic and atmospheric models. The (continuing) problem of discordant scales. An editorial comment. Climatic Change. 27 (4), 345–350.

Iglesias, A., Estrela, T., Gallart, F. 2005. Impactos sobre los recursos hídricos. En: J.M. Moreno (coord.). Evaluación preliminar de los impactos en España por efecto de cambio climático. Ministerio de Medio Ambiente, Madrid. España. pp. 303-353.

Ilstedt, U., Malmer, A., Verbeeten, E., Murdiyarso, D. 2007. The effect of afforestation on water infiltration in the tropics: a systematic review and meta-analysis. Forest Ecology and Management. 251 (1–2): 45–51. http://dx.doi.org/101016/jforeco200706014.

IPCC, 1990. Report prepared for Intergovernmental Panel on Climate Change by Working Group I [(Houghton, J.T., Jenkins, G.J., Ephraums, J.J (eds.)]. Cambridge University Press, Cambridge, Great Britain, New York, NY, USA and Melbourne, Australia, 410 pp.

IPCC, 1996. Climate Change 1996: Contribution of Working Group II to the Second Assessment Report of the Intergovernmental Panel on Climate Change [Watson, R.T., Zinyowera, M.C., Moss, R.H., Dokken, D.J. (ed.s)]. Cambridge University Press, Cambridge, Great Britain, New York, NY, USA, 891pp.

IPCC SRES, 2000. Special Report on Emissions Scenarios [Nebojsa, Nakicenovic, Swart (eds.)]. Cambridge University Press, UK. pp 570.

IPCC, 2001: Climate Change 2001: Synthesis Report. A Contribution of Working Groups I, II, and III to the Third Assessment Report of the Intergovernmental Panel on Climate Change [Watson, R.T. and the Core Writing Team (eds.)]. Cambridge University Press, Cambridge, United Kingdom, and New York, NY, USA, 398 pp.

IPCC, 2007 Climate Change 2007. Contribution of Working Groups I, II and III to the Fourth Assessment Report of the Intergovernmental Panel on Climate Change. [(Pachauri, R.K. and Reisinger, A. (eds.)]. IPCC, Geneva, Switzerland. pp 104

IPCC, 2013: Climate Change 2013: The Physical Science Basis. Contribution of Working Group I to the Fifth Assessment Report of the Intergovernmental Panel on Climate Change [Stocker, T.F., D. Qin, G.-K. Plattner, M. Tignor, S.K. Allen, J. Boschung, A. Nauels, Y. Xia, V. Bex and P.M. Midgley (eds.)]. Cambridge University Press, Cambridge, United Kingdom and New York, NY, USA, 1535 pp, doi:10.1017/CBO9781107415324.

IPCC, 2014: Climate Change 2014: Synthesis Report. Contribution of Working Groups I, II and III to the Fifth Assessment Report of the Intergovernmental Panel on Climate Change [Core Writing Team, R.K. Pachauri and L.A. Meyer (eds.)]. IPCC, Geneva, Switzerland, 151 pp.

Jacobeit, J. 2000. Rezente Klimaentwicklung im Mittelmeerraum. Petermanns Geographische Mitteilungen. 144, 22–33.

Jajarmizadeh, M., Harun, S., Salarpour, M. 2012. A review on theoretical consideration and types of models in hydrology. Journal of Environmental Sciences Technology, 5 (5): 249-261.

Jothityangkoon, C., Sivapalan, M., Farmer, D.L. 2001. Process controls of water balance variability in a large semi-arid catchment: downward approach to hydrological model development. Journal of Hydrology. 254,174–198. http://dx.doiorg/10.1016/S0022-1694(01)00496-6.

Katz, R.W., Parlange, M. B., Naveau, P. 2002. Statistics of extremes in hydrology, Adv. Water Resources. 25, 1287–1304.

Khon, V.C., Mokhov, I.I., Roeckner, E., Semenov, V.A. 2007 Regional changes of precipitation characteristics in north northern Eurasia from simulations with global climate model. Global and Planetary Change. 57, 118–123.

Kiely, G. 1999. Climate change in Ireland from precipitation and streamflow observation. Advances in Water Resources. 23, 141–151.

Kovats, S., Valentini, R. 2014. IPCC WGII AR5 – Chapter 23 Europe. 1–93 IPCC Intergovernmental Panel on Climate Change.

Leavesley, G.H. 1994. Modeling the effects of climate change on water resources – a review. Climatic Change. 28, 159–177.

Lehner, B., Döll, P., Alcamo, J., Henrichs, T., Kaspar, F. 2006. Estimating the impact of global change on flood and drought risks in Europe: a continental, integrated analysis. Climtic Change. 75 (3), 273–299.

Lespinas, F., Ludwig, W., Heussner, S. 2014. Hydrological and climatic uncertainties associated with modeling the impact of climate change on water resources of small Mediterranean coastal Rivers. Journal of Hydrology. 511, 403 – 422. http://dx.doi.org/10.1016/j.jhydrol.2014.01.033.

Littlwood, I.G., Jakeman, A.J. 1994. A new method of Rainfall-Runoff modeling and its application in catchment hydrology. In: Contemporary Hydrology, Wilby, R. (Ed.). John Wiley and Sons, England, Pp: 155-157.

Lopez-Bustins, J.-A., Martin-Vide, J., Sanchez-Lorenzo, A. 2008. Iberia winter rainfall trends based upon changes in teleconnection and circulation patterns. Global and Planetary Change. 63, 171–176.

López-Moreno, J.I., Beniston, M., García-Ruiz, J.M. 2008. Environmental change and water management in the Pyrenees facts and future perspectives for Mediterranean mountains. Global and Planetary. Change. 61, 300–312.

López-Moreno, J.I., Vicente-Serrano, S.M., Beguería, S., El Kenawy, A.M., Angulo, M. 2010. Trends in daily precipitation on the north-eastern Iberian Peninsula 1955– 2006. International Journal of Climatology 120, 248–257.

Lorenzo-Lacruz, J., Vicente-Serrano, S.M., Lopez-Moreno, J.I., Moran-Tejeda, E., Zabalza, J. 2012. Recent trends in Iberian streamflows (1945–2005). Journal of Hydrology. 414–415, 463–475. http://dx.doi.org/10.1016/j.jhydrol.2011.11.023.

Ludwig, R., May, I., Turcotte, R., Vescovi, L., Braun, M., Cyr, J.F., Fortin, L.G., Chaumont, D., Biner, S., Chartier, I., Caya, D., Mauser, W. 2009. The role of hydrological model complexity and uncertainty in climate change impact assessment. Advances in Geosciences. 21, 63–71. http://dx.doi.org/10.5194/adgeo-21-63-2009.

Machín, J., Navas, A., Domenche, S., López-Vicente, M. 2005. El río Arlanza en cabecera evolución reciente y tendencias en condiciones de cambio global. Cuadernos de Investigación Geográfica. 31, 77–95.

Mann, M., Bradley, R., Hughes, M. 1998. Global scale temperature patterns and climate forcing over the past six centuries. Nature. 392, 779–787.

Martínez-Fernández, J., Sánchez, N., Herrero-Jiménez, C.M. 2013. Recent trends in rivers with near-natural flow regime: the case of the river headwaters in Spain. Progress in Physical Geography. 37 (5), 685–700. http://dx.doi.org/10.1177/0309133313496834.

Mediero, L., Kjeldsen, T.R., Macdonald, N., Kohnova, S., Merz, B., Vorogushyn, S., Wilson, D., Alburquerque, T., Bloeschl, G., Bogdanowicz, E., Castellarin, A., Hall, J., Kobold, M., Kriauciuniene, J., Lang, M., Madsen, H., Gul, G.O., Perdigao, R.A.P., Roald, L.A., Salinas, J.L., Toumazis, A.D., Veijalainen, N., Porarinsson, O. 2015. Identification of coherent flood regions across Europe by using the longest streamflow records. Journal of Hydrology. 528, 341-360. http://.dx.doi.org/10.1016/j.jhydrol.2015.06.016.

Meehl, G.A., Covey, C., Delworth, T., Latif, M., McAvaney, B., Mitchell, J.F.B., Stouffer, R.J., Taylor, K.E. 2007. The WCRP CMIP3 multimodel dataset - A new era in climate change research. Bulletin of the American Meteorological Society. 88(9), 1383. http://dx.doi.org/10.1175/BAMS-88-9-1383.

Meinshausen, M., Smith, S.J., Calvin, K., Daniel, J.S., Kainuma, M.L.T., Lamarque, J.-., Matsumoto, K., Montzka, S.A., Raper, S.C.B., Riahi, K., Thomson, A., Velders, G.J.M., van Vuuren, D.P.P. 2011 The RCP greenhouse gas concentrations and their extensions from 1765 to 2300. Climatic Change. 109 (1-2), 213-241. http://dx.doi.org/10.1007/s10584-011-0156-z.

Milly, P C.D., Dunne, K.A., Vecchia, A.V. 2005 Global pattern of trends in streamflow and water availability in a changing climate. Nature. 438 (7 066), 347–350. http://dx.doi.org/10.1038/nature04312.

Mimikou, M.A., Baltas, E., Varanou, E., Pantazis, K. 2000. Regional impacts of climate change on water resources quantity and quality indicators. Journal of Hydrology. 234, 95–109.

MMA, 2000. Libro blanco del agua en España. Ministerio de Medio Ambiente.

Mokhov, E.R., Semenov, V.A., Khon, V.C. 2005 Extreme precipitation regimes in Northern Eurasia in the 20th century and their possible changes in the 21st century. Doklady Earth Sciences. 403,767–770.

Moncho, R., Chust, G., Caselles, V. 2009 Análisis de la precipitación del País Vasco en el período 1961–2000 mediante reconstrucción espacial. Nimbus. 23-24, 149–170.

MOPTMA, 1995. Programa Nacional del Clima. Ministerio de Obras Públicas, Transporte y Medio Ambiente.

Moradkhani, H., Sorooshian, S. 2008. General review of rainfall-runoff modeling: model calibration, data assimilation, and uncertainty analysis. Hydrological modeling and the water cycle. Springer. 291 p. ISBN 978-3-540-77842-4.

Morán-Tejeda, E., Ceballos-Barbancho, A., Llorente-Pinto, J. M. 2010. Hydrological response of Mediterranean headwaters to climate oscillations and land-cover changes: The mountains of Duero river basin (central Spain). Global and Planetary Change. 72 (1–2), 39-49. http://dx.doi.org/10.1016/j.gloplacha.2010.03.003.

Morán-Tejeda, E., Ignacio Lopez-Moreno, J., Ceballos-Barbancho, A., Vicente-Serrano, S.M. 2011. River regimes and recent hydrological changes in the Duero basin (Spain). Journal of Hydrology. 404, 241-258. http://dx.doi.org/10.1016/j. jhydrol.2011.04.034.

Morán-Tejeda, E., Ignacio Lopez-Moreno, J., Vicente-Serrano, S.M., Lorenzo-Lacruz, J., Ceballos-Barbancho, A. 2012. The contrasted evolution of high and low flows and precipitation indices in the Duero basin (Spain). Hydrological Sciences Journal-Journal Des Sciences Hydrologiques. 57, 591-611. http://dx.doi.org/10.1080/02626667.2012.673722.

Morán-Tejeda, E., Zabalza, J., Rahman, K., Gago-Silva, A., López-Moreno, J. I., Vicente-Serrano, S., Lehmann, A., Tague, C.L., Beniston, M. 2015. Hydrological impacts of climate and land-use changes in a mountain watershed: Uncertainty estimation based on model comparison. Ecohydrology. 8 (8), 1396-1416. http://dx.doi.org/10.1002/eco.1590.

Moriondo, M., Good, P., Durao, R., Bindi, M., Giannakopoulos, C., Corte-Real, J. 2006. Potential impact of climate change on fire risk in the Mediterranean area. Climate Research. 31, 85–95.

Mosmann, V., Castro, A., Fraile, R., Dessens, J., Sánchez, J.L. 2004 Detection of statistically significant trends in the summer precipitation of mainland Spain. Atmospheric Research. 70, 43–53.

Nijssen, B., O'donnell, G.M., Hamlet, A.F., Lettenmaier, D.P. 2001. Hydrologic sensitivity of global rivers to climate change. Climatic Change. 50, 143–175.

Noorbakhsh, M.E., Rahnama, M.B., Montazeri, S. 2005. Estimation of instantaneous unit hydrograph with Clarks method using GIS techniques. Journal of Applied Sciences. 5: 455-458.

Nunes, A. 2007. Recursos hídricos na Bacia do Rio Côa: relaçoes com a variabilidade climática e mundanças no uso de solo. In: En Ifestas, A., Cunha, L., da Cruz Coelho, M.E., Jacinto, R. (Eds.), Territorios e Culturas Ibéricas II. Centro de Estudios Ibéricos, Guarda, pp. 71–86.

Nunes, J.P., Seixas, J., Pacheco, N.R. 2008. Vulnerability of water resources, vegetation productivity and soil erosion to climate change in Mediterranean watersheds. Hydrological Processes. 22 (16), 3115-3134. http://dx.doi.org/10.1002/hyp.6897.

O'Gorman, P.A., Schneider, T. 2009 The physical basis for increases in precipitation extremes in simulations of 21st century climate change. Proceedings of the National Academy of Sciences of the United States of America. 106,14773–14777.

Pascual, D., Pla, E., Lopez-Bustins, J. A., Retana, J., Terradas, J. 2015. Impacts of climate change on water resources in the Mediterranean basin: A case study in Catalonia, Spain. Hydrological Sciences Journal-Journal Des Sciences Hydrologiques. 60 (12), 2132-2147. http://dx.doi.org/10.1080/02626667.2014.947290.

Pérez Martín, M.A. 2005. Modelo distribuido de simulación del ciclo hidrológico y de la calidad del agua, integrado en sistemas de información geográfica, para las grandes cuencas. Aportación al análisis de presiones e impactos de la Directiva Marco del Agua. Tesis Doctoral. Universitat Politècnica de València.

Prieto, C. 1996. La evolución de los recursos hídricos en España. 2ª Conferencia Internacional de Hidrología Mediterránea. Los recursos hídricos en los países Mediterráneos. Iberdrola. Instituto Tecnológico. Bilbao.

Pérez, F., Boscolo, R. 2010. Clima en España: pasado, presente y futuro. Red Telemática CLIVAR-España.

Petisco, S.E., Martín, J.M. 2006. Escenarios de temperatura y precipitación para la España peninsular y Baleares durante el período 2001-2100 basados en "downscaling" estadístico mediante métodos de análogos. XXIX Jornadas Científicas de la Asociación Meteorológica Española. Pamplona.

Prudhomme, C., Young, A., Watts, G., Haxton, T., Crooks, S., Williamson, J., Davies, H., Dadson, S., Allen, S. 2012. The drying up of Britain? A national estimate of changes in seasonal river flows from 11 regional climate model simulations. Hydrological Processes. 26 (7), 1115-1118. http://dx.doi.org/10.1002/hyp.8434.

Rahmana, M.B, Noury, M. 2008. Developing of Halil river rainfall-runoff model, using conjunction of wavelet transform and artificial neutral networks. Research Journal of Environmental Sciences. 2: 385-392.

Rasilla, D.F., Garmendia, C., Garcia-Codron, C.J. 2013. Climate change projections of streamflow in the Iberian Peninsula. International Journal of Water Resources Development. 29 (2), 184-200. http:/dx.doi.org/10.1080/07900627.2012.721716.

Ribalaygua, J., Pino, M.R., Pórtoles, J., Roldán, E., Gaitán, E., Chinarro, D., Torres, L. 2013. Climate change scenarios for temperature and precipitation in Aragón (Spain). Science of the Total Environment. 463–464 (0), 1015-1030. http://dx.doi.org/10.1016/j.scitotenv.2013.06.089.

Rodrigo, F.S., Trigo, R.M. 2007. Trends in daily rainfall in the Iberian Peninsula from 1951 to 2002. International Journal of Climatology. 27, 513–529.

Rojas, R., Feyen, L., Bianchi, A., Dosio, A. 2012. Assessment of future flood hazard in Europe using a large ensemble of bias-corrected regional climate simulations. Journal of Geophysical Research-Atmospheres. 117, D17109. http://dx.doi.org/10.1029/2012JD017461.

Ruelland, D., Hublart, P., Tramblay, Y. 2015. Assessing uncertainties in climate change impacts on runoff in Western Mediterranean basins. Hydrologic Non-Stationarity and Extrapolating Models to Predict the Future. 371, 75-81.

Sáenz, J., Zubillaga, J., Rodríguez-Puebla, C. 2001. Interannual winter temperature variability in the north of the Iberian Peninsula. Climatic Research. 16, 169–179

Sarris, D., Christodoulakis, D., Körner, C. 2007. Recent decline in precipitation and tree growth in the eastern Mediterranean. Global Change Biology. 13, 1187–1200. http://dx.doi.org/10.1111/j.1365-2486.2007.01348.x.

Shaw, E.M. 1983. Hydrology in practice. Chapman and Hall, London, UK. Pages: 569.

Serra-Diaz, J.M., Ninyerola, M., Lloret, F. 2012. Coexistence of Abies alba (Mill.) – Fagus sylvatica (L.) and climate change impact in the Iberian Peninsula: a climatic-niche perspective approach. Flora – Morphology, Distribution, Functional Ecology of Plants. 207 (1), 10–18. http://dx.doi.org/10.1016/j. flora.2011.10.002.

Serrano, A., Mateos, V.L., García, J.A. 1999 Trend analysis of monthly precipitation over the Iberian Peninsula for the period 1921–1995. Physics and Chemistry of the Earth Part b-Hydrology Oceans and Atmosphere. 24, 85–90.

Shorthouse, C., Arnell, N. 1999. The effects of climate variability on spatial characteristics of European river flows. Physics and Chemistry of the Earth. 24 (1–2), 7–13.

Singh, V.P., Frevert, D.K. 2005. Watershed models. Boca Raton, FL: CRC Press. Taylor and Francis, 245-272.

Solman, S., Nunez, M. 1999. Local estimates of global climate change: a statistical downscaling approach. International Journal of Climatology. 19, 835–861.

Stahl, K., Hisdal, H., Hannaford, J., Tallaksen, L.M., van Lanen, H.A.J., Sauquet, E., Demuth, S., Fendekova, M., Jodar, J. 2010. Streamflow trends in Europe: evidence from a dataset of near-natural catchments. Hydrology and Earth System Sciences. 14 (12), 2367–2382. http://dx.doi.org/10.5194/ hess-14-2367-2010.

Stahl, K., Tallaksen, L. M., Gudmundsson, L., Christensen, J. H. 2011. Streamflow data from small basins: a challenging test to high resolution regional climate modeling. Journal of Hydrometeorology. 12, 900–912.

Steele-Dunne, S., Lynch, P., McGrath, R., Semmler, T., Wang, S., Hanafin, J., Nolan, P. 2008. The impacts of climate change on hydrology in Ireland. Journal of Hydrology. 356 (1-2), 28-45. http://dx.doi.org/10.1016/j.jhydrol.2008.03.025.

Svensson, C., Kundzewicz, W.Z., Maurer, T. 2005. Trend detection in river flow series: 2. Flood and low flow index series. Hydrological Sciences Journal. 50 (5), 37– 41. http://dx.doi.org/10.1623/hysj.2005.50.5.811.

Szêpszô, G., Lingemann, I., Klein, B., Kovacs, M. 2014. Impact of climate change on hydrological conditions of Rhine and upper Danube rivers based on the results of regional climate and hydrological models. Natural Hazards. 72 (1), 241-262. Http://dx.doi.org/10.1007/s11069-013-0987-1.

Tavakoli, M., De Smedt, F., Vansteenkiste, T., Willems, P. 2014. Impact of climate change and urban development on extreme flows in the Grote Nete watershed, Belgium. Natural Hazards. 71(3), 2127-2142. http://dx.doi.org//10.1007/s11069-013-1001-7.

Taylor, K.E., Stouffer, R.J., Meehl, G.A. 2011 An overview of CMIP5 and the experiment design. Bulletin American Meteorological Society. 93, 485-498.

Teng, J., Vaze, J., Chiew, F.H.S., Wang, B., Perraud, J.M. 2012. Estimating the relative uncertainties sourced from GCMs and hydrological models in modeling climate change impact on runoff. Journal of Hydrometeorology. 13 (1), 122–139. http://dx.doi.org/10.1175/JHM-D-11-058.1.

Trenberth, K.E., Dai, A., Rasmussen, R.M., Parsons, D.B. 2003 The changing character of precipitation. Bulleting of American Meteorological Society. 84, 1205–1217

Trigo, R.M., Valente, M.A., Trigo, I.F., Miranda, P.M.A., Ramos, A.M., Paredes, D., García-Herrera, R. 2008 The impact of North Atlantic wind and cyclone trends on European precipitation and significant wave height in the Atlantic. Trends and Directions in Climate Research. 1146, 212-234.

UNESCO 2011. The impact of Global Change on Water Resources: The response of UNESCO´s International Hydrological Program. UNESCO, Division Water Sciences. Paris. France.

URA (Agencia Vasca del Agua), 2015. Plan hidrológico parte española de la demarcación del cantábrico oriental revisión 2015-2021. http://www.uragentzia.euskadi.eus/informacion/plan-hidrologico-de-la-demarcacion-hidrografica-del-cantabrico-oriental-2015-2021/u81-0003333/es/. Accessed 4 April 2017.

Valverde, P., Serralheiro, R., de Carvalho, M., Maia, R., Oliveira, B., Ramos, V. 2015. Climate change impacts on irrigated agriculture in the Guadiana river basin (Portugal). Agricultural Water Management. 152 (0), 17-30. http://dx.doi.org/10.1016/j.agwat.2014.12.012.

Vaze, J., Teng, J. 2011. Future climate and runoff projections across New South Wales, Australia: results and practical applications. Hydrological Processes. 25 (1), 18– 35. http://dx.doi.org/10.1002/hyp. 7812.

Vicente-Serrano, S.M., Gouveia, C., Julio Camarero, J., Begueria, S., Trigo, R., Lopez-Moreno, J.I., Azorin-Molina, C., Pasho, E., Lorenzo-Lacruz, J., Revuelto, J., Moran-Tejeda, E., Sanchez-Lorenzo, A. 2013. The response of vegetation to drought time-scales across global land biomes. Proceedings of the National Academy of Sciences of the United States of America. 110 (1), 52–57. http://dx.doi.org/10.1073/pnas.1207068110.

Wagener, T., Wheater, H.S., Gupta, H.V. 2004. Rainfall-Runoff modeling in gauged and ungauged catchments. Imperial College Press, London, UK.

Wilby, R.L., Dawson, C.W., Barrow, E.M. 2002. SDSM-A decision support tool for the assessment of regional climate change impacts. Environmental Modeling & Software. 17, 145-157. http://dx.doi.org/10.1016/S1364-8152(01)00060-3.

Wilby, R.L., Charles, S.P., Zorita, E., Timbal, B., Whetton, P., Mearns, L.O. 2004. Guidelines for use of climate scenarios developed from statistical downscaling methods. Data Distribution Center of the Intergovernmental Panel on Climate Change. (Available at http://ipcc-ddc.cru.uea.ac.uk).

Wilby, R.L., Harris, I. 2006. A framework for assessing uncertainties in climate change impacts: low-flow scenarios for the River Thames, UK. Water Resources Research. 42 (2), W02419. http://dx.doi.org/10.1029/2005WR004065.

Wilby, R.L., Dessai, S. 2010. Robust adaptation to climate change. Weather. 65, 180–185, 2010.

Willems, P. 2000. Probabilistic modeling of the emission receiving surface waters. PhD Thesis, Faculty of Engineering, Katholieke Universiteit, Leuven, Belgium.

Wilson, D., Hisdal, H., Lawrence, D. 2010 Has streamflow changed in the Nordic countries? — Recent trends and comparisons to hydrological projections. Journal of Hydrology. 394 (3–4), 334–346. http://dx.doi.org/10.1016/j.jhydrol.2010.09.010.

Xu, C.Y. 1999. From GCMs to river flow: a review of downscaling methods and hydrologic modeling approaches. Progress in Physical Geography. 23 (2), 229–249.

Xu, C.Y., Halldin, S. 1997. The effect of climate change on river flow and snow cover in the NOPEX area simulated by a single water balance model. Nordic Hydrology. 28, 273–282.

Yue, S., Kundzewicz, Z.W. Linghui, W. 2012. Changes in flood risk in Europe. Special Publication. No. 10. Wallingford, UK: IAHS Press.

Zabaleta, A., Morales, T., Meaurio, M., Gorria, C., Antiguedad, I. 2012. Regional hydrological signs for climate change in Southern Europe (Basque Country). International Conference on Water, Climate and Environment. ISBN 978-608-4510-10-9.

Zabaleta, A., Antiguedad, I. 2012. Klimaren seinale hidrologikoak EAE-ko arroetako uremarien joeretan. Gerora begirako proiekzio hidrologikoak. EKAIA Euskal Herriko Unibertsitateko Zientzi eta Teknologi Aldizkaria, 25, 33-59. http://www.ehu.es/ojs/index.php/ekaia/article/view/5257/6366.

Zhang, Y.X., Sun, S., Olsen, S.C., Dubey, M.K., He, J. 2011. CCSM3 simulated regional effects of anthropogenic aerosols for two contrasting scenarios: Rising Asian emissions and global reduction of aerosols. International Journal of Climatology. 31, 95-114. http://dx.doi.org/10.1002/joc.2060.

2.

METHODOLOGY

2. METHODOLOGY

2.1 GENERAL CONTEXT OF THE STUDY AREA

The Basque Country is located between 43º 27' 50'' and between 42º 28' 45'' latitude and 3º 23' and 1º 43' W longitude. Its most important geographical limits are the Cantabrian Sea in the north (south of the Bay of Biscay) and the Ebro depression in the south (Fig. 2.1). Geologically, it is in the zone of the folds and overthrusts of the Pyrenees, more specifically in its western sector, in the Basque-Cantabrian Watershed. Mostly, it is composed of carbonate rocks (more than 70%) with more or less content in clays (Bodego et al., 2014).

An orographic characteristic of the Basque Country are its mountain ranges (betwen1550 1300 m above sea level) that have less altitude than the two

important north-Iberian mountain ranges (Pyrenees and the Asturian Massif). In general, the Basque mountain ranges have Cretaceous age materials and they generate abrupt relief and low developed soils. Their preferential orientation is NW-SE and the altitude increases from the coast to the inland. The mountains located in the north of Vitoria-Gasteiz, with more than 1000 m altitude, divide the Atlantic and Mediterranean Watersheds (Fig. 2.1). The Basque mountains determine the passage of Atlantic air masses with direction NW. The altitude of the mountains forces the air masses to ascend condensing them so that precipitation occurs. Thus, the Basque coast is the rainiest of the Cantabrian Watershed, but in leeward areas the precipitation is scarce.

The **Atlantic Watershed** is characterized by important slopes in short distances, high precipitation (see next paragraph) and hydric erosion. Hence, the rivers travel short distances in very hilly terrains. The main drainage network cuts the relief in the S-N direction, consequently the rivers are almost perpendicular to the main geological structures and the secondary fluvial network is parallel to these structures.

The climate is temperate and humid, without dry season. Due to the influence of the Atlantic Ocean that warms up the air masses, the thermic oscillation between winter and summer (mean annual value around 12 ° C), and night and day is not too high (around 10 ° C). Accordingly, the mean annual temperature is mild (around 14 °C) and the mean annual precipitation in this region is between 1200 and 2000 mm (www.euskalmet.euskadi.eus).

In the Atlantic Watershed, the forest is widespread, being the *Pinus radiata* and *Eucalyptus globulus* (in lesser proportion) plantations the most common land use. The native forests are relegated to the mountains where there are different types of oaks, scrublands and Cantabrian holm oak (Loidi et al., 2011). The Atlantic Watershed is the zone of the Basque Country with largest urban agglomerations, industrial concentration and infrastructures.

In the **Mediterranean Watershed**, the relief becomes more gentle. The altitude difference between the mountains and the base of the catchments is lower than in the Atlantic Watershed because the base level of the rivers is at

higher altitude (around 600 m). The Araba plain constitutes a great central plateau, which is crossed by the Zadorra river (Fig. 2.1) and is flanked by mountain ranges (with E-W direction) that separates it from the Ebro depression.

Climatologically, the largest part of the Basque Mediterranean Watershed is located in the transition zone between the Oceanic (Atlantic) and Mediterranean climates where the Atlantic characteristics are predominant because there is not a real dry season. Further to the south, in the Ebro depression zone the summers are dry and the winters are dry and cold, therefore the climate is typically Mediterranean. Thus, in some months of summer the mean temperatures can exceed the 22 °C and in winter the low temperatures are low enough so that frost and fog occur (www.euskalmet.euskadi.eus).

In the Mediterranean Watershed, the stockbreeding and mainly the agriculture are important land uses. Cultivation of cereals, potatoes, sugarbeets, sunflowers or rapeseed, in valleys and plains suitable for tillage is usual. In hilly zones the main land use is forestry (Loidi et al., 2011). Comparing with the Atlantic Watershed the Ebro catchment is less populated and the most part of the population lives near the city of Vitoria-Gasteiz.

In this context, to carry out this research four mountain headwater catchments representative of different contexts in the Basque Country have been chosen. All of them are part of bigger Hydrological Units (HU): Aixola (4.8 km^2) of Deba HU, Goi-Nerbioi (185 km^2) of Ibaizabal HU and Otxandio (36 km^2) and Audikana (82 km^2) of Zadorra HU. Thus, Deba and Ibaizabal Hydrological Units flow into the Cantabrian Sea (Atlantic Watershed) and the Zadorra drains into the Ebro river (Mediterranean Watershed) (Fig. 2.1).

From the climatic point of view, there are notable differences, especially in precipitation, between the study catchments. Aixola and Otxandio, although they are located in different Watersheds (Atlantic and Mediterranean respectively), both have an Oceanic (Atlantic) climate, namely humid and temperate. The mean annual precipitation is around 1400-1500 mm, distributed fairly evenly throughout the year. Goi-Nerbioi is in the beginning of the Transition Zone of the Atlantic and Mediterranean climate, although the Atlantic

characteristics are predominant (Sub-Atlantic climate). In this catchment, the mean annual precipitation is around 1000 mm. Finally, Audikana catchment is also located in the Transition Zone, nevertheless in this zone the Mediterranean climate characteristics are prevalent (Sub-Mediterranean climate). The mean annual precipitation is between 500 and 600 mm and summers can be dry. The mean annual temperature in Aixola, Goi-Nerbioi and Audikana is 12 °C, while in Otxandio, where the elevation is higher than in the other catchments, the mean temperature is a little bit lower (10 °C). The study catchments are located in the European *Atlantic Region* (Fig. 2.1) which geographical and climatic characteristics are defined in the section *1.1.5 El País Vasco en el contexto general del cambio climático.*

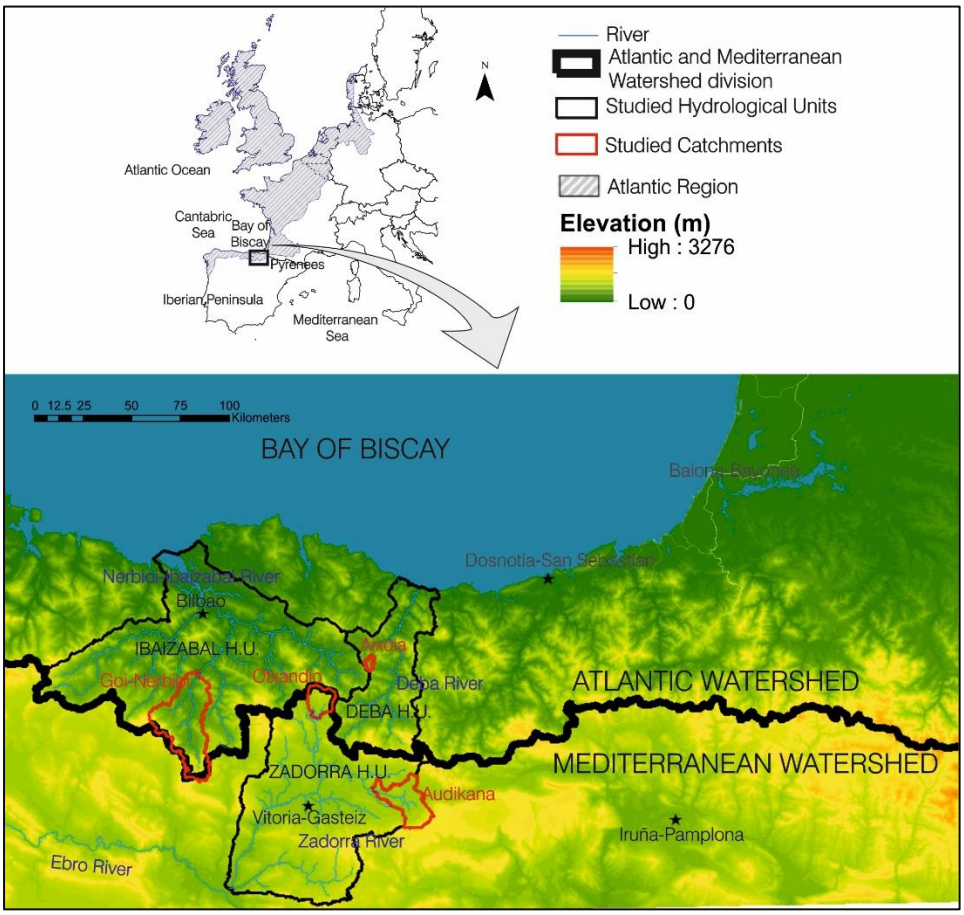

Figure 2.1. *Location of the study area in the Atlantic Region, Goi-Nerbioi, Aixola, Otxandio and Audikana catchments, the Hydrological Unit (H.U) in which they are located and the drainage area (Atlantic or Mediterranean Watershed).*

Regarding the physical characteristics, Otxandio and Aixola have the steeper slopes, in both catchments more than 50 % of the area have slopes bigger than 25 %. This feature has influence in the land use, in both cases the major land use is the forest, although in Aixola predominates exotic plantations while in Otxandio native forest. Audikana is relatively flat and in more than the 70 % of the area there are wheat plantations. In Goi-Nerbioi catchment the mean slope is of 17 % and in the flat areas there are pasturelands while in steeper slope areas the main land use is forest.

It is also important to mention that three of the studied catchments (Aixola, Otxandio and Audikana) drain to reservoirs used for water supply. Therefore, the climate change impact analysis of the hydrology of these catchments have an additional relevance.

In the sections related to the research of each catchment their characteristics are explained more in depth.

2.2 CLIMATE CHANGE PROJECTIONS

Over recent years different global and regional projects have been carried out to develop new generations of General Circulation Models (GCMs) or regionalize their climate outputs. At global level, the **Coupled Model Intercomparison Project (CMIP)** studies the outputs of GCMs. It was created in 1995 under the World Climate Research Programme (WCRP) and the entire international climate modelling community participates in the project. The CMIP provides climate models diagnosis, validation, intercomparison, documentation and data access. The research based on the phase three of CMIP (CMIP3) was included in the Fourth Assessment Report (AR4) of the Intergovernmental Panel on Climate Change (IPCC). Since 2008 the new set of coordinated climate model experiments **CMIP5** is promoted. According to the CMIP (http://cmip-pcmdi.llnl.gov/).

CMIP5 will notably provide a multi-model context for 1) assessing the mechanisms responsible for model differences in poorly understood feedbacks associated

with the carbon cycle and with clouds, 2) examining climate "predictability" and exploring the ability of models to predict climate on decadal time scales, and, more generally, 3) determining why similarly forced models produce a range of responses.

The results of the GCMs developed in the CMIP5 are those that have been used in the Fifth Assessment Report (AR5) of the IPCC.

At a European level, the European Commission under the 5th Framework Programme Priority financed from 2001 to 2004 the PRUDENCE project. This project was the first one that provided a series of high-resolution climate change scenarios for 2071-2100 for Europe. The 6th Framework (from 2004 to 2009) launched the **ENSEMBLES project** (http://ensembles-eu.metoffice.com/docs/Ensembles_final_report_Nov09.pdf) The objective of the project was to generate climate forecast for Europe, with the latest climate models available (AR3 and AR4). Thus, it was possible to obtain an objective probabilistic estimation of the uncertainties of the climate projections in Europe and therefore calculate more realistic future **regionalised** climate projections for this region.

To study the possible effects of climate change in the hydrology of catchments of the Basque Country the selected climate projections were those provided by the Spanish Meteorological Agency (AEMET). To deal with the problem of spatial resolution of climate models, AEMET has statistically downscaled the outputs of the Regional Circulation Models (RCMs) (PRUDENCE and ENSEMBLES) and GCMs (CMIP5). It is important to mention that AEMET projections do not cover the whole range of emission scenarios and downscaling methods, even though the meteorological agency has chosen and developed the more representative and suitable scenarios and downscaling techniques for making predictions over the Iberian Peninsula (Chirivella et al., 2015).

The climate projections released by AEMET are composed of daily precipitation and maximum and minimum temperature for specific weather stations. All the climate projections for the XXI century have a baseline period (1961-2000). The climate projections are determined by the GCM or RCM from different projects, the statistical downscaling method and the emission scenario

or the Regional Concentration Pathway (RCP). A short summary of the selection bases in this Thesis is included below:

- The project: in this research, the climate projections from PRUDENCE and ENSEMBLES projects and CMIP5 have been used. Thus, projections regionalized for Europe and the last version of GCMs are used.

- The Climate Model: in function of the project, the selection of the GCMs was based in different foundations that are explained more in detail in the following sections.

- The Statistical Downscaling method: AEMET has applied two downscaling methods: AEMET analogues (AN) and Statistical Downscaling Method (SDSM). According to Wigley (2004), *statistical downscaling methods are based on quantitative relationships between atmospheric variables (predictors) and local surface variables (predictands).*

- Analogues method (Schmidli et al., 2007): this method uses a two-step analogue technique, based on a search for analogues at geopotential heights of 500 and 1000 hPa. In the first step, a set of days with similar atmospheric configuration to the one simulated for the future with a GCM were identified. This set of days (analogues) were selected from a database obtained from the pre-analysis (Uppala et al., 2005), with data from 1958 to 2000, on the basis of the similarity of geostrophic wind speed (direction and velocity) at 500 and 1000 hPa. In the second step, different procedures were applied to estimate temperature and precipitation. For temperature, a multiple linear regression model was developed of atmospheric variables in the same vertical column as the selected weather station. This was done using maximum or minimum temperatures for the days selected in the previous step. Afterwards, this regression is applied to the atmospheric variables simulated with the GCM to estimate the maximum or minimum temperature on a certain future day for the selected weather station. In the case of precipitation, the mean values calculated for the ERA40 (meteoritical observations reanalysis produced by the European Centre of Medium-Range Weather

Forecest) most similar days are used instead of a regression. With this methodology AEMET provides two resolution approaches. The first, Analogues FIC (Foundation of Climate Research) (Schmidli et al., 2007) enables weather daily data to be obtained at each weather station. The second, Analogues-INM (National Institute of Meteorology, Spain) (AEMET, 2008) enables these to be obtained on a grid of 50 km x 50 km.

- Statistical Downscaling method (Wilby et al., 2002): this method is based on regression models among temperature and precipitation observed at weather stations and each predictand (precipitation and maximum and minimum temperature). These models were calibrated with data from 1961 to 1990 and then checked using historical records from 1991 to 2001. Using the calibrated regression models, projections were made for the XXI century.

The spatial resolution that offer the Analogues-INM is too poor for an area like the Basque Country where the climatological variability is important. Hence, to carry out this research, the statistical downscaling methods that offer weather station resolution were selected: The Analogues-FIC hereafter AEMET Analogues method (AN), and the Statistical Downscaling Method (SDSM).

- The emission scenario or the representative concentration pathway (RCP): The GCMs used in PRUDENCE and ENSEMBLES projects, consider the emission scenarios of the Special Report on Emissions Scenarios; SRES (IPCC SRES, 2000). Nevertheless, for the CMIP5 the RCPs were defined. In section *1. Introduction,* there is more explanation about the emission scenarios and the RCPs. For the PRUDENCE project, AEMET applied statistical downscaling for A2 and B2 emission scenarios and for ENSEMBLES A2, A1B and B1. In this Thesis, all the available emission scenarios from each project were used. In the case of CMIP5, two of the most widely used RCPs downscaled by AEMET were used: the climate projections for the stabilization scenario (RCP 4.5) and the high greenhouse gas emission scenario (RCP 8.5).

2.2.1 Selection of the climate projections: PRUDENCE Project

AEMET (2008) did an analysis to evaluate the reproduction of daily temperature and precipitation for 17 GCMs in the geographical area located between latitudes 27.5°N and 52.5°N and longitudes 22.5°E and 22.5°W. The conclusion was that the GCMs that better reproduce the European climate conditions were developed by some of the main European research centres (Max Planck Institute from Germany and Hadley Centre from UK). Based on this research, and considering the available data provided by AEMET two GCMs from the PRUDENCE project were selected (table 2.1).

The following nomenclature has been used in referring to the possible combinations in this work. First the RCM acronym (e.g. ECHAM4) is used followed by the downscaling method (e.g. AN referring to analogues method) and finally the greenhouse gases emission scenario (e.g. A2) is specified.

GCM acronym	Institution	Country	Downscaling method	E.S.	Climatic projection name
ECHAM4	Max-Planck-Institut für Meteorologie	Germany	AEMET AN	A2	ECHAM4_AN_A2
				B2	ECHAM4_AN_B2
CGCM2	Canadian Centre of Climate Modellig and Analysis	Canada	AEMET AN	A2	CGCM2_AN_A2
				B2	CGCM2_AN_B2

Table 2.1. *Overview of the General Circulation Models (GCMs) from the PRUDENCE project used in the present study, the institution in which they were developed, the country, the downscaling methods used for each GCM, the emission scenario (E.S.) and the name given to each climate projection (2010-2099). Note that the name of the baseline projections (1961-2000) follows the same system but without the emission scenario.*

2.2.2 Selection of the climate projections: ENSEMBLES Project

The selection of GCM provided by AEMET has been based upon two different research works that were carried out to study their validity in the Iberian Peninsula; Brands et al. (2011) have done a study of the ENSEMBLES global climate models in the south-west of Europe from a downscaling perspective. On the other hand, AEMET has published a report to evaluate the accuracy of the GCM in Spain and the Euro-Atlantic region (Casado et al., 2011). Using these studies and others such as Turco et al. (2011), Errasti et al. (2011) and Nieto & Rodriguez-Puebla (2006) to a lesser extent, EGMAM, EGMAM2, HADGEM2 and MPEH5 had been chosen. To have a better estimation of uncertainty, three

greenhouse gases emission scenarios (A2, A1B and B1) were used because an ensemble of GCM, downscaling methods and different emission scenarios give wider range of results than single-model simulations (Giorgi & Mearns, 2002; Murphy et al., 2004; Boorman & Sefton, 1997; IPCC, 2007). With the combination of GCM, downscaling methods and emission scenarios, 11 climatic projections were selected and these are shown in Table 2.2.

GCM acronym	Institution	Country	Downscaling method	RCP	Climatic projection name
EGMAM	Freie Universität Berlin	Germany	AEMET AN	A2	EGMAM_AN_A2
				A1B	EGMAM_AN_A1B
EGMAM2	Freie Universität Berlin	Germany	AEMET AN	A1B	EGMAM2_AN_A1B
			SDSM	A1B	EGMAM2_SDSM_A1B
HADGEM2	Met Office Hadley Centre	UK	AEMET AN	A1B	HADGEM2_AN_A1B
MPEH5	Max-Planck-Institut für Meteorologie	Germany	AEMET AN	A2	MPEH5_AN_A2
				A1B	MPEH5_AN_A1B
				B1	MPEH5_AN_B1
			SDSM	A2	MPEH5_SDSM_A2
				A1B	MPEH5_SDSM_A1B
				B1	MPEH5_SDSM_B1

Table 2.2. *Overview of the General Circulation Models (GCMs) from ENSEMBLES project used in the present study, the institution in which they were developed, the country, the downscaling methods used for each GCM, Representative Concentration Pathway (RCP) and the name given to each climate projection (2010-2099). Note that the name of the baseline projections (1961-2000) follows the same system but without the emission scenario.*

2.2.3 CMIP5

From all the GCMs downscaled by AEMET, a selection of 5 was made for this research (Table 2.3). For that purpose, firstly, the results of research works such as that by Perez et al. (2014) were taken into consideration -in which the CMIP5 models performance is evaluated for the north-east Atlantic region-. Secondly, the meteorological data for the climate projection baselines (1961-2000) of 9 GCMs (downscaled with AN and SDSM methods) were compared to the data observed at meteorological stations of the studied area, selecting those that best fitted. This step was necessary because the CMIP5 models are recent and the evaluation studies of their results are not so abundant.

GCM name	Institution	Country	Downscaling method	RCP	Climatic projection name
ACCESS1-0	CSIRO-BOM	Australia	AEMET AN	4.5	ACCESS1-0_AN_R45
				8.5	ACCESS1-0_AN_R85
BNU-ESM	College of Global Change and Earth System Science	China	AEMET AN	4.5	BNU-ESM_AN_R45
				8.5	BNU-ESM_AN_R85
			SDSM	4.5	BNU-ESM_SDSM_R45
				8.5	BNU-ESM_SDSM_R85
CMCC-CESM	Centro Euro-Mediterraneo per I	Italy	AEMET AN	8.5	CMCC-CESM_AN_R85
			SDSM	8.5	CMCC-CESM_SDSM_R85
MPI-ESM-LR	Max-Planck-Institut für Meteorologie	Germany	AEMET AN	4.5	MPI-ESM-LR_AN_R45
				8.5	MPI-ESM-LR_AN_R85
			SDSM	4.5	MPI-ESM-LR_SDSM_R45
				8.5	MPI-ESM-LR_SDSM_R85
MPI-ESM-MR	Max-Planck-Institut für Meteorologie	Germany	AEMET AN	4.5	MPI-ESM-MR_AN_R45
				8.5	MPI-ESM-MR_AN_R85
			SDSM	4.5	MPI-ESM-MR_SDSM_R45
				8.5	MPI-ESM-MR_SDSM_R85

Table 2.3. *Overview of the General Circulation Models (GCMs)from CMIP5 project used in the present study, the institution in which they were developed, the country, the downscaling methods used for each GCM, Representative Concentration Pathway (RCP) and the name given to each climate projection (2010-2099). Note that the name of the baseline projections (1961-2000) follows the same system but without the emission scenario.*

2.3 BIAS CORRECTION

Although the downscaled GCMs chosen were the ones that a priori best fitted the observed data provided by AEMET, there are still important differences between the climate projection baselines and the observed meteorological data (especially when precipitation is considered; see chapter *4. Evaluation of climate change impacts on water resources*). To correct these differences in precipitation and temperature, a linear-scaling approach following the methodology explained by Lenderink & Seibert (2007) was performed. The linear scaling works with the correction in a monthly scale based on the differences between the observed and simulated values. The values for each month are adjusted with the same correction factor (Teutschbein et al., 2013) and this factor is time independent. This method preserves the trend while adjusting the mean value (Hempel et al., 2013).

The linear-scaling approach in the case of precipitation is defined as:

$$P^*_{CP}(d) = P_{CP}(d) \cdot \left[\frac{\bar{P}_{obs}}{\bar{P}_{CP}}\right] \quad (2\text{-}1)$$

Where,

$P^*_{CP}(d)$ is the bias-corrected precipitation for the climate projection (baseline or future) in a daily time step

$P_{CP}(d)$ is the precipitation for the climate projection (baseline or future) in a daily time step

$\bar{P}_{obs}$ is the monthly mean observed precipitation (baseline)

$\bar{P}_{CP}$ is the monthly mean precipitation for the climate projection (baseline)

And for maximum and minimum temperature:

$$T^*_{CP}(d) = T_{CP} + \bar{T}_{obs} - \bar{T}_{CP} \quad (2\text{-}2)$$

Where,

$T^*_{CP}(d)$ is the bias-corrected temperature for the climate projection (baseline or future) in a daily time step

T_{CP} is the temperature for the climate projection (baseline or future) in a daily time step

$\bar{T}_{obs}$ is the monthly mean observed temperature (baseline)

$\bar{T}_{CP}$ is the monthly mean temperature for the climate projection (baseline)

This approach was selected with a view to altering the downscaled GCMs as little as possible (Graham et al., 2007) without affecting possible trends in future climate projections and derived hydrological projections. For this reason, although once the linear-scaling approach is applied the difference between monthly precipitation (or temperature) amount for the baseline is minimum, the precipitation and hot/cold days distribution between them is different. It is important to bear in mind that when the bias correction method is chosen, the selected method will also have associated uncertainties.

The bias-corrected values were the input climate values for hydrological modelling with SWAT.

2.4 HYDROLOGICAL MODELLING: GENERAL DESCRIPTION OF SOIL AND WATER ASSESSMENT TOOL (SWAT)

SWAT is a continuous time, semi-distributed, river catchment scale hydrological and environmental code. It was developed for the US Department of Agriculture (USDA), Agricultural Research Service, to predict the effect of land

management practices on water, sediment and agricultural chemical yields. The model simulates hydrological processes, sediment yield, nutrient loss, and pesticide losses into surface/groundwater and the effects of agricultural management practices and it was developed to apply in large ungauged catchments (Arnold et al., 1998).

SWAT code was developed to operate on a daily time step. SWAT 2005 has limited capability to operate sub-daily, nevertheless in the last years physically-based new algorithms were implemented on SWAT 2012 to simulate hydrological processes (Jeong et al., 2010) and sediment erosion, transport and deposition at sub-daily time-step (Jeong et al., 2011). Therefore, since this option was incorporated it is possible to analyse processes that can't be contemplated in a daily basis. Some examples are the research carried out by Maharjan et al. (2013) to estimate sub-daily runoff in a small catchment and the one conducted by Furl et al. (2015) where they analyse large erosion events on unit source catchments. However, these type of research studies are not very common, on the one hand because the implementation of such algorithms is relatively new and on the other hand because sub-daily observed data are not always available.

Below there is a description of the processes modelled by SWAT to simulate the flow and sediment in daily and sub-daily time steps. The description is focused on the equations and parameters that have been the most influential to the simulation in the study areas of the present Thesis. There are more details about the equations and its components in Neitsch et al. (2011).

2.4.1 Selection of hydrological model: SWAT

The selection of the hydrological code to use in a research project should be done based on the objectives of the research work and the available data. SWAT is a widely-used model to study hydrological and environmental impacts of the climate change (e.g. Bouraoui et al., 2005; Abbaspour et al., 2009; Lirong & Jianyun, 2012; Awan & Ismaeel, 2014; Zhang et al., 2014; Grusson et al., 2015; Lin et al., 2015) because of its capability to do long–term continuous simulations. Initially, SWAT was developed and used in large agronomic catchments therefore its application in small and/or forested catchments, could be questioned.

However, in the last decade it was applied in small and forest catchments with satisfactory results (e.g. Arabi et al., 2006; Behera & Panda, 2006; Watson et al., 2008; Parajuli, 2010; Zhou et al., 2011). One of the handicaps in small catchments is that as Qiu et al. (2012) reported, SWAT is not able to simulate precipitation patterns in terms of intensity and temporal distribution and therefore, daily flow and sediment peaks could be underestimated. Nevertheless, it is possible that this fact could be solved with the sub-daily simulation and this will be valued in section 3.4. Finally, SWAT has been employed in small size catchments located near the study areas, with satisfactory results (Cerro et al., 2014; Epelde et al., 2015; Peraza-Castro et al., 2015) Besides this, the input data required are not as numerous as in other types of models (scarcity of measured data) and there is a high facility to solve modelling problems thanks to its users community, it was considered that SWAT was appropriate to carry out the present research.

2.4.2 Catchment configuration

The first step in the modelling process with SWAT is to partition the catchment into subunits. Thus, based on topographic information, the catchment is divided into sub-catchments or sub-basins and these, in turn, in Hydrological Response Units (HRUs) (Fig. 2.2).

The sub-basins are the first level of subdivision. They have a geographic position in the catchment and variables like flow, sediments, nutrients and pesticides route from one sub-basin to another adjacent sub-basin. Its delineation is done with the surface topography (topographic map, digital elevation model (DEM)…), in this manner the whole area within a sub-basin flows to the sub-basin outlet. Each one has at least one HRU, a tributary and a reach or main channel to which they are connected.

The second level of subdivision are the HRUs. These are areas inside the sub-basin with homogeneous land use, slope and soil characteristics (Arnold et al., 2012) (Fig. 2.2). In this case, there is not interaction between HRUs. Loadings (water and variables that can be transported with such; sediments, nutrients and pesticides) are calculated for each HRU and summed together to determinate the total loadings from the sub-basin (Neitsch et al., 2011). These loadings enter in

the channel network of the catchment through the associated reach segment in each sub-basin. The reach segment transports the loadings of the sub-basin and also the outputs of the sub-basin up-stream (already added in the reach).

The surface runoff generated in each HRU is routed through tributary channels. This allows to calculate the concentration time and transmission losses through the tributary channel. The remaining water is added as lateral flow and baseflow (cumulatively called water yield) of the HRU and added to the reach for routing.

SWAT is flexible in catchment discretization; the user can place a control point anywhere in a reach of the catchment, which will then be taken as the outlet of that sub-basin. This makes it possible to obtain the results of the simulation relating to water quantity (including the separation of the hydrograph) and quality for any previously selected points.

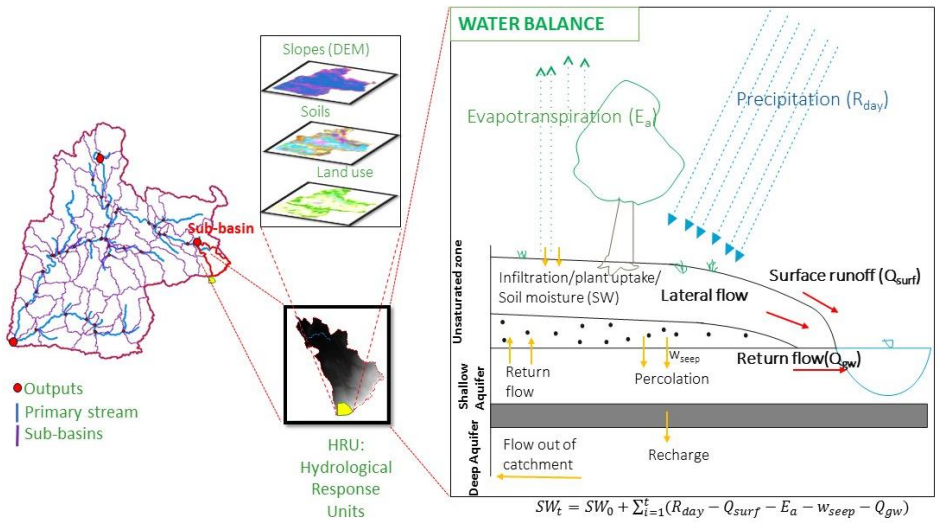

Figure 2.2. *Representation of the spatial distribution of the SWAT model.*

2.4.3 Water flow

SWAT considers the catchment hydrology in two major phases. The first one is the land phase and controls all the processes occurred in an HRU before the water, sediments… enter in the reach. The second one is the routing phase of the hydrologic cycle, which considers the movement of water, sediments... through the channel network to the catchment outlet.

LAND PHASE

It is possible to divide the hydrological processes simulated by SWAT in the land phase in the following general groups: 1) precipitation/interception, 2) evapotranspiration, 3) surface runoff and infiltration to soil and root zone, 4) soil water percolation or evaporation, and 5) baseflow/groundwater flow (Arnold et al., 1998).

1) Precipitation/interception

For each sub-basin, SWAT uses the data from the meteorological station nearest to its centroid. Meteorological data that may be introduced into the model are: daily or sub-daily precipitation, maximum/minimum air temperatures, solar radiation, wind speed and relative humidity. SWAT incorporates a weather generator but the use of measured precipitation is strongly recommended (Neitsch et al., 2011).

As the precipitation depends on the altitude, when the meteorological station network is not enough to represent this variability, the user can introduce “elevation bands”. In this case, the difference between the band and the elevation of the station will add to the measured precipitation.

The water enters to the system as precipitation (or snow). Nevertheless, it is possible to lose this water by evaporation (channels or reaches, soil or intercepted precipitation by plant canopy) or transpiration (plants). Normally it is difficult to separate the two terms so both are calculated through evapotranspiration. The plant canopy (CANMX parameter) is a function of the leaf area index of the plant and affect the interception , infiltration, surface runoff and evapotranspiration.

2) Potential evapotranspiration

SWAT incorporates three methods to calculate the potential evapotranspiration (PET): the Penman-Monteith method (Monteith, 1965; Allen, 1986; Allen et al., 1989), the Priestley-Taylor method (Priestley & Taylor, 1972) and the Hargreaves method (Hargreaves & Samani, 1985). The Food and Agriculture Organization (FAO, 1998) recommends the use of Penman-Montheith method when the data required for the equation are available. When only the

precipitation and maximum and minimum temperature are available this organization recommends the use of Hargreaves method:

$$\lambda E_0 = 0.0023 \cdot H_0 \cdot (T_{max} - T_{min})^{0.5} \cdot (\overline{T}_{av} + 17.8) \quad (2\text{-}3)$$

Where,

λ is the latent heat of vaporization (MJ kg^{-1})

E_0 is the potential evapotranspiration (mm d^{-1})

H_0 is the extra-terrestrial radiation (MJ m^{-1} d^{-1})

$T_{max} and\ T_{min}$ are the maximum and minimum air temperature (°C) respectively

$\overline{T}_{av}$ is the mean air temperature (°C)

3) Surface runoff and infiltration to the soil and root zone

There are two methods to simulate surface runoff: the modified **SCS curve number** (USDA; Soil Conservation Service, 1972) and the Green & Ampt Mein Larson infiltration method (Mein & Larson, 1973). The first one is an empiric method that considering the initial abstractions and the precipitation, calculates the surface runoff:

$$Q_{surf} = \frac{(R_{day} - 0.2S)^2}{(R_{day} + 0.8S)} \quad (2\text{-}4)$$

Where,

Q_{surf} is the amount of surface runoff on day i (mm)

R_{day} is the amount of precipitation on a day i (mm)

S is the retention parameter. Note that initial abstractions are commonly approximated as 0.2S:

$$S = 25.4\left(\frac{1000}{CN} - 10\right) \quad (2\text{-}5)$$

CN is the curve number for each day (usual values in USDA; Soil Conservation Service, 1972). This empiric parameter is a function of the soil hydrological group (soil with similar runoff potential under similar storm and cover condition; NRCS Soil Survey Staff, 1996), antecedent soil water content, a retention parameter and a slope adjustment. Therefore, as the antecedent soil

water changes over time, CN is adjusted at each time step, and as soil characteristic varies on the catchment, this parameter also changes spatially.

The antecedent moisture condition is divided into 3 groups; I is the dry condition (wilting point), II is the average moisture and III is the wet condition (filed capacity). There are two possibilities to calculate the retention parameter, the traditional one is the soil moisture method in which the parameter varies with soil profile water content. The second one is the plant evaporation method. With this method the CN is calculated as a function of plant evapotranspiration, in this way the value is more dependent on the antecedent climate. When the retention parameter varies with the soil storage:

$$S = S_{max} \cdot \left(1 - \frac{SW}{(SW + \exp(w1 - w2 \cdot SW))}\right) \quad (2\text{-}6)$$

Where,

S is the retention parameter for a given day (mm)

S_{max} is the maximum value S can achieve on a given day (mm)

SW is the soil water content of the entire profile excluding the amount of water held in the profile at wilting point (mm)

$w1\ and\ w2$ are the shape coefficients (more details in Neitsch et al. (2011)

When the retention parameter is function of the plant evapotranspiration:

$$S = S_{prev} + E_0 \cdot exp\left(\frac{-cncoef \cdot S_{prev}}{S_{max}}\right) - R_{day} + Q_{suf} \quad (2\text{-}7)$$

Where,

S is the retention parameter for a given day (mm)

S_{prev} is the retention parameter of the previous day (mm)

E_0 is potential evapotranspiration for the day (mm d^{-1})

$w1\ and\ w2$ are the shape coefficients (more details in Neitsch et al. (2011).

$cncoef$ is the weighting coefficient used to calculate the retention coefficient for daily curve number calculations dependent on plant evapotranspiration

S_{max} is the maximum value S can achieve on a given day (mm)

R_{day} is the amount of precipitation on a given day (mm)

Q_{surf} is the amount of surface runoff on a given day (mm)

The CN values for soil moisture II are tabulated in function of the hydrologic soil group, land use, cover type… (Soil Conservation Service (SCS), 1986). Nevertheless, these values were calculated for 5 % slope so when it is necessary to correct the CN value, SWAT uses the equation developed by Williams (1995).

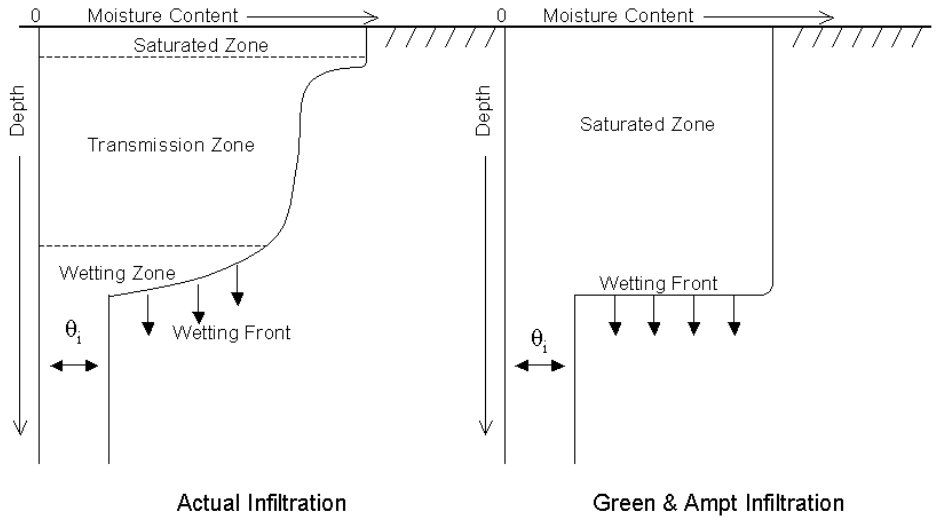

Figure 2.3. *Moisture in the soil profile. On the left the typical observed soil moisture distribution is represented while on the right it is displayed the modelled by Green & Ampt (Neitsch et al., 2011).*

As previously mentioned, the other method that SWAT has to calculate the surface runoff is the **Green & Ampt Mein Larson method (hereafter GAML)**. This is based on the Green & Ampt (Green & Ampt, 1911) equation that is a physically based model that allows continuous simulation of infiltration process. To use this equation, it is necessary to assume that the soil profile is homogeneous and the soil moisture is distributed uniformly in the profile. The figure 2.3 illustrates the simplification that this method does in the distribution of the soil moisture.

Mein and Larson (1973), using the Green & Ampt equation, developed a methodology to estimate the ponding time in the infiltration. The GAML method simulates continuous surface runoff using physical parameters based on the

direct relationship between the infiltration and the precipitation (Jeong et al., 2010). This method requires sub-daily precipitation as input. The equation is expressed as:

$$f(t) = K_e(1 + \frac{\psi \cdot \Delta\theta}{F(t)}) \quad (2\text{-}8)$$

Where,

$f(t)$ is the infiltration rate at time t (mm h^{-1})
$F(t)$ is the cumulative infiltration (mm)
K_e is the effective hydraulic conductivity (mm h^{-1})
ψ is the wetting front matric potential (mm)
$\Delta\theta$ is the change of moisture content (mm mm^{-1})

The cumulative infiltration (F) is a function of the infiltrated volume that varies according to the previous infiltration rates (f). When the precipitation intensity is less than the infiltration rate, the cumulative infiltration will be the sum of precipitation and previous infiltrations. To calculate the hydraulic conductivity parameter (K_e) from the GAML equation (2-8) SWAT uses an equation developed by Nearing et al. (1996). This equation incorporates the saturated hydraulic conductivity (K_{sat}) and the CN:

$$K_e = \frac{56.82 \cdot {K_{sat}}^{0.286}}{1 + 0.051 \cdot \exp(0.062 \cdot CN)} - 2 \quad (2\text{-}9)$$

Where,

K_e is the effective hydraulic conductivity (mm h^{-1})
K_{sat} is the saturated hydraulic conductivity (mm h^{-1})
CN is the curve number

Wetting front matric potential (ψ) (equation 2-8) is calculated as a function of porosity and sand-clay percentage (Rawls & Brakensiek, 1985). The change of moisture content across the wetting front $\Delta\theta$ is a function of the soil water content of the entire profile (SW), the amount of water in the soil profile at field capacity (FC) and the porosity.

The infiltration calculation is done for each time step (for SCS the time step is daily) and each HRU and all the water that does not enter in the soil profile will be surface runoff. The time (concentration time) that the surface runoff needs to arrive to the sub-basin outlet is calculated with the following equation:

$$t_{con} = \frac{{L_{spl}}^{0.6} \cdot n^{0.6}}{18 \cdot spl^{0.3}} \quad (2\text{-}10)$$

Where,

t_{con} is the concentration time of surface runoff (h)

L_{spl} is the sub-basin slope length (m)

n is the Manning's roughness coefficient for the sub-basin (values in Engman, 1983)

spl is the average slope in the sub-basin (m m^{-1})

When the time of concentration is big (greater than 1 day) not all the surface runoff reaches the main channel. To estimate the surface runoff lag SWAT incorporates the SURLAG parameter. For higher values of SURLAG higher fraction of water reaches the channels:

$$Q_{surf} = (Q`_{surf} + Q_{stor,i-1}) \cdot \left(1 - exp\left(\frac{-surlag}{t_{conc}}\right)\right) \quad (2\text{-}11)$$

Where,

Q_{surf} is the surface runoff discharged to the main channel on a given day i (mm)

$Q`_{surf}$ is the amount of surface runoff generated in the sub-basin on a given day i (mm)

$Q_{stor,i-1}$ is the surface runoff stored or lagged from the previous day (mm)

$surlag$ is the surface lag coefficient

t_{con} is the concentration time of surface runoff (h)

According to the modified Rational Formula (Chow et al., 1998) SWAT calculates the peak flow rate for each sub-basin outlet:

$$q_{peak} = \frac{\alpha_{tc} \cdot Q_{surf} \cdot area}{3.6 \cdot t_{con}} \quad (2\text{-}12)$$

Where,

q_{peak} is the peak runoff rate ($m^3\ s^{-1}$)

α_{tc} is the fraction of daily rainfall that occurs during the time of concentration

Q_{surf} is the surface runoff (mm)

$area$ is the sub-basin area (km^2)

t_{con} is the concentration time of surface runoff (h)

It is possible to observe some parameters needed in the estimation of surface runoff in the Table 2.4.

VARIABLE NAME	*RANGE*	*DEFINITION*
IEVENT	CN or GAML	Rainfall, runoff, routing method
ICN	0 or 1	Daily curve number calculation method: 0 calculate daily CN value as a function of soil moisture; 1 calculate daily CN value as a function of plant evapotranspiration
CNCOEF	0.5-2	Weighting coefficient used to calculate the retention coefficient for daily CN calculations dependent on plant evapotranspiration
CN2 and CNOP		CN in moisture condition.
IDT		Length of time step (min): Δt=IDT/60
SOL_BD	1.1-1.9	ρ_b: Moist bulk density (Mg m^{-3}): soil porosity =1 - ρ_b / 2.65
CLAY		% clay content
SILT		% silt content
OV_N	0.01-0.5	Manning's "n" value for surface runoff
SURLAG	0.1-24	Surface runoff lag coefficient.

Table 2.4. *Some parameters needed in the estimation of surface runoff. In bold type, parameter related to SCS and GAML methods, in an underscored type those affecting SCS and italicized those affecting GAML method.*

4) Soil water percolation and evaporation

The water that enters in the soil profile can have different destinies; it may be removed from the soil by plant uptake or evaporation, it can percolate to recharge the aquifer or can move laterally to contribute the streamflow (Fig. 2.2). In SWAT the soil is divided into different layers and the calculations are done for each layer. It assumes that the water is uniformly distributed in the layer, thus the horizontal flow in unsaturated zones is eliminated.

The potential water uptake for each layer is estimated with the next equation:

$$w_{up} = \frac{E_t}{[1-\exp(-\beta_w)]} \cdot \left[1 - exp\left(-\beta_w \cdot \frac{z}{z_{root}}\right)\right] \quad (2\text{-}13)$$

Where,

w_{up} is the potential water uptake from the soil surface to a specified depth z (mm)

E_t is the maximum plant transpiration on a given day (mm)

β_w is the water-use distribution parameter (10 in SWAT, thus most of the plant uptake occur in the upper part of the soil where the root density is bigger)

z is the water-use distribution parameter (mm)

z_{root} is the depth of root development in the soil (mm)

The plant uptake in each soil layer is calculated with the difference between its value in the lower boundary and the upper. Nevertheless, sometimes there is not enough water in the upper layers to meet the potential water uptake so SWAT allows to compensate the lower layer with the *epco* parameter (Table 2.5). *Epco* is the plant uptake compensation factor (between 0 and 1) the higher its value, the higher the amount of water uptake demand to be met by lower layers in the soil will be higher.

The evaporative demand in different soil layer is estimated with:

$$E_{soil} = E_s \cdot \frac{z}{z+\exp(2.374-0.00713 \cdot z)} \quad (2\text{-}14)$$

Where,

E_{soil} is the potential evaporative demand at depth z (mm)

E_s is the maximum soil water evaporation on a given day (mm)

z is the depth below the surface

The evaporative demand at each soil layer is the difference between its value in the upper and the lower boundaries of the layer. SWAT incorporates the *esco* parameter that allows the user to modify the depth distribution used to meet the soil evaporative demand (Table 2.5). *Esco* is the soil evaporation compensation factor (between 0 and 1), when its value is smaller, the model is able to have more evaporative demand from lower levels.

Percolation from the bottom of the root zone is considered as recharge to the shallow aquifer. With SWAT the water in the soil only can move downwards (percolation) when the water content of the upper layer exceeds the field capacity

(FC) and the underlying layer is unsaturated. The plant available water or available water capacity (AWC) is the difference between the field capacity and the wilting point (WP) so FC will be the sum of WP and AWC. The AWC (of each layer) is an input stablished by the user while the WP is:

$$WP = 0.40 \cdot \frac{m_c \cdot \rho_b}{100} \quad (2\text{-}15)$$

Where,

WP is water content at wilting point expressed as a fraction of the total soil volume (%)

m_c is the clay percentage content of the layer (%)

ρ_b is the bulk density of the soil layer (Mg cm^{-3})

Another condition for the percolation to occur is that the hydraulic conductivity of the underlying layer needs to be lower than the overlaying one. To calculate the amount of water that percolates from one layer to the underlying layer SWAT uses the Storage Routing Methodology. This depends on the amount of water that surpasses the FC and the travel time for percolation:

$$TT_{perc} = \frac{SAT - FC}{K_{sat}} \quad (2\text{-}16)$$

Where,

TT_{perc} is the travel time for percolation (h)

SAT is the amount of water in the soil layer when completely saturated (mm)

FC is the water content at field capacity (mm)

K_{sat} is the saturated hydraulic conductivity (mm h^{-1})

In SWAT the amount of water in the soil layer when this is completely saturated (SAT), is an approximation of the soil porosity. If we assume that the soil particles density is 2.65 Mg cm^{-3} SAT is defined as:

$$SAT \approx \emptyset = 1 - \frac{\rho_b}{2.65} \quad (2\text{-}17)$$

Where,

SAT is the amount of water in the soil layer when completely saturated (mm)

$\emptyset$ is the soil porosity expresses as a fraction of the total soil volume

ρ_b is the bulk density of the soil layer (Mg cm^{-3})

In the soil in addition to percolation, water flow can happen in other directions in saturated and unsaturated conditions. SWAT only considers the movement in other directions in saturated conditions but in the unsaturated zone there may be a movement when there is a water demand for evapotranspiration. Therefore, unsaturated flow between layers will be controlled by the plant uptake and the soil water evaporation. In addition, SWAT defines the *revap* parameter (Table 2.6). This will be the shallow aquifer water to return to the root zone because of evaporation and/or transpiration (Fig. 2.2).

Finally, in saturated soil layers lateral flow may happen. For it to exist, it is necessary that the underlying layers have lower hydraulic conductivity than the overlaying ones. As it happened to the SURLAG parameter in the surface runoff, for lateral flow there exists a parameter called LAT_TTIME to control the lag time or the delay of this flow (Table 2.5). As its value increases a lower fraction of water reaches the channels.

VARIABLE NAME	*RANGE*	*DEFINITION*
CLAY	0-100	m_c: Percent clay content
SOL_BD	1.1-1.9	ρ_b: Moist bulk density (Mg m^{-3}): soil porosity =1 - ρ_b / 2.65
SOL_AWC	0-1	AWC available water capacity
SOL_K	0.05-10	K_{sat}: Saturated hydraulic conductivity (mm h^{-1})
ESCO	0-1	Soil evaporation compensation coefficient
EPCO	0-1	Plant uptake compensation factor
LAT_TTIME	0-180	Lateral flow travel time (days)

Table 2.5*. Some parameters related to the soil water content.*

5) Baseflow/groundwater

SWAT considers two aquifers in each sub-basin (Fig. 2.2); shallow (from 2 to 20 m) and deep aquifer (>20 m). The first one contributes to the flow in main channel or reach. The water that percolates in the deep aquifer is lost from the simulated catchment (Arnold et al., 1993). The water balance in the shallow aquifer is:

$$aq_i = aq_{i-1} + w_{rchrg} - Q_{gw} - w_{revap} - w_{pump} \quad (2\text{-}18)$$

Where,

aq_i is the amount of water stored in the shallow aquifer on day i (mm)

aq_{i-1} is the amount of water stored in the shallow aquifer on day i-1 (mm)

w_{rchrg} is the amount of recharge entering the aquifer on day i (mm)

Q_{gw} is the groundwater flow, or baseflow into a main channel on day i (mm)

w_{revap} is the amount of water moving into the soil zone in response to water deficiencies on day i (mm)

w_{pump} is the amount of water removed from the shallow aquifer by pumping on day I (mm)

The shallow aquifer contributes to baseflow. When the aquifer exceeds a threshold value given by the GWQMN parameter (Table 2.6), the baseflow contributes to the reach or the channel. The groundwater or baseflow that enters in the reach or channel in steady (Hooghoudt, 1940):

$$Q_{gw} = \frac{800 \cdot K_{sat}}{L_{gw}} \cdot h_{wtbl} \quad (2\text{-}19)$$

Where,

Q_{gw} is the groundwater or baseflow into a main channel on day i (mm)

K_{sat} is the hydraulic conductivity of the aquifer (mm day^{-1})

L_{gw} is the distance from the ridge or sub basin divide for the groundwater system to the main channel (m)

h_{wtbl} is the water table depth (m)

When there is a non-steady state the groundwater/baseflow is calculated with the methodology defined by Smedema & Rycroft (1983). In this case, an important parameter is the recession constant:

$$\alpha = \frac{1}{N} \cdot ln\left[\frac{Q_{gw,N}}{Q_{gw,0}}\right] \quad (2\text{-}20)$$

Where,

α is the baseflow recession constant.

N is the time lapsed since the start of the recession (day)

$Q_{gw,N}$ is the groundwater flow on a day N (mm)

$Q_{gw,0}$ is the groundwater flow at the start of the recession (mm)

VARIABLE NAME	*RANGE*	*DEFINITION*
GW_DELAY	0-500	Delay time for aquifer to recharge (days)
GWQMN	0-5000	Threshold water level in shallow aquifer for baseflow (mm)
ALPHA_BF	0-1	Baseflow recession constant
REVAPMN	0-1000	Threshold water level in shallow aquifer for revap (mm)
GW_REVAP	0.02-0.2	Revap coefficient
RCHRG_DP	0-1	Deep aquifer percolation coefficient
GW_SPYLD	0-0.4	Specific yield of the shallow aquifer (m m^{-1})

***Table 2.6**. Some parameters influencing groundwater.*

Finally, the water balance equation is applied in each HRU to model the hydrological cycle:

$$SW_t = SW_0 + \sum_{i=1}^{t}(R_{day} - Q_{surf} - E_a - w_{seep} - Q_{gw}) \quad (2\text{-}21)$$

Where,

SW_t is the final soil water content (mm)

SW_0 is the initial soil water content on day i (mm)

R_{day} is the amount of precipitation on a day i (mm)

t is the time

Q_{surf} is the amount of surface runoff on day i (mm)

E_a is the amount of evapotranspiration on day i (mm)

w_{seep} is the amount of water entering the vadose zone from the soil profile on day i (mm)

Q_{gw} is the amount of return flow into the river on day i (mm)

ROUTING PHASE

The routing phase (Table 2.7) starts when the water reaches the channel. SWAT uses the Manning´s equation to calculate the volumetric rate (with the flow velocity and the channel section) and the velocity of the water.

$$v_c = \frac{R_{ch}^{2/3} \cdot slp_{ch}^{1/2}}{n} \quad (2\text{-}22)$$

Where,

v_c is the flow velocity (m^3 s^{-1})

R_{ch} is the hydraulic radius for a given depth of flow (m)

slp_{ch} is the slope along the channel length (m m^{-1})

n is the Manning's coefficient for the channel

There are two methods to route the water in the channel network; variable storage coefficient method (Williams, 1969) or the Muskingum routing method (Overton, 1966). Both methods are based on the kinematic wave model.

VARIABLE NAME	*RANGE*	*DEFINITION*
CH_N	-0.01-0.3	Manning´s n value for the main channel or tributary channel.
CH_K	-0.01-500	Effective hydraulic conductivity in main channel or tributary channel alluvium (mm/hr).
MSK_X	0-0.3	Weighting factor
MSK_CO(1-2)	0-16	Weighting factor for influence of normal flow on storage time constant value,

Table 2.7*. Some parameters for flow routing phase.*

2.4.4 Sub-daily water flow

SWAT was developed as a long-term simulations model that operates in a daily time step. Nevertheless, the need of understanding better the hydrological processes has led to incorporate new algorithms to be able to simulate individual storms, so SWAT is capable of doing long-term continuous and event-based simulations in catchment scales. For the sub-daily modelling, not all the processes are modelled at sub-daily time steps; surface runoff and discharge routing phase, are routed at sub-daily time step but base flow and evapotranspiration are calculated on a daily basis and distributed for each time step. The figure 2.4 shows processes occurred in a sub-daily simulation and their time steps. All the details about the sub-daily capability of SWAT are explained in the work carried out by Jeong et al. (2010).

LAND PHASE

To calculate the infiltration and the surface runoff in each HRU in a sub-basin in sub-daily time steps, SWAT uses the GAML method explained above (equation 2-8; Fig. 2.3; Table 2.4). Once the surface runoff is calculated, a lag fraction at the end of the time step is determined with a variation of 2-11 equation that incorporates the SURLAG parameter:

$$Q_{surf} = (Q`_{surf} + Q_{stor,i-1}) \cdot \left(1 - exp\left(\frac{-surlag}{t_{conc}/\Delta t}\right)\right) \quad (2\text{-}23)$$

Where,

Q_{surf} is the surface runoff discharged to the main channel on a given day i (mm)

$Q`_{surf}$ is the amount of surface runoff generated in the sub-basin on a given day i (mm)

$Q_{stor,i-1}$ is the surface runoff stored or lagged from the previous day (mm)

$surlag$ is the surface lag coefficient

t_{con} is the concentration time of surface runoff (h)

Δt is the time interval

The lag amount is added to the excess precipitation that occurs in the next time step and the HRU output values are aggregated at sub-basin scale for flow routing.

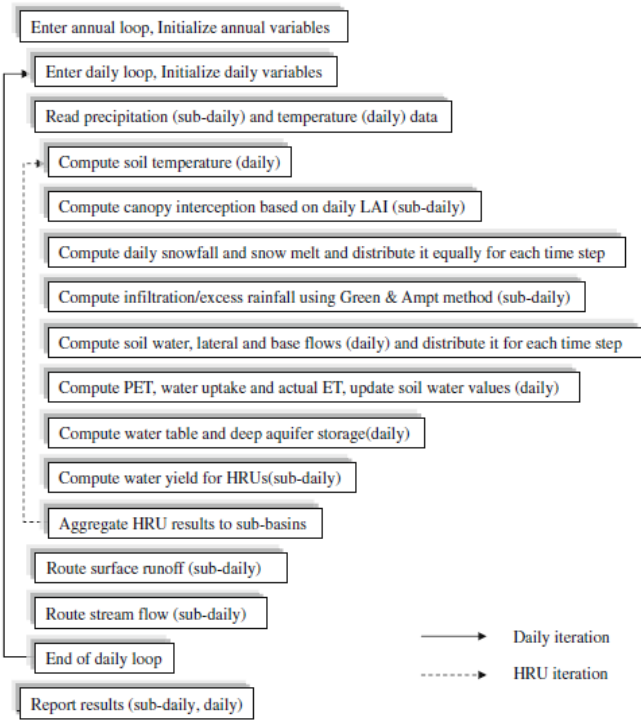

Figure 2.4. *Schematic flow chart showing the stream of processes in the sub-hourly simulation model (Jeong et al., 2010).*

ROUTING PHASE

The dimensionless Unit Hydrograph (UH) is used to route the surface runoff generated at each time step. Then, the time to peak flow is estimated based on the Soil Conservation Service (SCS) dimensionless Unit Hydrograph (SCS, 1972) method in which 37.5 % of the total volume is assigned to the rising side.

The methods to route the discharge through the channel network are the same as in daily time step (variable storage coefficient method and the Muskingum routing method; Table 2.7), nevertheless the routes of channel were modified in order to run at intervals as small as a 1 minute.

2.4.5 Erosion and sediment content

Sediment transport, as with the flow, consists on two components; land phase and channel or routing phase.

LAND PHASE

One of the most used method to predict the loss of the soil is the Universal Soil Loss Equation (USLE) developed by Wischmeier & Smith (1965). This empirical equation allows to calculate average annual gross erosion generated by rainfall energy. SWAT uses the Modified Universal Soil Loss Equation (MUSLE) (Williams, 1975) to calculate sediment from sheet erosion for each HRU because in this modified equation the rainfall energy is replaced with a runoff factor (it implicitly accounts for the soil moisture and runoff production). This change improves the sediment prediction accuracy and also allows to calculate sediment yield in single storms (Neitsch et al., 2011).

The MUSLE equation applied in SWAT is:

$$sed = 11.8 \cdot (Q_{surf} \cdot q_{peak} \cdot A_{HRU})^{0.56} \cdot K_{USLE} \cdot C_{USLE} \cdot P_{USLE} \cdot LS_{USLE} \cdot CFRG \quad (2\text{-}24)$$

Where,

sed is the sediment yield (t) on a given day

Q_{surf} is the surface runoff volume (mm ha^{-1})

q_{peak} is the peak runoff rate (m^3 s^{-1}) (equation 2-12)

A_{HRU} is the area of the HRUs (ha)

K_{USLE} is the USLE soil erodibility factor

C_{USLE} is the USLE cover and management factor

P_{USLE} is the USLE support practice factor

LS_{USLE} is the USLE topographic factor

$CFRG$ is the coarse fragment factor

The factors that come from USLE are explained on "SWAT theoretical documentation" (Neitsch et al., 2011).

Water and sediment yield calculated in each HRU are outlined in each sub-basin and then routed through the stream network to the catchment outle (Table 2.8)t.

VARIABLE NAME	*RANGE*	*DEFINITION*
USLE_C		Minimum value of USLE C factor for water erosion applicable to the land cover/plant.
USLE_K	0-0.65	USLE equation soil erodibility (K) factor
USLE_P	1.5-3	USLE equation support practice factor.

Table 2.8. *Some parameters related to the land phase of sediment.*

CHANNEL PHASE

To control the sediment transport in the channel (Table 2.9), SWAT considers degradation and deposition simultaneously. The deposited sediment (Bagnold, 1977) is calculated as:

$$sed_{dep} = (conc_{sed,ch,i} - conc_{sed,ch,mx}) \cdot V_{ch} \quad (2\text{-}25)$$

Where,

sed_{dep} is the sediment deposited (ton)

$conc_{sed,ch,i}$ is an initial sediment concentration in the reach (ton m^{-3} or kg L^{-1})

$conc_{sed,ch,mx}$ is the maximum concentration of sediment that can be transported by the water (ton m^{-3} or kg L^{-1})

V_{ch} is the volume of water in the reach segment (m^3)

The deposited degraded (Williams, 1975) is calculated as:

$$sed_{deg} = (conc_{sed,ch,mx} - conc_{sed,ch,i}) \cdot V_{ch} \cdot K_{ch} \cdot C_{ch} \quad (2\text{-}26)$$

Where,

sed_{deg} is the amount of sediment re-entrained in the reach segment (ton)

$conc_{sed,ch,mx}$ is the maximum concentration of sediment that can be transported by the water (ton m^{-3} or kg L^{-1})

$conc_{sed,ch,i}$ is an initial sediment concentration in the reach (ton m^{-3} or kg L^{-1})

V_{ch} is the volume of water in the reach segment (m^3)

K_{ch} is the channel erodibility factor (cm/h/Pa)

C_{ch} is the channel cover factor

VARIABLE NAME	*RANGE*	*DEFINITION*
CH_COV1	0-1	Channel erodibility factor.
CH_COV2	0-1	Channel cover factor.
SPCON	0.0001-0.01	Linear parameter for calculating the maximum amount of sediment that can be re-entrained during channel sediment routing.
SPEXP	1-2	Exponent parameter for calculating sediment re-entrained in channel sediment routing
ADJ_PKR	0.1-2	Peak rate adjustment factor for sediment routing in the sub-basin (tributary channels).

Table 2.9. *Some parameters related to the routed phase of sediment.*

2.4.6 Erosion and sediment content on sub-daily time step

In SWAT, upstream erosion and sediment yield are estimated for each HRU with the MUSLE equation (Williams, 1975). Nevertheless, this equation is typically applied for estimating long-term average erosion and generally is not appropriate for continuous simulations with short (sub-daily) time steps (Jeong et al., 2011). For this reason, new algorithms were implemented on SWAT 2012 and thus a new structure for erosion and sediment processes was created (Fig. 2.5).

In the new structure, the calculation of the surface runoff is done separately for pervious and impervious areas in each HRU. The processes in the pervious areas are going to be described in the following chapters because they are the most relevant for the current Thesis work.

The **erosion by rainfall** also called **splash erosion** can be significant in short-duration/high-intensity storms because its high kinetic energy can generate important amounts of eroded sediment in short time:

$$D_R = k \cdot KE \cdot e^{-\varphi^* h} \quad (2\text{-}27)$$

Where:

D_R is the soil detachment by raindrop impact (g m^{-2} s^{-1})

k is an index of the detachability of the soil (g J^{-1})

KE is the total kinetic energy of the rain (J m^{-2})

φ^* is an exponent varying from 0.9 to 3.1

h is the surface runoff depth (mm)

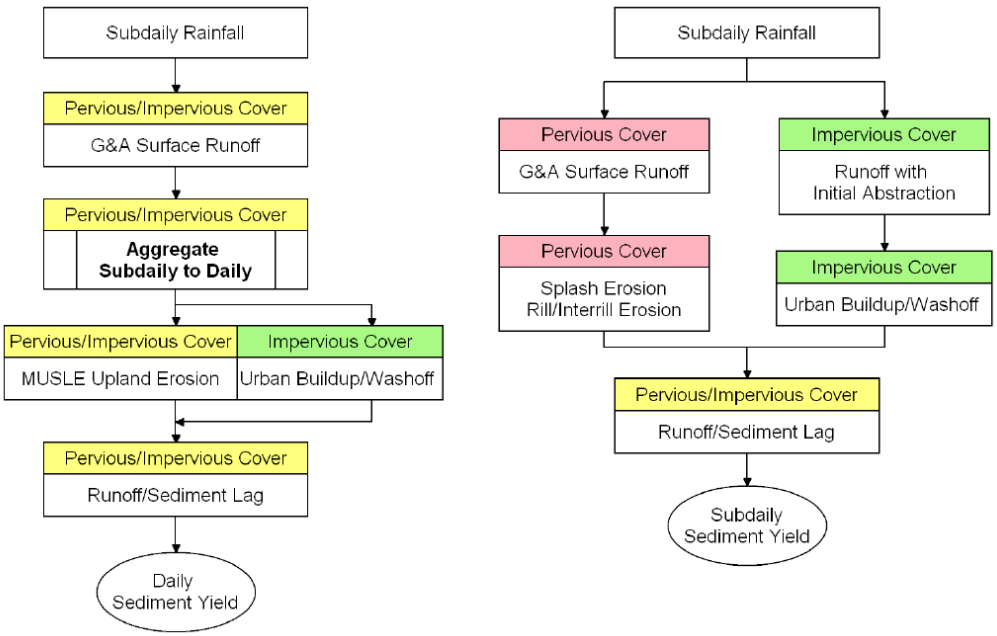

Figure 2.5. *Daily erosion processes in SWAT2005 (left) compared to sub-daily erosion processes (right) in SWAT 2012 (Jeong et al., 2011).*

For the calculation of the kinetic energy (KE) it is decisive the canopy interception. In this way, the KE is partitioned into direct through-fall estimated by Wischmeier & Smith (1978) and leaf drainage, estimated by Brandt (1990).

In addition to the splash erosion the **surface runoff routing** through the soil also generates erosion:

$$D_F = 11.02 \cdot \alpha^* \cdot K_f \cdot C_f \cdot \tau^{\beta^*} \quad (2\text{-}28)$$

Where:

D_F is the soil erosion rate (kg m^{-2} h^{-1})

K_f is the flow erodibility factor

C_f is the crop factor (Wischmeier, 1975)

α^* and β^* are calibration parameters

τ is the reach-average be shear stress (N m^{-2})

In stream, SWAT uses the Bagnold (1977) stream power function for the routing. Nevertheless, Richardson et al. (2011) suggest that this function does not work well in intermediate and small catchments. Hence, for the sub-daily **sediment routing** other two models were implemented: Yang (1996) and Brownlie (1982) functions. The first one achieves better results in small rivers (width < 10 m) and the second one in intermediate (width = 10 – 50 m).

VARIABLE NAME	*RANGE*	*DEFINITION*
EROS_SPL	0.9-3.1	Splash erosion coefficient
RILL_MULT	0.5-2	Rill erosion coefficient – multiplier to USLE_K for soil susceptible to rill erosion
EROS_EXPO	1.5-3	Exponential coefficient for overland flow
SUBD_CHSED	0=Bagnold 1=Brownlie 2=Yang	Instream sediment model
C_FACTOR	0.001/0.03/0.45	Scaling parameter for cover and management factor for overland flow erosion
CH_D50	10/50/100	Median particle diameter of main channel (mm)
SIG_G	1/1.57/5	Geometric standard deviation of particle size

***Table 2.10**. Some parameters for sub-daily erosion.*

The erosion and sediment transport models incorporated in SWAT for sub-daily predictions are physically based mechanistic models (Jeong et al., 2011).

In addition to the parameters described above (Tables 2.8 and 2.9) in the Table 2.10 in addition there are some other parameters described that have influence in the sub-daily sediment modelling.

2.4.7 Modelling process and evaluation methods

The modelling process can vary according to the select code, nevertheless the fundamental steps should be the same or at least similar. These fundamental steps are outlined in the figure 2.6.

The first steps are related to the definition of the objectives, the understanding of the natural system and the selection of the hydrological code. Once the code is selected, the objectives defined and the field data and the inputs collected, it is possible to proceed with the model construction. As already noted, in order to perform a modelling project with SWAT it is necessary to introduce a DEM, a land use map, a soil map and meteorological data. Having done that, the **evaluation criteria** are stablished, in any hydrological modelling project it is important to use several evaluation criteria (e.g. Legates & McCabe, 1999; Boyle et al., 2000). These criteria can vary depending on the objectives. In this case, as the objective of the hydrological modelling is to perform future hydrological projections, the evaluation criteria have been more restrictive than in other types of studies. Thus, several evaluation criteria (**statistical indices**) were used to evaluate the performance of the model (for calibration and validation):

- Nash-Sutcliffe efficiency (NSE): is a normalized statistic that determines the relative magnitude of the residual variance ("noise") compared to the measured data variance ("information") (Nash & Sutcliffe, 1970).

$$NSE = 1 - \left[\frac{\sum_{i=1}^{n}(Y_i^{obs} - Y_i^{sim})^2}{\sum_{i=1}^{n}(Y_i^{obs} - Y^{obs\,mean})^2}\right] \quad (2\text{-}29)$$

Where:

Y_i^{obs} is the *i*th observation value for the constituent being evaluated

Y_i^{sim} is the *i*th simulated value for the constituent being evaluated

$Y^{obs\,mean}$ is the mean of observed data for the constituent being evaluated

n is the total number of observations

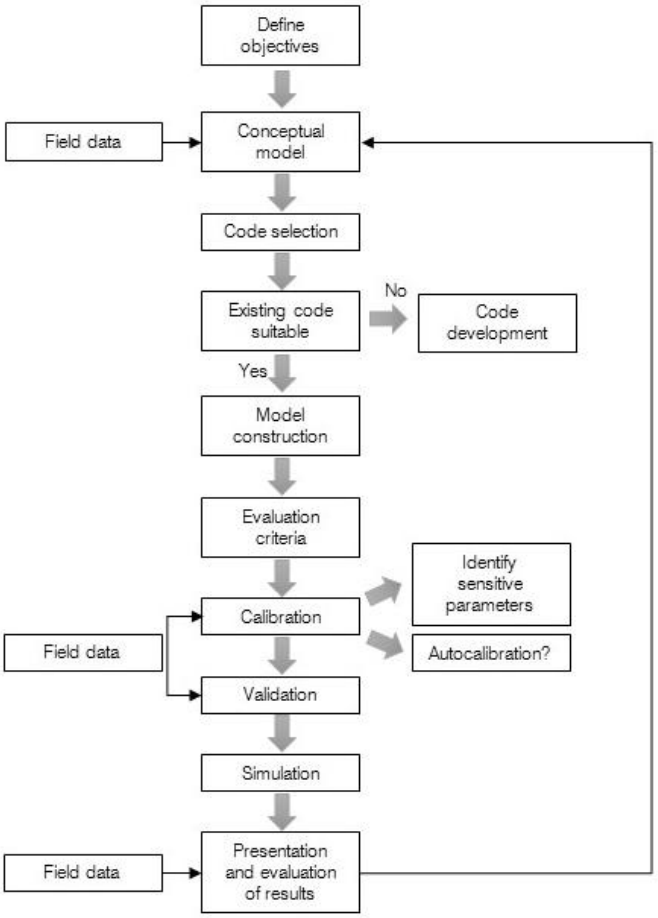

Figure 2.6. *Fundamental steps in the hydrological modelling (modified from Refsgaard, 1997).*

NSE ranges between $-\infty$ and 1, with NSE $=1$ being the optimal value. This statistical index is sensitive to extreme values due to the squared differences (Krause et al., 2005) and cannot help in the identification of model bias. In addition, it is not recommended to use the index for single-event simulation because it does not identify the magnitude and the timing of peak flows and the shape of recession curves. Nevertheless, it is a very commonly used index, hence, it can be used for comparison purposes. Besides, the index is good to be used with continuous long-term simulations and it is robust and can be used to evaluate the model performance for several outputs and time steps.

- The coefficient of determination (R^2): describes the degree of collinearity between simulated and measured data, specifically, the proportion of the variance in measured data explained by the code.

$$R^2 = \left[\frac{\sum_{i=1}^{n}(Y_i^{obs} - Y^{obs\,mean})(Y_i^{sim} - Y^{sim\,mean})}{\sqrt{\sum_{i=1}^{n}(Y_i^{obs} - Y^{obs\,mean})^2}\sqrt{\sum_{i=1}^{n}(Y_i^{sim} - Y^{sim\,mean})^2}} \right]^2 \quad (2\text{-}30)$$

Where:

Y_i^{obs} is the *i*th observation value for the constituent being evaluated
Y_i^{sim} is the *i*th simulated value for the constituent being evaluated
$Y^{obs\,mean}$ is the mean of observed data for the constituent being evaluated
$Y^{sim\,mean}$ is the mean of simulated data for the constituent being evaluated
n is the total number of observations

r^2 ranges from 0 to 1, with higher values indicating less error variance. The index overestimates the high extreme values (Krause et al., 2005) and does not indicate the additive and proportional differences between simulated and observed data (Legates & McCabe, 1999). This is a widely used statistical index in hydrological modelling therefore, as in the case of NSE, can be used to compare with other research works.

- The percent bias (PBIAS): measures the average tendency of the simulated data to be larger or smaller than their observed counterparts (Gupta et al., 1999).

$$PBIAS = \left[\frac{\sum_{i=1}^{n}(Y_i^{obs} - Y^{sim}) * 100}{\sum_{i=1}^{n}(Y_i^{obs})} \right] \quad (2\text{-}31)$$

Where:

Y_i^{obs} is the *i*th observation value for the constituent being evaluated
Y_i^{sim} is the *i*th simulated value for the constituent being evaluated
n is the total number of observations

The optimal value of PBIAS is 0; positive values indicate model underestimation bias, and negative values indicate model overestimation bias. This index cannot

be used in a single-event or to determine trends in the outputs. Nevertheless, it can be used to determine how well the model simulates average magnitudes, it is good for long-term simulations, it is robust and commonly used and it can help in the identification of average simulation bias. It is recommendable to use the PBIAS with other statistical indexes and graphical methods because when the simulation underpredicts as much as overpredicts, the index will be close to 0 even though the results are poor.

- Standard deviation ratio (RSR): is the ratio of the root mean square error to the standard deviation of measured data (Moriasi et al., 2007).

$$RSR = \left[\frac{\sum_{i=1}^{n} \sqrt{\left(Y_i^{obs} - Y^{sim}\right)^2}}{\sum_{i=1}^{n} \sqrt{\left(Y_i^{obs} - Y^{sim\ mean}\right)^2}} \right] \quad (2\text{-}32)$$

Where:

Y_i^{obs} is the *i*th observation for the constituent being evaluated

Y_i^{sim} is the *i*th simulated value for the constituent being evaluated

$Y^{sim\ mean}$ is the mean of simulated data for the constituent being evaluated

n is the total number of observations

RSR varies from the optimal value of 0 to $+\infty$. It gives more weight to high values and it can be applied to various output responses. It is a relatively new statistical index therefore has not been widely used in hydrological modelling studies.

Based on Moriasi et al. (2007), table 2.8 shows the values of statistical indexes to consider de calibration and validation “very good”, “good”, “satisfactory” or “unsatisfactory”. In 2015, the same author (Moriasi et al., 2015) published a research work with new evaluation values for statistical indexes. In this work, the simulations are at least “satisfactory” when $r^2 > 0.60$, NSE>0.50, and PBIAS$\leq \pm 15\%$ for streamflow and $r^2 > 0.40$, NSE >0.45 and PBIAS$\leq \pm 20$ % for sediment.

Performance rating	RSR	NSE	PBIAS %	
			Streamflow	Sediment
Very good	0≤RSR≤0.5	0.75<NSE≤1	PBIAS≤±10	PBIAS≤±15
Good	0.5≤RSR≤0.6	0.65<NSE≤0.75	±10≤PBIAS<±15	±15≤PBIAS<±30
Satisfactory	0.6≤RSR≤0.7	0.5<NSE≤0.65	±15≤PBIAS<±25	±30≤PBIAS<±55
Unsatisfactory	RSR>0.7	NSE≤0.5	PBIAS≥±25	PBIAS≥±55

Table 2.11. *General performance ratings for recommended statistics indexes for a monthly time step (From Moriasi et al., 2007). * Values of R^2 greater than 0.5 are considered "acceptable" based on criteria reported by Santhi et al. (2001) and Van Liew et al. (2003).*

To ensure that the model is simulating well not only the mean hydrograph values but also the high and low values, the observed discharge and the simulated were separated in surface runoff and baseflow with an automated digital filter program; Base Flow Filter Program-BFP (Arnold et al., 1995). Once the observed and simulated discharges were divided in these two components, the statistical indexes described before were used to evaluate the model performance for surface runoff and baseflow.

To ensure the goodness of the modelling process and determine its uncertainty for future hydrological projections, these statistical indices were also used in differentiated climate conditions. Considering that future climate scenarios often project a more extreme climate than that observed in recent decades for the North of the Iberian Peninsula (e.g. Brunet et al, 2009; CEDEX, 2010; IPCC, 2013), as proposed by Brigode et al. (2013), the 3 consecutive driest and wettest years were chosen to analyse whether the calibrated model is able to correctly simulate extreme conditions. The driest and wettest years were selected by calculating an "Aridity Index" (hereafter AI) for all the available data (calibration and validation period), where this index is deemed to be the ratio between potential evapotranspiration and precipitation (Görgen et al., 2010; Brigode et al., 2013).

Finally, the SWAT CUP program (Abbaspour et al., 2007a) using the SUFI2 algorithm (Abbaspouret al., 2004, 2007a) was used to do an

autocalibration and evaluate the uncertainty. The program calculates two factors to quantify the degree of uncertainty of each iteration. The p-factor is the percentage of measured data bracketed by the 95 % prediction uncertainty (95PPU). A value of 1 indicates 100 % bracketing of the measured data. The r-factor is the average thickness of the 95PPU band divided by the standard deviation of the measured data. The r-factor seeks to bracket most of the measured data with the smallest possible value (Abbaspour et al., 2007b). A working value of >0.7 for p-factor and <1.5 for r-factor is recommended (Abbaspour et al., 2015).

Thus, it is possible to apply the model evaluation criteria for daily discharge in different time periods (annually and seasonally) and in years with low and high AI. With this information, it is achievable to evaluate whether the performance of the model is good enough to simulate the future climate projections and also to identify where the largest uncertainties are.

When the observed and the simulated variables do not fit well, the usual process is the **calibration** which consist on adjusting the value of the parameters of the model to obtain a better simulation. The first step in the calibration process is to identify the most **sensitive parameters** for the catchment. To achieve this, SWAT 2005 interface offered the Latin Hypercube One-At-a-Time sensitivity analysis (van Griensven et al., 2006). This method involves taking a certain number of Latin Hypercube sample points for the same number of intervals and varying each of these sample points several times by changing each of the parameters one at a time, as is characteristic of the One-At-a-Time design. It ensures that the full range of the parameters are sampled with a certain precision and ensures that the changes in the output in each model run can be unambiguously attributed to the parameter that was changed. SWAT 2012 does not offer any sensitivity analysis, instead it is necessary to use the SWAT CUP program. With this program it is possible to perform a One-At-a-Time and a global sensitivity analysis. The methodology for the global sensitivity analysis is the same as the One-At-a-Time but instead of changing each parameter one at a time, all the parameters are changed simultaneously. According to Arnold et al. (2012) *the two analyses may yield different results, however both procedures*

provide insight into the sensitivity of the parameters and are necessary steps in model calibration.

In order to facilitate the calibration process and to obtain better results, the **autocalibration** tools for hydrological modelling emerged. These tools help considerably to achieve the best values of the parameters (or ranges), saving much of the effort involved in manual calibration (van Liew et al., 2005). The autocalibration program changes the values of the parameters over and over again until it achieves the defined criteria (a value in an objective function).

The specific methodology used in this Thesis to calibrate the model is defined bellow:

1. Select the calibration and validation years. The observed data must include wet, average and dry years (Gan et al., 1997). Because the future climate is generally expected to change, this criterion is even more important in studies of climate change impacts.

2. Perform a sensitivity analysis with the One-At-a-Time methodology. For flow and sediment this analysis was made with the highest number of parameters that influences each variable.

A manual calibration of the most sensitive parameters was made. The objective of this calibration was to identify the reasonable value range of each parameter. The calibration was made continuously comparing the observed variables (field data) and the simulated with the model and with the statistical indices described above. SWAT input parameters are process based therefore they must be changed within a realistic uncertainty range (Arnold et al., 2012).

3. Once the value range of each parameter was determined, they were introduced in the SWAT CUP program to perform an autocalibration with the SUFI2 algorithm (Abbaspour et al., 2004, 2007a). The objective function was different depending on the objectives but the most usual were the PBIAS and the R^2.

4. When the statistical indices calculated by SWAT CUP and the p and r-factor were at least satisfactory, it was possible to perform the rest of the

evaluation criteria (statistical indices of baseflow and surface runoff and aridity index) and decide if the calibration was good enough. If so, it was possible to start with the validation, otherwise it was necessary to continue with the calibration. In addition, in all the process it was verified that other important model outputs were reasonable.

After the calibration, the **validation** is conducted. This process consists on performing a simulation using parameters that were determined during calibration and comparing the results with observed data not used in the calibration. As reported by Refsgaard (1997) the model validation is the process of demonstrating that a given modelling project (specific for the study catchment) can make sufficiently accurate simulation, although "sufficiently accurate" can vary based on project objectives. The evaluation criteria described above were those used for both calibration and validation.

Finally, when the model is calibrated and validated it is possible to perform simulations changing input parameters like meteorological data or land uses.

2.5 METHODOLOGY TO EVALUATE THE HYDROLOGICAL IMPACT OF THE CLIMATE PROJECTIONS

For the purpose of studying the impact of the climatic projections (discharge and sediments), these have been divided in three 30 year future horizons: 2030s, 2060s and 2090s. When examining the hydrologic and sediment flux effects of future climate scenarios, changes were calculated relative to the results from the GCM baseline simulations rather than the historic observations. This convention avoids, at least to first order, the effects of model bias (Nijssen et al., 2001). This evaluation was done at annual and seasonal scales.

Besides that, a study of trends for high (Q80), average (Qm) and low flow (Q20) discharge series was made following the methodology described in Zabaleta et al. (2012). To make this analysis, the duration of high and low flow periods and the severity of low flows were calculated (Hisdal et al., 2001; Wilson et al., 2010) and their trends analysed. The **duration** is considered as the period

of time (in days) with a discharge value lower than the 0.2 percentile (Q20) for low flows and higher than the 0.8 percentile (Q80) for high flows (Fig. 2.7). Annual and seasonal durations were taken into consideration. The use of Q20 and Q80 percentiles, diminishes the weight of extreme maximum and minimum values, which may be subject to measurement error, and provides robustness to the results obtained in the statistical analysis. **Severity** defines the discharge deficit (volume) below Q20 for low flow and is considered annually. Quantiles, duration, or deficit, have been used by several authors to assess low flows (Smakhtin, 2001; Ouarda et al., 2008).

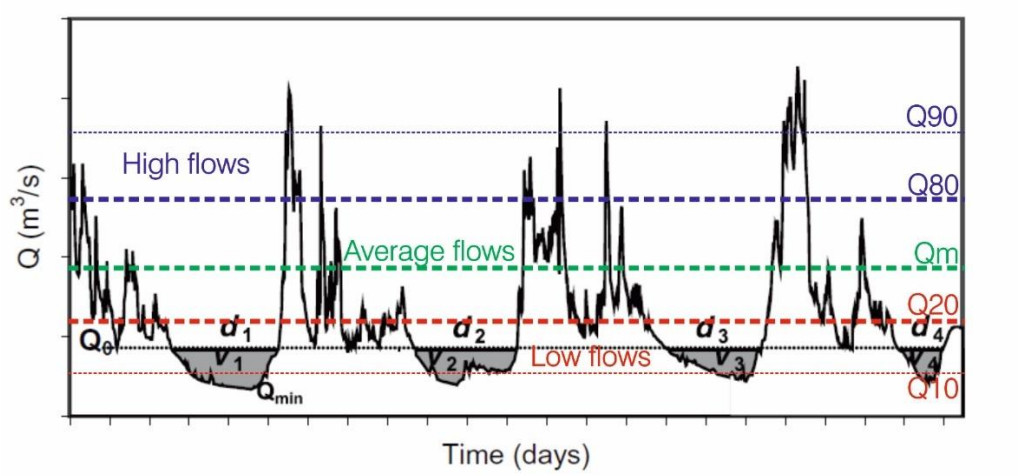

Figure 2.7. *Division of the hydrograph and associated percentiles (Q) (Modified from Wilson et al., 2010; Zabaleta & Antiguedad, 2012).*

The Mann-Kendall nonparametric trend test (Mann, 1945; Kendall, 1975) was applied to the series calculated for these variables (average flows, duration of high and low flows and severity of low flows). This is a non-parametric test that evaluates the data as time series and compares the relative magnitudes of the data instead of their values. It is usual to assume that the data series are serially independent, nevertheless streamflow series may frequently display statistical significant serial correlation. To avoid these possible distorting influences, an approach developed by Yue et al. (2002) was applied to the output series. In this method, the slope of the trend is estimated by the approximation of Theil-Sen; if this is very close to zero, it is not necessary to perform the trend analysis (since it is assumed that there is no trend), if it separates from zero it is assumed that

this trend is linear, the trend of the series is eliminated by the slope obtained and the autocorrelation at time step 1 of the series without trend is calculated. This procedure is known as Trend Free Pre-whitening (TFPW). The residual series, once the autocorrelation is eliminated, should be an independent series. To conclude, this independent series and the estimated trend at the beginning of the procedure are used to apply the Mann-Kendall test to this new series and to evaluate the statistical significance of the trend. The test procedure is as follows:

1. Calculate the statistic S of Kendall´s tau that is defined as:

$$S = \sum_{i=1}^{n-1} \sum_{j=i+1}^{n} sgn(X_j - X_i) \quad (2\text{-}33)$$

Where,

X_j are the sequential data values

n is the length of the data set and $sgn(X_j - X_i)$ is:

$$sgn(X_j - X_i) = \begin{cases} 1 \; if \; X_j - X_i > 0 \\ 0 \; if \; X_j - X_i = 0 \\ -1 \; if \; X_j - X_i < 0 \end{cases} \quad (2\text{-}34)$$

The null hypothesis is that the sample of data is independent and identically distributed. The alternative hypothesis is that a trend exists in X. A very high positive value of S indicates an increasing trend and a very negative value indicate a decreasing trend.

2. Calculate the variance of S:

$$VAR(S) = \frac{1}{18}[n(n-1)(2n+5) - \sum_{m=1}^{n} t_m m(m-1)(2m+5)] \quad (2\text{-}35)$$

Where,

t_m is the number of ties of extent *m*

n is the number of data points

3. Compute a normalized test statistic Z:

$$Z = \begin{cases} \frac{S-1}{\sqrt{VAR(S)}} & S > 0 \\ 0 & S = 0 \\ \frac{S+1}{\sqrt{VAR(S)}} & S < 0 \end{cases} \quad (2\text{-}36)$$

4. Compute the probability associated with this normalized test statistic. Z follows the normal distribution with a mean of 0 as standard deviation of 1.

The trend test was carried out with the help of the package zyp version 0.10-1 (Bronaugh & Werner, 2014) of Free Software R (R Studio, version 0.98.1087).

Therefore, with the Mann-Kendall test it is possible to identify increasing and decreasing trends and the probability of occurrence (P) of those trends. The value of P can vary between 0 and 1, where 0 indicates that there is no probability of occurrence in the trend and 1 indicates maximum probability. The criteria suggested by the IPCC (IPCC, 2013) in its 5th report was used to evaluate P. In this document, likelihood refers to a probabilistic assessment of some well-defined past or future outcomes. The categories defined and used in this research are described in Table 2.12:

TERMINOLOGY	PROBABILITY OF OCCURRENCE
Virtually certain trend	>0.99 probability of occurrence
Extremely probable trend	>0.95 probability of occurrence
Very probable trend	>0.90 probability of occurrence
Probable trend	>0.66 probability of occurrence

Table 2.12. *The criteria suggested by the IPCC (IPCC, 2013) to evaluate the provability of occurrence (P). Values of P below 0.66 are considered to represent non-probable trends in this Thesis, therefore there are not represented in this table.*

2.6 REFERENCES

Abbaspour, K.C., Faramarzi, M., Ghasemi, S.S., Yang, H. 2009. Assessing the impact of climate change on water resources in Iran. Water Resources Research. 45, W10434.

Abbaspour, K.C., Johnson, C.A., van Genuchten, M.T. 2004. Estimating uncertain flow and transport parameters using a sequential uncertainty fitting procedure. Vadose Zone Journal. 3 (4), 1340–1352. http://dx.doi.org/10.2113/3.4.1340.

Abbaspour, K.C., Rouholahnejad, E., Vaghefi, S., Srinivasan, R., Yang, H., Kløve, B. 2015. A continental-scale hydrology and water quality model for Europe: Calibration and uncertainty of a high-resolution large-scale SWAT model. Journal of Hydrology. 524 (0), 733-752. http://dx.doi.org/10.1016/j.jhydrol.2015.03.027.

Abbaspour, K.C., Vejdani, M., Haghighat, S. 2007a. SWATCUP calibration and uncertainty programs for SWAT. International Congress on Modelling and Simulation (MODSIM). 7, 1603-1609.

Abbaspour, K.C., Yang, J., Maximov, I., Siber, R., Bogner, K., Mieleitner, J., Zobrist, J., Srinivasan, R. 2007b. Modelling hydrology and water quality in the pre-alpine/alpine Thur watershed using SWAT. Journal of Hydrology. 333(2–4), 413-430. http://dx.doi.org/10.1016/j.jhydrol.2006.09.014.

AEMET. 2008. Generación de escenarios regionalizados de cambio climático para España. Madrid: Ministerio de Medio Ambiente, Medio Rural y Marino.

Allen, R.G. 1986. A Penman for all seasons. Journal of Irrigation and Drainage Engineering, ASCE. 112(4), 348-368.

Allen, R.G., Jensen, M.E., Wright, J.L., Burman, R.D. 1989. Operational estimates of evapotranspiration. Agronomy Journal. 81:650-662.

Arabi, M., Govindaraju, R.S., Hantush, M.M., Engel, B.A. 2006. Role of watershed subdivision on modeling the eff ectiveness of best management practices with SWAT. Journal of the American Water Resources Association. 42(2):513–528. http://dx.doi.org/10.1111/j.1752-1688.2006.tb03854.x.

Arnold, J.G., Allen, P.M., Bernhardt, G. 1993. A comprehensive surface-groundwater flow model. Journal of Hydrology. 142(1–4), 47-69. http://dx.doi.org/10.1016/0022-1694(93)90004-S.

Arnold, J.G., Allen, P.M., Muttiah, R., Bernhardt, G. 1995. Automated base flow separation and recession analysis technique. Ground Water. 33(6), 1010–1018. http://dx.doi.org/10.1111/j.1745-6584.1995.tb00046.x.

Arnold, J.G., Moriasi, D.N., Gassman, P.W., Abbaspour, K.C., White, M.J., Srinivasan, R., Santhi, C., Harmel, R.D., van Griensven, A., van Liew, M.W., Kannan, N., Jha, M.K.

2012. SWAT: Model use, calibration, and validation. Transactions of the ASABE. 55 (4), 1491-1508.

Arnold, J.G., Srinivasan, R., Muttiah, R.S., Williams, J.R. 1998. Large area hydrologic modeling assessment: part I. Model development. Journal of American Water Resources Association. 34(1), 73–89.

Awan, U.K., Ismaeel, A. 2014. A new technique to map groundwater recharge in irrigated areas using a SWAT model under changing climate. Journal of Hydrology. 519, Part B, 1368-1382. http://dx.doi.org/10.1016/j.jhydrol.2014.08.049.

Bagnold, R. 1977. Bed load transport by natural rivers. Water Resources Research. 13(2), 303-312. http:/dx.doi.org/10.1029/WR013i002p00303.

Behera, S., Panda, R.K. 2006. Evaluation of management alternatives for an agricultural watershed in a sub-humid subtropical region using a physical process model. Agriculture, Ecosystems & Environment. 113(1–4):62–72. http://dx.doi.org/10.1016/j.agee.2005.08.032.

Bodego, A., Mendia, M., Aranburu, A., Apraiz, A. 2014. Geología de la Cuanca Vasco-Cantábrica. Ed. Euskal Herriko Unibertsitatea. Argitarapen Zerbitzua. ISBN: 8498609917.

Boorman, D.B., Sefton, C.E.M. 1997. Recognizing the uncertainty in the quantification of the effects of climate change on hydrological response. Climatic Change 35 (4), 415–434.

Bouraoui, F., Benabdallah, S., Jrad, A., Bidoglio, G. 2005. Application of the SWAT model on the Medjerda river basin (Tunisia). Physics and Chemistry of the Earth, Parts A/B/C. 30, 497-507.

Boyle, D.P., Gupta, H.V., Sorooshian, S. 2000. Toward improved calibration of hydrologic models: Combining the strengths of manual and automatic methods. Water Resources Reserch. 36(12), 3663-3674.

Brands, S., Herrera, S., San-Martin, D., Gutierrez, J.M. 2011. Validation of the ENSEMBLES global climate models over southwester Europe using probability density functions, from a downscaling perspective RID C-5754-2009. Climate Ressearch. 48(2-3),145-161.

Brandt, C. J. 1990. Simulation of the size distribution and erosivity of raindrops and throughfall drops. Earth Surface Processes and Landforms. 15(8), 687-698. http://dx.doi.org/10.1002/esp.3290150803.

Brigode, P., Oudin, L., Perrin, C. 2013. Hydrological model parameter instability: A source of additional uncertainty in estimating the hydrological impacts of climate change? Journal of Hydrology. 476 (0), 410-425. http://dx.doi.org/10.1016/j.jhydrol.2012.11.012.

Bronaugh, D., Werner, A. 2014. Zhang + Yue-Pilon trends package. R Package 'zyp'.

Brownlie, W. 1982. Prediction of flow depth and sediment discharge in open channels. PhD diss. Pasadena, Cal.: California Institute of Technology.

Brunet, B., Casado, M.J., de Castro, M., Galán, P., López, J.A., Martín, J.M., Pastor, A., Petisco, E., Ramos, P., Ribalaygua, J., Rodríguez, E., Sanz, I., Torres, L., 2009. Generacio□n de Escenarios Regionalizados de Cambio Clima□tico para Espan□a. Spanish Meteorological Agency (AEMET).http://www.aemet.es/documentos/es/serviciosclimaticos/cambio_climat/datos_diarios/Informe_Escenarios.pdf. Accessed 5 August 2015.

Casado, M.J., Martín, J.M, Pastor, M.A., Rodríguez, E. 2011. Evaluación de los modelos climáticos globales participantes en el Cuarto Informe de Evaluación del IPCC sobre España y la región euroatlántica. Agencia Estatal de Meteorología, Madrid.

CEDEX (Centro de Estudios y Experimentación de Obras Públicas) 2010. Necesidades de adaptación al cambio climático de la red troncal de infraestructuras de transporte en España. Informe final. http://www.adaptecca.es/sites/default/files/editor_documentos/accit_informe_final_septiembre_2013.pdf. Accessed 5 August 2015.

Cerro, I., Antiguedad, I., Srinavasan, R., Sauvage, S., Volk, M., Sanchez-Perez, J.M. 2014. Simulating land management options to reduce nitrate pollution in an agricultural watershed dominated by an alluvial aquifer. Journal of Environmental Quality. 43, 67-74. http:/dx.doi.org/10.2134/jeq2011.0393.

Chirivella, V., Capilla, J. E., Pérez-Martín, M. A. 2015. Modelling regional impacts of climate change on water resources: The Jucar basin, Spain. Hydrological Sciences Journal. 60 (1), 30-49. http://dx.doi.org/10.1080/02626667.2013.866711.

Chow, V.T., Maidment, D.R., Mays, L.W. (Eds.). 1998. Applied Hydrology. McGrawHill, New York, USA.

Engman, E.T. 1983. Roughness coefficients for routing surface runoff. Proc. Spec. Conf. Frontiers of Hydraulic Engineering.

Epelde, A.M., Cerro, I., Sanchez-Perez, J.M., Sauvage, S., Srinivasan, R., Antigueedad, I. 2015. Application of the SWAT model to assess the impact of changes in agricultural management practices on water quality. Hydrological Sciences Journal-Journal Des Sciences Hydrologiques. 60, 825-843.

Errasti, I., Ezcurra, A., Sáenz, J., Ibarra-Berastegi, G. 2011. Validation of IPCC AR4 models over Iberian Peninsula. Theoretical and Applied Climatology. 103, 61-79.

FAO, 1998. Allen, R.G., Pereira, L.S., Raes, D., Smith, M. Crop evapotranspiration - Guidelines for computing crop water requirementsEd: Food and Agriculture Organization of the United Nations. SBN 92-5-104219-5

Furl, C., Sharif, H., Jeong, J. 2015. Analysis and simulation of large erosion events at central Texas unit source watersheds. Journal of Hydrology. 527, 494-504. http://dx.doi.org/10.1016/j.jhydrol.2015.05.014.

Gan, Y.T., Dlamini, E.M., Biftu, G.F. 1997. Effects of model complexity and structure, data quality, and objective functions on hydrologic modeling. Journal of Hydrology. 192, 81-103. http://dx.doi.org/10.1016/S0022-1694(96)03114-9.

Giorgi, F., Mearns, L.O. 2002. Calculation of average, uncertainty range, and reliability of regional climate changes from AOGCM simulations via the ''reliability ensemble averaging'' (REA) method. Journal of Climate. 15, 1141–1158.

Görgen, K., Beersma, J., Brahmer, G., Buiteveld, H., Carambia, M., de Keizer, O., Krahe, P., Nilson, E., Lammersen, R., Perrin, C., Volken, D. 2010. Assessment of Climate Change Impacts on Discharge in the Rhine River Basin: Results of the RheinBlick2050 Project, CHR Report. 1–23, 229 pp, Lelystad. ISBN 978-90-70980-35-1.

Graham, L.P., Andréasson, J., Carlsson, B. 2007. Assessing climate change impacts on hydrology from an ensemble of regional climate models, model scales and linking methods – a case study on the Lule River Basin. Climatic Change. 81 (1), 293-307. http://dx.doi.org/10.1007/s10584-006-9215-2.

Green, W.H., Ampt, G.A. 1911. Studies on soil physics. The Journal of Agricultural Science. 4(1), 1-24. http://dx.doi.org/10.1017/S0021859600001441.

Grusson, Y., Sun, X., Gascoin, S., Sauvage, S., Raghavan, S., Anctil, F., Sáchez-Pérez, J. 2015. Assessing the capability of the SWAT model to simulate snow, snow melt and streamflow dynamics over an alpine watershed. Journal of Hydrology. 531, Part 3, 574-588.

Gupta, H.V., Sorooshian, S., Yapo, P.O. 1999. Status of automatic calibration for hydrologic models: Comparison with multilevel expert calibration. Journal of Hydrologic Engineering. 4 (2), 135-143.

Hargreaves, G.H., Samani, Z.A. 1985. Reference crop evapotranspiration from temperature. Applied Engineering in Agriculture. 1, 96-99.

Hempel, S., Frieler, K., Warszawski, L., Schewe, J., Piontek, F. 2013. A trend-preserving bias correction – the ISI-MIP approach. Earth System Dynamics. 4, 219-236. http://dx.doi.org/10.5194/esd-4-219-2013.

Hisdal, H., Stahl, K., Tallaksen, L.M., Demuth, S. 2001. Have streamflow droughts in Europe become more severe or frequent? International Journal of Climatology. 21, 317–333. http://dx.doi.org/10.1002/joc.619.

Hooghoudt, S.B. 1940. Bijdrage tot de kennis van enige natuurkundige grootheden van de grond. Versl. Landbouwkd. Onderz. 46: 515-707.

http://cmip-pcmdi.llnl.gov/

http://ensembles-eu.metoffice.com/docs/Ensembles_final_report_Nov09.pdf

IPCC 2013 Climate Change 2013: The Physical Science Basis. Contribution of Working Group I to the Fifth Assessment Report of the Intergovernmental Panel on Climate Change (Cambridge: Cambridge University Press).http://doi.org/10.1175/2009JCLI2681.1.

IPCC SRES. 2000. Special Report on Emissions Scenarios: A special report of Working Group III of the Intergovernmental Panel on Climate Change (Cambridge University Press).

IPCC. 2007. Climate Change 2007: The Physical Science Basis. Contribution of Working Group I to the Fourth Assessment Report of the Intergovernmental Panel on Climate Change (Cambridge: Cambridge University Press).

Jeong, J., Kannan, N., Arnold, J., Glick, R., Gosselink, L., Srinivasan, R. 2010. Development and Integration of Sub-hourly Rainfall-Runoff Modeling Capability Within a Watershed Model. Water Resources Management. http://dx.doi.org/10.1007/s11269-010-9670-4.

Jeong, J., Kannan, N., Arnold, J.G., Glick, R., Gosselink, L., Srinivasan, R., Harmel, R.D. 2011. Development of Sub-Daily Erosion and Sediment Transport Algorithms for SWAT. Transactions of the ASABE. 54(5), 1685-1691. http://dx.doi.org/10.13031/2013.39841.

Kendall, M.G. 1975. Rank correlation measures. Charles Griffin. London, UK.

Krause, P., Boyle, D., Bäse, F. 2005. Comparison of different efficiency criteria for hydrological model assessment. Advances in Geosciences. 5, 89-97. http://dx.doi.org/10.5194/adgeo-5-89-2005.

Legates, D.R., McCabe, G.J. 1999. Evaluating the use of “goodness-of-fit” measures in hydrologic and hydroclimatic model validation. Water Resources Research. 35(1), 233-241. http://dx.doi.org/10.1029/1998WR900018.

Lenderink, G., Buishand, A., van Deursen, W., 2007. Estimates of future discharges of the river Rhine using two scenario methodologies: direct versus delta approach. Hydrology and Earth System Sciences. 11 (3), 1145–1159. http://dx.doi.org/10.5194/hess-11-1145-2007.

Lin, B., Chen, X., Yao, H., Chen, Y., Liu, M., Gao, L., James, A. 2015. Analyses of landuse change impacts on catchment runoff using different time indicators based on SWAT model. Ecological Indicators. 58, 55-63.

Lirong, S., Jianyun, Z. 2012. Hydrological response to climate change in Beijiang river basin based on the SWAT model. Procedia Engineering. 28, 241-245. http://dx.doi.org/10.1016/j.proeng.2012.01.713.

Loidi, J., Biurrun, I., Campos, J.A., García-Mijangos, I., Herrera, M. 2011. La vegetación de la Comunidad Autónoma del País Vasco. Leyenda del mapa de series de vegetación a escala 1:50.000. ISBN/ISSN: 978-84-694-4731-4. https://web-argitalpena.adm.ehu.es/pdf/UWLGBI7314.pdf (25/3/2017).

Maharjan, G.R., Park, Y.S., Kim, N.W., Shin, D.S., Choi, J.W., Hyun, G.W., Jeon, J.H., Ok, Y.S., Lim, K.J. 2013. Evaluation of SWAT sub-daily runoff estimation at small agricultural watershed in Korea. Frontiers of Environmental Science and engineering. 7(1), 109-119. http://dx.doi.org/10.1007/s11783-012-0418-7.

Mann, H.B. 1945. Non-Parametric tests against trend. The Econometric Society. 13, 245–259. http://dx.doi.org/10.2307/1907187.

Monteith, J.L. 1965. Evaporation and the environment. In The state and movement of water in living organisms, XIXth Symposium. Society for Experimental Biology. p. 205-234. Swansea, Cambridge University Press.

Moriasi, D.N., Arnold, J.G., van Liew, M.W., Bingner, R.L., Harmel, R.D., Veith, T.L. 2007. Model evaluation guidelines for systematic quantification of accuracy in watershed simulations RID H-4911-2011. Transactions of the ASABE. 50, 885-900.

Moriasi, D.N., Gitau, M.W., Pai, N., Daggupati, P. 2015. Hydrologic and Water Quality Models: Performance Measures and Evaluation Criteria. Transactions of the ASABE. 58, 1763-1785.

Murphy, J.M., Sexton, D.M.H., Barnett, D.N., Jones, G.S., Webb, M.J., Collins, M., Stainforth, D.A. 2004. Quantification of modelling uncertainties in a large ensemble of climate change simulations. Nature. 430, 768–772.

Nash, J.E., Sutcliffe, J.V. 1970. River flow forecasting through conceptual models: Part 1. A discussion of principles. Journal of Hydrology. 10(3), 282-290. http://dx.doi.org/10.1016/0022-1694(70)90255-6.

Natural Resources Conservation Service (NRCS) Soil Survey Staff. 1996. National soil survey handbook, title 430-VI. U.S. Government Printing Office, Washington, D.C.

Nearing, M.A., Liu, B.Y., Risse, L.M., Zhang, X. 1996 Curve numbers and Green–Ampt effective hydraulic conductivities. JAWRA Journal of the American Water Resources Association. 32, 125–136.

Neitsch, S.L., Arnold, J.G., Kiniry, J.R., Williams, J.R. 2011. Soil and Water Assessment Tool user's manual version 2009. Available in: wwwswat.tamu.edu.

Nieto, S., Rodriguez-Puebla, C. 2006. Comparison of precipitation from observed data and general circulation models over the Iberian peninsula. Journal of Climate. 19(17), 4254-4275.

Nijssen, B., O'donnell, G.M., Hamlet, A.F., Lettenmaier, D.P. 2001. Hydrologic sensitivity of global rivers to climate change. Climate Change. 50, 143–175.

Ouarda, T.B.M.J., Charron, C., St-Hilaire, A. 2008. Statistical models and the estimation of low flows. Canadian Water Resources Journal. 33 (2), 195-206. http://dx.doi.org/10.4296/cwrj3302195.

Overton, D. 1966. Muskingum flood routing of upland streamflow. Journal of Hydrology. 4, 185-200.

Parajuli, P.B. 2010. Assessing sensitivity of hydrologic responses to climate change from forested watershed in Mississippi. Hydrological Processes. 24(26):3785–3797. http://dx.doi.org/10.1002/hyp.7793.

Peraza-Castro, M., Ruiz-Romera, E., Montoya-Armenta, L.H., Sanchez-Perez, J.M., Sauvage, S. 2015. Evaluation of hydrology, suspended sediment and Nickel loads in a small watershed in Basque Country (Northern Spain) using eco-hydrological SWAT model. Annales De Limnologie-International Journal of Limnology. 51, 59-70.

Perez, J., Menendez, M., Mendez, F., Losada, I. 2014. Evaluating the performance of CMIP3 and CMIP5 global climate models over the north-east Atlantic region. Climate Dynamics. 43 (9-10), 2663-2680. http://dx.doi.org/10.1007/s00382-014-2078-8.

Priestley, C.H.B., Taylor, R.J. 1972. On the assessment of surface heat flux and evaporation using large-scale parameters. Monthly Weather Review. 100:81-92.

Qiu, L., Zheng, F., Yin, R. 2012. SWAT-based runoff and sediment simulation in a small watershed, the loessial hilly-gullied region of China: Capabilities and challenges. International Journal of Sediment Research. 27(2), 226-234.

qiuMein, R., Larson, C. 1973. Modeling infiltration during a steady rain. Water Resources Research. 9(2), 384–394. http://dx.doi.org/10.1029/WR009i002p00384.

Rawls, W.J., Brakensiek, D.L. 1985. Prediction of soil water properties for hydrologic modeling. p. 293-299. In E.B. Jones and T.J. Ward (eds). Watershed management in the 80's. ASCE, New York, N.Y.

Refsgaard, J.C.. 1997. Parameterisation, calibration and validation of distributed hydrological models. Journal of Hydrology. 198, 69-97.

Richardson, E., Simons, D., Lagasse, P. 2011. River Engineering for Highway Encroachments: Highways in the River Environment. Publication No. FHWA NHI 01-

004. Washington, D.C.: U.S. Department of Transportation, Federal Highway Administration.

Santhi, C., Arnold, J.G., Williams, J.R., Dugas, W.A., Srinivasan, R., Hauk, L.M. 2001. Validation of the SWAT model on a large river basin with point and nonpoint sources. JAWRA Journal of the American Water Resources Association. 37(5),1169–1188. http://dx.doi.org/10.1111/j.1752-1688.2001.tb03630.x.

Schmidli, J., Goodess, C.M., Frei, C., Haylock, M.R., Hundecha, Y., Ribalaygua, J., Schmith, T. 2007. Statistical and dynamical downscaling of precipitation: An evaluation and comparison of scenarios for the European Alps. Journal of Geophysical Research. 112: D04105. http://dx.doi.org/10.1029/2005JD007026.

Smakhtin, V.Y. 2001. Low flow hydrology: a review. Journal of Hydrology. 240, 147-186. http://dx.doi.org/10.1016/S0022-1694(00)00340-1.

Smedema, L.K., Rycroft, D.W. 1983. Land drainage—planning and design of agricultural drainage systems, Cornell University Press, Ithica, N.Y.

Soil Conservation Service (USDA). 1972. Section 4: Hydrology In National Engineering Handbook. SCS. Hydrology Section 4 (Chapters 4–10).

Soil Conservation Service Engineering Division (USDA). 1986. Urban hydrology for small watersheds. U.S. Department of Agriculture, Technical Release 55.

Teutschbein, C., Seibert, J. 2013. Is bias correction of regional climate model (RCM) simulations possible for non-stationary conditions? Hydrology and Earth System Sciences. 17, 5061-5077. http://dx.doi.org/10.5194/hess-17-5061-2013.

Turco, M., Quintana-Segui, P., Llasat, M.C., Herrera, S., Gutierrez, J.M. 2011. Testing MOS precipitation downscaling for ENSEMBLES regional climate models over Spain. Journal of Geophysical Ressearch Atmospheres. 116, D18109.

Uppala, S.M., Kallberg, P.W., Simmons, A.J., Andrae, U., Da Costa Bechtold, V., Fiorino, M., Gibson, J.K., Haseler, J., Hernandez, A., Kelly, G.A., Li, X., Onogi, X., Saarinen, S., Sokka, N., Allan, R.P., Andersson, E., Arpe, K., Balmaseda, M.A., Beljaars, A.C.M., Vandeberg, L., Bidlot, J., Bormann, N., Caires, S., Chevallier, F., Dethof, A., Dragosavac, M., Fisher, M., Fuentes, M., Hagemann, S., Holm, E., Hoskins, B.J., Isaksen, L., Janssen, P.A.E.M., Jenne, R., McNally, A.P., Mahfouf, J.F., Morcrette, J.J., Rayner, N.A., Saunders, R.W., Simon, P., Sterl, A., Trenberth, K.E., Untch, A., Vasiljevic, D., Viterbo, P., Woollen, J. 2005. The ERA40 Reanalysis. Quarterly Journal of the Royal Meteorological Society. 131, 2962-3012.

van Griensven, A., Meixner, T., Grunwald. S. 2006. A global sensitivity analysis tool for the parameters of multi-variable catchment models. Journal of Hydrology. 324, 10-23. http://dx.doi.org/10.1016/j.jhydrol.2005.09.008.

van Liew, M.W., Arnold, J.G., Bosch, D.D. 2005. Problems and potential of autocalibrating a hydrologic model. Transactions of the ASAE. 48(3), 1025-1040.

van Liew, M.W., Arnold, J.G., Garbrecht, J.D. 2003. Hydrologic simulation on agricultural watersheds: Choosing between two models. Transactions of the ASAE. 46(6),1539–1551.

Watson, B.M., McKeown, R.A., Putz, G., MacDonald, J.D. 2008. Modification of SWAT for modelling streamflow from forested watersheds on the Canadian Boreal Plain. Journal of Environmental Engineering Sciences. 7(S1):145–159. http://dx.doi.org/10.1139/S09-003.

Wigley, T.M.L. 2004. Input needs for downscaling of climate data. Discussion Paper. California Energy Commission.

Wilby, R.L., Dawson, C.W., Barrow, E.M. 2002. SDSM-A decision support tool for the assessment of regional climate change impacts. Environmental Modeling & Software. 17; 145-157. http://dx.doi.org/10.1016/S1364-8152(01)00060-3.

Williams, J.R. 1969. Flood routing with variable travel time or variable storage coefficients. Transactions of the ASAE. 12(1), 100-103.

Williams, J.R. 1975. Sediment – yield prediction with universal equation using runoff energy factor. Proceedings of the Sediment-Yield Workshop, USDA Sedimentation Laboratory, Oxford, Mississippi.

Williams, J.R. 1995. The EPIC model. Chapter 25: p. 909-1000. In V.P. Singh (ed). Computer models of watershed hydrology. Water Resources Publications, Highlands Ranch, CO.

Wilson, D., Hisdal, D., Lawrence, D. 2010. Has streamflow changed in the Nordic countries? – Recent trends and comparisons to hydrological projections. Journal of Hydrology. 394, 334-346. http://dx.doi.org/10.1016/j.jhydrol.2010.09.010.

Wischmeier, W. 1975. Estimating the soil loss equation's cover and management factor for undisturbed areas. In Proc. Sediment Yield Workshop: Present and Prospective Technology for Predicting Sediment Yield and Sources, 118-124. Washington, D.C.: USDA-ARS.

Wischmeier, W., Smith, D. 1965. Predicting rainfall erosion losses from cropland east of the Rocky Mountains. Washington, D. C., U. S. Department of Agriculture. Agricultural Handbook 282. 45 p.

Wischmeier, W., Smith, D. 1978. Predicting Rainfall Erosion Losses: A Guide to Conservation Planning. Washington, D.C. USDA Science and Education Administration.

Yang, C. 1996. Sediment Transport: Theory and Practice. New York, N.Y.: McGraw-Hill.

Yue, S., Pilon, P., Phinney, B., Cavadias, G. 2002. The influence of autocorrelation on the ability to detect trend in hydrological series. Hydrological Processes. 16, 1807– 1829. http://dx.doi.org710.1002/hyp.1095.

Zabaleta, A., Antiguedad, I. 2012. Klimaren seinale hidrologikoak EAEko arroetako uremarien joeretan. Gerora begirako proiekzio hidrologikoak. Ekaia 25, 89-118.

Zabaleta, A., Meaurio, M., Ruiz, E., Antiguedad, I. 2014. Simulation climate change impact on runoff and sediment yield in a small watershed in the Basque Country, northern Spain. Journal of Environmental Quality. 43, 235–245. http://dx.doi.org/10.2134/jeq2012.0209.

Zabaleta, A., Morales, T., Meaurio, M., Gorria, C., Antiguedad, I. 2012. Regional hydrological signs for climate change in Southern Europe (Basque Country). International Conference on Water. Climate and Environment. ISBN 978-608-4510-10-9.

Zhang, X., Xu, Y., Fu, G. 2014. Uncertainties in SWAT extreme flow simulation under climate change. Journal of Hydrology. 515, 205-222. http://dx.doi.org/10.1016/j.jhydrol.2014.04.064.

Zhou, G., Wei, X., Wu, Y., Liu, S., Huang, Y., Yan, J., Zhang, D., Zhang, Q., Liu, J., Meng, Z., Wang, C., Chu, G., Liu, S., Tang, X., Liu, X. 2011. Quantifying the hydrological responses to climate change in an intact forested small watershed in Southern China. Global Change Biology. 17(12), 3736–3746. http://dx.doi.org/10.1111/j.1365-2486.2011.02499.x.

3.

EVALUATION OF THE PERFORMANCE OF THE HYDROLOGICAL MODEL

3. EVALUATION OF THE PERFORMANCE OF THE HYDROLOGICAL MODEL

3.1 INTRODUCTION

Understanding runoff generation processes is essential for predicting water quantity and quality (Ladouche et al., 2001; Uhlenbrook, 2006). Consideration of these processes becomes necessary when climate and land use conditions change (Naef et al., 2002; Negley & Eshleman, 2006; Stewart & Fahey, 2010) or when management decisions have to be taken. Managers commonly use modelling as a tool to understand how these changes impact at the catchment scale. In most cases, models are applied with little knowledge of the hydrological processes occurring in the studied area. However, as Beven (2007) suggests,

neglecting processes because of a lack of understanding of how the systems work, ultimately influences how well the system can be predicted by a model. In this regard, Yu & Schwartz (1999) noted that the performance of the numerical models would be enhanced by analysing and taking into account the runoff generation processes in the catchment under study when modelling. These authors showed that separation of the hydrograph can provide data that can be useful when calibrating numerical models.

In the Basque Country, SWAT has been used in several catchments for different purposes. The model was employed in the Alegria catchment to study the transport of pollutants in an agricultural area (Cerro et al., 2014; Epelde et al., 2015) and in Oka catchment, small and forested, to evaluate the hydrology, and suspended sediment and Nickel loads (Peraza-Castro et al., 2015). Some authors have noted that SWAT needs some improvements in small catchments (e.g. Qiu et al., 2012) therefore a performance evaluation is needed.

Bearing all this in mind, in the present chapter, the Soil and Water Assessment Tool (SWAT) (Arnold et al., 1998) was applied and tested at different time-steps (daily and hourly) in Aixola catchment. In this case, the evaluation was done for streamflow and also for suspended sediment yield which plays a key role in environmental conditions of small mountainous catchments and, thus, is of great interest for integrated river basin management. In this Thesis, data obtained in the field between 2012 and 2015 (soil properties and continuous series of electrical conductivity in the main tributaries and the outlet of the catchment) made it possible to perform and evaluate the simulation results of runoff generation processes.

Many studies have used electrical conductivity (EC) as an environmental indicator for hydrograph separation (Pilgrim et al., 1979; Matsubayashy et al., 1993; Caissie et al., 1996; Cey et al., 1998; Stewart et al., 2007; Hayashi et al., 2012), applying a mass balance approach. EC was also applied in the Aixola catchment (Zabaleta & Antiguedad, 2013) to make a preliminary approximation of the baseflow/surface runoff contribution in storm events. In the present Thesis, discharge data for the main two sub-catchments were obtained through the

electrical conductivity-based mass balance approach (CMB). These data were used to better understand the runoff generation processes throughout Aixola catchment in order to help provide a more realistic simulation.

Summarizing, in this chapter SWAT projects were performed to evaluate model capacity to accurately simulate streamflow and sediment yield in a small forested catchment considering:

⇒ The model performance to simulate streamflow and sediment yield at daily time-step with little knowledge on specific soil characteristics and water origin in the catchment (section *3.4 Streamflow and sediment yield simulation in Aixola catchment*).

⇒ The model daily performance to simulate streamflow spatial origin (section *3.5 Evaluation of SWAT model performance to simulate streamflow spatial origin*) considering:

- Is it possible to obtain good approximation of the water contribution from different parts of the catchment along with a good result in the outlet?
- Analyse simulation of the surface/baseflow amount to point out where the highest uncertainties occur: 1) in the contribution from different parts of the catchment or 2) in the surface/baseflow contribution.

⇒ Evaluation of the model performance to simulate streamflow and sediment load at sub-daily time-step (section *3.6 Evaluation of SWAT model performance to simulate streamflow and sediment yield at sub-daily time-step)* considering:

- Is it possible to obtain better daily results when the simulation is done at sub-daily time-step?
- Analyse the capability of the SWAT sub-daily code to simulate different types of discharge events.

3.2 STUDY AREA: AIXOLA CATCHMENT

The Aixola catchment is located in the central part of the Basque Country in its Atlantic watershed, at an average latitude of 43° N and an average longitude of 1° W (Fig. 3.1). It covers an area of 4.6 km^2 and is comprised of two main streams; the catchment can therefore be divided into two main sub-catchments. The smallest sub-catchment, Txulo, covers 25 % of the entire catchment (1.1 km^2) and is located in the north, whilst the largest, Elgeta, covers 75 % (3.5 km^2). The two streams converge near the gauging station (40 m upstream), which was selected as the outlet of the catchment. The Aixola river drains into the Aixola reservoir, which has a capacity of 2.79 hm^3 and is used for drinking water supply. The prevailing climate in the region is humid and temperate. The mean annual precipitation is about 1480 mm, distributed fairly evenly throughout the year; the mean annual temperature is 12 °C, and the mean annual discharge is 600 mm, around 0.092 $m^3\ s^{-1}$ (2003-2008).

The elevation in the catchment ranges from 340 m at the outlet of the catchment to 750 m at the highest peak. Most slopes have less than 30 %. The lithology is highly homogeneous with most of the bedrock (94 %) consisting of practically impervious Upper Cretaceous Calcareous Flysch (Santonian-Mid Maastrichtian). The main types of soil are cambisols and regosols (FAO, 1998), with depths ranging from less than 1 m to more than 13 m, and a loam texture (Fig. 3.1b)).

The land use is very homogeneous and represents a good reference for reforested catchments in the Cantabrian watershed of the Basque Country. Reforested species (*Pinus radiata*) cover more than 80 % of the area and in the rest of the catchment, *Larix decidua* and *Abies alba*, small remaining patches of mixed forest of *Fagus sylvatica* and *Quercus robur*, some pasturelands (covering the 10 % of the catchment) and urban areas (3 %) are found. (Fig. 3.1c)).

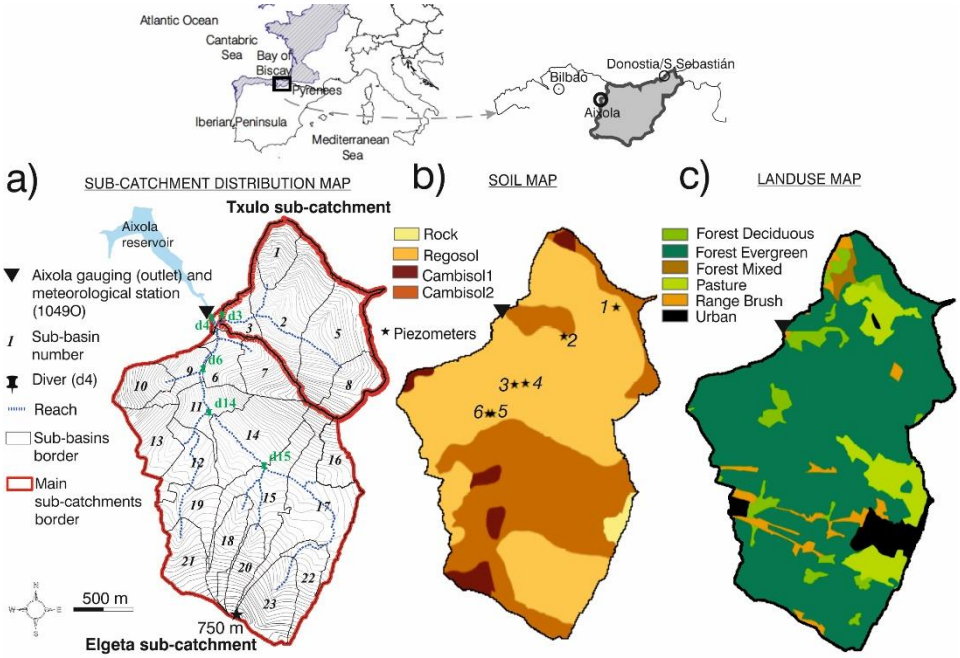

Figure 3.1. *Location of Aixola catchment and a) contour line map, b) soil map and c) land use map. In a) the two main sub-catchments (Elgeta/Txulo), the location of the electrical conductivity CTD_Diver and the sub-basin subdivision made using SWAT can be observed. In b) the location of piezometers is shown, the soil general characteristics are described in Table 3.1. In c) the land use map is displayed; forest deciduous correspond with Fagus sylvatica and Quercus robur and forest evergreen with Pinus radiata and in minor proportion with Larix decidua and Abies alba.*

3.2.1 Instrumentation and measurement

Precipitation, air temperature and discharge are measured every 10 minutes in the gauging station (Fig. 3.1a). With the purpose of better understand the spatial origin of water inside the catchment, in April 2011 a CTD-Diver probe (Eijkelkamp) was installed in the gauging station (d4) to measure the specific electrical conductivity of water (at 25 ºC, hereafter EC; μS cm^{-1}) every 20 minutes. In October 2011, another two probes were installed; one along Elgeta stream (d6) and the other one in Txulo stream (d3) (Fig. 3.1a)). The EC is easy to measure and the installation required is minimum.

In January 2012 six piezometers where installed in the catchment. Thanks to the description of the soil cores obtained in the drilling the characteristics of the soils are better known. In the Fig. 3.1b) is possible to observe the location of the piezometers and in Table 3.1 are described their general characteristics. In

general, the soils are deep, with depths ranging from about 1 m in the lower zones (near the river) to 13 m in higher areas. The texture varies from loam to clay loam, and the organic matter in the first horizon is around 1-5 %. In addition, in Appendix 1 there is more information about the soil profiles and the chemical and physical properties of the soils.

NAME	HORIZONS	DEPTH (m)	O. M.	F.C.	TEXTURE
1 Egoetxeaga	A1	0.5	3.57	35	Clay Loam
	B1	1.25		47.7	Clay Loam
	C1	2.2		43	Loam
	C2	7.4		38.1	Loam
	R	>7.4		-	Limestone and marl
2 Txulo	A	0.35	1.47	47.4	Loam
	B1	1.3		46.4	Loam
	B2	1.7		43.7	Loam
	R	>1.7		-	Limestone with some sandstone
3 Bastarrika 1	A	0.65	1.36	51.7	Clay Loam
	B1	1.2		49	Loam
	B2	4.4		43.7	Loam
	Bg	7.8		46.2	Loam
	R	>7.8		-	Marl
4 Bastarrika 2	B1	1.6		49.7	Loam
	B2	11.8		39.8	Loam
	B3	13.2		38.1	Loam
	R	>13.2		-	Marl
5 Aixola 1	A	0.4	5.01	53	Loam
	B1	0.95		36.5	Loam
	C1	1.05		-	Clay Loam
	R	>1.05		-	Limestone
6 Aixola 2	A	0.4	5.01	50.4	Loam
	B1	1.3	0.9	43.2	Loam
	CB	3.94	0.69	45.4	Loam
	R	>3.94	-	-	Limestone

Table 3.1*. Soil properties of Aixola catchment. The first column represents the location of the piezometers in the catchment in the Fig. 3.1 b). Horizons were defined following the guidelines established by FAO (1998) and the depth of each horizon (meters) was measured from the cores. The volumetric organic matter (O.M; PEC/EN/A-098), the field capacity (F.C) and the texture (PEC/EN/A-098) are also represented. For more information see the Appendix 1.*

3.3 HYDROLOGICAL MODELLING METHODOLOGY IN THE SWAT MODEL PERFORMANCE EVALUATION

The first SWAT project carried out in Aixola catchment was performed with SWAT 2009 (Fig. 3.2, 1.Project, hereafter *1P*). The SWAT model requires inputs

describing topography, soils, land use, and meteorology. Table 3.2 summarizes these inputs and the sources of the corresponding data used for this study. The main outlet of the catchment was set at the Aixola gauging station (Fig. 3.1 a)). The digital elevation model (DEM) was used to delimit the drainage area of the catchment and taking the topographic parameters into consideration the hydrological model partitioned the catchment into 23 sub-basins (Fig. 3.1 a)), resulting in an average sub-basin area that corresponds to 4 % of the total catchment area in this study. This division is in agreement with delineation recommendations reported in several previous SWAT studies (FitzHugh & MacKay, 2000; Jha et al., 2004; Arabi et al., 2006), which show that the runoff and especially sediments are highly influenced by catchment subdivision.

Data type	Description / properties	Source
Topography	LIDAR DEM 2008 (5 x 5 m)	Basque Government; Geoeuskadi (www.geoeuskadi.net)
Land use	Land use classification, 2005 (1:10000)	Basque Government; Geoeuskadi (www.geoeuskadi.net)
Soils	Soil types (1:25000)	Basque Government; Geoeuskadi (www.geoeuskadi.net)
Meteorology	Precipitation and minimum and maximum temperature	Gipuzkoa Provincial Council (http://www4.gipuzkoa.net/oohh/web/eus/index.asp)

***Table 3.2**. Summary of the inputs introduced in the model.*

The parameterization of the different types of land use was based on the SWAT land use classes (Table 3.3). The properties for the soil types of the study area were taken from the geographical database of the Government of the Basque Country (GeoEuskadi, 2012) and their properties are listed in Table 3.3 (*1P*). Slopes were classified on the basis of the DEM into four different slope ranges: 0-5 %, 5-35 %, 35-50 % and >50 % (Table 3.4).

As mentioned above, during drilling (January 2012) of the soil cores (Fig. 3.1b)), soil properties, such as the depth of the soils, their horizons, root depth, the texture for each horizon and in some cases the amount of organic matter were described (Table 3.1). Taking the Basque Government's Soil Types map as a reference and including these new data, the cambisols where divided into cambisol1 and cambisol2 (Fig. 3.1b)). In addition, the SWAT soil properties database was modified to include the new data (Table 3.3, 2.Project, hereafter *2P*). Using the same DEM and land use as the *1P* (Table 3.2) but changing the

soil properties (Table 3.3, *2P*), a new project was performed with SWAT 2012 (Fig. 3.2, *2P*). Before calibration, an evaluation of the effect of the new soil map and properties obtained from the analysis of soil cores on the simulation was done. To do so, a simulation was performed on the *2P* with the values of the calibrated parameters described in the *1P* (Table 3.4).

			1.LAYER			2.LAYER			3.LAYER			4.LAYER		
		Area %	Z	Texture	O.M.	Z	Texture	O.M.	Z	Texture	O.M.	Z	Texture	O.M.
1.P	REGOSOL	40	0.2	Loam	1.86	1.8	Clay loam	1.86	-	-	-	-	-	-
	CAMBISOL	59.6	0.2	Silty Clay	1.8	0.9	Clay	1.8	-	-	-	-	-	-
	LUVISOL	0.4	0.2	Silty Clay	8.26	0.5	Clay	1.46	-	-	-	-	-	-
2.P	REGOSOL	55	0.7	Loam	0.79	1.4	Loam	0.29	2.75	Loam	-	5	Loam	0
	CAMBISOL1	4	0.4	Loam	2.32	-	Loam	-		-	-	-	-	-
	CAMBISOL2	40	0.4	Loam	2.32	1	Loam	0.47	3	Clay Loam	0.05	-	-	-

Table 3.3. *Comparison between soil data introduced in the SWAT database in the 1.Project (Fig. 3.2, 1P) and in the 2.Project (Fig.3.2, 2P). The database was modified because new soil properties were obtained from the soil cores (Table 3.1). Area % is the percentage of each soil type in relation to the whole catchment, Z is the depth from soil surface to bottom of layer in meters, O.M. is the percentage of the organic matter. 1 % of the catchment area in the 2P is rock.*

The next action (Fig 3.2, 2.Project Step 1 hereafter *2P S1*) was to calibrate the model using the daily discharge ($m^3 s^{-1}$) measured in the gauging station. In 2011 CTD-divers were installed in the catchment (Fig 3.1 a)). Using the conductivity data measured with the divers, a mass balance approach (hereafter CMB) (Stewart et al., 2007) was applied with two goals: 1) to quantify the discharge contribution of each sub-catchments to the main outlet, and 2) to separate the hydrograph observed at the outlet into two components: baseflow (groundwater and subsurface flow) and surface runoff. The discharge data of the main two sub-catchments derived from the CMB approach were also taken into consideration to calibrate the model in *2P S1* (Fig. 3.2). In this way, it was intended to study whether the use of these new data and the consideration of the associated hydrological processes might help improve the results of the simulation. In addition, an evaluation of the model performance to simulate the baseflow and the surface runoff amount was done.

Finally, *2P* was calibrated and validated hourly (Fig. 3.2, 2.Project Step 2, hereafter *2P S2*). Continuous simulations are necessary to investigate long term

impacts, nevertheless, to adequately capture hydrologic processes, it is important to simulate individual storm events furthermore, in small catchments where the response to precipitation is usually fast. Aixola catchment shows a quick response to almost all the rainfall events (Zabaleta & Antiguedad, 2013) therefore daily time-step could be not enough to simulate the magnitude of storm events.. Thus, it was possible to evaluate the model sub-daily performance for a long period (continuous simulation) and also for different storm events.

3.3.1 Sub-catchment contribution

The discharge of the two main sub-catchments to the entire catchment (Fig. 3.1a)) was calculated in a daily time-step. For this purpose, a daily CMB was conducted for data recorded between 1/10/2011 and 31/12/2012. According to this approach, water from different sources will possess different hydrochemical characteristics. The relative contributions of these sources can be evaluated by measuring both stream discharge and chemical quality of the mixed water flowing into the stream. CMB does not take into account the hydrodynamic dispersion which might affect the degree of mixing between waters from different sources (Jones et al., 2006). For this reason, in some cases this method has been called into question (Rice and Hornberger, 1998; Jones et al., 2006). However, this approach has been successfully applied in other cases. Martínez-Santos et al. (2014) applied the CMB approach to separate the hydrograph in the Oka river (Bizkaia province, very close to the Aixola river). They considered that the small size of the catchment (31.5 km^2), the steep slopes and the quick response to precipitations led to greater consideration being given to processes driven by hydraulic gradients than those caused by hydrodynamic dispersion. A preliminary EC-based mass balance was also applied in the Aixola catchment (Zabaleta & Antiguedad, 2013) to separate discharge during storm events. These authors show that an EC based-approach may be suitable to provide insights on the runoff generation processes in certain types of catchments.

Points d3 and d6 were established as references for the chemical characteristics of waters from the Txulo and Elgeta sub-catchments respectively (Fig 3.1 a)). The

CMB was performed using these data and the EC and discharge data in the outlet (d4).

$$Q_{d4}C_{d4} = Q_{d6}C_{d6} + Q_{d3}C_{d3} \quad (3\text{-}1)$$

$$Q_{d4} = Q_{d6} + Q_{d3} \quad (3\text{-}2)$$

Where,

Q is the discharge (in this case in $m^3\ s^{-1}$)

C is the EC (in this case in $\mu s\ cm^{-1}$)

subscripts d4, d6 and d3 are the points in the catchment where the EC was measured

The results obtained from the CMB approach were used in the SWAT calibration process performed in the *2P S1* (Fig. 3.2).

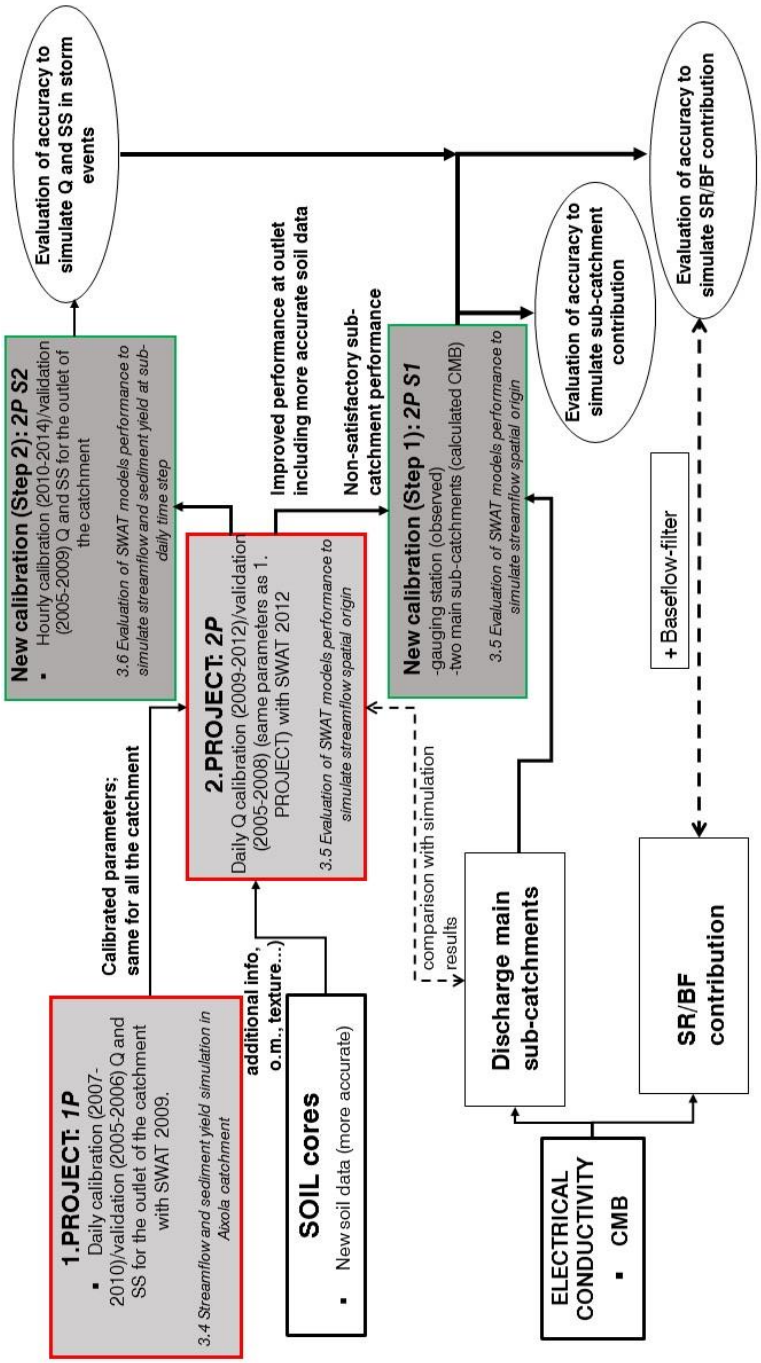

Figure 3.2. *Methodology chart.*

3.3.2 Hydrograph separation

Subsequently, in order to better understand the hydrological processes occurring in the catchment and test the hydrological simulation, two different methods were used to separate the hydrograph at the outlet of the catchment.

Firstly, a tracer-based method was used to separate the hydrograph into baseflow (groundwater + subsurface) and surface runoff. To achieve this, an EC-based method (CMB) was applied. In this case the CMB assumes that: 1) baseflow conductivity is equal to streamflow conductivity at lowest flows, 2) surface runoff conductivity is equal to streamflow conductivity at highest flows, and 3) the baseflow and surface runoff EC values given in Points 1) and 2) remain constant throughout the period analysed (Stewart et al., 2007). This two-component mixing model and the relationship between EC and discharge can be expressed as:

$$Q_t C_t = Q_{BF} C_{BF} + Q_{SR} C_{SR} \quad (3\text{-}3)$$

$$Q_t = Q_{BF} + Q_{SR} \quad (3\text{-}4)$$

Where,

Q is the discharge (in this case in $m^3\ s^{-1}$)

C is the EC (in this case in $\mu s\ cm^{-1}$)

Subscripts t, BF and SR refer to the total, baseflow and surface runoff respectively.

During very intense storm events, in the available data series the electrical conductivity drops to minimum values of around 150 $\mu S\ cm^{-1}$; this value was taken as the EC of surface runoff. The maximum values were recorded before the drop in conductivity caused by storm events at the end of the summer period; highest electrical conductivity was commonly around 380 $\mu S\ cm^{-1}$; this value was taken as the baseflow EC. These values were used to apply the CMB approach to the daily EC and discharge data recorded in the gauging station between 13/04/2011 and 31/12/2012, making it possible to decompose the hydrograph into baseflow and surface runoff.

Secondly, as proposed in the SWAT model website (http://swat.tamu.edu) an automated digital filter programme (Baseflow Filter Program – BFP) (Arnold et al., 1995) was used to separate the daily discharge into the two components; in this process a low-pass filter is applied separating the "low-frequency" baseflow component from the "high-frequency" runoff component (Stewart et al., 2007). In this kind of filter, the operator determines the degree of filtering by adjusting a filter coefficient and selecting the number of passes the filter makes through the discharge data set (Nathan & McMahon, 1990; Mau & Winter, 1997). The BFP passes over the discharge three times (forward, backward and forward). This is a non-tracer-based technique which, although it has only a graphical basis, is objective and reproducible (Arnold & Allen, 1999). The equation for the filter is:

$$q_t = \beta\, q_{t-1} + (1+\beta)/2 * (Q_t - Q_{t-1}) \qquad (3\text{-}5)$$

where,

q_t is the filtered surface runoff at the time-step t (one day)

Q is the original discharge

β is the filter parameter (by default 0.925)

Baseflow, b_t, is calculated using the equation:

$$b_t = Q_t - q_t \qquad (3\text{-}6)$$

The filter method is comparable in accuracy with the manually separated baseflow and gives results similar to the automated model of Rutledge (1993) (Arnold et al., 1995). This methodology is described in greater detail by Arnold & Allen (1999) and Arnold et al. (1995).

Data obtained from the hydrograph separation (baseflow and surface runoff) using the CMB method and BFP have been compared with that obtained from the model simulation. This was possible because SWAT offers different flow components as output data. In this case only the distinction between surface runoff and baseflow was considered for comparison. Decomposition of the hydrograph was only used to test the model performance but not to calibrate the model.

3.4 STREAMFLOW AND SEDIMENT LOAD SIMULATION IN AIXOLA CATCHMENT (1P)

SWAT 2009 was used to perform the *1P* (Fig. 3.2). The objective of the modelling was to provide new insights into how potential changes in precipitation and temperature may affect suspended sediment yields in forested headwater catchments. It is possible to observe the results of this research in the section *4.1 Simulation climate change impact on runoff and sediment yield in Aixola catchment*. It has been considered necessary to explain the calibration and validation of the *1P* in the present section because it is the base of the next projects and steps. When this project was performed neither soil characteristics measured in the soil profiles (Fig. 3.1a)) nor EC in the river were available for the modelling.

3.4.1 Hydrological model input, calibration and validation

With the DEM and the control points introduced in the model, the catchment was divided in 23 sub-catchments, and these, in turn, with the slope classification, land use map, and soil type maps were then overlaid to derive 165 unique HRUs (Table 3.4).

Daily river flow ($m^3\ s^{-1}$) and sediment load (t) data measured at the Aixola gauging station were used for calibrating and validating the model (Fig. 3.1a)). The model was run with a daily time-step for 6 years; the period from 2007 to 2010 (4 years) was used for calibration and the period from 2005 to 2006 (2 years) for validation. The period from October 2003 to December 2004 was also simulated but considered as a warm-up. No sediment load data were available from June 2008 onwards; accordingly, although discharge calibration was performed using a four-year-long series, data were only available for 18 months for the calibration of sediment loads. In the two-year period used for validation, sediment yield registered at the gauging station was higher than in the calibration period due to the tree harvesting management practices used in small parts of the pine tree plantations. As described before, the dominant land use in the catchment is pine tree plantations. Tree cutting and site preparation for reforestation (scalping and

downslope ripping) were observed in the catchment, directly in the field and also in orthophotos taken each year from 2004 to 2009. Such practices increase the sediment available to be delivered to the Aixola reservoir, as the soil in these areas remains bare for a period of time. These management practices were only used in a few very small patches in the catchment from 2004 to 2006 (Zabaleta et al., 2007); the total area was about 1.05 ha per year (from 2004 to 2006), in different zones on each occasion. Nevertheless, in order to simplify the inclusion of these management practices in the model, a single small area of 1.05 ha of bare soil, serving as a source of sediment, was included on the vegetation map for the 2004 to 2006 validation period. From 2007 to 2010 (calibration period) no land use changes or management activities were detected.

Sensitivity analysis was carried out to identify the most sensitive parameters for the model calibration using the Latin Hypercube One-At-a-Time (LH-OAT) approach offered in the SWAT sensitivity analysis interface (van Griensven et al., 2006). This method involves taking a certain number of Latin Hypercube sample points for the same number of intervals, and then varying each of these sample points several times by changing each of the parameters one at a time, as is characteristic of the OAT design. It ensures that the full range of the parameters are sampled with a certain precision and ensures that the changes in the output in each model run can be unambiguously attributed to the parameter that was changed. The sensitive parameters and their calibrated values are listed in Table 3.5.

Land use type	Swat land use code	Slope class	number HRUs	Catchment percentage	Sediment yield (%) calibration	Sediment yield (%) validation
Forest evergreen	FRSE	0-5	1	0.47	0.06	0
Forest evergreen	FRSE	5-35	36	35.2	7.64	1
Forest evergreen	FRSE	35-50	36	24.08	10.76	1.47
Forest evergreen	FRSE	>50	26	21.75	10.11	1.09
Forest deciduous	FRSD	5-35	4	0.48	1.28	0.07
Forest deciduous	FRSD	35-50	7	0.83	2.44	0.22
Forest deciduous	FRSD	>50	8	1.86	6.18	0.67
Forest mixed	FRST	35-50	1	0.21	0.24	0.02
Forest mixed	FRST	>50	1	0.64	0.03	0.04
Pasture	PAST	5-35	14	7.18	17.03	1.74
Pasture	PAST	35-50	8	1.77	12.46	1.18
Pasture	PAST	>50	3	0.74	6.17	0.64
Range-Brush	RNGB	0-5	1	0.02	0.03	0
Range-Brush	RNGB	5-35	5	0.47	4.97	0.43
Range-Brush	RNGB	35-50	5	0.39	8.64	0.83
Range-Brush	RNGB	>50	4	0.46	7.22	0.8
Residential	URBN	0-5	1	1.15	1.92	0.22
Residential	URBN	5-35	1	2.26	2.55	0.35
Bare*	BARE	5-35	2	0.03	0	89.25
Bare*	BARE	>50	1	0.01	0	0

Table 3.4. *Land use types and their SWAT code, and slope classes introduced in the model. Number of HRU with each of the combinations and related percentage of the total catchment can also be found. Additionally, the percentage of suspended sediment yield attributed by the model to each land use-slope class combination during the calibration and the validation periods was included in the table. * Only for validation.*

Change type	Parameter name	Description	Sensitivity		Actual value used
			Flow	Sediments	
r	CN2.mgt	Curve number for moisture condition II	1	3	↓10%
v	CH_K2.rte	Main channel conductivity	2	13	100
v	SURLAG.bsn	Surface runoff lag coefficient	3	5	1
v	ALPHA_BF.gw	Baseflow alpha factor	4	11	0.021
v	ESCO.bsn	Soil evaporation compensation factor	5	10	0.9
v	GWQMN.gw	Threshold depth of water in shallow aquifer required for return flow to occur	6	16	700
v	CH_N2.rte	Manning's *n* value for the main channel	7	8	No change
	SLOPE	Mean slope within the HRU	8	7	No change
v	CANMX.hru	Maximum canopy storage	9	4	8
v	GW_REVAP.gw	Groundwater "revap" coefficient	10	21	0.19
	BLAI (crop.dat)	Maximum potential leaf area index	11	1	No change
r	SOL_K.sol	Saturated hydraulic conductivity	12	15	↑10%
r	SOL_AWC.sol	Available water capacity of the soil layer	13	14	↓4%
	SOL_Z.sol	Depth from soil surface to bottom of layer	14	18	No change
v	GW_DELAY.gw	Groundwater delay time	15	20	40
v	REVAPMN.gw	Threshold water in shallow aquifer	16	23	No change
	EPCO.bsn	Plant uptake compensation factor	17	19	No change
	SLSUBBSN.hru	Average slope length	18	12	No change
v	BIOMIX.mgt	Biological mixing efficiency	19	17	0.9
	USLE_P.mgt	USLE equation support practice factor	-	2	No change
v	SPCON.bsn	Channel sediment routing parameter	-	6	0.0001
v	SPEXP.bsn	Exponent parameter for calculating sediment re-entrained in channel	-	9	1.5
v	RSDCO.bsn#	Residue decomposition factor			0.1
v	LAT_TTIME.hru#	Lateral flow travel time			5
v	LAT_SED.hru#	Sediment concentration in lateral and groundwater flow			0.5
v	OV_N.hru#	Manning's *n* value for overland flow			0.6
v	SHALLST.gw#	Initial depth of water in the shallow aquifer			1000
v	DEEPST.gw#	Initial depth of water in the deep aquifer			0
	RCHR_DP.gw#	Deep aquifer percolation factor			0
v	USLE_K.mgt#	USLE equation soil erodibility factor			cambisol 0.25 regosol 0.35

Table 3.5. Description and rank in sensitivity of SWAT parameters selected for calibration. *v: means the default parameter is replaced by a given value, and r means the existing parameter value is changed relatively. #: parameters not included in the model sensitivity analysis.

3.4.2 Results: model calibration and validation

The initial sensitivity analysis resulted in the selection of parameters that were manually calibrated as listed in Table 3.5. This table shows the most sensitive parameters for streamflow and sediment that were adjusted from the SWAT default values to fit the model simulated with the observed discharge and sediment data. Some of the parameters were not included in the model sensitivity analysis routine (Table 3.5) but proved to be very sensitive during the manual calibration process, especially LAT_TTIME and USLE_K.

The model streamflow and sediment predictions were calibrated and validated against daily data from the Aixola gauging station as shown in Fig. 3.3. Note that sediment data from June 2008 to December 2010 are not presented in the calibration period as there are missing data. According to the criteria of Santhi et al. (2001), Van Liew et al. (2003) and Moriasi et al. (2007), the simulated and observed runoff and sediment data for the calibration period would show an acceptable level of agreement for recommended statistics on a monthly basis. Since, in our case, the data are evaluated using daily time-steps it can be said that they are, at least, *satisfactory* (Table 3.6) as indicated by NSE, R2, PBIAS, and RSR values for discharge of 0.62, 0.81, -16 %, and 0.62, respectively, and 0.56, 0.76, 47 %, and 0.66, respectively, for sediment. The fit between simulated and measured discharge and sediment data for the validation period can also be considered *satisfactory*: with values for NSE of 0.6 and 0.54, R2 of 0.85 and 0.8, PBIAS of 2 % and 42 %, and RSR of 0.64 and 0.68, for discharge and sediments respectively. These results indicate that the performance of the model for the Aixola catchment using the set of parameters given in Table 3.6 was acceptable.

	calibration		validation	
	flow	sediment	flow	sediment
NSE	0.62	0.56	0.6	0.54
R^2	0.81	0.76	0.85	0.80
PBIAS	-16	47	2	42
RSR	0.62	0.66	0.64	0.68

Table 3.6. *Summary statistical indices obtained for NSE, R^2, PBIAS and RSR.*

Daily discharge and sediment peaks were, however, underestimated by the model (Fig. 3.3). These inaccuracies might be related, as Qiu et al. (2012)

reported, to the inability of SWAT to simulate precipitation patterns, in terms of intensity as well as temporal distribution. For the Aixola catchment, it has been shown that precipitation intensity during rainfall events strongly influences runoff, especially the magnitude of increase in discharge during the runoff event, and that both precipitation intensity and runoff increase are the factors that most influence the value of the sediment peak (Zabaleta et al., 2007). Underestimation of the runoff could also be responsible for less channel and bank erosion resulting, in turn, in a lower suspended sediment concentration at the catchment outlet.

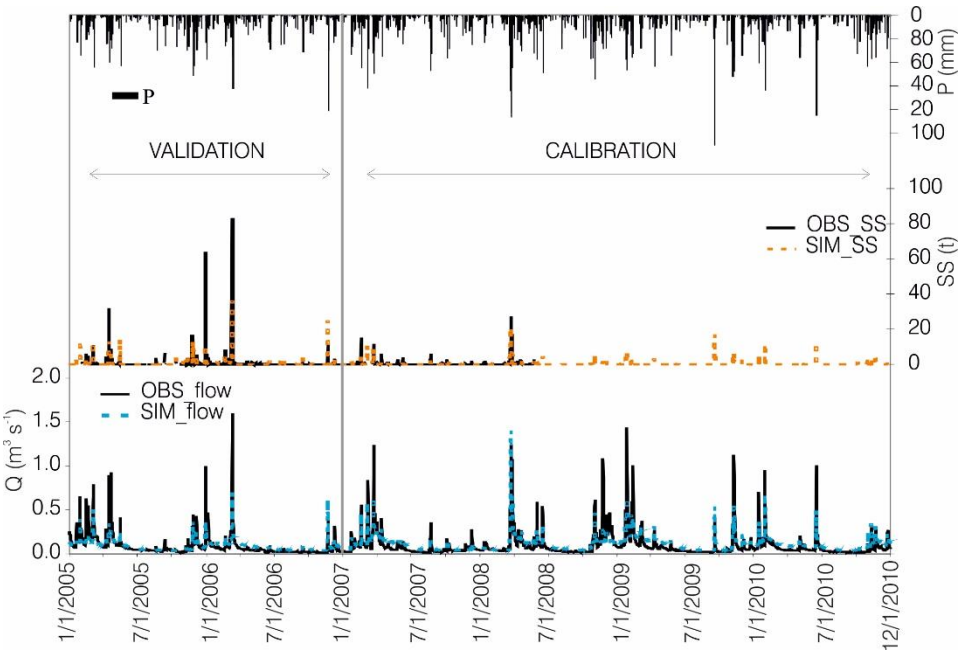

***Figure 3.3**. Daily runoff ($m^3\ s^{-1}$) and sediment load (t) calibration and validation. Daily precipitation of the period was included.*

As it was mentioned before, there are some differences in the land use inputs for the calibration and validation periods. Despite these changes affecting a very small patch of land (0.04 % of the total catchment) (Table 3.4), they have a great impact on the total suspended sediment yield and on the proportion of sediment coming from each land use class (Table 3.4). As Zabaleta et al. (2007) noted, the existence of unprotected soil and unconsolidated sediment increases the amount of sediment available for transport, indicating the impact of land management

practices and land use changes on the total suspended sediment yield and on the type of sediment delivered from the catchment. Indeed, almost 90 % of the sediment yield simulated during the validation period comes from bare soils, while during the calibration period pasture is the land use type that, considering its area, contributes most to sediment yield accounting for just 30 % (Table 3.4).

3.4.3 Discussion and conclusions

The *1P* (Fig. 3.2) was calibrated from 2007 to 2010 and validated from 2005 to 2006 at daily time-step. To do so, the river flow ($m^3 s^{-1}$) and the sediment load (t) measured at Aixola gauging station were used. The parameters calibrated in this project (Table 3.3) are the usual in streamflow and sediments simulation (Arnold et al., 2012).

Although the model underestimated daily peak discharges and sediment load, statistics assessing the fit between simulated and observed data series (NSE, R^2, PBIAS, and RSR) indicated that the results were satisfactory in both cases (Table 3.5). Precipitation intensity during rainfall events and the magnitude of discharge increase during the runoff event are the factors that most influence the value of the sediment peak (Zabaleta et al., 2007); therefore, the simulation results could probably be improved if the SWAT took precipitation distribution into account and by using sub-daily data that would consider the rapid (sub-daily) response to precipitation of this small catchment. In any case, the results in terms of both calibration and validation of the model show that, despite Aixola being a small and forested catchment, SWAT can be used in this catchment to develop a model that performs satisfactorily to simulate discharge as well as sediment loads (Moriasi et al., 2007).

3.5 EVALUATION OF SWAT MODEL PERFORMANCE TO SIMULATE STREAMFLOW SPATIAL ORIGIN

In this study, a new SWAT project (SWAT 2012) was created (Fig. 3.2, *2P*) in an attempt to improve on that previously applied (Fig. 3.2, *1P*). This was possible thanks to the new field data (discharge obtained from the EC and soil properties) obtained in Aixola catchment.

3.5.1 Hydrological model input, calibration and validation

As it was already mentioned, the DEM and the land use are the same as *1P* (Table 3.2) except for the soil properties database and soil map where cambisols have been divided in cambisol 1 and cambisol 2 because of the different depth of those soils (Fig. 3.2 b)). In Table 3.3 is possible to observe the most important differences of the soil properties in both projects.

The catchment configuration is very similar to 1.Project (sub-basin and HRU quantity and slope classification). Txulo sub-catchment was divided into 5 sub-basins (1, 2, 3, 5 and 8), while the Elgeta sub-catchment was distributed into 18 sub-basins (4, 6, 7, 9-23). The location of the CTD-divers was set as the outlet of the main two sub-catchments, located in d3 in Txulo and d6 in Elgeta (Fig. 3.1 a)).

	Observed (indirec data)		Simulated *2P*		Simulated *2P S1*	
	TXULO	**ELGETA**	**TXULO**	**ELGETA**	**TXULO**	**ELGETA**
AUTUMN 2011	30	70	28	72	32	68
WINTER 2012	41	59	31	69	36	64
SPRING 2012	45	55	29	71	40	60
SUMMER 2012	92	8	27	73	82	18
AUTUMN 2012	45	55	29	71	35	65

Table 3.7*. Percentage of seasonal discharge contribution for Elgeta and Txulo sub-catchments to the Aixola river for the data estimated with the mass balance approach (observed) and the simulated data (simulated 1.Project; 1P and 2.Project Step1; 2P S1).*

Before calibration (Fig. 3.2, *2P*), the effect on the simulation of the new soil properties obtained from the analysis of soil cores was evaluated. With this purpose, the simulated data obtained for the gauging station in *2P* were compared with the results of *1P* (Fig. 3.4). In addition, the contribution of main sub-catchments was also analysed. Discharge data were not available for Txulo and Elgeta sub-catchment when *1P* was performed, therefore the simulated discharge for these points in *2P* was only contrasted with the calculated discharge with the CMB approach (Table 3.7). This analysis showed that *2P* did not simulate well the spatial distribution of main sub-catchments, especially in the driest seasons.

To achieve a more realistic simulation a second calibration was done (Fig. 3.2, 2.Project Step 1 hereafter *2P S1*) from 1/1/2009 to 31/12/2012 using the daily

discharge ($m^3 \cdot s^{-1}$) measured in the gauging station and also discharge data of the main two sub-catchments derived from the CMB approach for the period between 1/10/2011 and 31/12/2012. Therefore for the last period, a calibration with 3 points (gauging station, Elgeta (d6) and Txulo (d3)) was conducted. It was intended to study whether the use of these new data and the consideration of the associated hydrological processes might help improve the results of the simulation.

Calibration was performed manually and automatically using the SWAT CUP program (Abbaspour et al., 2007). The SWAT CUP program was used for autocalibration. However, the results obtained with this method for the calibrated outlets (gauging station, Elgeta and Txulo sub-catchments) were not any better than those achieved manually and therefore the results shown refer to a manual calibration. This was made comparing the observed discharge on the gauging station and the calculated from the CMB approach to Elgeta and Txulo sub-catchments with the simulation results. The evaluation was performed with the statistics explained in the *2.4.7 Modelling processes and evaluation methods* and with graphical methods. During validation (1/1/2005-31/12/2008), only the discharge in the gauging station (outlet) of the catchment was considered since no records of EC data existed for that period.

Table 3.8 shows the parameters that were adjusted from the model default values during calibration. These parameters were obtained from a thorough sensitivity analysis for the entire catchment, using SWAT CUP's one-at-a-time approach to know how sensitive the parameters and their sensitivity range were. Then a global analysis was done to understand the sensitivity ranking. The parameters have been modified separately for each of the sub-catchments due to their slightly different hydrological behaviour, although both sub-catchments manifest a swift response to precipitation. Elgeta (sub-basins 4, 6, 7, 9-23) has higher runoff coefficient thus more streamflow generated than Txulo (sub-basins number 1, 2, 3, 5 and 8). However, when there is a lack of rainfall (summer) Txulo shows a higher regulation capacity because most of the streamflow is contributed from this sub-catchment. (Fig. 3.4, Table 3.7). This is also a reason for the difference in the parameterization of sub-catchments on the key water budget components.

The lateral flow travel time (LAT_TTIME) is considerably higher in the Txulo sub-catchment than Elgeta (Table 3.8), thereby the pathways of water movement takes longer through the soil profile. Additional soil properties, such as the available water capacity (SOL_AWC) and the moist bulk density (SOL_BD) of the soil layer in Txulo catchment, were also increased during calibration and, therefore, the increase in water holding capacity also increased the potential for more evapotranspiration by vegetation. On the other hand, parameters such as Manning's n value for overland flow (OV_N) and the baseflow alpha factor (ALPHA_BF) decreased in Txulo, so that surface water and ground water travel time has increased. In Txulo, with the maximum canopy storage (CANMX), evapotranspiration was reduced, therefore, the overall water yield increased. In order to better match the high flows, the Curve Number for moisture condition II (CN2) was increased by 10 % in Txulo. In addition, elevation bands (ELEVB, ELEV_FR) were used to account for orographic effects on precipitation and temperature of the Aixola catchment.

Change type	Parameter name	Description	Flow		1. Project
			Txulo	Elgeta	
r	CN2.mgt	Curve number for moisture condition II	↑10%	No change	↓10%
v	CH_K2.rte	Main channel conductivity	52	7	100
v	SURLAG.bsn	Surface runoff lag coefficient	1	1	1
v	ALPHA_BF.gw	Baseflow alpha factor	0.005	0.015	0.021
v	ESCO.bsn	Soil evaporation compensation factor	0.9	0.9	0.9
v	GWQMN.gw	Threshold depth of water in shallow aquifer required for return flow to occur	700	700	700
v	CANMX.hru	Maximum canopy storage	5	10	8
v	GW_REVAP.gw	Groundwater "revap" coefficient	0.05	0.15	0.19
	SOL_K.sol	Saturated hydraulic conductivity	No change	No change	↑10%
r	SOL_AWC.sol	Available water capacity of the soil layer	↑22%	No change	↓4%
r	GW_DELAY.gw	Groundwater delay time	450	450	40
r	SOL_BD.sol	Moist bulk density of first soil layer	1.7	No change	No change
r	ELEV. sub	Elevation at the centre of the elevation band	450	19	No change
r	ELEV_FR. sub	Fraction of sub-basin area within the elevation	1	12	No change
r	SPCON.bsn	Channel sediment routing parameter	0.0001	0.0001	0.0001
v	SPEXP.bsn	Exponent parameter for calculating sediment re-entrained in channel	1.5	1.5	1.5
v	LAT_TTIME.hru	Lateral flow travel time	82	3.57	5
v	OV_N.hru	Manning's *n* value for overland flow	0.1	0.6	0.6
v	SHALLST.gw	Initial depth of water in the shallow aquifer	1000	1000	1000
v	DEEPST.gw	Initial depth of water in the deep aquifer	0	0	0
v	RCHR_DP.gw	Deep aquifer percolation factor	0	0	0

Table 3.8. *SWAT parameters selected for calibration, their description and modifications carried out during calibration for each of the sub-catchments. *v means that the default parameter is replaced by a given value, and r means the existing parameter value is changed relatively.*

The values of the parameters of the Elgeta sub-catchment are very similar to those set in the *1P* (, in which the values of the parameters were the same throughout the catchment.

In order to evaluate the performance of the model in the Aixola catchment and Txulo and Elgeta sub-catchments, simulated data were compared with data taken from field measurements using several widely-used model evaluation methods, explained in the *2.4.7 Modelling processes and evaluation methods*.

3.5.2 Results: Contribution from-sub-catchments

As mentioned previously, *2P* has the same input data and calibrated parameters as the *1P* with the exception of soil map and soil properties (Fig. 3.2). Fig. 3.5 shows the results for the discharge for both calibration (1/1/2009-31/12/2012) and validation (1/1/2005-31/12/2008) periods for the gauging station. It can be observed that merely introducing more realistic characteristics of soils (*2P*) improves the simulation, increasing the high flow peaks, especially in the driest seasons where low flow decreases in a more realistic simulation (Fig. 3.5, compare *1P* and *2P*). However, in these periods small storm events occur and the model is still unable to simulate these effects. Although the simulation in gauging station improves in *2P*, Fig. 3.4 and Table 3.7 show that the spatial distribution of sub-catchments is not yet correct, in general overestimating Elgeta sub-catchments contribution and underestimating Txulo.

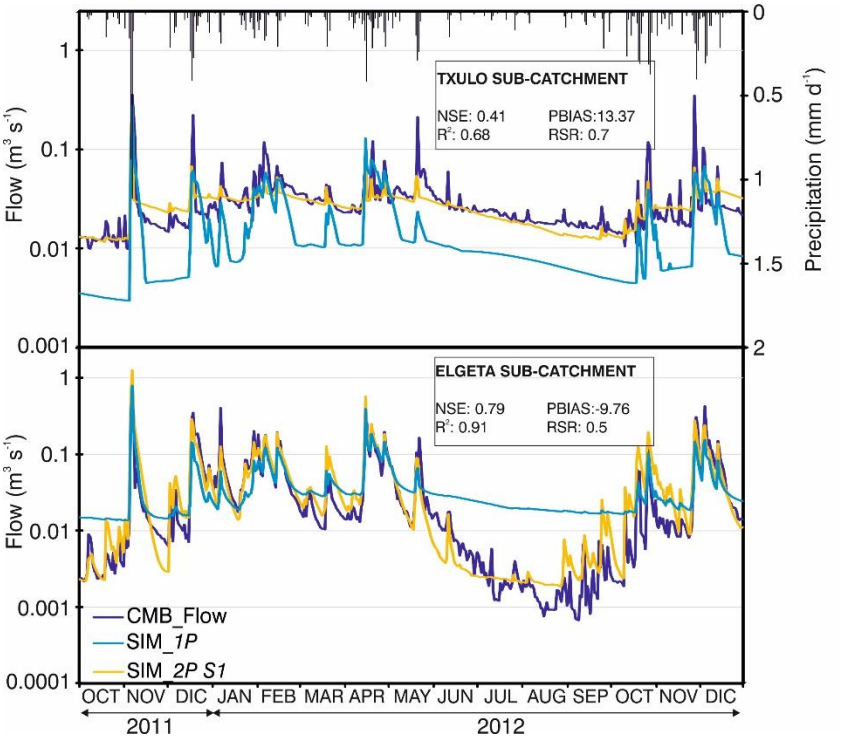

Figure 3.4. *Daily discharge derived from the CMB method (CMB_Flow) and simulated in 1.Project (SIM_1P) and 2.Project Step 1 (SIM_2P S1). Model evaluation statistics for Txulo and Elgeta (2P S1) sub-catchments are also shown. Precipitation of the period is included.*

The daily flow obtained from the CMB approach (1/10/2011-31/12/2012) was used to calibrate and evaluate the model daily discharge in the outlets of Elgeta and Txulo sub-catchment (Fig. 3.1a) points d6 and d3). Once calibration has been performed considering sub-catchments contribution (*2P S1*), peaks produced by storm events in gauging station are simulated correctly (Fig. 3.5, *2P S1*), obtaining a much more adjusted simulation in high and low flows. After *2P S1*, simulated discharge in Elgeta sub-catchment fits well with the discharge obtained from electrical conductivity, showing *very good* performance of the model (Fig. 3.4) – even better than in the outlet (Fig. 3.5), according to NSE, R^2, PBIAS and RSR. Therefore, for the discharge in Txulo, and using the recommended statistics, data for the calibration period would show only acceptable levels of agreement (Fig. 3.4).

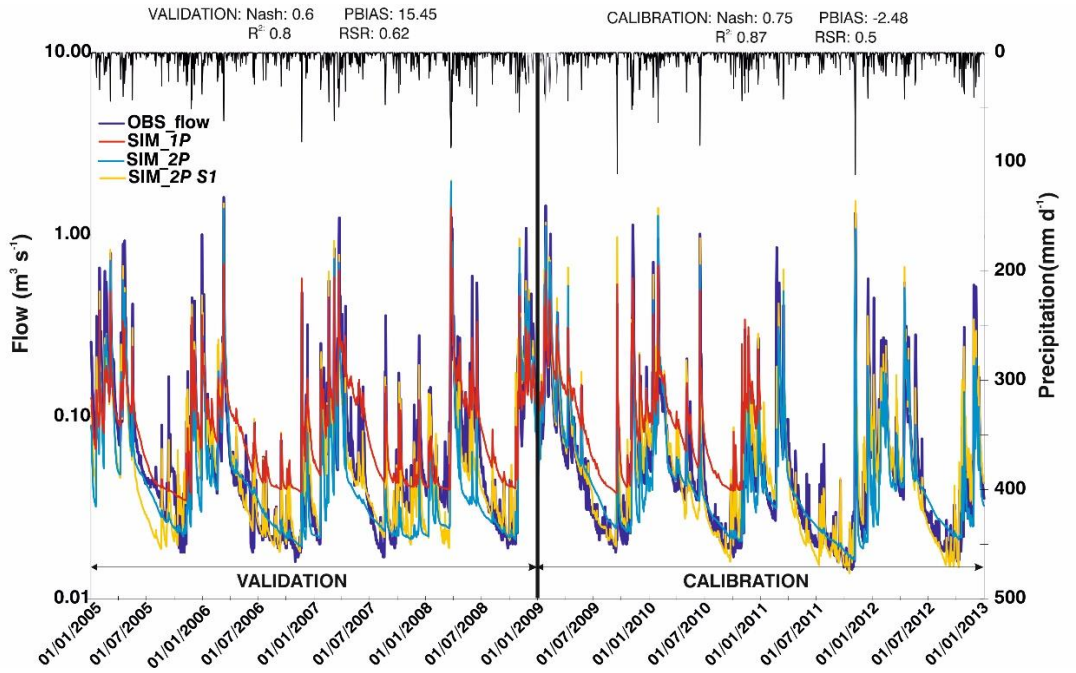

Figure 3.5. *Simulated (SIM_1P for 1.Project, SIM_2P for 2.Project and SIM_2P S1 for 2.Project Step 1, see Fig. 3.2) and observed daily discharge (OBS_flow) for calibration and validation period and the model evaluation statistics for the outlet of the catchment. Precipitation of the period was included.*

During calibration, the parameters related to the retention capacity of the Txulo sub-catchment were changed as shown in the previous section (Table 3.5) obtaining better results for discharge between runoff events (Table 3.7 and Fig. 3.4). Nevertheless, these changes led to a decline in the simulation of rainfall events, as runoff response was not as quick and direct as the response observed in data obtained from the CMB. This may be one of the reasons why the simulation of Txulo was just acceptable. However, another issue should also be considered - the small size of the sub-catchment (1 km^2) may be critical for the correct performance of the SWAT model at a daily time-step, or there may be gaps in the knowledge of the physical properties of this sub-catchment. Underestimation of the peak flows in the Txulo sub-catchment has a direct effect on simulation of the discharge in the outlet of Aixola catchment, and therefore the largest errors and uncertainties come from this small area.

Nevertheless, it should be noted that the use of data obtained from the CMB approach was essential in the calibration process. Considering the input data

from Txulo and Elgeta are quite similar, if SWAT is not forced it is always going to simulate more water quantity in the larger sub-catchment (Table 3.7, *2P*). Therefore, use of this methodology revealed the importance of the Txulo sub-catchment (Fig. 3.4, Table 3.7) which, although much smaller than Elgeta, provides a larger quantity of water in the driest seasons (summer). Regarding the temporal (seasonal) distribution of the streamflow contribution of each of the sub-catchments into Aixola river, the results of the simulation present *good* results for the calibration. Table 3.7 shows the percentage of the model simulated in *2P* and *2P S1*, and the streamflow contribution estimated from the CMB for each season and sub-catchment. From these data, it may be concluded that the model underestimates the percentage of water contributed to the Aixola river from the Txulo sub-catchment for all seasons. Conversely, it overestimates the percentage of water coming from Elgeta.

Autumn is the only season for which two years of data could be compared. For this season, it is noteworthy that while for 2011 the results fit well, there are important differences in 2012. These differences may be related to the fact that a storm event occurred in the area during October 2012 which the model was unable to correctly simulate for the Txulo sub-catchment (Fig. 3.4).

3.5.3 Results: Surface runoff/baseflow contribution

The simulated surface runoff and baseflow (Fig. 3.2, *2P S1*) were compared with that obtained applying the CMB and BFP methods to evaluate the performance of the model. The three methods used to separate the hydrograph (SWAT-model-based separation, tracer-based CMB and non-tracer-based BFP) show the important contribution of baseflow (Fig. 3.6) in the Aixola catchment (13/04/2011-31/12/2012).

Comparing the results of the simulation for the entire period and seasonally, *2P* generates a higher amount of baseflow. During the calibration phase the model does not simulate the discharge peaks caused by small storm events. Note, that in *2P* calibration each sub-catchment contribution was not considered and the results obtained in *2P S1* are therefore the ones that will be compared with the other methods to decompose the hydrograph.

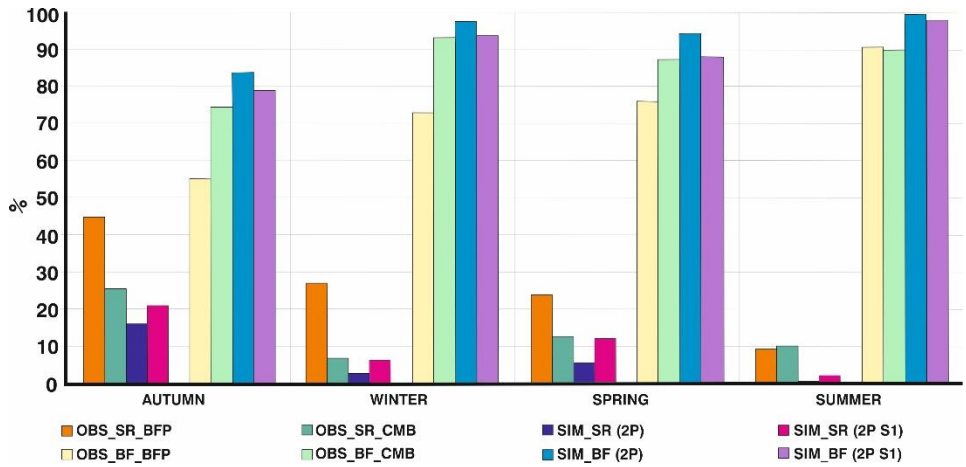

Figure 3.6. *Observed (OBS) and simulated (SIM, 2.Project (2P) and 2.Project Step 1 (2P S1)) surface runoff (SR) and baseflow (BF) calculated using the CMB method (CMB) and baseflow filter program (BFP). Data are expressed as a percentage, taking the observed discharge in the case of the decomposition of the observed hydrograph, and taking the simulated discharge for the simulated surface runoff and baseflow. The period under consideration was 13/4/2011-31/12/2012.*

The results obtained from the CMB approach and the results of the simulation (*2P S1*) are very similar; around 15 % surface runoff and 85 % baseflow in annual terms. The BFP apportioned the observed discharge of the outlet in 30 % surface runoff and 70 % baseflow. When this distribution is analysed seasonally (Fig. 3.6), decomposition obtained from the CMB approach and the SWAT simulation (*2P S1*) are usually similar. These methods give baseflow contribution values of around 80 % for autumn, and around 90 % for spring, winter and summer. The BFP gives a similar distribution but with slightly different contribution percentages. In this case, baseflow contributes around 60 % in autumn, less than 80 % in both spring and winter, and around 90 % in summer. Autumn is the season with the greatest differences between the three methods. When using BFP, which is comparable in accuracy with the manually separated graphical method (Arnold et al., 1995), the baseflow is lower than that calculated by CMB and SWAT simulation (*2P S1*). Research at a catchment located near Aixola with similar physical characteristics (Martínez-Santos et al., 2014) concluded that the graphical methods might underestimate the baseflow contribution, and use of this method only becomes viable for storm events where surface runoff is

dominant. A previous study (Zabaleta & Antiguedad, 2013) carried out in Aixola catchment, showed that the amounts of baseflow (in storm events) were important and it may therefore be assumed that the BFP is underestimating the baseflow contribution. It should also be taken into account that two of the three methods used (CMB and SWAT simulation outputs) show practically the same results (Fig. 3.6).

The data obtained through the CMB and BFP were not used for the calibration but they were used to evaluate the accuracy of the simulation compared with SWAT outputs. The results differ, depending on the hydrograph separation method. However, in general it can be seen that when SWAT is calibrated taking additional field data into consideration (soil characteristics and sub-catchment contribution) the results are similar to those obtained with BFP and to an even greater extent with CMB, which presents more reliable results, as shown before. Therefore, the uncertainty related to the baseflow / surface runoff contribution could be considered negligible.

Not only was *good* simulation for the outlet achieved, runoff spatial distribution in the catchment was simulated accurately as well. It should be noted that it was necessary to use data derived from field measurements to apply this approach.

3.5.4 Discussion and conclusions

Installation of probes in the river to measure the specific electrical conductivity (EC) allowed us to quantify the amount of discharge from the two sub-catchments in Aixola and showed that the smaller sub-catchment, Txulo, has higher regulation capacity than the larger one, Elgeta. When discharge contributions based on EC data are not taken into account in calibration, SWAT always simulates higher discharge from the Elgeta sub-catchment, due to the apparent homogeneity of the catchment.

According to habitually used statistics, *good* simulation results were obtained for the discharge in the outlets of the Aixola catchment (1/1/2009-31/12/2012 calibration, 1/1/2005-31/12/2008 validation) and Elgeta and Txulo sub-catchments (1/10/2011-31/12/2012), for daily time-step and seasonally. The Conductivity Mass Balance approach (CMB) and the Baseflow Filter Program

(BFP) were used to separate the discharge observed in the outlet of the catchment (13/4/2011-31/12/2012), into baseflow and surface runoff. The results obtained using the CMB method were very similar to the simulation results, showing that the baseflow contribution in Aixola is very important (85 %). Baseflow contribution calculated with the BFP (70 %) is usually lower than that calculated with the other methods. Hence, the greatest uncertainties relating to modelling of the Aixola catchment with the SWAT model come from the spatial distribution of streamflow, specifically that from the smallest sub-catchment, Txulo. When this distribution is analysed seasonally good performance is observed, with autumn being the season with most uncertainties. In terms of the baseflow / surface runoff relation, the model performs well.

This research shows the importance of understanding hydrological processes in the catchment during modelling. Even though Aixola is a small catchment (4.6 km^2), it was possible to achieve an acceptable performance of the SWAT model in the catchment outlet. However, as results show, an acceptable simulation of discharge in the outlet of a catchment does not mean either a good performance of runoff generation processes in the catchment or an acceptable spatial contribution of discharge.

It was therefore necessary to use field data that is usually not considered in calibration processes, in order to achieve acceptable performance of the hydrological processes taking place in the catchment. Thus, taking field data into consideration helped make the simulation more realistic.

3.6 SUB-DAILY STREAMFLOW AND SEDIMENT LOAD SIMULATION

The *2P* was calibrated one more time at hourly time-step (Fig. 3.2, 2.Project Step 2 hereafter *2P S2*). The aim of this step was to evaluate the influence of the modelling time-step on the results. Aixola is a small catchment with important slopes and quick response to the precipitation, maybe this is the reason why,

SWAT underestimates the magnitude of the discharge peaks (sections *3.4 Streamflow and sediment yield simulation in Aixola catchment* and *3.5 Evaluation of the model performance to simulate streamflow spatial origin*, *1P* and *2P*). Therefore, it will be evaluated if performing the simulation at smaller time scale than daily improves the results; a) for the hourly calibration and validation, b) for the daily calibration and validation and c) in different type of storm events.

3.6.1 Hydrological model input, calibration and validation

In *2P S2*, the river flow (m^3 s^{-1}) and the sediment load (kg) measured at Aixola gauging station were used to calibrate (from 2010 to 2014) and validate (from 2005 to 2009) the model. The surface runoff and the baseflow obtained with the CMB approach were not used for the calibration. Nevertheless, these data were used to evaluate if the simulated distribution is coherent. This analysis was done at daily time-step because as it was explained in the *2. Methodology* chapter *2.4 Hydrological modelling: general description of Soil and Water Assessment Tool (SWAT)* section, although the simulation is done sub-daily, SWAT calculates the surface runoff/baseflow distribution at daily time-step.

Before starting the calibration, the parameter values used in the *2P S1*, were introduced in the *2P S2* (Fig. 3.2). Considering the statistical indices, the discharge results were not satisfactory because, for example, NSE value was -1.23 and R^2 0.16, and the graphical comparison between the measured discharge and the simulated also indicates a poor performance. This is the reason why the *2P* was calibrated again to simulate hourly discharge and sediment yield. Nevertheless, instead of starting a calibration from the beginning some of the values calculated in *2P S1* (Table 3.8) were used in this step and the calibration was specially focused on the parameters that can be used in the sub-daily calibration (explained in the next paragraphs). For example, in *2P S2* the parameters related with snow and the ground water have little influence and therefore, the values calculated in the *2P S1* were not modified (see Table 3.8 and Table 3.9).

Change type	Parameter name	Description	Flow/Sediment	
			Txulo	Elgeta
r	CN2.mgt	Curve number calculated with catchment slope	No change	
v	CH_K2.rte	Main channel conductivity	42.07	15.79
v	CH_N2.rte	Manning's "n" value for the main channel	0.023	0.152
v	SURLAG.bsn	Surface runoff lag coefficient	1	
v	SFTMP.bsn	Snowfall temperature (°C)	1.1	
v	SMTMP.bsn	Snow melt base temperature (°C)	4.5	
v	ICN.bsn	Daily curve number calculation method	Plant ET	
v	CNCOEF.bsn	Plant ET curve number coefficient	1.75	
v	ADJ_PKR.bsn	Peak rate adjustment factor for sediment routing	0.61	
v	MSK_CO1.bsn	Calibration coefficient in Muskingum method	5.8	
v	MSK_CO2.bsn	Calibration coefficient in Muskingum method	5.78	
v	MSK_X.bsn	Weighting factor in Muskingum method	0.18	
v	EROS_SPL.bsn	Splash erosion coefficient	1.09	
v	RILL_MULTL.bsn	Rill erosion coefficient	0.55	
v	EROS_EXPO.bsn	Exponential coefficient for overland flow	0.55	
v	SUBD_CHSED.bsn	Instream sediment model	2	
v	C_FACTOR.bsn	Cover and management factor for overland flow erosion	0.001	
v	CH_D50.bsn	Median particle diameter of main channel (mm)	0.75	
v	SIG_G.bsn	Geometric standard deviation of particle size	1.44	
v	ALPHA_BF.gw	Baseflow alpha factor	0.005	
v	ESCO.bsn	Soil evaporation compensation factor	0.9	
v	GWQMN.gw	Threshold depth of water in shallow aquifer required for return flow to occur	700	
v	CANMX.hru	Maximum canopy storage	0.07	
v	GW_REVAP.gw	Groundwater “revap” coefficient	0.05	0.15
	SOL_K.sol	Saturated hydraulic conductivity	No change	
r	SOL_AWC.sol	Available water capacity of the soil layer	No change	
r	GW_DELAY.gw	Groundwater delay time	450	
r	SOL_BD.sol	Moist bulk density of first soil layer	No change	
r	ELEV. sub	Elevation at the centre of the elevation band	450	19
r	ELEV_FR. sub	Fraction of sub-basin area within the elevation ba	1	12
r	SPCON.bsn	Channel sediment routing parameter	0.01	
v	SPEXP.bsn	Exponent parameter for calculating sediment re-entrained in channel	1.5	
v	LAT_TTIME.hru	Lateral flow travel time	3.918	
v	OV_N.hru	Manning’s *n* value for overland flow	0.3	
v	SHALLST.gw	Initial depth of water in the shallow aquifer	1000	
v	DEEPST.gw	Initial depth of water in the deep aquifer	0	
v	RCHR_DP.gw	Deep aquifer percolation factor	0	

Table 3.9. *SWAT parameters selected for hourly calibration (2P S2), their description and modifications carried out during calibration for each of the sub-catchments. *v means that the default parameter is replaced by a given value, and r means the existing parameter value is changed relatively.*

Accordingly, the beginning of the calibration started with Hargreaves evapotranspiration method, the values of the parameters related to the snow and ground water calculated in *2P S1* and the rest of the parameters had the default values. Changing only this few parameters the simulated hydrograph shape was

not the adequate because the simulated had more fluctuations and did not fit in time with the observed. To change the shape of the hydrograph, the parameters of the channel routing need to be changed and SWAT has two methods to simulate the channel routing: the variable storage water routing (Williams, 1969) and the Muskingum method (Overton, 1966) (see *2. Methodology* chapter *2.4. Hydrological modelling: general description of Soil and Water Assessment Tool (SWAT)* section). In this case, to simulate the channel routing, the Muskingum method was used because it has three parameters that can be changed to modify the shape of the hydrograph (MSK_CO1, MSK_CO2 and MSK_X, see Table 3.9) while the variable storage water routing has not calibration parameters. By changing the parameters that pertain to Muskingum method the simulated and observed hydrograph fit better. Nevertheless, the simulated surface runoff was too low for Aixola catchment (97 % baseflow and 3 % surface runoff). To decrease the lateral flow and increase the surface runoff the parameters related to the Green & Ampt Mein Larson infiltration method (Mein & Larson, 1973) were modified. For example, the clay amount of the soil was increased, and the soil saturated conductivity (SOL_K; K_{sat} in 2.9 equation) and the sand content decreased. Nevertheless, although these changes increased the surface runoff, it was in a low amount. In addition, some of these parameters (clay and sand content) were measured in the catchment, therefore although it is possible to modify their value, it is advisable to change their values as little as possible. Considering that the influence of these parameters on the amount of surface runoff was low and their values should be modified as little as possible, it was decided not to change the sand and clay contents of the soils and their permeability. CN was calculated using the plant evapotranspiration method (equation 2-7) which value is dependent on the antecedent climate. The plant evapotranspiration factor can be modified with the CNCOEF which is the weighting coefficient used to calculate the retention coefficient for daily curve number calculations dependent on plant evapotranspiration. This parameter was very sensitive and its calibration achieved an increase of the surface runoff and the decrease of the lateral flow (baseflow).

In the discharge calibration, the most sensitive parameters were the ones related to the Muskingum routing method and the CNCOEF. The values for these parameters were estimated with the SWAT CUP program (Abbaspour et al., 2007). The calibrated parameters are shown in the Table 3.9.

Considering the sediment calibration, the most sensitive parameters were calculated with the SWAT CUP's absolute sensitivity analysis (modified by Bressiani (2016) for sub-daily time-step), being those: the exponential coefficient for overland flow (EROS_EXPO), the mean particle diameter (CH_D50) and the scaling parameter for cover and management factor for overland flow erosion (C_FACTOR). In general, all the changes were done with the aim of increasing the sediment amount because the simulated sediment was considerably lower than the observed. The C FACTOR is the most sensitive parameter because it has a lot of influence in the erosion and therefore in the availability of suspended sediment. The influence of the rest of sensitive parameters is low comparing with C_FACTOR. In addition, some parameters were calibrated although they not appear in the sensitivity analysis as "sensitive". For example, the parameter SUBD_CHSED gives three possibilities to choose the instream sediment routing model. In this case, the number 2, Yang model, was selected because it is the most appropriate for small catchments (Yang, 1996). To increase the sediment simulation performance in peaks, the peak rate adjustment factor for sediment routing was calibrated (ADJ_PKR), nevertheless the influence of this parameter was limited. The rill erosion coefficient (RILL_MULT) was also increased with the aim of increasing the suspended sediment content in stream. The sensitivity of this parameter is high, nevertheless it should be changed carefully because it generates a lot of fluctuations. Other modified parameters are the channel sediment routing parameter (SPCON), exponent parameter for calculating sediment retrain in channel (SPEXP) and geometric standard deviation of particle size (SIG_G). The influence of these parameters in the performance of the sediment simulation was scarce although with their calibration the results were slightly better.

Parameters like plant canopy (CANMX) have influence in discharge and sediment simulation because its increase decreases the water that reaches the soil and

therefore the generated sediment is smaller. All the calibrated parameters values are in Table 3.9.

3.6.2 Storm events characterization and selection

As mentioned above, in this step (Fig. 3.2, *2P S2*) the evaluation of simulation results was done for the whole period (calibration from 2010 to 2014 and validation from 2005 to 2009) and for different types of events, all of them from the calibration period. Specifically, the events were selected from 2012 to 2014 because in this period the electrical conductivity was also measured in the streamflow of the Aixola gauging station and therefore it is possible to apply the CMB approach (see section *3.3.1 Sub-catchment contribution*) to separate the surface runoff (SR) and the baseflow (BF). The beginning of the event was stablished when the surface runoff stars, and the end when all the surface runoff is depleted. These patterns prove to be valid when it is a single-peak event. Nevertheless, in the Atlantic watershed the multiple-peak events are usual.

The events were characterized with five groups of parameters: conditions before the storm, precipitation that generates the event, the discharge during the event, surface runoff and baseflow in the event (at daily time-step) and the suspended sediments exported during the event.

To characterized the storm events, the total precipitation that generates the event (Pt, mm), the mean intensity during the rainfall (IP, mm h^{-1}) and the maximum intensity of it (Pmax, mm h^{-1}) were calculated. Nevertheless, the conditions before the event also were considered, thus the precipitation one hour before the event (bP1, mm), seven and twenty-one days before (bP7d, mm; bP21d, mm) and the mean discharge measured in the gauging station 24 hours before the event (bQ1d, L s^{-1}) were calculated.

The discharge during the storm event was expressed as the total water volume (Qt, mm) measured in the gauging station during the event, the mean (Qmean, L s^{-1}) and maximum (Qmax, L s^{-1}) discharges and the rate between the maximum discharge and the discharge before the event (Qmax/Qb). The mean (CSSmean, mg L^{-1}) and maximum suspended sediment concentration (CSSmax, mg L^{-1}) and the total load (SSt, kg) were also considered.

To analyse the hourly performance of SWAT model daily baseflow (BF, mm) and surface runoff (SR, mm) contribution were also considered at daily time step. In the case of the observed values these parameters were calculated with the CMB approach, and in the case of the simulated, both (BF and SR) are a daily output in SWAT. In addition, the relationship between the baseflow and the surface runoff was also calculated (BF/SR) and taken into account to characterize the events.

As the precipitation is an input variable it is only possible to consider the observed precipitation, nevertheless, all the parameters related to the discharge and the sediment were calculated for observed and simulated values. Fifteen storm events registered in the calibration period (from 2010 to 2014; Fig. 3.7) were analysed to evaluate the simulation performance on each type of event. These fifteen events represent different hydrologic situations; different antecedent conditions, rainfall intensity and/or discharge amount. Note that sediment data from 2012 March to November are missing and consequently there are not storm events analysed for this period.

3.6.3 Results: Model calibration and validation

The statistical indices for the hourly calibration (from 2010 to 2014) show that the discharge simulation is at least *good* (Table 3.10). For the validation period (from 2005 to 2009) NSE and RSR are satisfactory, these statistical indices are very sensitive to extreme values and may be concluded that the peaks fit better in the calibration than in the validation period. In the validation period the precipitation intensity of some events is higher than in the calibration and therefore, the discharge peaks are higher. The simulated peaks however, are not high enough to fit with the observed and this is reflected in the results of the statistical indices (Fig. 3.7). On the other hand, PBIAS and R^2 show that the discharge calibration and validation are very *good*.

	Calibration (2010-2014)		Validation (2005-2009)	
	flow	sediment	flow	sediment
NSE	0.71	0.24	0.55	0.30

R^2	0.85	0.5	0.79	0.7
PBIAS	-12	-0.22	5.87	10.88
RSR	0.54	0.87	0.66	0.83

Table 3.10. *Sub-daily summary statistics obtained for NSE, R^2, PBIAS and RSR.*

Considering the sediment load hourly simulation performance, as it is possible to observe in the Fig. 3.7 the magnitude of the simulated peaks is considerably lower than the observed, that is, the simulation does not generate as much sediment as the real system (Aixola catchment) in an event. This is the reason why the NSE and the RSR are *unsatisfactory*. The statistical indices are better for the validation period than by the calibration. This is because in November 2011 there is a flood that transports an important amount of sediment (≈8000 kg) that is not simulated for the model, which has a significant weight in the results of the statistical indices (Fig. 3.7).

Note that the statistical indices values to evaluate the simulation performance (Table 2.8) are stabilised for monthly simulation, and generally, as the evaluation time-step increases, a stricter performance rating is warranted (Moriasi et al., 2007).

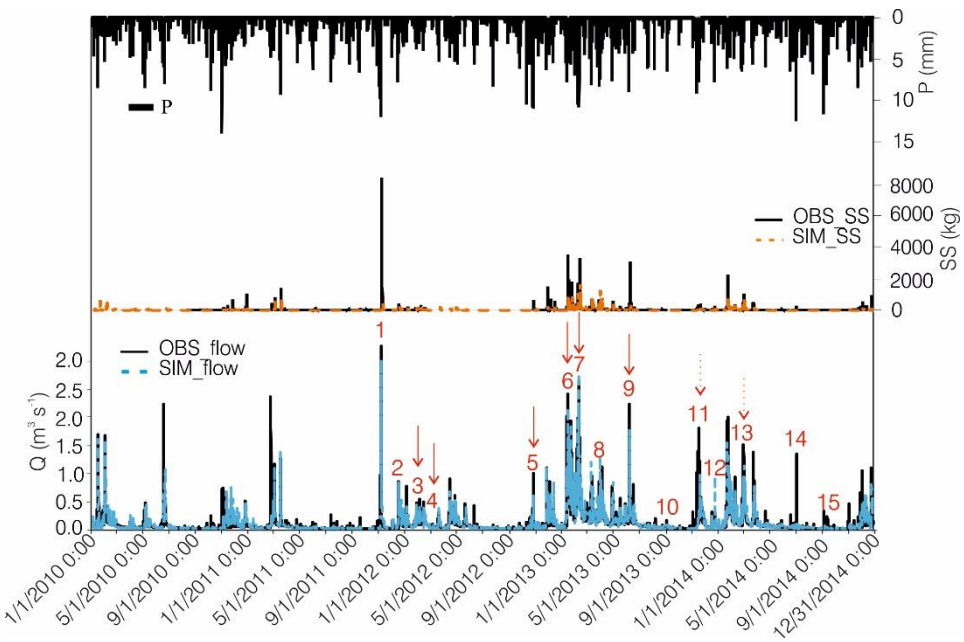

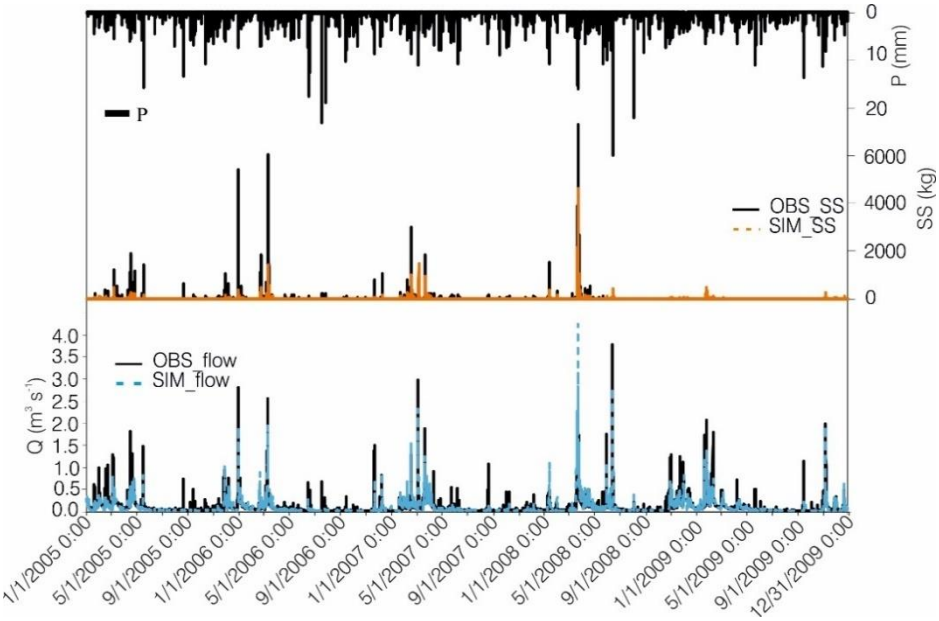

Figure 3.7. *Graphical results for the hourly discharge and sediment calibration (top image) and validation (image below). Precipitation of the period is included. In the top image the analysed event numbers and their performance is displayed; when the arrow is continuous the performance is at least satisfactory (based on R^2, RSR and graphics), when the arrow is discontinuous the simulation performance improves at the half-end of the event (based on graphics) and when there is not an arrow the performance is unsatisfactory.*

With the purpose of evaluating whether the sub-daily simulation increases the daily performance, the statistical indices were calculated at daily time-step. As it is possible to observe in the Table 3.11 the streamflow daily performance when the simulation is carried out at sub-daily time-step is better. In general, the simulated and observed peaks fit better (better NSE and RSR) and the PBIAS is lower but the improvement is small. Taking into account the sediment, the simulation improvement when the sediment simulated at sub-daily time-step is considered at daily time-step is considerable (Table 3.11, Sediment Step 2). Aixola catchment shows an immediate and important response to storm events (Zabaleta et al., 2007). However, the simulation does not show an immediate response so that the sediment load, instead of mainly concentrating during the event, is dispersed, especially after the event thus, after the event, the sediment load is exported lengthened in time. The hourly modelling improvement occurs when the simulated sediment load is accumulated in a day, and these data fit much better with the daily observed values.

In the 1.Project the sediment load was also simulated. The statistical indices for all the modelling periods are shown in Table 3.11. These values are worse than the obtained in Step 2, therefore, when the simulation is done at sub-daily time-step the daily results are better than when the simulation is done at a daily time-step. Nevertheless, it is important to have in mind that the discharge results from 1.Project were worse than in Step 2 and the error generated in the discharge simulation is transferred to the sediments.

	FLOW *2P S1* 2005-2012	FLOW *2P S2* 2005-2012	SEDIMENT *1P* 2005-2010	SEDIMENT *2P S2* 2005-2010
NSE	0.69	0.71	0.54	0.72
R^2	0.91	0.89	0.8	0.84
PBIAS	-10.72	-2.29	43.28	19.92
RSR	0.56	0.54	0.67	0.53

Table 3.11. *Daily summary statistics obtained for NSE, R2, PBIAS and RSR for flow (Fig.3.2 2P S1 and 2P S2) and sediments (Fig. 3.2 1P and 2P S2).*

3.6.4 Analysis of the model performance during different types of events

After evaluating the performance of the simulation as a whole, i.e. for calibration and validation, the next action was to evaluate the performance at event scale. Fifteen storm events from the calibration period were selected for the evaluation. The events are numbered in the top image of the Fig. 3.7.

In the figures 3.8 to 3.22, it is possible to observe the analysed events in detail. In each image, the hourly precipitation in mm, the observed and simulated sediment load (kg) and the observed and simulated dishcarge (m^3 s^{-1}) are represented. In both cases the RSR and R^2 results for each storm event can be observed on the graphics. NSE and PBIAS were not calculated because these statistical indices are not adequate for single-events (Moriasi et al., 2015). The event characteristics related to precipitation are represented in the top left of the image while those related to streamflow and suspended sediment, appear in a table at the bottom of each image. The baseflow and surface runoff values are calculated not for the event but instead for the whole days that the event occurs (starting at 0:00 and ending at 23:59). This is because SWAT calculates these variables at daily time-step and thus, the baseflow and surface runoff calculated with CMB and the

obtained with the simulation can be compared. Nevertheless, with the aim of identifying different types of events, the baseflow and the surface runoff calculated with CMB for each event were analysed and it is possible to observe the results in the Table 3.12.

Considering the values in Table 3.12, the observed storm events can be grouped into different types. In some events **surface runoff is greater than the 60 %.** These are events with important precipitation intensity and high discharge. They can be divided in two groups, summer events (**9, 14 and 15**) and autumn/winter events (**1 and 6**).

Event	Date	IP (mm h^{-1})	Pmax (mm h^{-1})	Qmean (L s^{-1})	Qmax/Qb	%BF	%SR	Flood P.	Sediment P.
1	11/4/2011 - 11/8/2011	3.7	11.9	649.91	160.31	25	75	X	X
2	12/16/2011 - 12/19/2011	1.7	7.7	368.49	39.38	50	50	≈*	X
3	1/28/2012 - 1/30/2012	1.0	3.8	223.29	5.31	73	27	√	√
4	2/14/2012 - 2/25/2012	1.2	3.9	247.84	5.89	80	20	√	≈*
5	11/26/2012 - 12/1/2012	1.0	6.2	263.69	43.97	49	51	√	X
6	1/12/13 - 1/23/13	1.3	7.8	763.20	31.45	37	63	√	≈*
7	2/4/2013 - 2/23/2013	1.0	10.7	586.85	8.76	53	47	√	X
8	4/29/2013 - 5/4/2013	0.6	7.6	214.16	8.35	68	32	X	√
9	6/8/2013 - 6/10/2013	1.7	8.9	631.67	13.18	37	63	√	X
10	8/8/2013	1.3	4.2	66.44	4.18	67	33	X	X
11	11/8/2013 - 11/26/2013	0.7	9.1	309.50	71.63	55	45	≈	X
12	12/26/2013 - 12/27/2013	2.6	7.8	111.16	2.20	69	31	X	√
13	2/28/2014 - 3/6/2014	1.0	6.5	588.58	14.51	51	49	≈	X
14	7/3/2014 - 7/4/2014	3.6	12.4	156.94	45.16	35	65	X	X
15	9/7/2014 - 9/8/2014	5.2	11.6	73.72	17.91	30	70	X	X

Table 3.12. *Event number and date and observed parameters: precipitation intensity (IP; mm h^{-1}), maximum precipitation (Pmax; mm h^{-1}), mean discharge (Qmean; L s^{-1}), relationship between maximum discharge and the discharge before the event (Qmax/Qb) and baseflow and surface runoff percentage (%). A summary of the performance of the model to simulate flow (Flow P.) and sediment load (Sediment P.) is included: X indicates an unsatisfactory performance, √ a satisfactory, ≈* intermediate (one of the statistical indices indicate satisfactory result and the other unsatisfactory) and ≈ indicates that at the half-end of the simulation performance is good.*

The events number 9 (Fig. 3.8), 14 (Fig. 3.9) and 15 (Fig. 3.10) are generated by summer storms. The precipitation intensity (IP: 1.1, 1.3 and 1.4 mm h^{-1} respectively) and maximum precipitation (Pmax: 8.9, 12.4 and 11.6 mm h^{-1} respectively) of these summer storms are high and they generate single-peak events (event 9 is not so clear, Fig. 3.8). The antecedent conditions between these three events are different, before the events 14 and 15 there were little

events but in general from April 2014, the spring, summer and even part of autumn were characterized by small events with low discharge (Fig. 3.7). Before event number 9 there were higher intensity events. Moreover, in 2013 winter, 2014 spring and the beginning of summer there were relatively high intensity consecutive events. This translates into more precipitation the days before (see bP7d and bP21d in Fig. 3.8, 3.9 and 3.10) and higher discharge the day before (bQ1d: 170.07 L s^{-1} in event 9, 29.87 and 18.59 L s^{-1} in 14 and 15 respectively).

The discharge simulation results of event number 9 are *very good* (RSR=0.41 and R^2=0.90). The simulated peak is a little bit lower than the observed (see Qmax in Fig. 3.8) but the fit between the simulated and the observed discharge recession is very good (Fig. 3.8). The simulated discharge results in events 14 and 15 are *unsatisfactory* (RSR=0.99 and R^2=0.22 for event 14 and RSR=1 and R^2=0.55 for 15). There is practically not response to precipitation and therefore there is not surface runoff (Figs. 3.9 and 3.10).

As for the discharge, in events 14 and 15 the suspended sediment simulation results are *unsatisfactory* (Figs. 3.9 and 3.10). The discharge results for event 9 are *very good*, nevertheless the simulated CSS and SST are considerably lower than the observed (Fig. 3.8), therefore the simulation results are *unsatisfactory*.

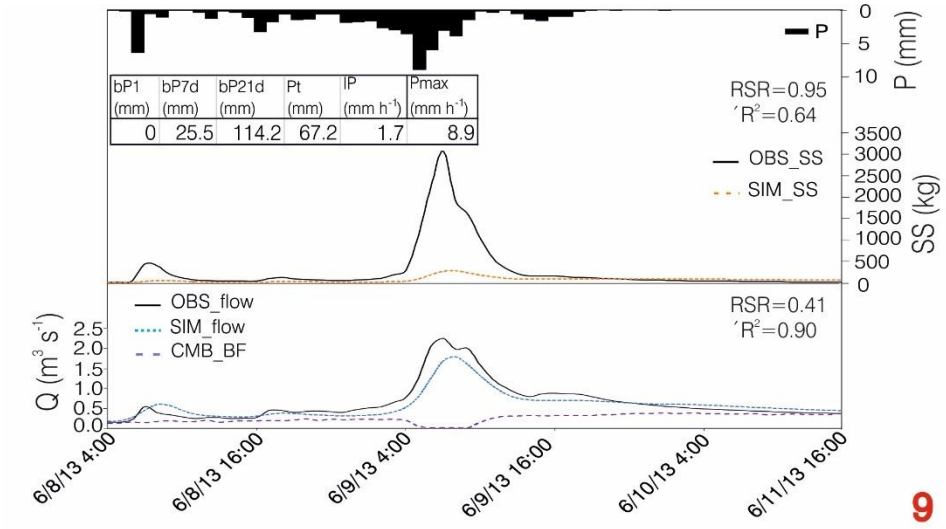

	bQ1d (L s $^{-1}$)	Qt (mm)	Qmean (L s $^{-1}$)	Qmax (L s $^{-1}$)	Qmax/Qb	BF mm	SR mm	BF/SR	CSSmean (mg L $^{-1}$)	CSSmax (mg L $^{-1}$)	SST (kg)
OBS	170.07	29.66	631.67	2241	13.18	13.38	18.86	0.71	76.66	380.22	16551.04
SIM	179.21	26.97	574.30	1780	9.93	15.94	33.04	0.48	31.14	43.80	4319.92

Figure 3.8. *Graphical and statistical (R^2 and RSR) results for the hourly discharge (bottom) and sediment load (top)for event 9.*

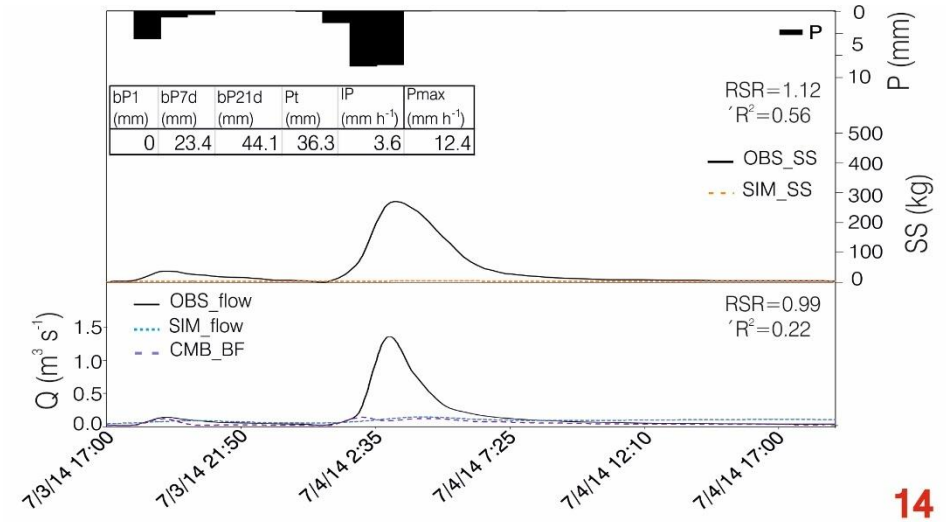

	bQ1d (L s $^{-1}$)	Qt (mm)	Qmean (L s $^{-1}$)	Qmax (L s $^{-1}$)	Qmax/Qb	BF mm	SR mm	BF/SR	CSSmean (mg L $^{-1}$)	CSSmax (mg L $^{-1}$)	SST (kg)
OBS	29.87	3.32	156.94	1349	45.16	1.64	2.07	0.79	46.46	124.72	1006.52
SIM	40.23	2.04	96.34	150	3.73	1.55	0.01	267.79	3.75	7.25	36.63

Figure 3.9. *Graphical and statistical (R^2 and RSR) results for the hourly discharge (bottom) and sediment load (top)for event 14.*

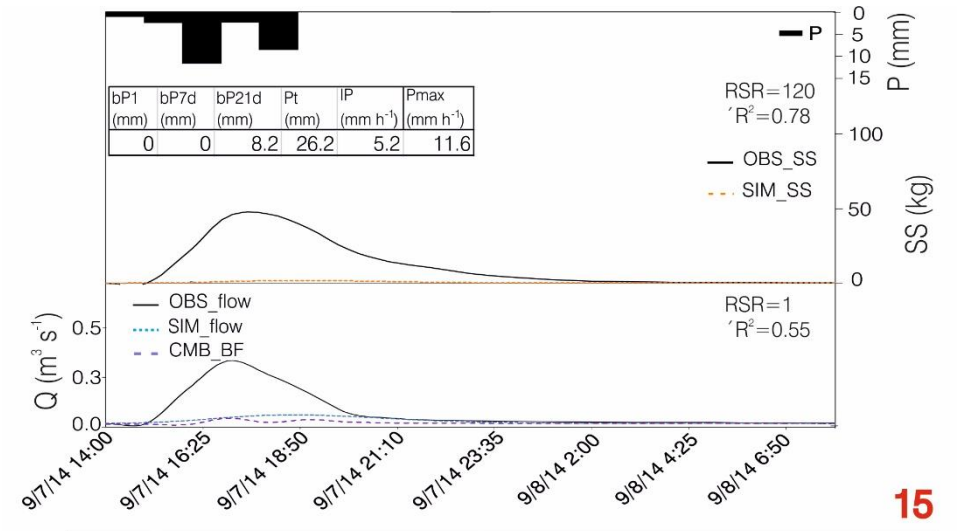

	bQ1d (L s⁻¹)	Qt (mm)	Qmean (L s⁻¹)	Qmax (L s⁻¹)	Qmax/Qb	BF mm	SR mm	BF/SR	CSSmean (mg L⁻¹)	CSSmax (mg L⁻¹)	SST (kg)
OBS	18.59	1.10	73.72	333	17.91	0.73	0.82	0.89	33.37	89.55	215.64
SIM	20.05	0.47	31.56	61	3.06	1.05	0.00	----------	4.54	8.15	11.56

Figure 3.10. *Graphical and statistical (R^2 and RSR) results for the hourly discharge (bottom) and sediment load (top)for event 15.*

Taking into account all the analysed events, the number 1 (Fig. 3.11) has the highest mean and maximum observed discharge (Qmean: 649.91 L s^{-1}, Qmax: 3280 L s^{-1}), surface runoff (71 %) and sediment concentration (CSSmean: 105.68 mg L^{-1}). The conditions before the event indicate that the discharge was low (bQ1d: 20.46 L s^{-1}) and the precipitation generates a high peak (Qmax/Qb: 160.31). After the dry season, in autumn 2011 this was the first flood.

The discharge simulation results are *unsatisfactory* (RSR=0.77 and R^2=0.43). The simulated flow increases after the observed discharge and the high discharge level maintains over time. In this case, although the observed and simulated peaks do not fit in time, the height is similar (simulated Qmax/Qb: 160.98). As the discharge, the sediments simulation results are *unsatisfactory* (RSR=1.02 and R^2=0.06). Fig. 3.11 shows that there is not a sediment peak when the flood occurs and the concentration in the water is maintained over time, probably influenced by the simulated discharge.

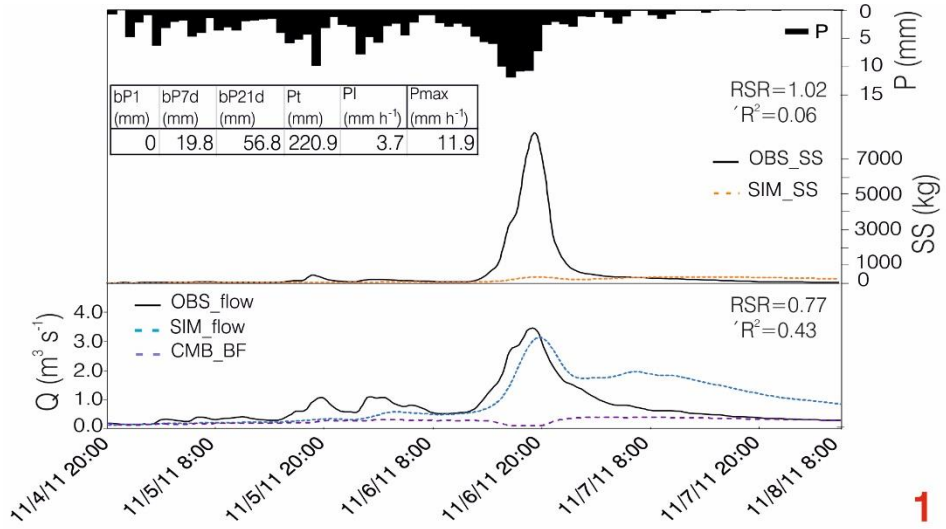

	bQ1d (L s $^{-1}$)	Qt (mm)	Qmean (L s $^{-1}$)	Qmax (L s $^{-1}$)	Qmax/Qb	BF mm	SR mm	BF/SR	CSSmean (mg L $^{-1}$)	CSSmax (mg L $^{-1}$)	SST (kg)
OBS	20.46	42.22	649.91	3280	160.31	12.82	31.55	0.41	105.68	717.82	8430.22
SIM	18.76	54.18	834.12	3020	160.98	29.60	46.58	0.64	31.85	78.00	10940.34

Figure 3.11. *Graphical and statistical (R^2 and RSR) results for the hourly discharge (bottom) and sediment load (top)for event 1.*

Number 6 (Fig. 3.12) is a winter multiple-peak event generated by a 293.1 mm precipitation, with high surface runoff (63 %; Table 3.12). The precipitation before the event was scarce (bP7d: 6.8 and bPd21: 30 mm) and the observed discharge one day before the event was 77.10 L s^{-1} while the simulated was around four times higher than the observed (286.24 L s^{-1}).

The discharge simulation results are *very good* (RSR=0.45 and R^2=0.83). The hydrograph shows (Fig. 3.12) that in the beginning and in the recession the simulated discharge is higher than the observed and specially in the first peaks the simulated flow is smaller than the observed. The simulated and observed mean and total discharge (see Qt and Qmean in Fig. 3.12) are similar, nevertheless the observed Qmax/Qb is 31.45 while the simulated one is 7.58. The difference is important for two main reasons. In the one hand, the simulated flow at the beginning was higher than the observed and in the other hand, the simulated peaks are lower than the observed. In addition, the relationship between the baseflow and surface runoff indicates that in the case of observed discharge most of it is surface runoff (BF/SR: 0.64) while in the simulated

discharge most of it is baseflow (BF/SR: 1.25). Therefore, although the discharge simulation results are *very good*, the processes are not being modelled well.

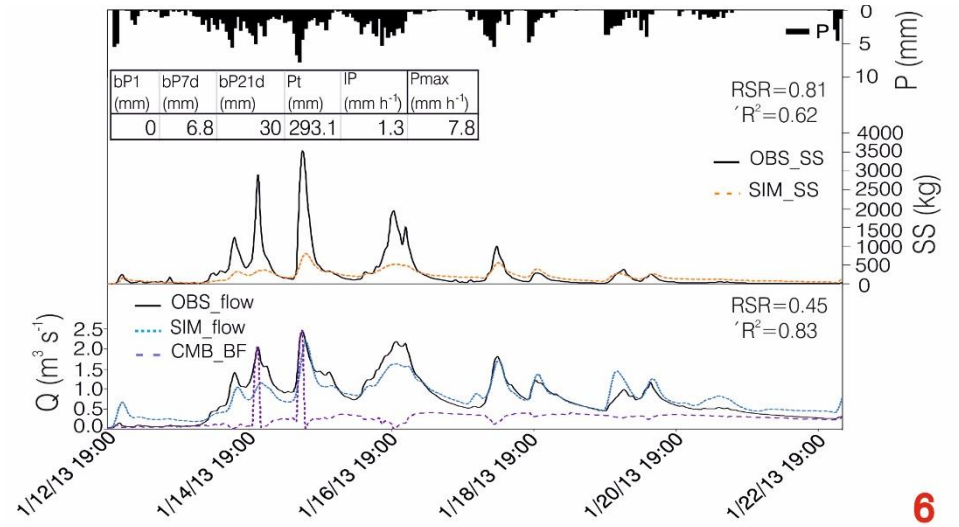

	bQ1d (L s $^{-1}$)	Qt (mm)	Qmean (L s $^{-1}$)	Qmax (L s $^{-1}$)	Qmax/Qb	BF mm	SR mm	BF/SR	CSSmean (mg L^{-1})	CSSmax (mg L^{-1})	SST (kg)
OBS	77.10	149.32	763.20	2425	31.45	60.70	94.44	0.64	82.73	747.50	69326.96
SIM	286.24	151.85	776.14	2170	7.58	114.89	91.74	1.25	64.25	103.00	48979.93

Figure 3.12. *Graphical and statistical (R^2 and RSR) results for the hourly discharge (bottom) and sediment load (top)for event 6.*

The simulated sediment load is around 20300 kg lower than the observed. The RSR is 0.81 indicating an *unsatisfactory* result and R^2 is 0.62 which can be considered satisfactory. Graphically, the simulated sediment load shows the same pattern than the observed but it is considerably lower in the peaks. Taking into account that most of the simulated streamflow is baseflow, it is normal that the sediment transport is smaller.

Other type events are those with **high baseflow (> 60 %)**. These are winter events (number 3, 4 and 12), spring event (number 8) and summer event (number 10). In general, they are generated by not too intense precipitations and mean discharge, and the discharge increase of the events (relationship Qmax/Qb) is small (Table 3.12).

The events 3 and 4 are consecutive and occurred in winter 2012 (Fig. 3.7). The precipitation accumulated during the 7 days before the event was 32 mm and 7.4 mm and 21 days before 49.5 mm and 104.7 mm for event 3 and 4 respectively.

In event 3, the observed discharge was around 20 L s^{-1} lower than the simulated and in event number 4 was 10 L s^{-1} higher. In both cases the precipitation that generated the events was not very intense and the total precipitation during the event was around 20-25 mm.

The results of the statistical indices of the discharge for event 3 are *good* (RSR=0.59 and R^2=0.75) and *very good* (RSR=0.42 and R^2=0.84) for event number 4. Additionally, in both events the observed and simulated values for Qt, Qmean, Qmax and Qmax/Qb are similar (see Fig. 3.13 and Fig. 3.14).

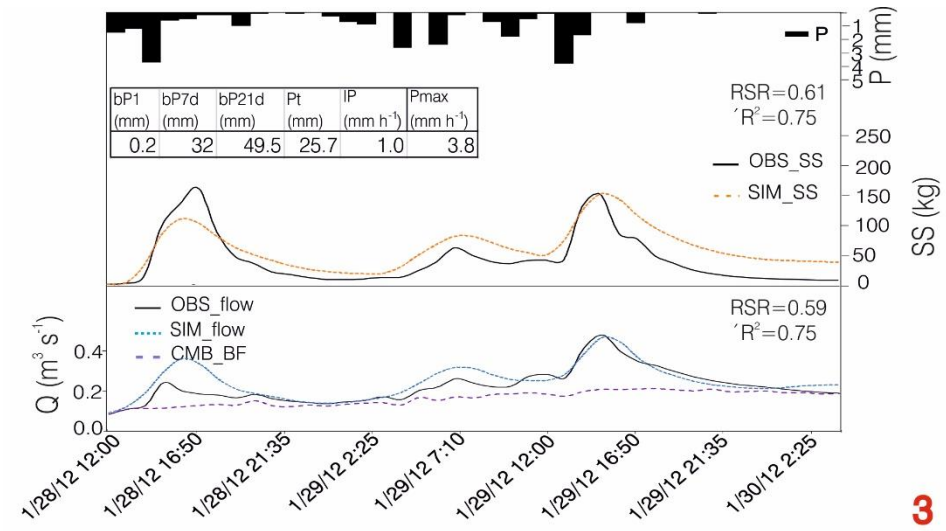

	bQ1d (L s $^{-1}$)	Qt (mm)	Qmean (L s $^{-1}$)	Qmax (L s $^{-1}$)	Qmax/Qb	BF mm	SR mm	BF/SR	CSSmean (mg L $^{-1}$)	CSSmax (mg L $^{-1}$)	SST (kg)
OBS	90.02	7.16	223.29	478	5.31	8.38	1.91	4.40	49.67	242.67	1748.08
SIM	114.71	7.90	246.14	467	4.07	10.94	3.63	3.01	63.66	90.90	2508.84

Figure 3.13. *Graphical and statistical (R^2 and RSR) results for the hourly discharge (bottom) and sediment load (top)for event 3.*

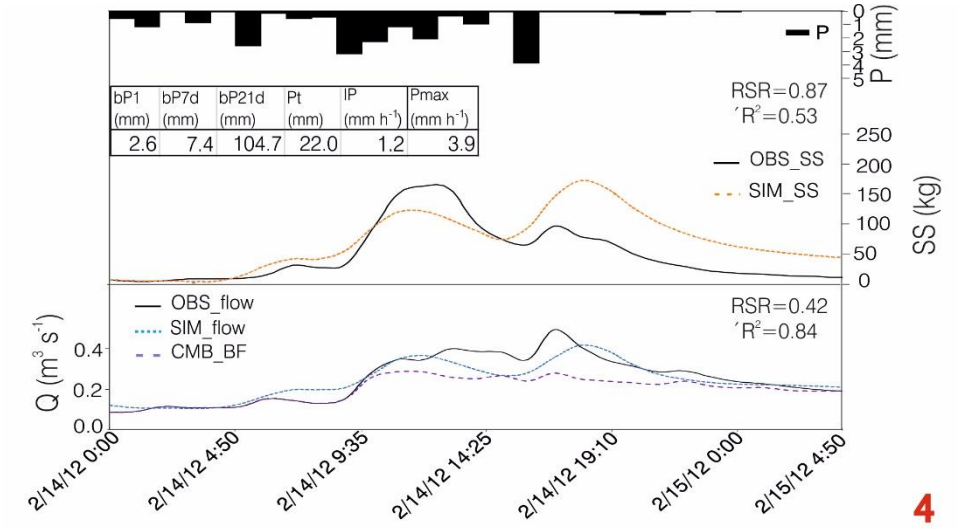

bP1 (mm)	bP7d (mm)	bP21d (mm)	Pt (mm)	IP (mm h⁻¹)	Pmax (mm h⁻¹)
2.6	7.4	104.7	22.0	1.2	3.9

	bQ1d (L s⁻¹)	Qt (mm)	Qmean (L s⁻¹)	Qmax (L s⁻¹)	Qmax/Qb	BF mm	SR mm	BF/SR	CSSmean (mg L⁻¹)	CSSmax (mg L⁻¹)	SST (kg)
OBS	84.34	5.62	247.84	497	5.89	7.07	1.13	6.25	45.59	130.79	1401.74
SIM	74.80	5.46	240.59	420	5.61	9.23	4.08	2.26	69.68	114.00	2032.63

Figure 3.14. *Graphical and statistical (R^2 and RSR) results for the hourly discharge (bottom) and sediment load (top)for event 4.*

The statistical indices show that the simulated sediment load performance is satisfactory (RSR=0.61 and R^2=0.75) in event 3 and *unsatisfactory* (RSR=0.87 and R^2=0.53) in 4. In both events the differences between observed and simulated CSSmean, CSSmax and SST are considerable. In Figs. 3.13 and 3.14, it is possible to observe that simulated sediment load maintains relatively high after the last peak of the event.

In Aixola catchment the simulated peaks are usually lower than the observed (Fig. 3.7), however in event number 12 the simulated discharge peak is higher than the observed. The precipitation 7 days before the event was 35.1 mm and 21 days before 42.6 mm. The precipitation intensity and the maximum precipitation that cause the event are high (PI: 2.6 mm h^{-1} and Pmax: 7.8 mm h^{-1}) but the total precipitation is only 19.1 mm. The simulated discharge one day before the event (bQ1d: 382.04 L s^{-1}) is much higher than the observed (bQ1d: 143.39 L s^{-1}).

The discharge simulation statistical results are *unsatisfactory* (RSR=3.55 and R^2=0.65) because although the peak fits in time, it is considerably higher than the observed and, in addition, in the recession the simulated flow is always above

the observed (Fig. 3.15). The Qt, Qmean and Qmax are higher for the simulated flow, nevertheless the Qmax/Qb parameter shows that the flow increase is similar for the observed and simulated discharge.

The results for sediment load indicate that the simulation performance is satisfactory (RSR=0.63 and R^2=0.8). The CSSmean is similar for the observed and simulated but the simulated total sediment load (SST) is much higher than the observed. This is due to the fact that the sediment transport keeps relatively high at the end of the event, probably due to the high discharges simulated for this stage of the hydrograph.

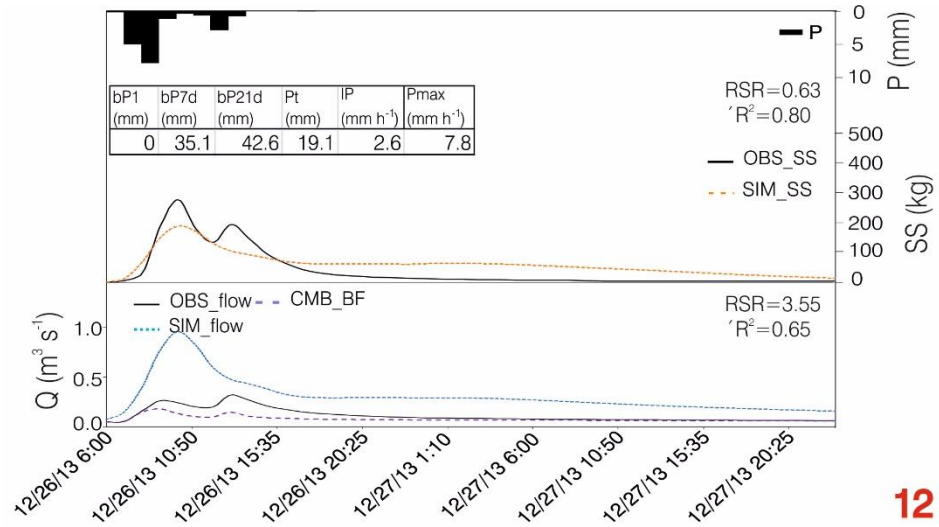

bP1 (mm)	bP7d (mm)	bP21d (mm)	Pt (mm)	IP (mm h^{-1})	Pmax (mm h^{-1})
0	35.1	42.6	19.1	2.6	7.8

	bQ1d (L s^{-1})	Qt (mm)	Qmean (L s^{-1})	Qmax (L s^{-1})	Qmax/Qb	BF mm	SR mm	BF/SR	CSSmean (mg L^{-1})	CSSmax (mg L^{-1})	SST (kg)
OBS	143.39	3.65	111.16	316	2.20	2.76	1.13	2.44	56.43	316.78	1580.92
SIM	382.04	10.12	307.97	953	2.49	6.02	4.92	1.22	50.35	60.80	2503.65

Figure 3.15. *Graphical and statistical (R^2 and RSR) results for the hourly discharge (bottom) and sediment load (top)for event 12.*

The event number 8 (Fig. 3.16) was generated by a weak mean intensity spring precipitation (0.6 mm h^{-1}) that is distributed in 5 days for which the maximum precipitation intensity (7.6 mm h^{-1}) is moderate. The precipitation 21 days before the event was 49.1 mm and 7 days before 16.4 mm. The observed discharge one day before was 91.80 L s^{-1} and the simulated was 135.13 L s^{-1}.

RSR=0.74 indicate that the discharge simulation performance is *unsatisfactory* while the R^2=0.67 is satisfactory. The hydrograph shows (Fig. 3.16) that the first days the simulated discharge is lower than the observed. Nevertheless, at the end the simulated discharge remains above the observe and therefore the Qt, Qmean and Qmax values are higher for the simulated flow.

The statistical indices show that the simulated sediment load performance is *very good* (RSR=0.39 and R^2=0.85). Graphically the fit is good although the simulated peaks are lower than the observed (see CSSmax in Fig. 3.16). On the contrary, the simulated CSSmean and SST are higher than the observed although they are similar.

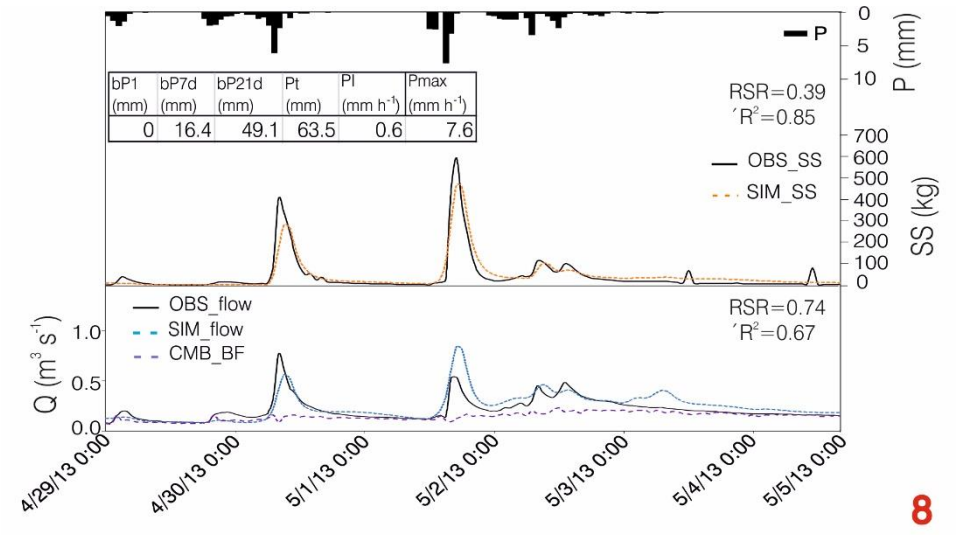

	bQ1d (L s $^{-1}$)	Qt (mm)	Qmean (L s $^{-1}$)	Qmax (L s $^{-1}$)	Qmax/Qb	BF mm	SR mm	BF/SR	CSSmean (mg L^{-1})	CSSmax (mg L^{-1})	SST (kg)
OBS	91.80	22.96	214.16	767	8.35	16.52	7.26	2.28	34.81	307.58	5552.99
SIM	135.13	26.01	242.60	841	6.22	20.05	5.60	3.58	35.15	157.00	5998.45

Figure 3.16. *Graphical and statistical (R^2 and RSR) results for the hourly discharge (bottom) and sediment load (top)for event 8.*

The last analysed event (number 10, Fig. 3.17) with high baseflow contribution, is a small (Qmean: 66.44 L s^{-1}) summer event. The antecedent conditions are similar to event number 8 but the observed discharge one day before is smaller (bQ1d: 46.30 L s^{-1}). The mean precipitation intensity during the event is low (IP: 1.3 mm h^{-1}) and it only takes a few hours, the total precipitation is 11.6 mm. The discharge simulation does not respond to this precipitation therefore the

statistical indices for discharge and sediment load are *unsatisfactory* (RSR=0.92 and R^2=0.65 and RSR=1.22 and R^2=0.60, respectively). In Fig. 3.17 it is possible to observe that there are not simulated peaks and discharge is overestimated before and after the observed peaks.

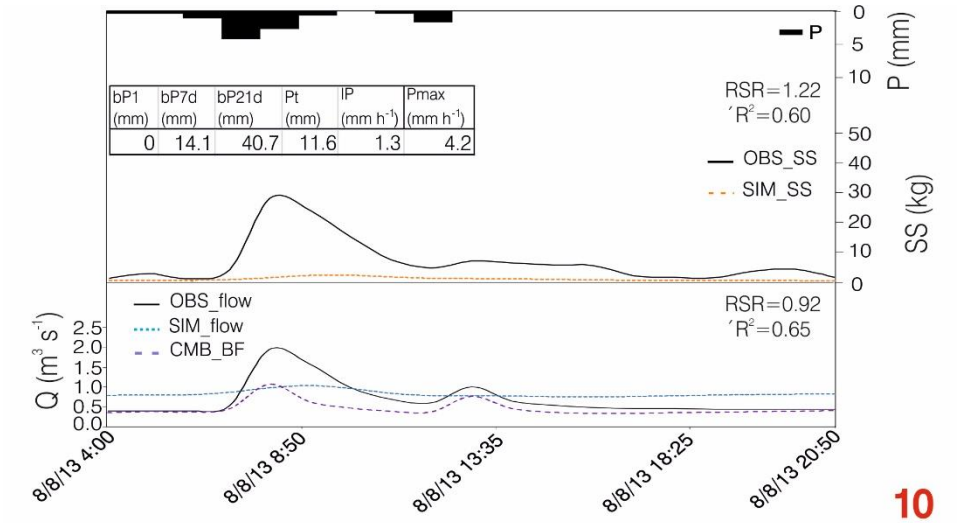

	bQ1d (L s $^{-1}$)	Qt (mm)	Qmean (L s $^{-1}$)	Qmax (L s $^{-1}$)	Qmax/Qb	BF mm	SR mm	BF/SR	CSSmean (mg L^{-1})	CSSmax (mg L^{-1})	SST (kg)
OBS	46.30	0.99	66.44	194	4.18	0.81	0.34	2.37	23.85	23.85	129.66
SIM	55.86	1.21	81.34	103	1.84	0.67	0.00	----------	3.68	6.80	20.96

Figure 3.17. *Graphical and statistical (R^2 and RSR) results for the hourly discharge (bottom) and sediment load (top)for event 10.*

Finally, the third type of events is characterized for having **similar surface runoff and baseflow quantity (around 50 %)**. These are autumn/winter multiple-peak events generated by precipitation intensities around 1 mm h^{-1}, with considerable Qmean and Qmax/Qb (Table 3.12). These are the events 2, 5, 7, 11 and 13.

In Fig. 3.18 it is possible to observe the discharge and the sediment load of event 2. The precipitation before the event was not high (bP7d: 9.7 mm and bP21d: 55.3 mm) and the observed discharge level neither (bQ1d: 21.83 L s^{-1}) and it is a bit higher than the simulated (bQ1d: 18.76 L s^{-1}). The precipitation intensity during the event is weak (IP: 1.7 mm h^{-1}) and the maximum precipitation fallen in an hour is 7.7 mm.

RSR=0.72 indicates that the discharge simulation performance is *unsatisfactory* while the R^2=0.78 is satisfactory. The hydrograph shows (Fig. 3.18) that the

simulated discharge is above the observed and therefore, Qt, Qmean, Qmax and Qmax/Qb are higher for the simulation. In addition, the BF/SR ratio indicates that the flow is mostly composed by surface runoff while the data obtained with the CMB indicate that the baseflow component is higher than the surface runoff.

Considering the sediments, the simulation results are *unsatisfactory* (RSR=0.81 and R^2=0.42) because as in other events (3, 4, 12) the peaks are underestimated and after the last peak a relatively high load of sediments can be observed, probably also influenced by the discharge simulation (Fig. 3.18). Thus, the simulated CSSmean and CSSmax are lower than the observed but the SST is higher.

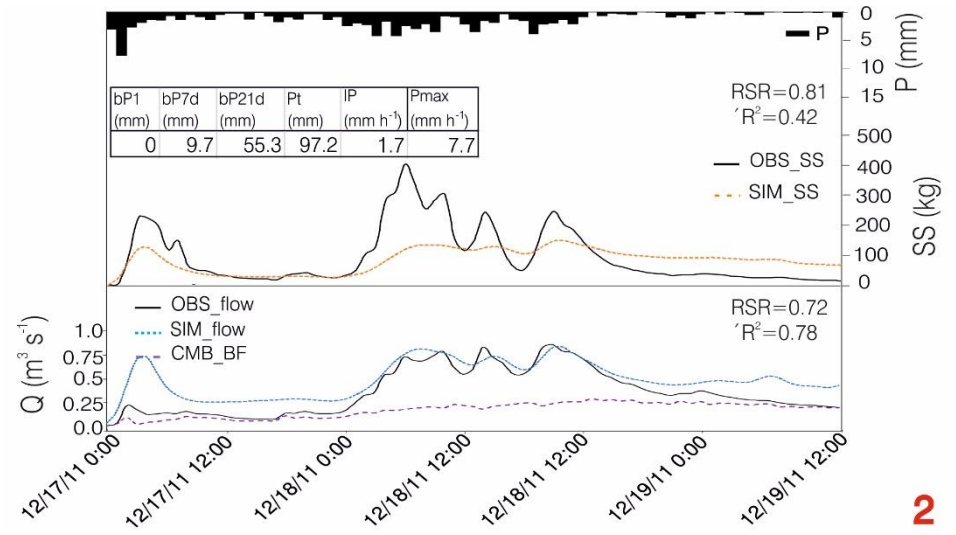

	bQ1d (L s $^{-1}$)	Qt (mm)	Qmean (L s $^{-1}$)	Qmax (L s $^{-1}$)	Qmax/Qb	BF mm	SR mm	BF/SR	CSSmean (mg L^{-1})	CSSmax (mg L^{-1})	SST (kg)
OBS	21.83	21.63	368.49	860	39.38	12.26	10.85	1.13	74.98	443.73	7071.76
SIM	18.76	54.18	834.12	3020	160.98	29.60	46.58	0.64	31.85	78.00	10940.34

Figure 3.18. *Graphical and statistical (R^2 and RSR) results for the hourly discharge (bottom) and sediment load (top)for event 2.*

The precipitation before event 5 (Fig. 3.19) was not too high (bP7d: 32 mm and bP21d: 51.2 mm). The precipitation that generates the event (Pt: 101 mm) was distributed during 5 days so that the mean precipitation intensity was 1 mm h^{-1} and the maximum precipitation intensity 6.2 mm h^{-1}.

The simulated and observed discharge before the event were very similar (bQ1d≈25 L s^{-1}). The statistical indices (RSR=0.36 and R^2=0.91) and the graphic and parameters comparison (Qt, Qmean, Qmax and Qmax/Qb in Fig. 3.19) indicate that the discharge simulations performance is *very good*.

The suspended sediments simulation performance is *unsatisfactory* (RSR=0.93 and R^2=0.19). The sediment increases a bit with the event but much less than the observed, thus, simulated CSS, CSSmax and SST are underestimated.

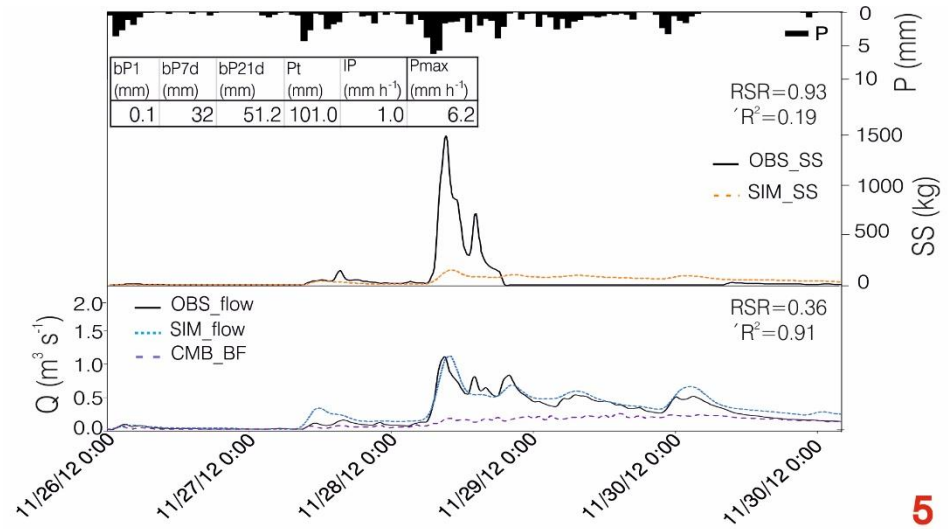

	bQ1d (L s^{-1})	Qt (mm)	Qmean (L s^{-1})	Qmax (L s^{-1})	Qmax/Qb	BF mm	SR mm	BF/SR	CSSmean (mg L^{-1})	CSSmax (mg L^{-1})	SST (kg)
OBS	25.26	25.80	263.69	1111	43.97	14.36	13.17	1.09	41.82	372.20	7714.60
SIM	25.51	30.13	307.99	1120	43.90	25.22	20.15	1.25	32.50	53.80	5737.35

Figure 3.19. *Graphical and statistical (R^2 and RSR) results for the hourly discharge (bottom) and sediment load (top)for event 5.*

Number 7 is a winter multiple-peak event generated after other winter events (Fig. 3.7) for which bP7d is 47.2 mm, bP21d 408.2 mm and observed bQ1d is 302.07 L s^{-1} (Fig. 3.20).

The discharge simulation result is *very good* (RSR=0.48 and R2=0.77). The graphic shows a good fit specially in the recession and the simulated and observed Qt, Qmax, Qmean and Qmax/Qb are similar; with the exception of Qmax the simulated discharge is lower than the observed.

As in previous events, the suspended sediment peaks are underestimated while the sediment load do not decrease as fast as the observed. Therefore, the observed CSSmax is considerably higher than the simulated but the CSSmean and SST are lower (Fig. 3.20). The statistical indices are in line with this, indicating that the sediment simulation is *unsatisfactory* (RSR=0.75 and R^2=0.46).

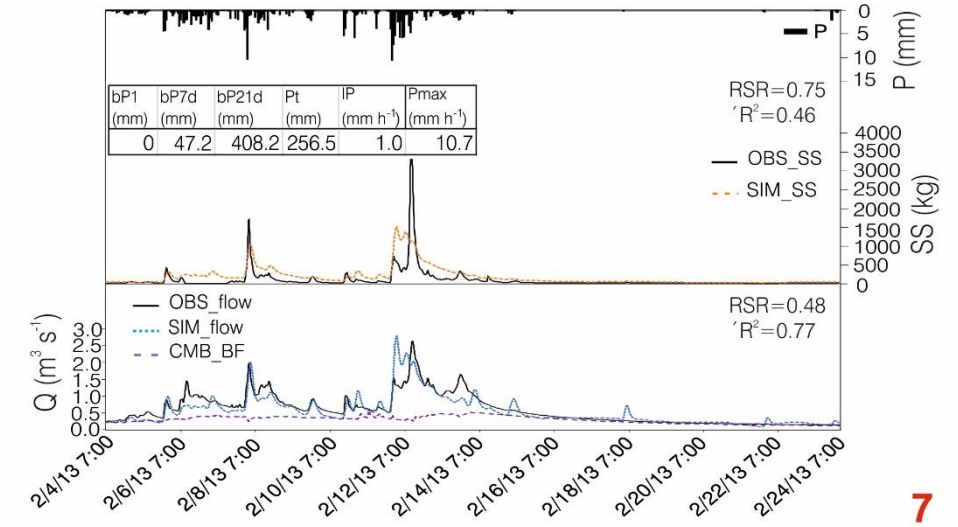

	bQ1d (L s $^{-1}$)	Qt (mm)	Qmean (L s $^{-1}$)	Qmax (L s $^{-1}$)	Qmax/Qb	BF mm	SR mm	BF/SR	CSSmean (mg L^{-1})	CSSmax (mg L^{-1})	SST (kg)
OBS	302.07	217.24	586.85	2646	8.76	115.72	103.00	1.12	20.63	397.85	39509.84
SIM	359.96	206.62	558.16	2780	7.72	175.32	78.46	2.23	52.53	169.00	74089.03

Figure 3.20. *Graphical and statistical (R^2 and RSR) results for the hourly discharge (bottom) and sediment load (top)for event 7.*

Flood number 11 (Fig. 3.21) is an event that occurs after the dry season (Fig. 3.7). The precipitation intensity is not too high (IP: 0.7 mm h^{-1}) but this is a multiple-peak event and its duration is 18 days, therefore the total precipitation is considerable (Pt: 297.3 mm) as well as the total discharge (Qt: 107.79 mm) and the sediment load (SST: 9628.96 kg). The simulated discharge (Qt: 67.24 mm) and sediment load (SST: 8553.03 kg) are lower than the observed. The first days of the event the simulation responds to the precipitation increasing the baseflow and consequently no peaks are formed in the moments of greater precipitation intensity. It is from November 21 when the simulated and observed discharge fit better. The sediment load also begins in this moment to adjust better. Nevertheless, in the peaks the simulated sediment does not have the same

magnitude as the observed, and after the peak the simulated sediment load instead of decreasing, it is maintained high over time.

The statistical indices show that the discharge and sediment simulation is *unsatisfactory* (RSR=0.90, R^2=0.40 and RSR=0.90, R^2=0.20, respectively).

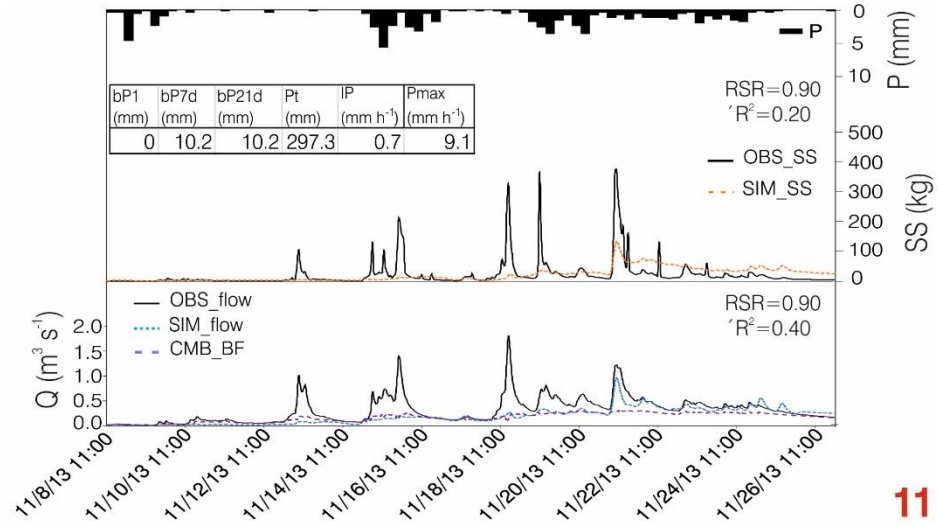

bP1 (mm)	bP7d (mm)	bP21d (mm)	Pt (mm)	IP (mm h^{-1})	Pmax (mm h^{-1})
0	10.2	10.2	297.3	0.7	9.1

	bQ1d (L s^{-1})	Qt (mm)	Qmean (L s^{-1})	Qmax (L s^{-1})	Qmax/Qb	BF mm	SR mm	BF/SR	CSSmean (mg L^{-1})	CSSmax (mg L^{-1})	SST (kg)
OBS	25.27	107.79	309.50	1810	71.63	59.17	48.83	1.21	12.87	167.67	9628.96
SIM	21.02	67.24	193.09	967	46.00	69.43	8.46	8.21	18.51	49.30	8553.03

Figure 3.21. *Graphical and statistical (R^2 and RSR) results for the hourly discharge (bottom) and sediment load (top)for event 11.*

The last analysed event is the number 13 which occurred in March 2014 with a precipitation of 141.4 mm distributed in 6 days (IP: 1 mm h-1 and Pmax: 6.5 mm h^{-1}) and considerable flow (observed Qmean: 588.58 L s^{-1}). The precipitation before the event was bP7d: 21.1 mm and bP21d: 95.4 mm and the observed discharge one day before the event was 104.35 L s^{-1} while the simulated was 152.50 L s^{-1}.

The simulation discharge pattern is similar to flood 11 where the fit is better at the end of the event. The simulated Qt, Qmean, Qmax and Qmax/Qb are lower than the observed and RSR=0.71 is *unsatisfactory* and R^2=0.57 satisfactory. In Fig. 3.22 it is possible to observe that with the suspended sediment occurs the other way around, at the beginning of the event the observed and simulated sediment

fit better and worse at the end. The statistical indices are *unsatisfactory* (RSR=0.90 and R^2=0.48).

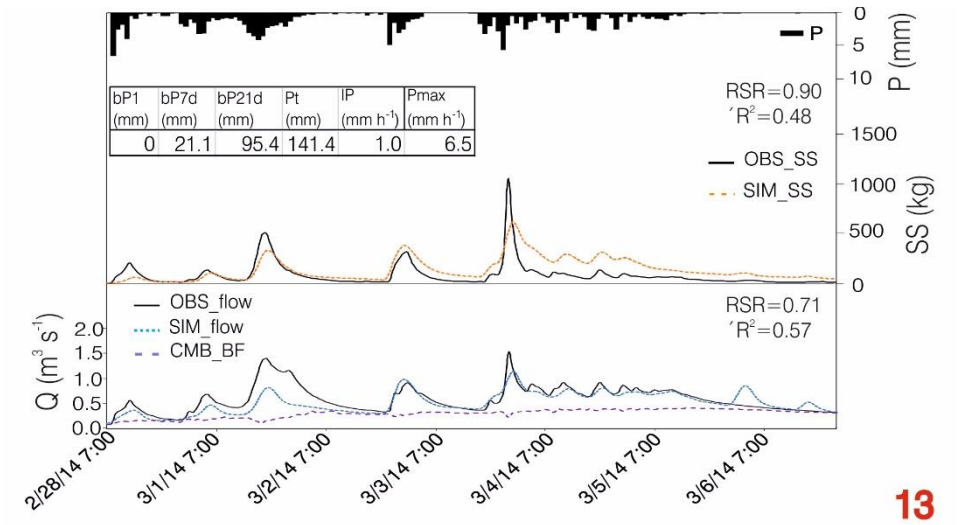

	bQ1d (L s $^{-1}$)	Qt (mm)	Qmean (L s $^{-1}$)	Qmax (L s $^{-1}$)	Qmax/Qb	BF mm	SR mm	BF/SR	CSSmean (mg L^{-1})	CSSmax (mg L^{-1})	SST (kg)
OBS	104.35	74.16	588.58	1514	14.51	38.60	36.03	1.07	30.88	191.57	12999.74
SIM	152.50	64.94	515.36	1140	7.48	62.17	20.15	3.09	62.79	150.00	21864.35

Figure 3.22. *Graphical and statistical (R^2 and RSR) results for the hourly discharge (bottom) and sediment load (top)for event 13.*

3.6.5 Discussion and conclusions

In the *2P S2* using the input data of *2P*, the hourly discharge (m^3 s^{-1}) and sediment load (kg) of Aixola catchment were calibrated (from 2010 to 2014) and validated (from 2005 to 2009). To do so, some of the parameters values calibrated in *2P* were used in this step although the related to sub-daily calibration were adjusted. Thus, in Aixola catchment in the discharge calibration the most sensitive parameters are those included in the Muskingum method (MSK_CO1,2 and MSK_X) and those related to the Green & Ampt Mein Larson infiltration method. The hourly statistical indices indicate that the sub-daily calibration performance for discharge is at least *good* and the validation is *satisfactory* (Table 3.10). Nevertheless, the decrease of the simulation time-step has not solved the underestimation of the simulated peaks observed in *1P* and *2P S1*. When the hourly data are used to calculate the daily discharge, it is possible to compare

the simulation performance of the *2P S1* and *2P S2* (Table 3.11). In general, the results for *2P S2* are a bit better, therefore, although the underestimation of the simulated peaks persists, the simulation performance is better when it is done at hourly time-step.

The most sensitive parameter in the sediment load calibration was the C FACTOR that controls the cover and management factor for overland flow erosion. The statistical indices that are more sensitive to extreme values (NSE and RSR) indicate that hourly sediment calibration and validation are *unsatisfactory* (Table 3.10). The graphical results (Fig. 3.7) show that the sediment load peaks are lower than the observed. Considering that the discharge peaks are also underestimated, these errors are transferred to the sediment load simulations. The PBIAS point out that the sediment calibration and validation is *very good* and the R^2 values are higher than 0.5 indicating at least a *satisfactory* simulation performance. Therefore, it is possible to conclude that although the observed and simulated sediment load peaks do not fit well the amount of sediment transported by water is simulated well. Hence, to achieve a better hourly sediment simulation performance the timing of sediment transportation should be improved. This idea is reinforced when the hourly sediment load simulation results are used to calculate the daily sediment load. The daily statistical indices (Table 3.11) indicate that from 2005 to 2010 the sediment simulation performance is *very good*. Comparing these results with the obtained in the *1P* where the results were *satisfactory*, the improvement is considerable. However, it is important to keep in mind that this improvement is not only the consequence of the reduction of the simulation time-step. The discharge simulation has been improved in the different projects and steps evaluated in this chapter and, therefore better discharge simulation performance helped achieving better sediment simulation results.

For the analysis made in 15 events occurred from 2012 to 2014 (Fig. 3.7), it is difficult to obtain clear conclusions on the type of events that show a better performance of the model. In Fig. 3.7 and in summer events that tend to be isolated events (10, Fig. 3.17; 14, Fig. 3.9; 15, Fig. 3.10), it is possible to observe that regardless the surface runoff/baseflow content or the characteristics of the precipitation that generates the event, the discharge and sediment performance

is *unsatisfactory*. Nevertheless, seems that the events that occur before a certain event play an important role in the discharge simulations performance. The event number 9 (Fig. 3.8) is also a summer event, however it is an event occurred after a consecutive series of events (Fig. 3.7) and in this case, the discharge simulation results are *very good*. Therefore, might be thought that the antecedent conditions have importance in the events simulation performance. The precipitation 7 days before the event (bP7d) and the discharge one day before the event (bQ1d) do not show a pattern that indicates better or worse discharge simulation, nevertheless, when the precipitation 21 days before the event (bP21d) is high (> 100 mm) the discharge is simulated *satisfactorily*. It is possible to observe this pattern in events 4 (Fig. 3.14), 7 (Fig. 3.20) and 9 (Fig. 3.8), all of them autumn and winter events. On the contrary, the first events after the dry season (low bP21d) are not well simulated (1; Fig. 3.11 and 11, Fig. 3.21). However, there are exceptions; events number 5 (Fig. 3.19) and 6 (Fig. 3.12) have low bP21d and the simulation results are *very good*. In general, it seems that the discharge simulation needs time to adjust and this is not only between event and event but also in autumn and winter multiple-peak events where the ending of the event fits much better with the observed values than the beginning of it (e.g. 3, Fig. 3.13; 11, Fig. 3.21; 13, Fig. 3.22). Therefore, in consideration of the above, the soil moisture level of the catchment plays a key role in the discharge sub-daily simulations performance because, in general, to achieve a good performance in the event simulation, the saturation level of the catchment needs to be high (Fig. 3.7). This conclusion is in agreement with Yan et al. (2015) which concluded that sub-daily SWAT simulation has better event results in wet seasons.

Regarding the sediments simulation on different type of events, the results are in general *unsatisfactory* because of the pattern of the simulated sediment does not fit the observed one: the simulated sediment load is relatively low during the peak and, on the contrary, it is relatively high towards the ned o the event. There are many examples in the analysed events; e.g. 2, Fig. 3.18; 3, Fig. 3.13; 4, Fig. 3.14; 12, Fig. 3.15; 13, Fig. 3.22. The events 8 (Fig. 3.16) and 12 (Fig. 3.15) show *very good* statistical results for the sediment simulation but in both cases, it is because

the discharge is overestimated. The event number 3 (Fig. 3.13) has *good* results for both, discharge and sediment simulation.

Finally, considering the surface runoff/baseflow contribution, except for event 2 (Fig. 3.18) and 6 (Fig. 3.12) the predominant flow (surface runoff or baseflow) is well simulated.

3.7 REFERENCES

Abbaspour, K.C., Yang, J., Maximov, I., Siber, R., Bogner, K., Mieleitner, J., Zobrist, J., Srinivasan, R. 2007. Modelling hydrology and water quality in the pre-alpine/alpine Thur watershed using SWAT. Journal of Hydrology. 333(2–4), 413-430. http://dx.doi.org/10.1016/j.jhydrol.2006.09.014.

Arabi, M., Govindaraju, R.S., Hantush, M.M., Engel, B.A. 2006. Role of watershed subdivision on modeling the effectiveness of best management practices with SWAT. Journal of the American Water Resources Association. 42(2), 513–528. http://dx.doi.org/10.1111/j.1752-1688.2006.tb03854.x.

Arnold, J.G., Allen, P.M. 1999. Automated methods for estimating baseflow and ground water recharge from streamflow records. Journal of the American Water Resources Association. 35(2), 411-424. http://dx.doi.org/10.1111/j.1752-1688.1999.tb03599.x.

Arnold, J.G., Allen, P.M., Muttiah, R., Bernhardt, G. 1995. Automated base flow separation and recession analysis technique. Ground Water. 33(6),1010–1018. http://dx.doi.org/10.1111/j.1745-6584.1995.tb00046.x.

Arnold, J.G., Moriasi, D.N., Gassman, P.W., Abbaspour, K.C., White, M.J., Srinivasan, R., Santhi, C., Harmel, R.D., van Griensven, A., van Liew, M.W., Kannan, N., Jha, M.K. 2012. SWAT: Model use, calibration, and validation. Transactions of the ASABE. 55 (4), 1491-1508.

Arnold, J.G., Srinivasan, R., Muttiah, S.R., Williams, J.R. 1998. Large area hydrologic modeling and assessment part I. Model development1. Journal of the American Water Resources Association. 34(1), 73-89. http://dx.doi.org/10.1111/j.1752-1688.1998.tb05961.x.

Beven,K. 2007. Towards integrated environmental models of everywhere: uncertainty, data and modelling as a learning process. Hydrology & Earth System Sciences .11(1), 460-467.

Bressiani, D. 2016. Coping with hydrological risks through flooding risk index, complex watershed modeling, different calibration techniques, and ensemble streamflow forecasting. PhD, Universidade de Sao Paulo.

Caissie, D., Pollock, T.L., Cunjak, R.A. 1996. Variation in stream water chemistry and hydrograph separation in a small drainage basin. Journal of Hydrology. 178, 137–157.

Cerro, I., Antiguedad, I., Srinavasan, R., Sauvage, S., Volk, M., Sanchez-Perez, J.M. 2014. Simulating land management options to reduce nitrate pollution in an agricultural watershed dominated by an alluvial aquifer. Journal of Environmental Quality. 43, 67-74. http://dx.doi.org/10.2134/jeq2011.0393.

Cey, E.E., Rudolph, D.L., Parkin, G.W., Aravena, R. 1998. Quantifying groundwater discharge to a small perennial stream in southern Ontario, Canada. Journal of Hydrology. 210(1-4), 21–27. http://dx.doi.org/10.1016/S0022-1694(98)00172-3.

Epelde, A.M., Cerro, I., Sanchez-Perez, J.M., Sauvage, S., Srinivasan, R., Antiguedad, I. 2015. Application of the SWAT model to assess the impact of changes in agricultural management practices on water quality. Hydrological Sciences Journal-Journal Des Sciences Hydrologiques. 60, 825-843.

FAO. 1998. World Reference Base for Soil Resources. Rome: Food and Agriculture Organization of the United Nations.

FitzHugh, T.W., Mackay, D.S. 2000. Impacts of input parameter spatial aggregation on an agricultural nonpoint source pollution model. Journal of Hydrology 236,35–53. http://dx.doi.org/10.1016/S0022-1694(00)00276-6.

GeoEuskadi. 2012. Territorial information system of the Basque Government (http://www.geo.euskadi.net/s69-15375/es/). Accessed 20 Jun 2016.

Hayashi, M., Vogt, T., Mächler, L., Schirmer, M. 2012. Diurnal fluctuations of electrical conductivity in a pre-alpine river: Effects of photosynthesis and groundwater exchange. Journal of Hydrology. 450–451(0), 93-104. http://dx.doi.org/10.1016/j.jhydrol.2012.05.020.

Jha, M., Gassman, P.W., Secchi, S., Gu, R., Arnold, J. 2004. Effect of watershed subdivision on SWAT flow, sediment, and nutrient predictions. Journal of the American Water Resources Association. 40(3),811–825. http://dx.doi.org/10.1111/j.1752-1688.2004.tb04460.x.

Jones, J.P., Sudicky, E.A., Brookfield, A.E., Park, Y-J. 2006. An assessment of the tracer-based approach to quantifying groundwater contributions to streamflow. Water Resources Research. 42, W02407.

Ladouche, B., Probst, A., Viville, D., Idir, S., Baque, D., Loubet, M., Probst, J-L., Bariac, T. 2001 Hydrograph separation using isotopic, chemical and hydrological approaches (Strengbach catchment, France). Journal of Hydrology. 242(3-4), 255–274. http://dx.doi.org/10.1016/S0022-1694(00)00391-7.

Martínez-Santos, M., Antigüedad, I., Ruiz-Romera, E. 2014. Hydrochemical variability during flood events within a small forested catchment in Basque Country (Northern Spain). Hydrological Processes. 28, 5367-5381. http://dx.doi.org/10.1002/hyp.10011.

Matsubayashi, U., Velasquez, G.T., Takagi, F. 1993. Hydrograph separation and flow analysis by specific electrical conductance of water. Journal of Hydrology. 152(1-4), 179–199. http://dx.doi.org/10.1016/0022-1694(93)90145-Y.

Mau, D.P., Winter, T.C. 1997. Estimating ground-water recharge and streamflow hydrographs for small mountain watershed in a temperate humid climate, New

Hampshire, USA. Ground Water. 35(2), 291-304. http://dx.doi.org/10.1111/j.1745-6584.1997.tb00086.x.

Mein, R., Larson, C. 1973. Modeling infiltration during a steady rain. Water Resources Research. 9(2), 384–394. http://dx.doi.org/10.1029/WR009i002p00384.

Moriasi, D.N., Arnold, J.G., Van Liew, M.W., Bingner, R.L., Harmel, R.D., Veith, T.L. 2007. Model evaluation guidelines for systematic quantification of accuracy in watershed simulations RID H-4911-2011. Transactions of the ASABE. 50(3), 885-900.

Moriasi, D.N., Gitau, M.W., Pai, N., Daggupati, P. 2015. Hydrologic and Water Quality Models: Performance Measures and Evaluation Criteria. Transactions of the ASABE. 58, 1763-1785.

Naef, F., Scherrer, S., Weiler, M. 2002. A process based assessment of the potential to reduce flood runoff by land use change. Journal of Hydrology. 267(1–2), 74-79. http://dx.doi.org/10.1016/S0022-1694(02)00141-5.

Nathan, R.J., McMahon, T.A. 1990. Evaluation of automated techniques for base flow and recession analysis. Water Resources Research. 26(7), 1465-1473. http://dx.doi.org/10.1029/WR026i007p01465.

Negley, T.L., Eshleman, K.N. 2006. Comparison of stormflow responses of surface-mined and forested watersheds in the Appalachian Mountains, USA. Hydrological Processes. 20, 3467–3483. http://dx.doi.org/10.1002/hyp.6148.

Overton, D. 1966. Muskingum flood routing of upland streamflow. Journal of Hydrology. 4, 185-200.

Peraza-Castro, M., Ruiz-Romera, E., Montoya-Armenta, L.H., Sanchez-Perez, J.M., Sauvage, S. 2015. Evaluation of hydrology, suspended sediment and Nickel loads in a small watershed in Basque Country (Northern Spain) using eco-hydrological SWAT model. Annales De Limnologie-International Journal of Limnology. 51, 59-70.

Pilgrim, D.H., Huff, D.D., Steele, T.D. 1979. Use of specific conductance and contact time relations for separating flow components in storm runoff. Water Resources Research. 15, 329–339. http://dx.doi.org/10.1029/WR015i002p00329.

Qiu, L., Zheng, F., Yin, R. 2012. SWAT-based runoff and sediment simulation in a small watershed, the loessial hilly-gullied region of China: Capabilities and challenges. International Journal of Sediment Research. 27(2), 226-234.

Rice, K.C., Hornberger, G.M. 1998. Comparison of hydrochemical tracers to estimate source contributions to peak flow in a small, forested headwater catchment. Water Resources Research. 34, 1755–1766. http://dx.doi.org/10.1029/98WR00917.

Rutledge, A.J. 1993. Computer programs for describing the recession of groundwater discharge and for estimating mean ground water recharge and discharge from streamflow records. U.S. Geological Survey Water Resources Investigations Report 93-4121.

Santhi, C., Arnold, J.G., Williams, J.R., Dugas, W.A., Srinivasan, R., Hauck, L.M. 2001. Validation of the SWAT model on a large river basin with point and nonpoint sources. Journal of the American Water Resources Association. 37(5),1169-1188. http://dx.doi.org/10.1111/j.1752-1688.2001.tb03630.x.

Stewart, M., Cimino, J.,Ross, M. 2007. Calibration of base flow separation methods with streamflow conductivity. Ground Water. 45(1), 17-27. http://dx.doi.org/10.1111/j.1745-6584.2006.00263.x.

Stewart, M.K., Fahey, B.D. 2010. Runoff generating processes in adjacent tussock grassland and pine plantation catchments as indicated by mean transit time estimation using tritium. Hydrology and Earth System Sciences. 14(6), 1021-1032. http://dx.doi.org/10.5194/hess-14-1021-2010.

Uhlenbrook, S. 2006. Catchment hydrology—a science in which all processes are preferential—invited commentary. Hydrological Processes. 20, 3581–3585. http://dx.doi.org/10.1002/hyp.6564.

van Griensven, A., Meixner, T., Grunwald, S., Bishop, T., Di Luzio, M., Srinivasan, R. 2006. A global sensitivity analysis tool for the parameters of multi-variable catchment models. Journal of Hydrology. 324(1-4):10-23.

van Liew, M.W., Arnold, J.G., Garbrecht, J.D. 2003. Hydrologic simulation on agricultural watersheds: Choosing between two models. Trans. ASAE. 46(6):1539-1551.

Williams, J.R. 1969. Flood routing with variable travel time or variable storage coefficients. Transactions of the ASAE. 12(1), 100-103.

www.geoeuskadi.net

Yang, C. T. 1996. Sediment Transport Theory and practice. The McGraw-Hill Companies, Inc., New York.

Yang, X., Liu, Q., He, Y., Luo, X., Zhang, X. 2016. Comparison of daily and sub-daily SWAT models for daily streamflow simulation in the Upper Huai River Basin of China. Stochastic Environmental Research and Risk Assessment. 30 (3). http://dx.doi.org/10.1007/s00477-015-1099-0

Yu, Z., Schwartz, W. 1999. Automated calibration applied to watershed-scale flow simulations. Hydrological Processes. 13(19), 191-209.

Zabaleta A., Martínez, M., Uriarte, J.A., Antiguedad, I. 2007. Factors controlling suspended sediment yield during runoff events in small headwater catchments of the Basque Country. Catena 71:179-190.

Zabaleta, A., Antiguedad, I. 2013. Streamflow response of a small forested catchment on different timescales. Hydrology and Earth System Sciences. 17(1), 211-223.

4.

EVALUATION OF CLIMATE CHANGE IMPACTS ON WATER RESOURCES AND SEDIMENT YIELD

4. EVALUATION OF CLIMATE CHANGE IMPACTS ON WATER RESOURCES AND SEDIMENT YIELD

4.1 INTRODUCTION

Climate change will have effects on hydrological systems, which in turn will impact ecological, social and economic systems (Bender et al., 1984; Dibike & Coulibaly, 2005; Brauman et al., 2007; Vörösmarty et al., 2010). These effects can be studied both at local and regional levels, providing important information for territorial and sectoral planning (Lahmer et al., 2001). In some areas where water scarcity is not a key aspect of the territorial management, as it is the case of the Basque Country (Bay of Biscay, Atlantic region), few studies have been carried out to evaluate the possible effects of the climate change on catchment water quality and quantity. In addition, climate change is probable to have an impact on disharge and the amount, concentration and distribution of fluvial sediments

in catchments. These parameters are used for characterizing the status of water bodies, are the focus of sediment environmental quality standards in general, and are key water quality indicators within the context of the European Water Framework Directive (WFD). Hence, it is important to investigate to what extent climate change would impair the current conditions and hinder the achievement of these standards and the objectives of the WFD. In relation to this, some long-term records of fluvial sediment show how surprisingly sensitive rivers can be to relatively modest changes in climate (Coulthard et al., 2000; Macklin & Lewin, 2003; Viles & Goudie, 2003); specifically, climate changes have been observed to have a rapid impact on suspended solid fluxes (Meybeck, 2005) and may do so in the future (Zhu et al., 2008). Indeed, the European Joint Research Centre (JRC, 2004) includes transport of solids among the factors sensitive to climate variability and change. The WFD does not explicitly mention the risks implied by climate change in the plan for achieving its environmental objectives. However, the time scale for the implementation process and achieving particular objectives extends into the 2020s, and climate models project that there will have been changes in average temperature and precipitation by then (Wilby et al., 2006). Thus, as previous studies have noted, it is important to assess potential impacts of climate change on hydrology (e.g. Nijssen et al., 2001; Menzel & Burger, 2002; Werritty, 2002; Andréasson et al., 2004), as well as on soil erosion rates and sediment flux (e.g. Xu, 2003; Michael et al., 2005; Sivitsky et al., 2005).

Europe is a representative region of global changes due to among other factors, climate warming (Shorthouse & Arnell, 1999). There is a clear contrast between the North and the South of the continent, hence, an increase in precipitation and, therefore, an increase in water discharge, has been pointed out in the North (e.g. Arnell, 1998; Kiely, 1999; Xu & Halldin, 1997; IPCC, 2007, 2014). By contrast, in the south the trend is reversed: a decrease of precipitation is predicted and, consequently, a decrease in discharge (e.g. Mimikou et al., 2000; Ayala-Carcedo & Iglesias, 2000; Ribalaygua et al., 2013; Lespinas et al., 2014; Touhami et al., 2015; Valverde et al., 2015; IPCC, 2014). Due to its location in the Bay of Biscay (Fig. 2.2), the arid climatological conditions projected for southern Europe do not seem to be representative for the Basque Country. However, it is neither clear

whether the hydrological changes projected in this region will follow the discharge increasing trend projected for northern Europe.

Coch & Mediero (2015) analyzed low flows to identify different areas of hydrologic trends of the Iberian Peninsula and Mediero et al., (2015) investigated the flood-prone regions in Europe. Both studies reached the same conclusion for the area studied in this Thesis: The Basque Country would be located in the area they called Atlantic region. This area is characterized by Atlantic frontal systems coming from the west, usually in autumn and spring, being summer the dry season. Furthermore, the 4th report of the International Panel on Climate Change (IPCC, 2007) provides a vulnerability map of Europe for the XXI century, where the Atlantic region encompasses the northern Iberian Peninsula, western France, the Netherlands, Belgium, northern part of Germany, western Denmark and the UK. As a general trend, the report predicts an increase in the future winter storms and flooding for this region.

From some research conducted since 2000 in the Atlantic region (Table 1.2), although it is difficult to interpret, general trends of mean discharge evolution can be derived considering those more clearly observed. A significant decrease of discharge is observed in all the studies for summer and spring seasons. This decrease is even more important towards the end of the century. In winter trends are not so clear. In the UK (b, in Table 1.2) and in the Iberian Peninsula (d, Table 1.2), both increase and decrease discharge can be expected depending on the study, whereas in France (c, Table 1.2) the observed trend is decreasing. Trends in spring are similar to those in winter though decrease of discharge prevails. Annual trends are determined by trends in winter and spring.

From the aforementioned research works (Table 1.2), it can be deduced the general idea that a transition zone exists between northern and southern Atlantic region, where expected trends in discharge (in winter and spring) change from increasing in the North to decreasing in the South. It is not an easy task to locate this transition zone, due to the low spatial resolution of climate models; according to Habets et al., (2013) this area is located in northern France and following IPCC, 2007 and Goubanova & Li (2007) it would be in the North of the Iberian Peninsula,

that includes the Basque Country. The uncertainties involved, precisely, in the climate predictions for that transition zone are large and difficult to identify. Therefore, it should be an in-depth studied area. However, compared with other European regions, the number of research works in this zone is low (Table 1.2); these evidences the strength of the current work.

Uncertainties related to the impact of climate change appear at the four levels of the sequence: GCMs; Representative Concentration Pathway (RCP) or emission scenario; downscaling and hydro-sedimentary projections. For example, Chen et al., (2011), assessed the uncertainty of downscaling methods and the results showed that impact studies based on only one downscaling method should be interpreted with caution. Wilby (2005) found that the uncertainty related to hydrological model calibration is comparable with that involved in greenhouse and other pollutant emissions. Wilby & Harris (2006) determined that the greatest uncertainties derive more from the choice of GCM and downscaling methods and less from the hydrological models and emission scenarios. Some research supports the argument that the choice of hydrological model has a relatively minor impact on the results of hydrological simulations based on climate projections (Boyer et al., 2010; Bates et al., 2008; Kay et al., 2006) and major uncertainties come from the GCM structure (Arnell, 1999; Bergstrom et al., 2001; Nijssen et al., 2001; Kay et al., 2009; Chen et al., 2011; Arnell, 2011; Teng et al., 2012). For this reason, the use of an ensemble of climate models gives a better estimate of uncertainty (e.g. IPCC, 2007; 2013; Stahl et al., 2011). Therefore, the inherent uncertainties of the methods used at each of these levels propagate the uncertainties of the previous levels of the sequence, with the result that all single uncertainties are then propagated in the hydrological models (Wilby et al., 2006).

Discharge and sediment flux (including soil erosion and sediment transport) are commonly studied using mathematical models. Several different types of models can be used in this kind of research (Merritt et al., 2003; Borah & Bera, 2004). In this Thesis SWAT code (Arnold et al., 1998) was selected to analyse the impact of climate change on streamflow and associated sediment yield. The SWAT model is widely used across the world and has been applied to many different size catchments and under considerably different conditions, usually with

satisfactory results (Gassman et al., 2007). It can be employed for very different objectives, from modelling just discharge to also assessing water quality, including sediments, nutrients and bacteria; it can work at different time steps, daily or subdaily; and daily, monthly, and annual statistics can be obtained for the outputs of the model at the sub-cathcment or hydrologic response unit (HRU) level. To date, SWAT has been widely used for studying and predicting the impact of climate change on pollutant loss, including suspended sediments (e.g., Hanratty & Stefan, 1998; Bouraoui et al., 2002; Nearing et al., 2005, Phan et al., 2011). Although it has been mostly applied to large agronomic catchment, there are several cases in which the application of SWAT to a small or/and forested catchment has been satisfactory (e.g. Kaur et al., 2004; Veith et al., 2005).

In this context, in this chapter it is performed a first insight on the climate change effects on hydrological systems of the Basque Country. In some cases the research is more focused on the suspended sediment response to climate change (*4.2 Simulation climate change impact on streamflow and sediment yield in Aixola catchment*) and in others in the water resources (*4.3 Evaluation of climate change impacts on water resources in Goi-Nerbioi catchment* and *4.4 Evaluación de los impactos del cambio climático en los recursos hídricos de la cuenca del Zadorra*).

4.2 SIMULATION CLIMATE CHANGE IMPACT ON STREAMFLOW AND SEDIMENT YIELD IN AIXOLA CATCHMENT

4.2.1 Introduction

Suspended sediment yield plays a key role in processes and environmental conditions in small mountainous catchments and is thus of great interest for environmental and river basin management. A great proportion of the sediment delivered to the oceans comes from small mountainous catchments, as small rivers have less area for storing flood-driven sediment. They are also more likely to respond to event-driven floods (Milliman & Syvitski, 1992; Farnsworth & Milliman, 2003).

Transport of solids is one of the optional (not obligatory) elements for characterizing rivers in the European WFD (European Commission, 2000). In fact, when the ecological status of a river is assessed under the WFD, only hydromorphological indicators that have an effect on biological health are considered. Ecology and hydromorphology are, however, strongly interconnected (Brierley & Fryirs, 2000). The need to understand the connection between sediments and ecological status is implicit in much of the WFD (Chave, 2001). Furthermore, the development of sediment EQS (Environmental Quality Standards) is called for by the Directive, but the proposals made for achieving them are technically controversial (Crane, 2003).

In this context, this research set out to provide new insights into how potential changes in precipitation and temperature may affect suspended sediment yields in a forested headwater catchment of the Basque Country (Atlantic region). Specifically, the objective of this section is to assess the potential long-term trends in sediment yield in a catchment of the Basque Country (Aixola catchment) due to climate change.

The evaluation of the performance of the SWAT code for the Aixola catchment was explained in the section 3.4 *Streamflow and sediment yield simulation in Aixola catchment*. Therefore, all the hydro-sedimentary projections given in the next pages are obtained from the 1.Project (Fig. 3.2).

4.2.2 Evaluation of climate projections

Simulations with the calibrated SWAT model were used to assess the potential long-term trends in streamflow and sediment yield in the area due to future climate change projections. The study of consequences of global climate change on hydrological systems, such as the Aixola catchment, requires scenarios of future temperature and precipitation changes as input to the hydrologic model. During the scenario simulations, it was assumed that there will be no changes in land use. In this way, it is possible to evaluate the likely impacts of the climate change alone on discharge and sediments.

As it was explained before, direct application of output from general circulation models (GCMs) is often inadequate for hydrologic and other assessments (e.g. von Storch et al., 1993) due to the coarse resolution of the GCM data, especially for precipitation. The statistical downscaling is based on empirical-statistical relationships between the regional climate and global-scale parameters (e.g. Wilby et al., 2004), which is the approach used in this study. The advantages and drawbacks of these two categories of downscaling approaches and their impacts on resulting simulations have been widely discussed in the literature (Murphy, 1999, 2000; Schmidli et al., 2007).

Daily precipitation and maximum and minimum temperatures from 1961 to 1990 and predictions for 2011 to 2100 were provided by Spanish Meteorology Agency (AEMET) for a meteorological station (1049O) located approximately 1 km away from the Aixola gauging station, for the respective baseline and future climate change scenarios used in the analysis. AEMET has used various different downscaling methods to regionalize data obtained from the GCMs and the one chosen for this study was the empirical regionalization based on the analogues of the Climate Research Foundation (FIC), hereafter AEMET Analogues method (AN). There is more explanation about this downscaling technique in the *2. Methodology* chapter *2.2 Climate change projections* section.

The simulations provided by the AN combine two IPCC SRES scenarios: A2 and B2, considered to be scenarios of medium-to-high and medium-to-low CO_2 emissions respectively (IPCC SRES, 2000) and two GCMs: CGCM2, (Flato & Boer 2001); and ECHAM4, (Roeckner et al., 1996). These yield four model-scenario combinations: CGCM2-A2, CGCM2-B2, ECHAM4-A2, and ECHAM4-B2 (Table 2.1).

In addition to providing regionalized data for the period 2011-2100, the downscaled projections also provide a control period (1961 to 1990), considered to be the baseline period for the GCM projections. These baselines were obtained by the same downscaling methodology and, therefore, one baseline is provided for each model. This control period has been compared with precipitation and temperature data measured at the 1049O station by AEMET between 1983 and

1990 (no earlier data are available). The simulated GCM baseline precipitation values were below the corresponding AEMET measurements for both models for the eight-year comparison period. The CGCM2 model underestimated mean annual precipitation by 3.5 % versus underestimations of as much as 35.5 % for the ECHAM4 model. In contrast, regarding the temperature, it was the ECHAM4 model that gave the best fit to the observed values, with a mean daily maximum temperature of 17 °C (matching the measurements) and a minimum of 7 °C (one degree lower than that measured). The CGCM2 model gave the closest match with the mean measured minimum temperature (8 °C), but it calculated a mean daily maximum temperature of 15 °C (2 °C lower than that measured).

The first and most important source of uncertainty in this kind of research on climate change impact is the selection of input climate data, especially the choice of GCM but the downscaling method is also key (Fowler et al., 2007). In any case, the aforementioned results illustrate the mismatch between observed and simulated data for the downscaled GCMs used for hydrologic simulation in the next step. Despite CGCM2 simulating annual precipitation relatively well, which is more difficult to simulate than temperature, the calculated daily maximum temperature is lower than that observed. As a result, evapotranspiration estimated during the simulation process will be affected, and so will discharge and, consequently, suspended sediment concentrations. Temperature results obtained after the downscaling for ECHAM4 are reasonably similar to those observed in the meteorological station, however, precipitation is greatly underestimated, which will undoubtedly influence hydrological results. It is necessary to keep these differences between the GCM baseline climate data and the actual historical climate data in mind when evaluating the potential hydrological impacts of climate change.

Regarding the downscaled data for the scenario period (2011-2100), to be used to simulate future hydrologic conditions in Aixola, some differences with the downscaled baseline conditions were observed. Precipitation was predicted to decrease (0.55 mm yr-1 for CGCM2-A2, 4.16 mm yr-1 for ECHAM4-A2, and 2.22 mm yr-1 for ECHAM4-B2) except under the CGCM2-B2 combination, for which precipitation would increase about 1.02 mm every year (Table 4.1). Specifically,

the projections estimate that by the year 2100 annual rainfall would be lower by 50 mm (CGCM2-A2), 200 mm (ECHAM4-B2) or even 374 mm (ECHAM4-A2) or higher by 98 mm (CGCM2-B2) relative to present conditions (mean of 1480 mm). As shown in Table 4.1, it was found that maximum and minimum temperatures would increase, to a greater or lesser extent, with all the model–scenario combinations considered.

	CGCM2				ECHAM4			
	A2		B2		A2		B2	
	Annual	2100	Annual	2100	Annual	2100	Annual	2100
P	-0.55	-50	1.02	98	-4.16	-374	-2.22	-200
Tmax	0.082	7.38	0.032	2.88	0.077	6.93	0.034	3.03
Tmin	0.032	2.88	0.01	0.9	0.031	2.79	0.029	2.61

Table 4.1. *Annual change and change until 2100 expected for precipitation (P, mm) and maximum and minimum temperature (Tmax and Tmin, °C) for 1049O weather station taking into account CGCM2-A2, CGCM2-B2, ECHAM4-A2 and ECHAM4-B2 climate projections.*

4.2.3 Analysis of the effects of climate change on the water resources and sediments of Aixola catchment

Annual time series of discharge (Q) and suspended sediments (SS) for the period of 2011 to 2100, simulated by the calibrated SWAT model using the four downscaled model-scenario combinations (CGCM2-A2, CGCM2-B2, ECHAM4-A2 and ECHAM4-B2) were analysed from two different points of view. As it was explained in the *2. Methodology* section, on the one hand, the results were grouped into three consecutive 30-year periods (2011-2040, 2041-2070, and 2071-2100, hereafter 2030s, 2060s and 2090s) and compared to the values simulated for the baseline period (1961-1990) (Fig. 4.1). Downscaled GCM data were also used for the baseline simulations. We should highlight that when examining the hydrologic and sediment flux effects of future climate scenarios, changes were calculated relative to the results from the GCM baseline simulations, rather than the historic observations. This convention avoids, at least to first order, the effects of model bias (Nijssen et al., 2001). On the other hand, the Mann-Kendall nonparametric trend test (Mann, 1945; Kendall, 1975) was applied to the output series in order to identify trends in the projected series and assess whether they were significant. In both cases, one simulation was

performed for the entire period from 2011 to 2100 for each of the four climate projections.

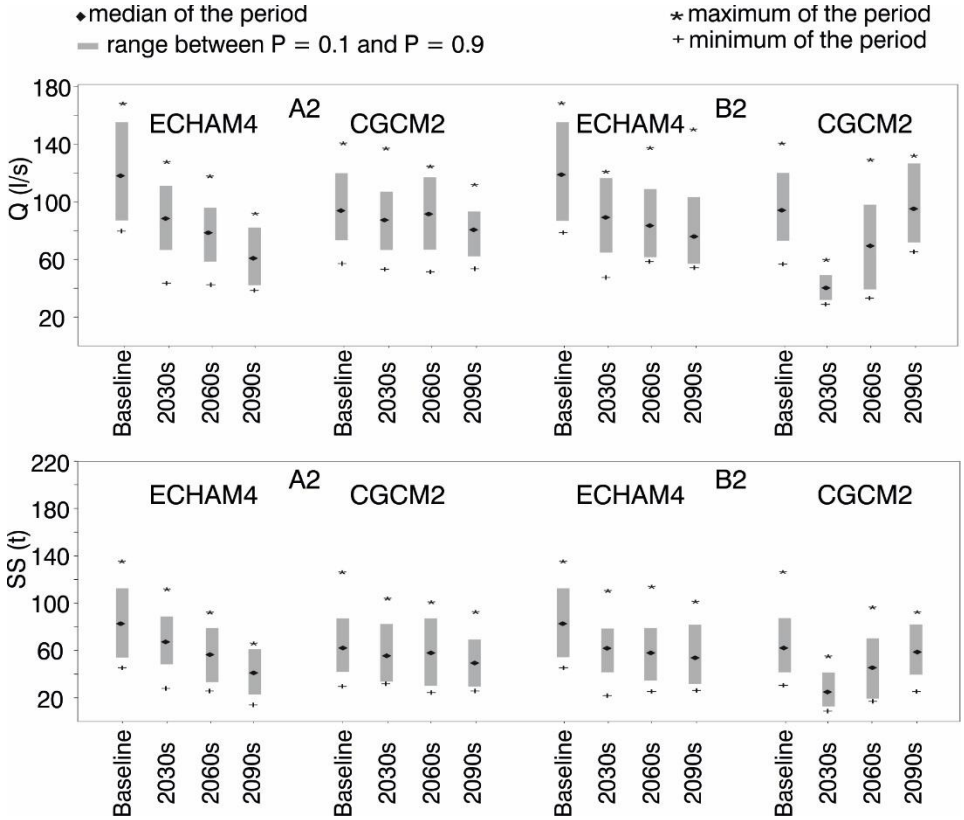

Figure 4.1. *Median, maximum, minimum and P0.1-P0.9 range of discharge and sediment for baseline and for 2030s, 2060s and 2090s.*

The results of the climate change scenarios are shown in Fig. 4.1, in which the median, maximum, and minimum values, as well as the range between percentile 10 and percentile 90 for the 2030s, 2060s and 2090s, were compared to the ones calculated for the outputs simulated under the baseline scenario (1961-1990) for each GCM (Fig. 4.1). Compared to baseline, under the same land use and management conditions, the median annual discharge and sediment yield would decrease for all the periods, as can be deduced from the climate projections summarized in Table 4.1. However, under one of the possible future climate conditions (the CGCM2 under the B2 emission scenario), average discharge and sediment yield values would be similar to the baseline ones for the 2090s after decreasing in the two previous periods. In addition, it can be observed in the

figure (Fig. 4.1), that not only the median value of discharge and sediment yield decreases, but also the inter-annual variability, as the range of data decreases from the baseline to the future periods.

The model-scenario combination that produces the greatest differences between the baseline and the projection for 2090s is ECHAM4-A2 (predicting the largest decrease in precipitation and increases in both maximum and minimum temperatures, Table 4.1); this resulted in a 50 % decrease in sediment yield, from 82 t year^{-1} at baseline to 41 t year^{-1}, in the 2090s. In contrast, the projection with CGCM2-B2 (indicating increases in precipitation and small increases in maximum and minimum temperatures, Table 4.1) yields notably similar results regarding sediment yield for the 2090s and the baseline, with only a slight decrease (6 %) being observed from 62 t year^{-1} to 58 t year^{-1}. Taking into account the high degree of uncertainty in climate and hydrological projections, this difference is essentially negligible. In fact, it could be that in this scenario the increase in precipitation is balanced by the increase in temperature and, as a result, in evapotranspiration. Simulations performed using the other two model-scenario combinations (CGCM2-A2 and ECHAM4-B2) give sediment yields 20 % and 35 % lower than baseline (1961-1990), respectively. Results obtained for the 2060s are similar, with decreases of around 30 % estimated for mean annual sediment yield for all the combinations except CGCM2-A2, for which the estimated decrease, compared with baseline, is not significant (6 %). It is also worth pointing out some of the differences for the first period (2030s), which corresponds to the first WFD period. Specifically, the simulations predict decreases in the mean annual sediment yield of 11 to 24 %, this time the exception being the CGCM2-B2 projection that estimates a decrease of 60 %.

Given these results, it seems that annual increases or decreases in sediment yield are a function of the change in annual precipitation and, to a lesser extent, a change in annual temperature. In fact, the total amount of precipitation in the Aixola catchment during a given event and suspended sediment delivery during that same event are strongly correlated (Zabaleta et al., 2007). Nevertheless, it is necessary to keep in mind that precipitation intensity is not taken into account in the simulation process because this is performed at daily time-step. Intensity is

closely related to the concentration of suspended sediment in water and being able to take it into account in hydrological simulation might well lead to different results.

The aforementioned results, nevertheless, give us an idea of the magnitude of changes in sediment yield that can be expected (compared to the baseline period). Subsequently, the Mann-Kendall nonparametric trend test (Mann, 1945; Kendall, 1975) was applied to the annual simulation outputs in order to identify trends in the projected series, from 2011 onwards, to assess their level of significance. To assess probabilities of occurrence we have applied the criteria suggested by the IPCC (2005) in its fourth report, for the following likelihood ranges: the result is "virtually certain" to happen when p (probability of occurrence) is > 0.99; "extremely probable" when p > 0.95; "very probable" when p > 0.9; "probable" when p > 0.66 (Table 2.10). Additionally, annual changes in the simulated series were quantified using linear regression analysis.

For the 2011 to 2100 ECHAM4 model inputs, discharge and sediments were found to be "very probable" (p > 0.9) to "virtually certain" (p > 0.99) to decrease by 0.23 to 0.45 $m^3 s^{-1}$ and 0.14 to 0.43 t every year, respectively, under the B2 and A2 scenarios. With the CGCM2-A2 model-scenario combination, discharge and sediment inputs to the reservoir were also found to be "probable" (p > 0.66) to decrease 0.13 $m^3 s^{-1}$ and 0.11 t yearly. Only with CGCM2-B2, both discharge and sediments were "virtually certain" (p > 0.99) to increase 0.94 $m^3 s^{-1}$ and 0.57 t every year, respectively.

For the period 2011 to 2100, sediment yield (Table 4.2) was found to be "very probable" to decrease by about 17 %, 25 % and 55 % for the CGCM2-A2, ECHAM4-B2 and ECHAM4-A2 combinations, respectively. In contrast, cumulative sediment yield would increase by as much as 285 % for the B2 scenario simulated using the CGCM2 model. In the nearer future, from 2011 to 2070, the estimated annual sediment yield was predicted to decrease by 11 %, 16 % or 37 % (CGCM2-A2, ECHAM4-B2 and ECHAM4-A2) or to increase by 190 % (CGCM2-B2). Finally, for the nearest future, that is, by 2040, sediment yield was predicted to decrease by 6 %, 8 % or 18 % for the CGCM2-A2, ECHAM4-B2

and ECHAM4-A2 model-scenario combinations, respectively, or increase by 95 % for the CGCM2-B2 model-scenario combination.

Time period	CGCM2		ECHAM4	
	A2	B2	A2	B2
2013-2040	-6	95	-18	-8
2013-2070	-11	190	-37	-16
2013-2100	-17	285	-55	-25

Table 4.2. *Total decrease (%) of suspended sediment yield predicted by each of the model-scenario combinations for the time periods analysed in this Thesis.*

4.2.4 Discussion and conclusions

Annual outputs from the simulations found that under the same land use and management conditions, the mean and interannual variations in annual streamflow and sediment yield would decrease compared to the baseline period (1961-1990). Hydrological models are usually designed to be used in stationary conditions, despite it being known that hydrological parameters may change with climate change. In relation to this, changes other than climatic ones, such as variations in land use or management, would tend to increase the uncertainty in the parameterization of the model. Taking only climatic variations into account, however, the largest decrease in sediment yield is observed for ECHAM4-A2, the combination that generates the largest decrease in precipitation and large increases in both maximum and minimum temperature, resulting in an environment with higher rates of evapotranspiration and lower precipitation in which less discharge would be produced. Sediment yield decreases observed for simulations under ECHAM4-B2 and CGCM2-A2 are similar and smaller than those for the ECHAM4-A2 model-scenario combination. With ECHAM4-B2, there is a larger decrease in precipitation but the increase in temperatures, especially maximum temperatures, is smaller than for CGCM2-A2; hence, for the former the decrease in streamflow and sediments is more related to decreases in precipitation, while for the latter they are more related to a higher rate of evapotranspiration.

Results obtained for simulations under CGCM2-B2 differ from the other model-scenario combinations: specifically, in the long term (by 2100), annual sediment

yield would not change much from that simulated for the baseline (1961-1990). However, a strong increasing trend would be observed between 2011 and 2100. This is the only combination for which, as well as rises in minimum and maximum temperatures, precipitation would also slightly increase. In this catchment, precipitation is the input variable that most affects hydrological response, more than temperature, in annual terms. This is consistent with the findings of other authors, such as Todd et al., (2011), who have reported that the variability in the hydrological response observed when applying different climatic projections is mostly driven by differences in precipitation forecast in the different climate models considered by the IPCC.

The uncertainty in the projections of climate models is, considerably greater than that generated due to the parameterization of the underlying hydrological model (Todd et al., 2011). Often, though, the use of certain GCMs, emission scenarios and downscaling methods is conditioned by availability of the necessary data, as is the case in this study. In this section, two emission scenarios, A2 and B2, two GCM and one downscaling method have been discussed, these being the climatic projections available for the area considered.

A2 and B2 are not the most extreme scenarios, but rather are moderate mid-range ones, and the uncertainty that is involved in the selection of these emission scenarios is considerably less than that implied in the climate models and downscaling methods. An estimation of the uncertainty generated by these other aspects of the simulation process can potentially be provided using multi-model approaches (Willems & Vrac, 2011), but is beyond the scope of the present Thesis. Accordingly, given the inherent uncertainties, this should be regarded as a preliminary study of the application of projections coming from various GCMs to assess the hydrologic impact of climate change in a specific catchment of the Basque Country. Clearly, the impact ranges would widen further if more climate models, including regional ones, were to be considered. Indeed, there is no doubt that simulations with data provided for more GCM and different downscaling methods are needed to obtain a wider range of results and for a better evaluation of potential impacts.

This research presents a first attempt to estimate future changes in sediment yields in the Basque Country that may be used as a starting point to expand our understanding of future hydrological impacts in the area and provide some data to decision makers.

4.3 EVALUATION OF CLIMATE CHANGE IMPACTS ON WATER RESOURCES IN GOI-NERBIOI CATCHMENT

4.3.1 Introduction

In Goi-Nerbioi catchment (Fig. 2.2), hydrological projections were performed using as input climate projections from ENSEMBLES and CMIP5 (Coupled Model Intercomparison Project) projects. As in sub-section 4.2, it was assumed that there will be no changes in land use.

The projected climate variables from ENSEMBLES and CMIP5 projects were introduced in the Soil and Water Assessment Tool or SWAT model (Arnold et al., 1998) to evaluate the hydrological impact of climate change, focusing on the following partial objectives:

- To evaluate the baselines of considered downscaled projections of climate variables with respect to the observed data (1961-2000).
- To study the average hydrological impact of future climate projections in three horizons: 2030s, 2060s, 2090s (annual, seasonal and monthly).
- To assess possible trends in extreme daily discharges (2011-2099/2100) and compare the observed figures for the reference period (1961-2000).
- To identify the differences between climate projections and identify the greatest uncertainties in the different steps of the followed methodology.
- Compare the hydrological projections performed with climate projections from ENSEMBLES and from CMIP5.

4.3.2 Study area

The study area is the catchment of the Nerbioi River (185 km^2), which is located at an average latitude of 43° and longitude of 3° (Fig. 4.2). Its direction South-North, is very common in catchments of the Basque Country, as well as its geology and land use. The catchment is located at the interface between the Atlantic climate in the North and the Mediterranean climate in the South. In addition, this is one of the catchments with longest records of hydro-meteorological parameters in this zone.

Average annual rainfall is about 1000 mm and it is distributed quite evenly throughout the year: close to 300 mm in winter and autumn; 230 mm in spring and 30 mm in summer, as an average (1961-2014). The mean annual temperature is around 12 °C, being the seasonal averages for winter and summer 8 °C and 20 °C (1961-2014), respectively.

The mean elevation of the catchment is around 200 m above sea level (m.a.s.l.) (Fig. 4.2). The lithology is dominated by siltstones, clays and sandstones with medium-low permeability (Geographical Database of the Basque Government, www.geoeuskadi.net). In the southeast part, at an average altitude of 1100 m.a.s.l., there is a highly permeable late Cretaceous limestone platform. The main soil types are Cambisols, Rankers and Gleysols (FAO, 1977), which are characterized by high clay and silt contents. Land use in the catchment is divided between native forests, exotic plantations and pasturelands. The areas with the highest slopes (>35 %) are covered by forest and tree plantations, while the flatter areas (7-15 %) host pasturelands. The average slope in the catchment is around 17 %.

Mean annual discharge at the outlet of the catchment is 3 $m^3\ s^{-1}$. The mean in spring and autumn is around 3.5 $m^3\ s^{-1}$; in winter 5 $m^3\ s^{-1}$ and in summer 0.8 $m^3\ s^{-1}$ (1996-2013). Discharge data from a gauging station (Gardea; http://www.bizkaia.eus) located at the outlet of the catchment (Fig. 4.2) were used in this work to calibrate and validate the hydrological model. Discharge data have been recorded at this gauging station since 1995. This station was designed to measure mean and high flows.

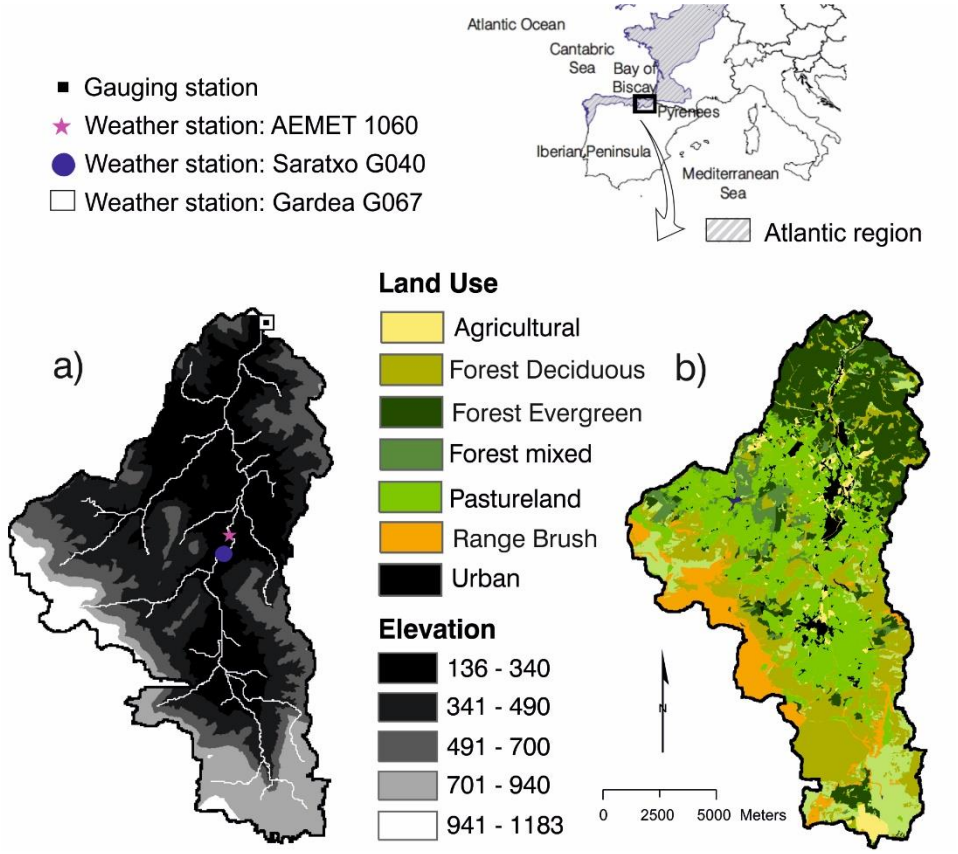

Figure. 4.2. *Location of Goi-Nerbioi catchment and a) digital elevation model, b) land use map. In a) the Nerbioi river and the location of the gauging and weather stations can be observed.*

4.3.3 Hydrological model input and data source

SWAT requires topographic, land use/cover, soil and meteorological data. The source for the Digital Elevation Model (LIDAR 2008, 5x5m), land use classification (2005, 1: 10,000) and part of the soil map (1: 25,000) is the Basque Government's Geographical Database (www.geoeuskadi.net). The remainder of the soil map was obtained from the soil map of Araba province (1:200,000) (Iñiguez et al., 1980). Soil properties were obtained from these two sources and the plant growth properties for each land cover were directly obtained from the SWAT database.

For the calibration and the validation of the model, daily maximum and minimum temperature and precipitation (1996-2013) for the Gardea (G067), Saratxo (G040) and Amurrio (AEMET 1060) meteorological stations were used (Fig. 4.2, a)). The

meteorological data for the Gardea and Saratxo stations and the daily observed discharge for the Gardea G067 gauging station (Fig. 4.2, a)) were obtained from the Basque Meteorological Agency (www.euskalmet.euskadi.eus) and Bizkaia Provincial Council (http://www.bizkaia.eus), while the meteorological data for Amurrio were provided by the Spanish Meteorological Agency (AEMET). The climate variables of the daily maximum and minimum temperature and precipitation used to model the climate scenarios were downloaded from the AEMET website (http://escenarios.aemet.es/). These climate variables were given for Amurrio meteorological station (AEMET 1060) (Fig. 4.2, a)) for baseline periods (1961-2000 for each GCM) and future scenarios (2006-2100). For the baseline period there is a small number of years with available discharge data (1995-2000). However, for Amurrio station (AEMET 1060), previous observed meteorological data (1961-2000) are available. These meteorological data were used to generate (using SWAT) discharge series from 1961-2000. The modelled series was termed OBS_SIM.

4.3.4 Model calibration and validation

Daily river flow ($m^3 s^{-1}$) observed at the Gardea G067 gauging station was used for the model calibration and validation. The model was run daily; the period from 1996 to 2006 was used for calibration and the period from 2007 to 2013 for validation. The purpose of this selection of the calibration and validation years was to consider similar hidro-meteorological conditions for both periods. The 18 years of simulation ensures that wet, dry and average years are all included.

The first step in calibration was to identify the most sensitive parameters for the catchment. To achieve this, a “one-at-a-time” sensitivity analysis (van Griensven et al., 2006) was conducted with 22 flow-related parameters. The most sensitive parameters are listed in Table 4.3. Later, a realistic value-range was introduced for the most sensitive parameters in the SWAT CUP program (Abbaspour et al., 2007a) to make an autocalibration using the SUFI2 algorithm (Abbaspour et al., 2004, 2007a) (Table 4.3). The program calculates a p-factor to quantify the degree of uncertainty of each iteration. The p-factor is the percentage of measured data bracketed by the 95% prediction uncertainty (95PPU). A value of

1 indicates 100% bracketing of the measured data. The r-factor is the average thickness of the 95PPU band divided by the standard deviation of the measured data. The r-factor seeks to bracket most of the measured data with the smallest possible value (Abbaspour et al., 2007b). A working value of >0.7 for p-factor and <1.5 for r-factor is recommended (Abbaspour et al., 2015). In this way, besides achieving good results for the calibration, the uncertainty of the simulation is also quantified. Finally, the validation process was performed using the parameter set for the calibration period and comparing the observed and simulated discharge (2007-2013).

Change type	Variable name	Description	Range	Best value
r	Cn2	Curve number	-0.2-+0.2	-0.07
v	Esco	Soil evaporation compensation factor	0.77-0.86	0.83
v	Gwqmn	Depth of water in the shallow aquifer required for return flow to occur	614-655	625.36
r	Sol_Awc	Available water capacity	0.1-0.5	0.48
v	Epco	Plant uptake compensation factor	0.8-0.95	0.87
v	Revapmn	Threshold water in shallow aquifer	768-900	892.21
v	Ch_K2	Main channel conductivity	10-44	38.66
v	Alpha_BF	Base flow alpha factor	0.6-0.9	0.77
v	Surlag	Surface runnoff lag coefficient	0.5-2.5	1.32
v	Smtmp	Snow melt base temperature (ºC)	3-9	4.77
v	Gw_Delay	Delay time for aquifer recharge	1-20	1.4
v	Sftmp	Snowfall temperature (ºC)	0.39-1.5	0.62
v	GW_Revap	Groundwater “revap” coefficient	0.017-0.04	0.026

Table 4.3*. Most sensitive parameters (ranked from 1 the most sensitive and 13 the less sensitive) in the Goi-Nerbioi River catchment, their description, the range used for the autocalibration (p-factor 0.81 and r-factor 0.41) and the best value. “v” means the default parameter is replaced by a given value; “r” means the existing parameter value is changed relatively.*

To evaluate the performance of the model (for calibration and validation), the evaluation criteria explained in the chapter *2. Methodolgy*, section *2.4.7 Modelling process and evaluation methods* was used. According to Moriasi et al. (2007), the discharge simulation is satisfactory in a monthly time step when NSE>0.5, R^2>0.5 and the slope and intercept of the linear regression between simulated and observed discharges are close to 1 and 0 respectively (Arnold et al., 2012), RSR≤0.7, and PBIAS<25%. In addition to this and in order to ensure the

goodness of the modeling process and determine its uncertainty for future hydrological projections, these statistical indices were also used in differentiated climate conditions. The driest and wettest years were selected by calculating an "Aridity Index" (hereafter AI) for all the available data (1996-2013), where this index is deemed to be the ratio between potential evapotranspiration and precipitation. The three consecutive calendar years with the lowest AI are 2003, 2004 and 2005 while the years with the highest AI value are 2010, 2011 and 2012. Thus, using the model evaluation methods for daily discharge in different time periods (annually and seasonally) and in years with low and high AI, it is possible to evaluate whether the performance of the model is good enough to simulate the future climate projections and also to identify where the largest uncertainties are.

4.3.5 Evaluation of climate projections: ENSEMBLES and CMIP5

ENSEMBLES PROJECT

ENSEMBLES is a European climate change project which has regionalized (RCMs) the results of multiple climate models (GCMs). The statistical downscaling methods applied in the regionalized GCMs are the AEMET analogues (AN) and the Statistical Downscaling Method (SDSM). Therefore, the climate projections used in this section have been downscaled in two steps: a dynamical downscaling in the ENSEMBLES project and a statistical performed by AEMET. To reduce uncertainty, three greenhouse gases emission scenarios (A2, A1B and B1) were used because an ensemble of GCM, downscaling methods and different emission scenarios give better results than single-model simulations (Giorgi & Mearns, 2002; Murphy et al., 2004; Boorman & Sefton, 1997; IPCC 2007). With the combination of 4 GCMs (EGMAM, EGMAM2, MPEH5, HADGEM2), two downscaling methods (AN and SDSSM) and three emission scenarios (A2, A1B and B1), 11 climate projections (Table 2.2) were selected.

AEMET supplies daily climate variables for the Amurrio (AEMET 1060) meteorological station (Fig. 4.2, a)), for each downscaled GCM for the baseline period (1961-2000) and for future climate projections (2011-2099).

To analyze the performance of the selected climate projections, the baselines (1961-2000) of each downscaled GCM were compared with real measured data. The seasonal and annual differences between each baseline projection and the real measured data were calculated for both precipitation (%) and mean temperature (%) on a monthly mean basis (Fig. 4.3).

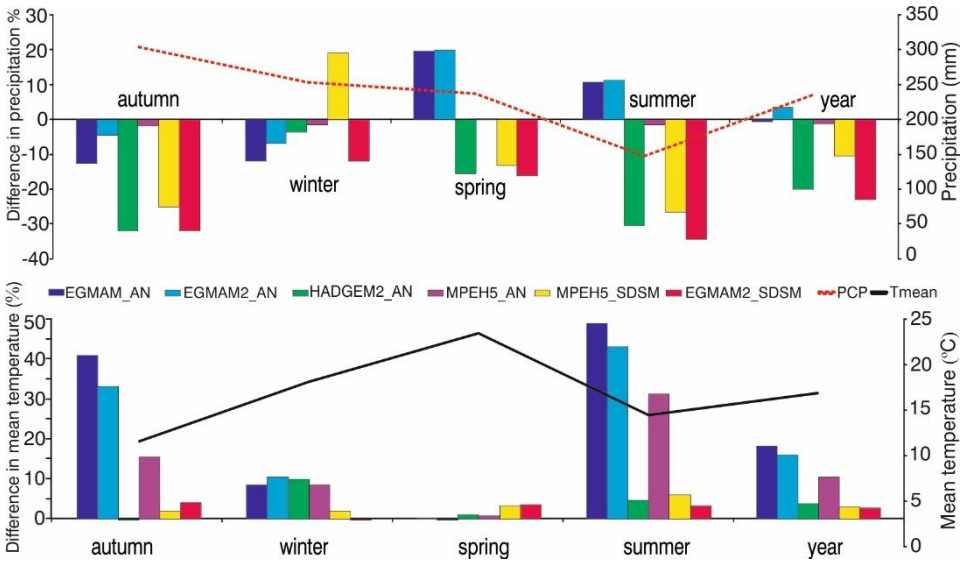

Figure 4.3. *Difference between observed meteorological parameters; precipitation (PCP) and average temperature (TMEAN)) and climate baselines (1961-2000) before applying bias correction at annual and seasonal scales.*

Focusing on precipitation, annual EGMAM_AN, EGMAM2_AN and MPEH5_AN precipitations are closer to the observed precipitation levels (-0.8 % and 3.4 % respectively) than the other projections, while precipitation outputs from EGMAM2_SDSM and HADGEM2_AN differ the most (around -20 %). With regard to seasons, autumn and summer are the ones that differ the most from the real measured data, whereas, the results for winter are closer to the observed data. In general, it can be said that the models simulate less precipitation than the observed.

Regarding the mean temperature, as opposite to precipitation, simulations from EGMAM_AN, EGMAM2_AN and MPEH5_AN differ the most from real data as they simulate 18 %,16 % and 10 % (2.4 °C, 2.1 °C and 0.5 °C) more in a yearly base. For the other models, the results do not differ much from real data (less than3.6

%). With respect to the seasons, the two climate projections mentioned show the biggest differences chiefly for autumn and summer. EGMAM_AN and EGMAM2_AN simulate 40 % and 33 % more in autumn and in summer the differences are higher; 48 and 40 % more, respectively. That means around 4 °C more in summer and 3.5 °C in autumn. In contrast to precipitation, the models simulate higher mean temperatures compared with the measured ones.

Therefore, there is a considerable difference between the climate projections baselines and the measured meteorological data. This is the reason why a bias correction was performed (*chapter 2. Methodology, 2.3 Bias correction section*). Hence, a linear-scaling approach following the methodology explained by Lenderink et al. (2007) was performed to these data. This methodology eliminates the monthly differences between the measured and the projected baseline climate values, but for example the rainfall distribution is not corrected.

The Fig. 4.4, shows monthly mean monthly discharge (m^3 s^{-1}) of the results obtained from the simulation made with the bias-corrected climate projections baselines and the modelled with real observed meteorological data (OBS_SIM). The figure shows that in all the cases the simulated flow using the baselines of climate projections is lower than the OBS_SIM. Annually, EGMAM2_SDSM and MPEH5_SDSM are the projection baselines that best fit, simulating 14 % less discharge than the OBS_SIM. The biggest difference is for MPEH5_AN, it simulates 35 % less flow. With regard to seasonal projections, the biggest differences are for summer; EGMAM2_SDSM and MPEH5_SDSM simulate -51 and -64 % respectively, showing the smallest differences for this season. The rest of baselines project a difference of about -80 %. In spring, the projected discharge is 22 % and 58 % less than the OBS_SIM. Winter is the season with more similarities (around -5 and -10 %) following by autumn (-8 and -42 %). In general, the climate models downscaled with SDSM method show results more similar to the observed.

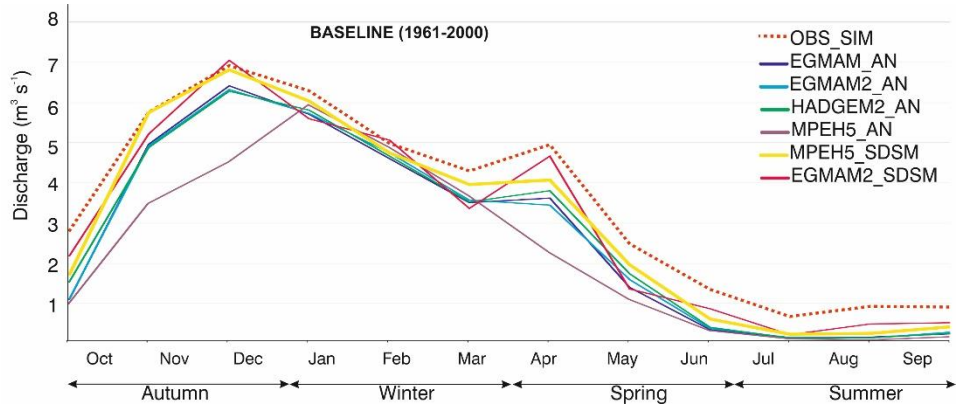

Figure 4.4. *Monthly mean discharge (m^3 s^{-1}) from 1961 to 2000 obtained from the simulation with observed meteorological data (OBS_SIM) and from the simulation with the downscaled and bias-corrected baseline climate projections from ENSEMBLES.*

***CMIP5* PROJECT**

The last generation of GCMs is coordinaited by the CMIP5. AEMET has done a statistical downscaling to the climate projections obtained from these GCMs and supplies daily climate variables for the Amurrio (AEMET 1060) meteorological station (Fig. 4.2, a)), for each downscaled GCM for the baseline period (1961-2000) and for future climate projections (2006-2100). 5 GCMs (ACCESS1-0, BNU-ESM, MPI-ESM-RL, MPI-ESM-MR, CMCC-CESM), 2 RCPs (8.5 and 4.5) and 2 downscaling methods (AN and SDSM) were used in this research. As it has been explained before, an ensemble of different scenarios gives more reliable results than single-model simulations. With these combinations, 16 climate projections were implemented, as shown in Table 2.3.

As mentioned above, in order to select the downscaled GCMs their climate projection baselines (1961-2000) were compared to the meteorological data observed in the catchment. The seasonal and annual differences between each baseline projection and the observed data were calculated for both, precipitation (%) and mean temperature (%) and they are displayed in Fig. 4.5. For the precipitation, annual projections baselines of CMCC-CESM_SDSM, MPI-ESM-LR_SDSM and MPI-ESM-MR_SDSM are closer to observed precipitation levels (-29 %) than other projections, while BNU-ESM_AN and CMCC-CESM_AN show the largest differences with observed (around -50% less precipitation). It is clear

that at both annual and seasonal scales the baselines downscaled with the SDSM method fit the observed precipitation better than those downscaled with AN method (Fig. 4.5). Focusing on mean temperature, BNU-ESM_AN scenario shows the highest difference compared to the observed values as it simulates 12 % higher temperatures in an annual basis. MPI-ESM-MR_AN fits very well and the results of the other models baseline projections do not differ greatly from the observed data (5.5 % as an average). In general, at annual and seasonal scale, the models tend to simulate higher temperatures than those observed, with the exception of summer and especially spring, when some climate projection baselines show lower temperatures than observed ones. Although the downscaled GCMs chosen were the ones that *a priori* best fitted the observed data provided by AEMET, there are still important differences between the climate projections baselines and the observed meteorological data (especially when precipitation is considered). In order to correct these differences, as it was done with the climate projections from ENSEMBLES, a linear-scaling approach was performed (*chapter 2. Methodology, 2.3 Bias correction section*). The bias-corrected values were introduced as meteorological input in SWAT.

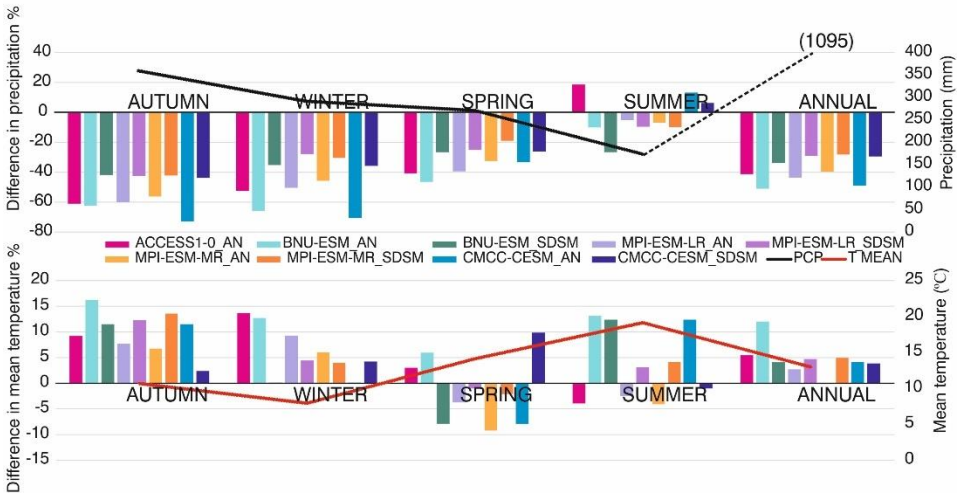

Figure 4.5. *Difference between observed meteorological parameters; precipitation (PCP) and average temperature (TMEAN) and climate baselines (1961-2000) before applying bias correction at annual and seasonal scales.*

The bias-corrected precipitation and maximum and minimum temperature for the baseline of each downscaled GCM was introduced in the calibrated and validated SWAT project. The first step was to assess how the hydrological simulations obtained for baseline (1961-2000) adjust to the ones performed using observed meteorological data (OBS_SIM) for the same period. The mean monthly discharges ($m^3 s^{-1}$) obtained are shown in Fig. 4.6. This figure shows that as in the case of precipitation, hydrological simulations obtained using the baseline climate projections downscaled with the SDSM method fit much better to OBS_SIM than those downscaled with the AN method. In fact, the adjustment for discharge series obtained using SDSM downscaling to OBS_SIM is really good in autumn (-9 %) and winter (-2 %) whereas in spring and summer the discharge is underestimated by about 22 % and 71 %, respectively. However, those differences are higher in all seasons for the discharge series obtained using the AN method; around -22 % in autumn, -11 % in winter, -46 % in spring and -83 % in summer.

Therefore, it is clear that, in this case, the choice of the downscaling method is the cause of a higher uncertainty source in the obtained discharge series than the choice of the GCM itself.

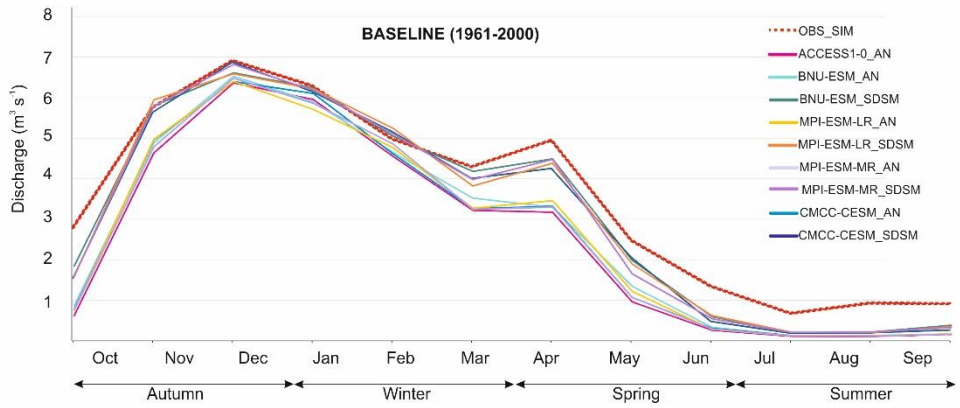

Figure 4.6. *Monthly mean discharge ($m^3 s^{-1}$) from 1961 to 2000 obtained from the hydrological simulation with observed meteorological data (OBS_SIM) and from the hydrological simulation with the downscaled and bias-corrected GCMs baselines.*

4.3.6 Results: model calibration and validation

The parameters changed in the calibration process of SWAT for the Goi-Nerbioi, their value-range used in the autocalibration and the final values are shown in Table 4.3. These are some of the most common parameter changes usually performed in SWAT to calibrate the model (Arnold et al., 2012) and all of them were changed taking into account the catchment characteristics. The results of the calibration (1996-2006) and the validation (2007-2013) are displayed in a daily hydrograph with the observed and simulated discharge (Fig. 4.7). The calibration can be seen to fit the observed data well, although the peak magnitude is underestimated in some high flows. In previous works carried out with the SWAT model (daily time step) in the Basque Country, the underestimation of the peak magnitude is usual (Zabaleta et al., 2014; Peraza et al., 2015; Epelde et al., 2015; Meaurio et al., 2015). This inaccuracy may be related to the inability of the model to properly consider precipitation intensity and spatial-temporal distribution when simulating rapid hydrological responses at the daily time step (Qiu et al., 2012).

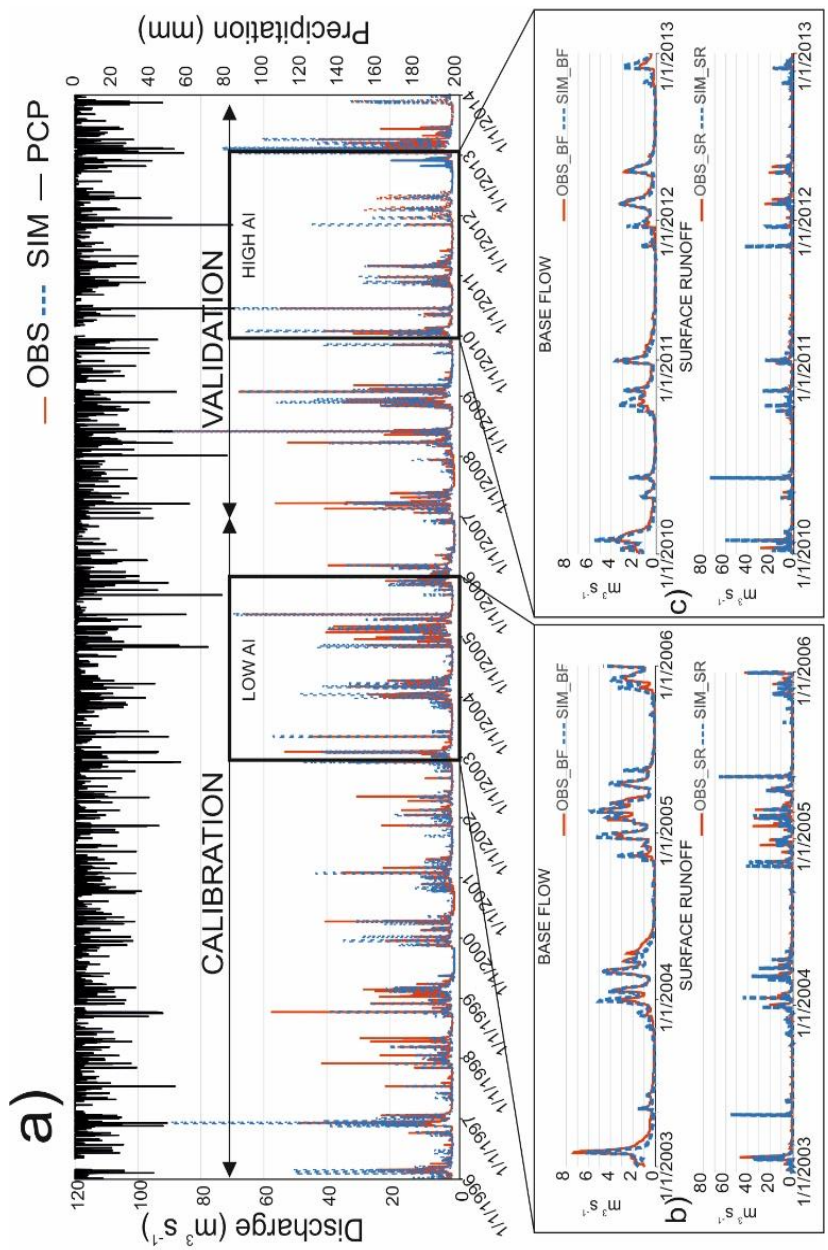

Figure 4.7. *a) Daily observed (OBS) and simulated (SIM) discharge for both the calibration (1996-2006) and the validation (2007-2013) periods, and the precipitation (PCP) observed in Amurrio station (AEMET 1060). b) Zoom of the Low Aridity Index (LOW AI) period (2003-2005) where the observed and simulated base flow (on top) and surface runoff (below) are represented. c) Zoom of the High Aridity Index (HIGH AI) period (2010-2013) where the observed and simulated base flow (on top) and surface runoff (below) are represented. For additional information the statistical indices are shown in Table 4.4. In general, simulated discharge peaks fit observed data better during the validation (Fig. 4.7). The set of statistical indices calculated for daily discharge (Table 4.4) shows that the model performs satisfactorily during both, calibration and validation (Moriasi et al., 2007).*

Analyzing years with a low and high aridity index (AI), it is possible to assess whether the simulation is good enough to make long-term hydrologic projections and evaluate when the greatest uncertainties are found (low or high AI). In Fig. 4.7 it is possible to observe that the model is able to simulate well the years with low and high AI not only for mean discharge but also for base flow and surface runoff. The set of statistical indices (Table 4.4) shows that simulation performance for years with low and high AI is at least *good*, although some parameters are slightly poorer for years with high AI (more uncertainty).

		DISCHARGE				
	Scale	**NSE**	**R2**	**slope/int.**	**PBIAS**	**RSR**
CALIBRATION	1996-2006	0.63	0.68	0.85/0.35	-1.00	0.61
VALIDATION	2007-2013	0.75	0.77	0.91/0.24	0.17	0.50
HIGH AI	2010-2012	0.67	0.76	1.02/0.16	-10.51	0.58
LOW AI	2003-2005	0.74	0.76	1.01/0.16	-5.16	0.51
ALL 1996-2013	1996-2013	0.69	0.72	0.89/0.3	-0.51	0.56
	WINTER	0.66	0.68	0.81/0.62	6.26	0.58
	SPRING	0.74	0.76	0.87/0.1	17.74	0.51
	SUMMER	0.29	0.40	0.61/0.06	12.23	0.84
	AUTUMN	0.61	0.72	0.98/0.77	-26.78	0.63

* According to Moriasi et al. (2007) the discharge simulation is satisfactory at monthly time step when the NSE > 0.5, R^2 > 0.5, RSR ≤ 0.7, and PBIAS < 25%. The best value for slope is 1 and 0 for intercept (Arnold et al., 2012).

Table 4.4. *Values obtained for the statistical indices used in the evaluation of the SWAT model performance at daily time-step. Seasonal statistical values are calculated for the 1996-2013 period.*

In addition, the set of statistical indices were also applied for the entire period (1996-2013) on a seasonal scale. It is thus possible to evaluate the model performance considering low (summer), intermediate (spring and autumn) and high (winter) flows and determining where the largest uncertainties are. Winter and spring present *good* statistical results, autumn is at least *satisfactory* and the statistical indices show that although the hydrograph seems not to fit properly in summer (low R^2, NSE and RSR), the water yield is simulated correctly (low PBIAS). Note that summer discharges, being the lowest, are more vulnerable to measurement errors. Therefore, although the simulation does perform well, summer is the season associated to the highest modelling uncertainty. However,

according to Moriasi et al. (2007) the values of most of the statistical indices shown in Table 4.4 were *good* or *very good* at monthly time step. Since these analyses were made with daily values they are considered to be at least *good*. Additionally, the p-factor and r-factor obtained with the SWAT-CUP program (the range of the parameters is shown in Table 4.3) for calibration and validation are 0.81 and 0.41 respectively, which is considered *good* (Abbaspour et al., 2015). As a consequence, it can be said that the performance of the model is good enough for carrying out future hydrological projections with a certain degree of confidence.

4.3.7 Analysis of the effects of climate change on the water resources of Goi-Nerbioi catchment. Projections of ENSEMBLES project

To evaluate the impact of climate change on the hydrology of the Goi-Nerbioi catchment area, the baseline (1961-2000) discharge simulated for each downscaled GCM was compared with its future hydrological projections, divided in three horizons (2030s, 2060s and 2090s). The difference (in %) between average discharge for each model baseline and future projections, is represented in the Fig. 4.8.

Most of the projections show that the discharge will decrease in all the seasons and, therefore, also annually. The difference between baselines (1961-2000) and the future projection is bigger when the century draws on. More specifically, having into account all the projections, the difference for the 2030s is -5 %, for 2060s is -15 % and for 2090s is -28 % (Table 4.5). Winter is the season with less difference, for the end of the century the decrease respect the baseline is -20 %. In autumn, spring and summer the difference is around -35 %.

Two downscaling methods (AN and SDSM) have been used and it is possible to compare their results as they were applied in the same GCM (MPEH5) for three emission scenarios (A2, B1 and A1B). The SDSM downscaling method in general projects (annually and seasonally) bigger decrease respect baseline than AN method (difference in %).

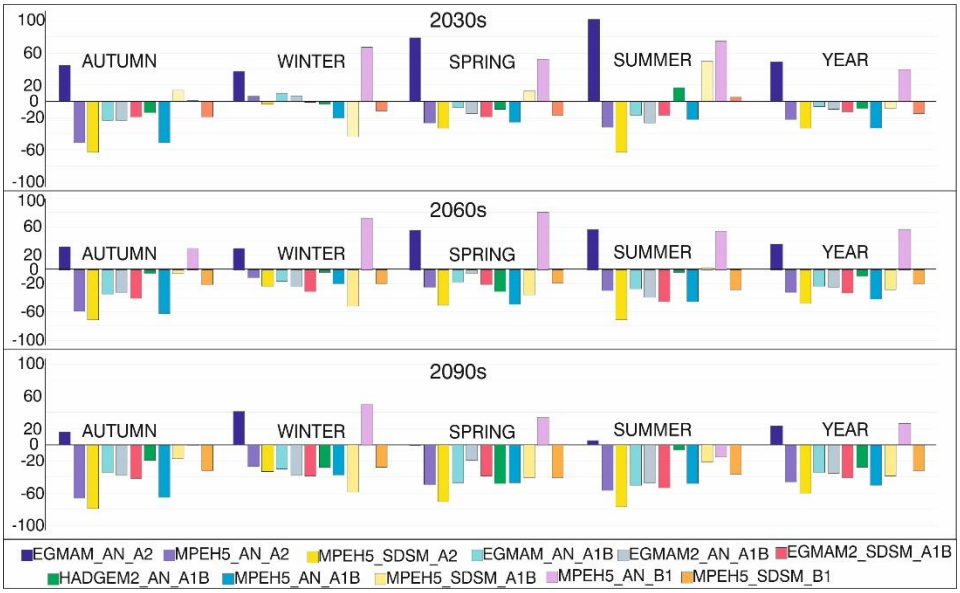

***Figure 4.8**. Annual and seasonal discharge (m^3 s^{-1}) difference in %, between each hydrological projection and its baseline projections (1961-2000), divided into 3 horizons (ENSEMBLES project models).*

Taking into account the emission scenarios, with the exception of EGMAM_AN_A2, the A2 emission scenario projects less discharge than the other two. For 2090s A2 predicts around -52 %, A1B -44 % and B1 -3 %, less discharge.

	Mean difference value		
	2030s	**2060s**	**2090s**
AUTUMN	-18	-24	-34
WINTER	5	-9	-20
SPRING	0	-10	-33
SUMMER	7	-16	-36
YEAR	-5	-15	-28

***Table 4.5**. Summary of the discharge differences (%) mean values, between baseline and future projections (divided in three horizons).*

Annually and seasonally EGMAM_AN_A2 and MPEH5_AN_B1 (Fig. 4.8) simulate an increase in discharge for all three periods (in contrast to the rest of projections), although for the 2090s the increase is lower. Specifically, EGMAM_AN_A2 projects 49 % more discharge for 2030s, 36 % for 2060s and 24 % for 2090, while MPEH5_AN_B1 estimates 39 % for 2030s, 57 % for 2060s and 27 % for 2090s.

Fig. 4.9 is an ensemble of the combination of the analysed 11 hydrological projections (mean monthly discharge) and their temporal evolutions measured in the analysed 3 horizons. The possible discharge range is the highest in winter (varies from 2.27 $m^3 s^{-1}$ to 7.90 $m^3 s^{-1}$) and in autumn (from 1.54 $m^3 s^{-1}$ to 5.86 $m^3 s^{-1}$) and spring (from 0.88 $m^3 s^{-1}$ to 2.78 $m^3 s^{-1}$) this range is still large. Summer displays the lowest range (from 0.09 $m^3 s^{-1}$ to 0.41 $m^3 s^{-1}$) and the discharge is always lower than the OBS_SIM. Therefore, the trend shows that the summer discharge will be lower than in the OBS_SIM, while in the other three seasons could be lower or higher.

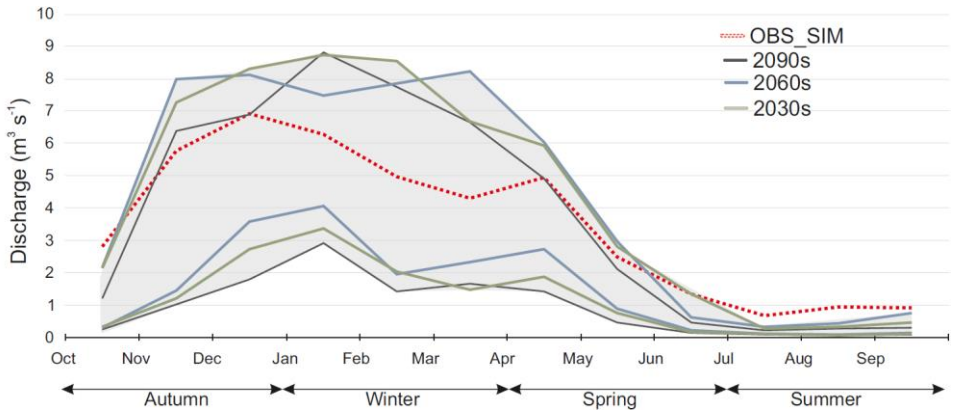

Figure 4.9. *Mean monthly discharge ($m^3 s^{-1}$) calculated with the values of 11 climate projections (ENSEMBLES). The highest discharge values represent the maximum value of the mean monthly discharge of all the projections by month, while the lowest values represent the minimum. The grey colour represents the range of possible discharge values and the observed mean monthly discharge (1961-2000) is shown (OBS_SIM).*

Evaluation of trends in duration and severity of low and high flows (Q20 and Q80)

The results from the duration trends analysis for low (Q20) and high (Q80) flows are shown in Tables 4.6 and Fig. 4.10. This analysis has been done for the reference period 1961-2000 and for the future periods 2011-2039, 2011-2069 and 2011-2099.

Analysing the duration (in days) of low flows (<Q20) from 1961 to 2000 (Table 4.6), the discharge simulated for the reference period (OBS_SIM) does not show any significant annual trend. At seasonal scale, a significant trend is only detected in spring, when the low flow duration shows a "probable" increasing trend. Some of the discharge series simulated using the six climate baselines, show significant

trends; a decreasing in autumn (MPEH5 GCM) and increasing in spring (SDSM downscaling method), and depending on the GCM considered it is possible to observe an increase or decrease in winter, summer and at annual scale (Table 4.6).

		OBS_SIM	EGMAM_AN	EGMAM2_AN	HADGEM2_AN	MPEH5_AN	MPEH5_SDSM	EGMAM2_SDSM
Q20	YEAR	0.39	**-0.68**	***0.99***	0.10	**-0.70**	0.34	***1.00***
	AUTUMN	-0.52	-0.27	0.28	0.03	**-0.70**	**-0.81**	0.47
	WINTER	0.61	**-0.84**	0.00	0.51	-0.62	0.00	***0.95***
	SPRING	***0.86***	-0.38	0.21	0.09	0.32	***0.99***	***0.97***
	SUMMER	0.32	0.09	***1.00***	-0.34	**-0.81**	0.32	***1.00***
Q80	YEAR	**-0.99**	***0.83***	**-1.00**	-0.47	0.13	-0.49	**-1.00**
	AUTUMN	**-0.75**	-0.19	**-0.85**	-0.21	0.25	-0.39	**-0.90**
	WINTER	**-0.68**	***0.76***	**-0.99**	0.41	0.64	0.62	**-0.80**
	SPRING	**-0.74**	0.45	**-0.71**	**-0.73**	**-0.91**	**-0.96**	**-1.00**
	SUMMER	**-0.91**	0.60	0.00	0.23	0.00	0.00	**-1.00**

Table 4.6. *Sign (+ or -) and probability of occurrence (P) of the annual and seasonal trends detected for the duration (days) of the period below Q20 and above Q80 between 1961 and 2000. Trends with a P higher than 0.66 are represented in bold; positive values are italicised.*

In Fig. 4.10 are displayed the future low flow (Q20) duration trends (2011-2099). As it was explained above, when the series is longer (more years included in the analysis), the number of projections with significant trends is greater, thus 2011-2099 is the period with more significant trends (Fig 4.10). The period 2011-2039 and 2011-2069 show homogeneous increasing low flow duration trends both, annually and seasonally. The clearest homogeneous trends appear on 2011-2069 where in the analysed eleven projections, ten show an increasing trend annually and in summer, and most of them are “virtually certain” or “extremely probable”. In autumn seven of the projections show increasing trends while in spring and winter the number of projections with trend is lower (Fig. 4.10). For the period 2011-2099 although the number of projections with significant trend is higher, some of them show negative sign. For example, four of the projections show increasing annual low flows duration in 2011-2069 while in 2011-2099 there are decreasing. In winter and autumn there are not homogeneous trends due to their sign can be positive or negative. In spring, the number of projections with increasing trend rises considerably; from three projections in 2011-2069 to ten in

2011-2099. Therefore, it is possible to conclude that in short term, the number of low flow days will increase annually and in summer and although the trend is not so evident seems to will occur something similar in autumn. When all the century is considered (2011-2099) there are more uncertainties in the annual values and the projections with trends in summer decrease. There are not homogeneous trends in winter and autumn whereas low flows show an increase in spring, something that also occurred in the baseline with the observed values trend (OBS_SIM).

OBS_SIM shows a “virtually certain” decreasing annual trend in high flow duration (>Q80) for 1961-2000 (Table 4.6), “very probable” in summer and “probable” decreasing trend in autumn, winter and spring. Regarding the simulated baselines, EGMAM2 model results (downscaled with SDSM and AN methods) are similar to the OBS_SIM. Most of the baselines show a decreasing trend in spring while there are not clear homogeneous trends for the other seasons.

The future periods (Fig. 4.10), show most homogeneous trends for low flows than for high flows, mainly because the sign of the trends change more. Therefore, the decreasing trends are predominant especially in 2011-2069. In this period (Fig. 4.10), the annual decreasing trend is homogeneous and is possible to observe the same pattern in winter and autumn. Considering 2011-2099 period, the number of projections with significant trend are higher but there are not so homogeneous. The annual trends, in summer and spring are heterogeneous, while winter and autumn in general show decreasing homogeneous trends. Therefore, during the century, it seems that the high flow days, as occurred with the OBS_SIM, will decrease in autumn and winter.

Considering the severity of low flows (2011-2100), the hydrological projections performed with EGMAM2 GCM show to “very probable” to “virtually certain” increasing trends (Table 4.7). The MPEH5_AN projection presents a “probable” decreasing trend and the other projections do not show probable trends; therefore, there is not possible to obtain clear conclusions about the severity of low flows.

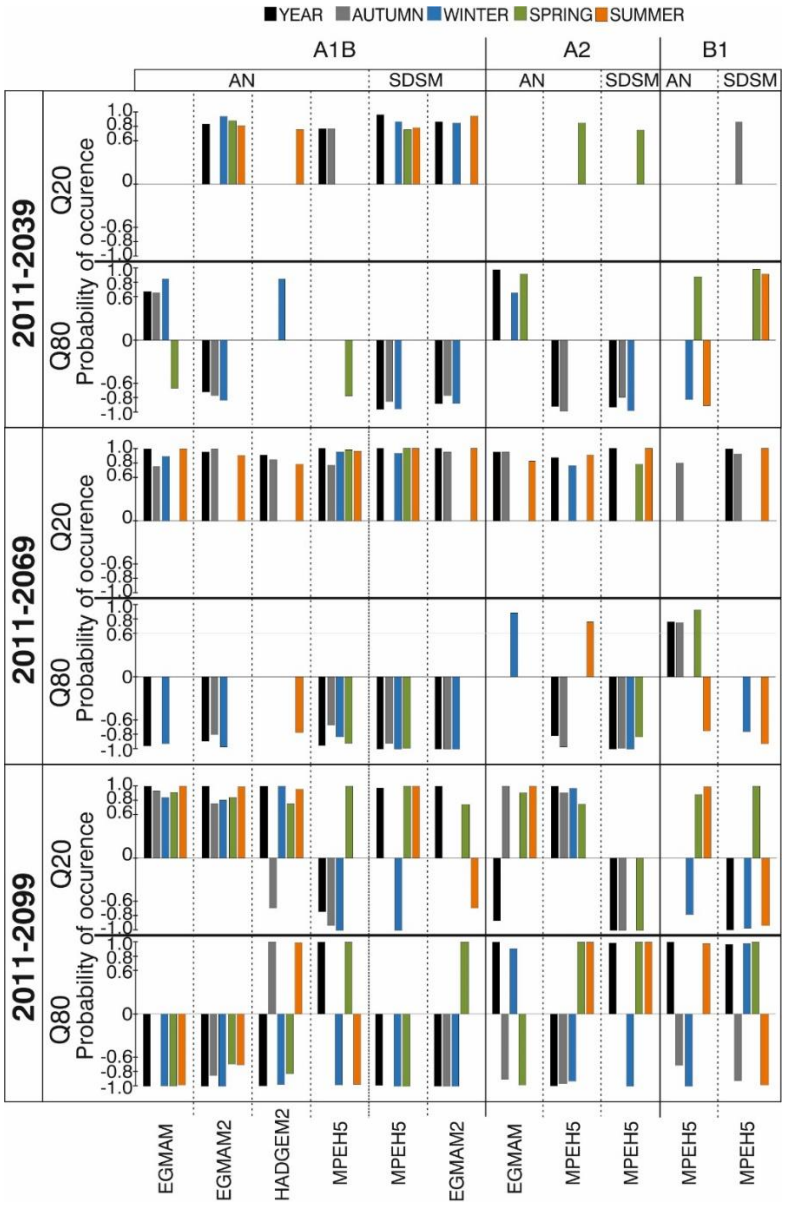

Figure 4.10. *Trends for low flow (Q20) duration and high flow (Q80) duration displayed at annual and seasonal scales for the 2011–2099 period. Only values with a probability of occurrence higher than 0.66 are shown.*

	Q10	Q20
EGMAM_AN	-0.44	-0.60
EGMAM2_AN	**0.94**	**0.98**
EGMAM2_SDSM	**0.99**	**1.00**
HADGEM2_AN	0.37	0.10
MPEH5_AN	**-0.83**	**-0.77**
MPEH5_SDSM	-0.60	-0.19

Table 4.7*. Trends for the severity of low flows (Q10 and Q20) of Goi-Nerbioi catchment obtained on an annual scale for the period 2011-2099. The probability of occurrence values are shown. The sign, none for the increasing and - for the decreasing, refers to the sign of the trend.*

4.3.8 Analysis of the effects of climate change on the water resources of Goi-Nerbioi catchment. Projections of CMIP5

The methodology for the evaluation of the impact of climate change on the hydrology of the Goi-Nerbioi catchment area, using the climate variables of CMIP5, is the same as the explained above. The annual discharge difference (%) between the 16 hydrological projections and its respective baseline simulations, divided into three 30-year horizons (2030s, 2060s, 2090s) is shown in Fig. 4.11. Focusing on the downscaling method (AN or SDSM), the hydrological projections derived from climate projections that use the AN method tend to predict a smaller discharge decrease than those downscaled with SDSM (with the exception of CMCC_CESM_AN_R85). Considering that climate projections obtained with the SDSM downscaling method fit better to OBS_SIM series data for the baseline period, it seems reasonable to consider that there is a higher probability of occurrence of the hydrological scenarios obtained under SDSM method, meaning those where the discharge decrease is more pronounced.

It is also important to compare the two different RCPs because, one would expect that the difference between the 2060s and 2090s for the projections with RCP 4.5 would be minimal, while for 8.5 the difference would continue to increase. Indeed, if the projections of CMCC-CESM are not considered, the difference in discharge at annual scale between the baseline and the projections with RCP 4.5 is -6 % for the 2030s, -8 % for the 2060s and -9 % for the 2090s, while for RCP 8.5 it is -13 % for the 2030s; -15 % for the 2060s and -20 % for the 2090s. In the RCP 4.5 scenario, the seasonal decrease of discharge throughout the century is lower (Fig.4.12). In some seasons, as in summer, a stabilization of the discharge can be observed, and in others (e.g. autumn) the increase in the average flow in the 2090s almost compensates for the decreases observed during the 2060s. This is not the case for the RCP 8.5 scenario where discharge continues to decrease until the end of the century (Fig. 4.12).

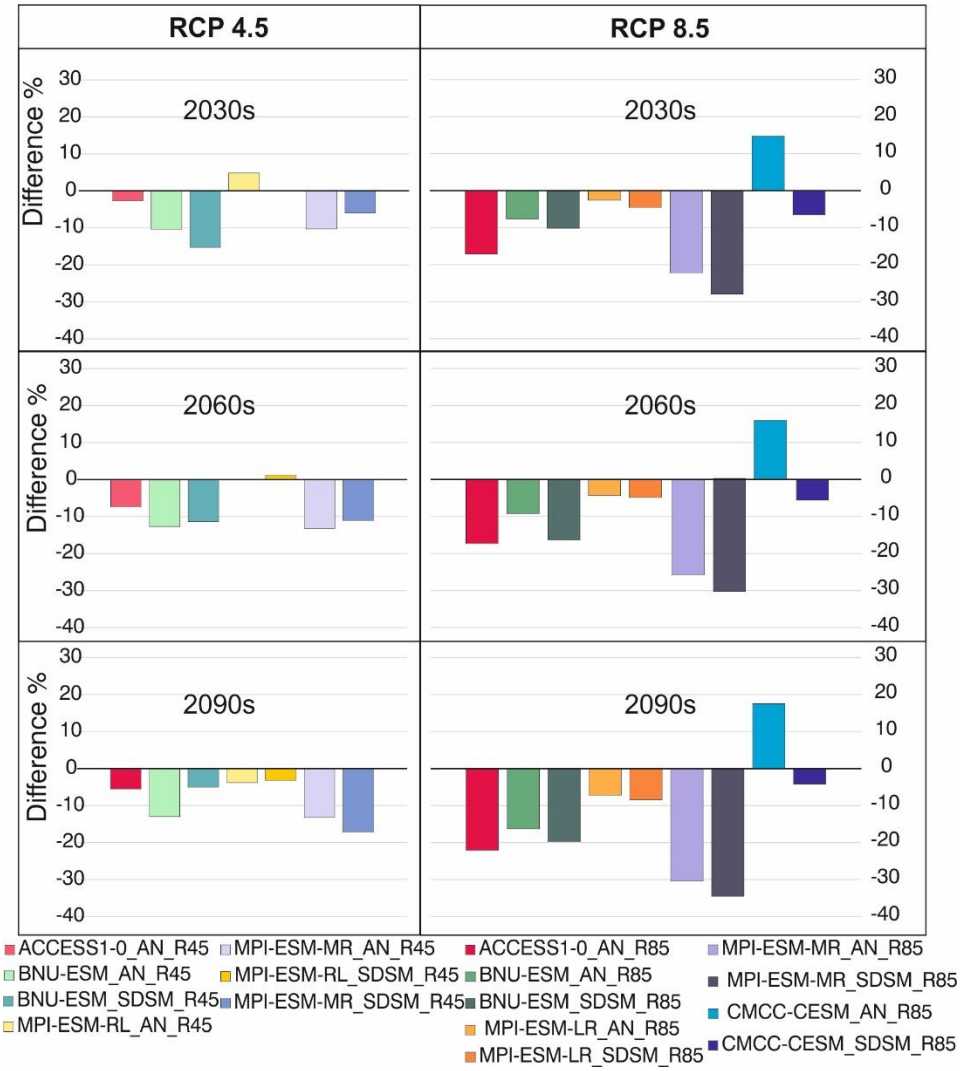

***Figure 4.11**. Annual discharge difference (%) between the 16 hydrological projections and its respective baseline simulations, divided into three 30-year horizons (2030s, 2060s, 2090s).*

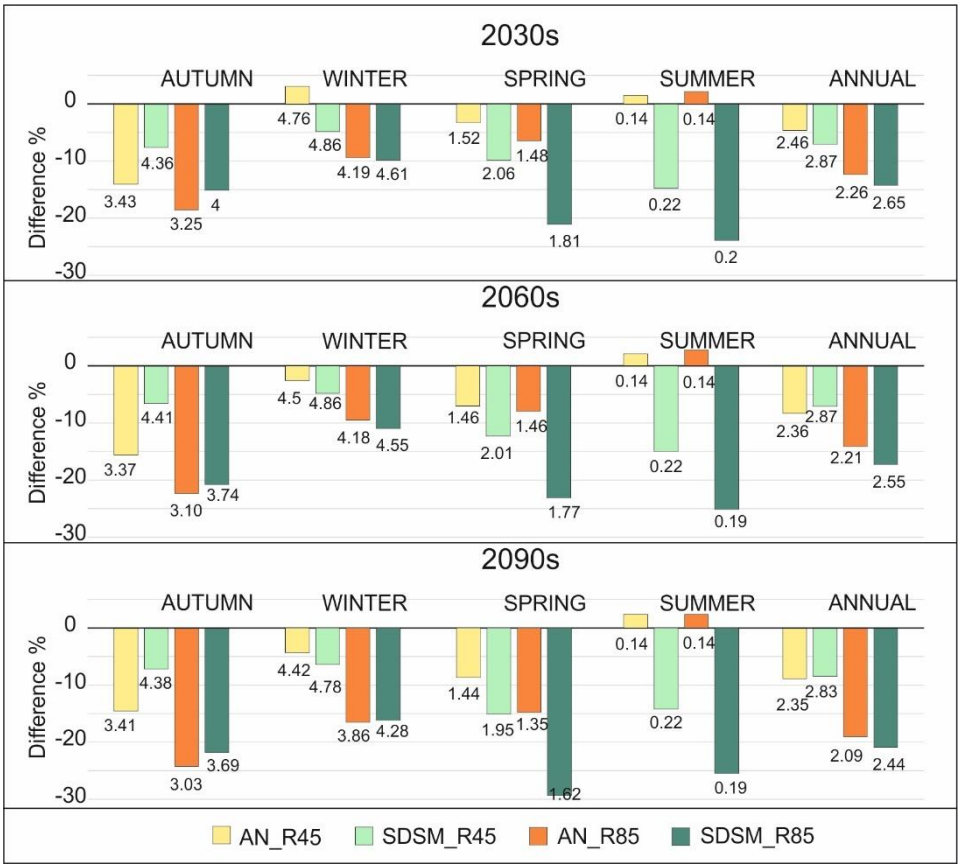

Figure 4.12. *Annual and seasonal discharge difference (%) between hydrological projections and their respective baselines grouped by downscaling method and RCP. The figure shows the mean difference between: - ACCES1-0_AN_R45, BNU-ESM_AN_R45, MPI-ESM-MR_AN_R45 and MPI-ESM-RL_AN_R45, represented as* ***AN_R45****. - BNUESM_SDSM_R45, MPI-ESM-MR_SDSM_R45 and MPI-ESM-RL_SDSM_R45, represented as* ***SDSM_R45****. - ACCES1-0_AN_R85, BNU-ESM_AN_R85, MPI-ESM-MR_AN_R85 and MPI-ESM-RL_AN_R85, represented as* ***AN_R85****. - BNU-ESM_SDSM_R85, MPI-ESM-MR_SDSM_R85 and MPI-ESM-RL_SDSM_R85, represented as* ***SDSM_R85****. The results are divided into 3 horizons (2030s, 2060s, 2090s). In addition, the mean annual and seasonal discharge (m^3 s^{-1}) is indicated in each bar.*

Undeniably CMCC_CESM_AN_R85 is most noteworthy because it projects higher discharge than the baseline. CMCC_CESM_SDSM_R85 decreases respect to the baseline, but as it happens with CMCC_CESM_AN_R85 the discharge increases throughout the century. The results for this GCM were analysed separately due to those different trends shown. Fig. 4.13 shows the difference (%) between CMCC-CESM_AN_R85 and CMCC-CESM_SDSM_R85 future discharges with regard to their baseline on a seasonal and annual scale.

In order to compare not only the trends but also the discharge, in terms of illustrative average flow for each period, the average discharge for each time horizon considered is also displayed in Fig. 4.13. These are the two projections that simulate highest discharge at annual scale as well as at seasonal scale.

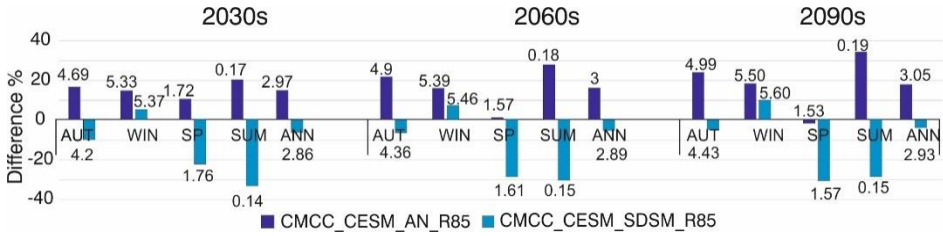

Figure 4.13. *Seasonal and annual discharge difference (%) between CMCC_CESM_AN_R85 and CMCC_CESM_SDSM_R85 hydrological projections and their respective baselines divided into three 30-year horizons (2030s, 2060s, 2090s). In addition, the mean annual and seasonal discharge (m^3 s^{-1}) is indicated in each bar.*

As discussed above, the downscaling method and the selection of RCP have a strong influence on the results. The projections were therefore classified taking into consideration the downscaling method (AN or SDSM) and the scenarios (RCP 4.5 or RCP 8.5) (Fig. 4.12), and analysed in four different groups (with the exception of the CMCC-CESM projections). Thus, the results are an ensemble of projections that makes it possible to analyse differences between these factors (downscaling method and RCP). At annual scale, and for the end of the century (2090s), discharge decreases by 9 % and 20 % for RCP 4.5 and RCP 8.5 scenarios, respectively, with little differences between downscaling methods. These results are consistent with most of the studies carried out in the Atlantic region of France and in the North of the Iberian Peninsula (Table 1.2). However, focusing on the seasonal changes, significant differences can be found depending on the use of the downscaling method. Summer is the season when the greatest differences can be observed; slightly increasing (<5 % for 2090s) for climate projections derived from AN downscaling, and clearly decreasing (-15 to -25 % for 2090s) for SDSM-derived ones. The AN downscaling method simulated considerably less discharge than the SDSM downscaling method. Hence, the differences between baseline and future projections are bigger for the SDSM method, although the projections downscaled with SDSM (independent of RCP)

always projected more discharge than those downscaled with the AN method (Fig. 4.12). In other seasons (autumn, winter and spring), discharge decreased regardless of the method chosen, with higher changes when using the AN method in autumn and smaller changes in spring. The results obtained using different downscaling methods are most similar in winter. This is the season that has most weight in the annual discharge, hence its effect can be observed at annual scale. Considering all the models, autumn is the season with the most significant discharge decrease (-17 %) followed by spring (-16 %), winter (-11 %), and summer (-7 %) for 2090s. These results are slightly different from previous studies undertaken in the Atlantic region of France and the north of the Iberian Peninsula (Table 1.2). In most of the research works carried out in these areas the highest discharge decreases occur in summer, and depending on the study are followed by autumn or spring (Table 1.2). In the present study, considering the average value, summer is not the most affected season in percentage. This could be explained by the influence of the projections downscaled with the AN method (Fig. 4.12).

Fig. 4.14 is an ensemble showing a combination of the 16 hydrological projections analysed (average of the mean monthly discharge ($m^3\ s^{-1}$) represented in a hydrological year) and their evolution over time measured at the 3 time horizons (2030s, 2060s and 2090s). In order to consider all the discharge predictions obtained, the projections were not divided based on the downscaling method or the RCP. The highest discharge values represent the maximum value of the mean monthly discharge of all of the projections, while the lowest values represent the minimum ones. The possible discharge range is the highest in winter and autumn. In these seasons the possible mean discharge may vary by 2.7 $m^3\ s^{-1}$. In spring the discharge may range between 1 and 2.1 $m^3\ s^{-1}$, while the range in summer may be the lowest: between 0.1 and 0.3 $m^3\ s^{-1}$. In spring, summer and the beginning of autumn, the projected discharge is always lower than the OBS_SIM. However, the results for spring and summer have to be considered with special care because, as discussed previously, the baseline of the hydrological projections are underestimated and it is therefore probable that a similar phenomenon happens in the case of future projections. With regard to

the evolution of the discharge over the century, the projected lowest discharge decreases from the 2030s to the 2090s. The projected highest discharges show the same trend in spring and summer, whereas they may even increase in autumn and winter.

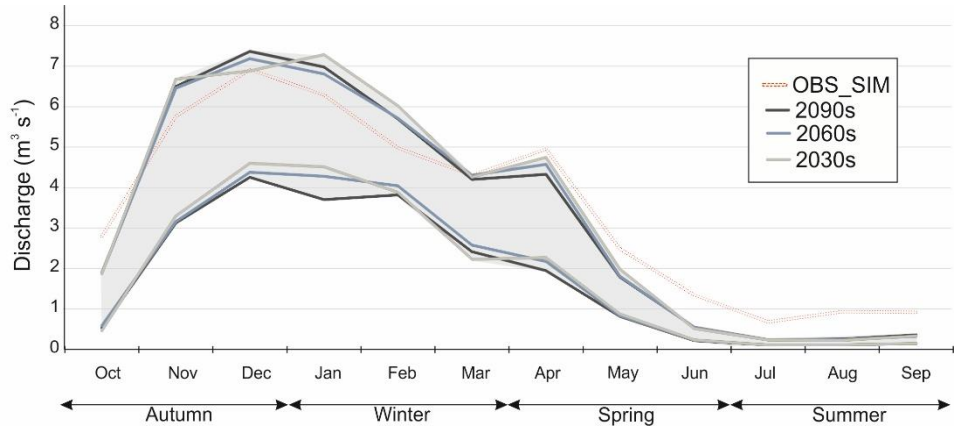

Figure 4.14. *Mean monthly discharge ($m^3 s^{-1}$) simulated with 16 climate projections (CMIP5). The highest discharge values represent the maximum value of the mean monthly discharge of all the projections, while the lowest values represent the minimum. The results are divided into three 30-year horizons (2030s, 2060s, 2090s). The grey color represents the range of possible discharge values and the observed mean monthly discharge (1961–2000) is shown (OBS_SIM).*

Evaluation of trends in duration and severity of low and high flows (Q20 and Q80)

The results obtained from trend analysis carried out for the duration of extreme flows are shown in Table 4.8 and Fig. 4.15. This analysis has been made for the reference period 1961-2000 (Table 4.8) and the future periods 2011-2040, 2011-2070 and 2011-2100 (Fig. 4.15). However, the most significant trends appear in the longest period (2011-2100) and hence, these are the results considered in this study. The results of the analysis for 2011-2040 and 2011-2070 are in Appendix 3.

		OBS_SIM	ACCESS1-0_AN	BNU-ESM_AN	BNU-ESM_SDSM	MPI-ESM-RL_AN	MPI-ESM-RL_SDSM	MPI-ESM-MR_AN	MPI-ESM-MR_SDSM	CMCC-CESM_AN	CMCC-CESM_SDSM
Q20	YEAR	0.39	0.58	0.34	***0.91***	-0.45	***0.73***	-0.45	0.5	***0.93***	0.34
	AUTUMN	-0.52	0.26	-0.08	0.37	-0.06	0.47	**-0.99**	0.04	0.65	***0.96***
	WINTER	0.61	0	0	0	0	0	0	0	0	0
	SPRING	***0.86***	0.08	***0.68***	0.16	0.47	***0.73***	-0.4	**-0.81**	-0.64	-0.05
	SUMMER	0.32	-0.21	0.52	***0.85***	**-0.78**	0.45	0.41	***0.81***	-0.64	-0.41
Q80	YEAR	**-0.99**	-0.17	**-0.91**	**-0.9**	0.02	0.02	0.32	0.47	0.37	0.34
	AUTUMN	**-0.75**	0.5	**-0.98**	**-1**	**-0.75**	-0.5	0.25	***0.71***	-0.62	-0.52
	WINTER	**-0.68**	**-0.76**	0.49	0.63	***0.76***	0.62	-0.28	-0.49	-0.62	0.53
	SPRING	**-0.74**	-0.64	0	-0.48	-0.42	0.37	0.65	0.37	***0.77***	0.39
	SUMMER	**-0.91**	0	**-0.84**	**-0.85**	0	0.09	0	0	-0.35	0

Table 4.8. *Sign (+ or -) and probability of occurrence (P) of the annual and seasonal trends detected for the duration (days) of the period below Q20 and above Q80 between 1961 and 2000. Trends with a P higher than 0.66 are represented in bold; positive values are italicised.*

Analysing the duration (in days) of low flows (<Q20) from 1961 to 2000 (Table 4.8), the discharge simulated for the reference period (OBS_SIM) does not show any significant annual trend. At seasonal scale, a significant trend is only detected in spring when the low flow duration shows a "probable" upward trend. However, some of the discharge series simulated using the nine climate baselines, show significant trends; an increase at annual scale and, depending on the GCM considered, an increase or decrease in spring, summer and autumn (Table 4.8).

In the evaluation of future low flow duration (2011-2100; Fig. 4.15), a general increasing trend can be observed, although, there are few decreasing trends. In spring and autumn there are many upward trends. In spring the number of projections with significant increasing trends is higher under RCP 8.5 than in RCP 4.5. On the contrary, in autumn this number is lower. Summer present random significant trends, mostly under RCP 8.5, that in general tend to be positive. There are few projections with significant trends in winter, therefore, is not possible to obtain clear conclusions for this season.

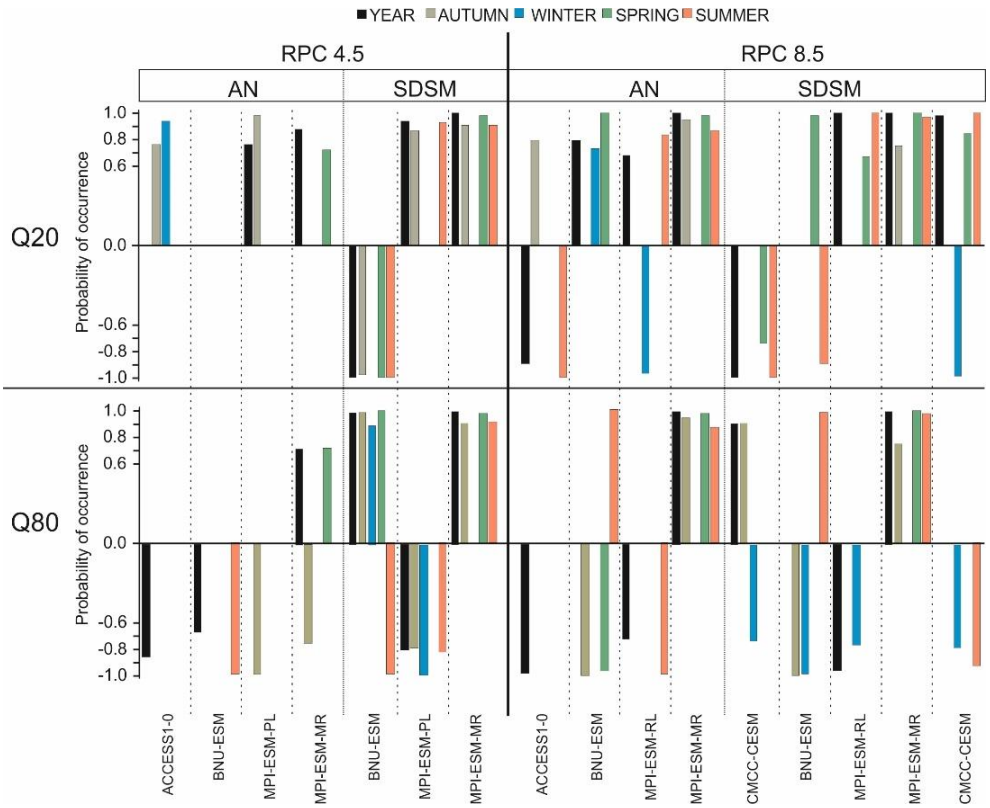

Figure 4.15. *Trends for low flow (Q20) duration and high flow (Q80) duration displayed at annual and seasonal scales for the 2011–2100 period. The projections under Representative Concentration Pathway 4.5 (RCP 4.5) and 8.5 (RCP 8.5) are displayed separately. Only values with a probability of occurrence higher than 0.66 are shown.*

OBS_SIM displays decreasing annual and seasonal trends for high flow duration (above Q80, between 1961 and 2000, baseline). Annually, the decreasing trend is "extremely probable", on summer is “very probable” and in autumn, winter and spring is “probable” (Table 4.8). In general, the high flow durations obtained using climate baselines, do not show significant trends. However, the most significant trends are for the model BNU-ESM showing “very probable” to “virtually certain” decreasing trends annually and for autumn.

The high flow duration (Q80) for future projections (2011-2100) show significant trends annually and in autumn, however, there are as many increasing as decreasing trends (Fig. 4.15). In spring there are few projections with significant trends being most of them increasing. In winter under RCP 8.5 there is a general

decreasing trend. In summer a change in general trend can be observed form RCP 4.5 to RCP 8.5: under RCP 4.5 decreasing trends prevail, while under RCP 8.5 are mostly increasing.

Understanding the lower part of the projected hydrographs is essential for an assessment of impact on freshwater ecosystems. Therefore, besides knowing the trend of the number of days with high (>Q80) and low (<Q20) flows, it is also important to know the volumetric deficit (severity) trend, especially for low flows. The OBS_SIM (1961-2000) low flow deficit does not display any significant trend. Most of the baselines do not show significant trends, nevertheless, the few of them where trend is detected, predict an increase in severity.

For 2011-2100 there are significant trends in most of the projected simulations for severity. However, these trends are opposite from each other and cannot be related to the use of given GCMs, downscaling methods or RCP scenarios. As a consequence, severity showed very high uncertainty in future hydrologic projection in the Goi-Nerbioi catchment.

4.3.9 Discussion and conclusions

In this study, to assess future climate change effects (up to year 2100) on the hydrological response of the Goi-Nerbioi catchment, climate projections from ENSEMBLES and CMIP5 were used. The bias-corrected climate projections were used to perform a hydrological simulation using the SWAT code. Before performing hydrological projections SWAT was calibrated and validated achieving satisfactory results (1996-2013, Table 4.4).

ENSEMBLES

11 climatic projections combining four GCM (EGMAM, EGMAM2, MPEH5, HADGEM2) two downscaling methods (AEMET analogues -AN- and Statistical Downscaling Method -SDSM-) and three greenhouse gases emission scenarios (A1B, A2 and B1) have been applied to the Goi-Nerbioi catchment.

There is a considerable difference between the climatic projections baselines (1961-2000) and the measured meteorological data (models simulate generally less precipitation, especially in summer and autumn), making it necessary to

apply a bias correction. In this research, a linear-scaling approach (Lenderink et al., 2007) was used to correct the bias and to prevent it being propagating in the future climate and derived hydrological projections. The discharge results obtained from the simulation with these projections are always lower than the observed, with the EGMAM2_AN being the projection that best fits on yearly basis (-29%); the biggest differences are for summer and autumn and the smallest ones are for winter. These differences have been taken into account for the discharge projections in the future scenarios.

As regards the hydrological impact of future climate scenarios (2030s for 2011-2039, 2060s for 2041-2069, 2090s for 2071-2099), most of the projections show that the discharge will decrease in all the seasons and therefore also annually, with the clearest decrease being in the last horizon. Compared with the reference period (1961-2000) summer is the season that displays the larggest decrease, even for the models (MPEH5_AN_B1, EGMAM_AN_A2) that predict an increase in annual discharge (associated with an increase in winter and spring). As far as downscaling is concerned, the SDSM method always projects less discharge than the AN method. For the combination of the 11 hydrological projections analysed in the three horizons, the wider range between the monthly highest and lowest discharge values will occur in winter and autumn and the narrower one is in summer.

The analysis performed with the low (<Q20) and high flows (>Q80) shows more trends for low flows than for high flows (2011-2099). In short term (2011-2039, 2011-2069) the low flow duration will increase annually and in summer and possibly in autumn. Nevertheless, when all the century is considered (2011-2099), there are more uncertainties due to the aleatoriety of the significant trends. The most generalized trend is the increasing trend in spring. For high flow (>Q80) duration it is more difficult to obtain homogeneous trends because the sign for the trends is more random. However, for 2011-2069 the decreasing trends are predominant. Considering the period from 2011 to 2099 the most homogeneous trends are the autumn and spring decreasing trends.

Considering the low flow (<Q20) severity, the half of the projections have significant trend, therefore their sign is different so it is not possible to obtain clear conclusions.

CMIP5

In the next part of the research, 16 climate projections combining five GCMs (ACCESS1-0, BNU-ESM, MPI-ESM-RL, MPI-ESM-MR, CMCC-CESM), two downscaling methods (AEMET analogues -AN- and Statistical Downscaling Method -SDSM-) and two Representative Concentration Pathways (RCP 4.5 and RCP 8.5) were considered to assess future climate effects (to 2100) on the hydrological response of the Goi-Nerbioi catchment.

There is a considerable difference between the baselines of the climate models (1961-2000) and the observed meteorological data (the models generally simulate less precipitation, especially in spring and summer), therefore, as with ENSEMBLES, a bias correction was applied to the climate projections. The discharge results obtained from the simulation carried out with these bias-corrected projections were compared with the discharge obtained from a simulation made with the observed meteorological data (OBS_SIM; 1961-2000). The comparison shows that the GCMs downscaled with the SDSM method achieve a better adjustment than those downscaled with the AEMET analogues (AN); nevertheless, they all underestimate the discharge amount. The greatest differences occur in summer and spring when the baselines of all the projections are lower than those observed (-77% and -34% respectively). In autumn and winter the projections downscaled using the SDSM method have a difference of less than -10%. These differences between SDSM and AN clearly show that in this case the influence of the downscaling methods is higher than that of the GCM.

Comparing the differences in discharge between projection baselines (1961-2000) and future projections (2030s for 2011-2040, 2060s for 2041-2070, 2090s for 2071-2100), four of the analysed GCMs (ACCESS1-0, BNU-ESM, MPI-ESM-RL and MPI-ESM-MR) show a similar trend; the discharge decreases with respect to the baseline at annual and seasonal scales and this decrease is higher

throughout the century. In addition, the projections with RCP 4.5 from the 2060s to 2090s become stable, while there is an important decrease for the projections with RCP 8.5. As far as downscaling is concerned, on an annual scale the differences between AN and SDSM are small but they become significant when the analysis is performed at a seasonal scale. The greatest differences occur in summer when the projections downscaled with the AN method project around 5% more discharge for the 2090s whereas SDSM projects 15-25% less. Considering the differences between baselines and future hydrological projections, and taking into account all the projections, autumn is the season that displays the largest decrease (-17% for 2090s) followed by spring (-16% for 2090s).

For the ensemble of the 16 hydrological projections analysed in the three horizons, the widest range between the monthly highest and lowest discharge values will occur in winter and autumn (around 2.9-5.6 $m^3 s^{-1}$) followed by spring (between 1-2.1 $m^3 s^{-1}$) while the narrowest one is in summer (between 0.1-0.3 $m^3 s^{-1}$). An understanding of the temporal evolution of discharges in the lower part of the hydrograph is essential for a projection of impacts on freshwater ecosystems. For spring, summer and the beginning of autumn, simulated discharge is always below the OBS_SIM. This could be a drawback for the future from an environmental point of view and considering the need to meet the objectives established by the Water Framework Directive (WFD).

The analyses performed with low (<Q20 percentile) and high flows (>Q80 percentile) show more homogeneous trends for projections with RCP 8.5. Most show a yearly downward trend in high flow duration (days), especially during autumn, winter and spring. For low flow duration the yearly general trend is not clear but in autumn and spring it is possible to see a homogeneous increasing trend. The sign of the severity (volume deficit in the discharge below Q20, in annual scale) varies randomly according to the projections, and it is therefore not possible to obtain a clear conclusion. Focusing on the uncertainties of the results, the analysis for high flows (duration) and low flows (duration and severity) show that the results are more conclusive for high flows and there is therefore less uncertainty in this part of the hydrograph.

GENERAL CONCLUSIONS

In this work, different generations of climate models were used to analyse the possible impacts of climate change in the water resources of Goi-Nerbioi catchment. On the one hand, the climate models of AR3 (IPCC, 2001) and AR4 (IPCC, 2007) were regionalized for Europe in the ENSEMBLES project and then AEMET did a statistical downscaling to the outputs of the regionalized climate projections. On the other hand, the last generation of climate models (AR5; IPCC, 2013) of CMIP5 was used with the same aim: evaluate the future water resources of Goi-Nerbioi catchment considering that due to the climate change the precipitation and temperature of the zone will change. The climate outputs of the models of CMIP5, as well as the ENSEMBLES project, were downscaled by AEMET statistically, but these data were not previously regionalized.

It should be taken into account that when considering hydrologic projections several different sources of uncertainties are involved in the simulation (GCM, downscaling method, RCP or emission scenario). However, these lie outside the scope of this study. Nevertheless, the fact that different global climate modelling projects (ENSEMBLES and CMIP5) have been used in this research allows to make a comparison between their results and to observe where are the greatest uncertainties.

The ENSEMBLES baseline (1961-2000) climate projections show lower difference in precipitation than the outputs of CMIP5. In general terms, considering all the projections used in this research, the baseline precipitation of ENSEMBLES models project -9 % less precipitation than the observed, while for CMIP5 the projected precipitation is -38 % lower. In addition, the CMIP5 projections show strong influence of the statistical downscaling method because the projections with AN always show higher differences from the measured precipitation and yearly they show differences from -40 % to -60 %. Considering the temperature, ENSEMBLES simulate around 9 % more temperature in annual base and CMIP5 around 3.5 % more. Therefore, the regionalization of the GCMs makes it possible to obtain baseline precipitation projections more similar to the observed, but the new generation of GCMs achieve better adjustment to the

observed temperature. The baseline discharge projections obtained introducing the bias-corrected climate projections in the hydrological code (SWAT) always project less discharge than the performed with the observed meteorological data (OBS_SIM). In addition, when all the hydrological projections (mean value) are considered, the difference with the OBS_SIM is similar for the ENSEMBLES and CMIP5 projections. Thus, they simulate around -20 % less discharge annually, -15 % in autumn, -35 % in spring, -75 % in summer and -10 % in winter. Furthermore, in both cases (ENSEMBLES and CMIP5) the hydrological projections with SDSM statistical downscaling show less difference with the OBS_SIM. Therefore, the results show that when the ensembles of hydrological projections is considered, the statistical downscaling is a higher source of uncertainty than the climate model generation.

The future hydrological projections from ENSEMBLES and CMIP5 climatic modelling projects (except for the projections of CMCC_CESM GCM) show an annual discharge decrease that it is higher throughout the century. Seasonally, the projections from ENSEMBLES indicate that the greater decreases may occur in summer while for CMIP5 are in autumn. In both cases winter is the season that projects less discharge decreases. In any case, the climate projections with SDSM statistical downscaling always project greater decreases respect the baseline than the downscaled with AN method.

For the end of the century (2090s) the annual and seasonal projections from ENSEMBLES show considerably more discharge decrease than CMIP5. Considering the ensembles of the mean monthly discharge (Figs. 4.9 and 4.14) the possible discharge range is higher for the projections from ENSEMBLES, therefore, the uncertainty is higher. Both model generations have in common that the summer projections are always lower than the OBS_SIM.

From the low flow (<Q20) duration obtained from the hydrological projections of ENSEMBLES, is possible to conclude that in short term and medium (2011-2039, 2011-2069) the low flow duration will increase annually and in summer and possibly in autumn. Some of the projections from CMIP5 show significant trends in short term, nevertheless is not possible to obtain general patterns. Considering

all the century the projections from ENSEMBLES show homogeneous increasing trends in spring while for CMIP5 the upward homogeneous trends are in spring and autumn.

The high flow duration (>Q80) for ENSEMBLES and CMIP5 are more uncertain than low flow because although there are many significant trends in the projections, their sign is random. The projections from ENSEMBLES display decreasing trends in winter and autumn and it is more difficult to obtain clear conclusions for CMIP5.

Considering the severity, there are only a few projections from ENSEMBLES with significant trend. For CMIP5 most of the projected simulations have a significant trend however they have opposite sign showing a high uncertainty.

The results obtained in this study show the need to consider a wide range of climate projections as well as evaluating the hydrological projections obtained beyond the most common annual mean discharges. Focusing on the seasonal variation of discharge enabled an approximation to future distribution of freshwater resources. This approximation, together with the consideration of the extremes of the hydrograph in the analysis will allow for better planning of future measures in terms of water quantity and quality in catchments of the Atlantic region (Bay of Biscay).

4.4 EVALUACIÓN DE LOS IMPACTOS DEL CAMBIO CLIMÁTICO EN LOS RECURSOS HÍDRICOS DE LA CUENCA DEL ZADORRA

4.4.1 Introducción

Esta investigación se ha llevado a cabo dentro del projecto EGHILUR (Zabaleta et al., 2017) de la convocatoria KLIMATEK, que tiene por objeto promover la realización de proyectos que contribuyan decididamente a asegurar la resiliencia del territorio vasco al cambio climático.

El área de estudio se centra en dos sub-cuencas de cabecera de la cuenca del Zadorra: Otxandio y Audikana. Esta cuenca se sitúa en la vertiente mediterránea

del País Vasco y ambas sub-cuencas, tienen características considerablemente diferentes; Otxandio es una sub-cuenca de cabecera de importantes pendiente en la que predomina el bosque, es bastante húmeda (clima atlántico) y el caudal medio anual es de 1.47 m^3 s^{-1} (1985-2015). Audikana es una sub-cuenca de cabecera mucho más llana en la que predomina el cultivo de cereal y es más árida (clima sub-meditarráneo) con un caudal medio diario de 1.20 m^3 s^{-1} (1985-2015).

El objetivo de este estudio se centra en evaluar los efectos del cambio climático en los recursos hídricos de ambas sub-cuencas. Para ello, se ha utilizado la misma metodología y el mismo código hidrológico (SWAT) que en las cuencas estudiadas con anterioridad. Las proyecciones climáticas que a posteriori se han introducido en el modelo SWAT han sido las del CMIP5, sin embargo, en esta ocasión, el estudio se ha centrado en caudales medios (Qm) y bajos (Q20). Además, también se ha realizado una aproximación a la evaluación del efecto del uso del suelo en los recursos hídricos.

4.4.2 Área de estudio

El río Zadorra es tributario del Ebro y su curso transcurre desde su nacimiento en las estribaciones de Sierra de Entzia (Araba) hasta su desembocadura al Ebro en Zambrana (Araba). La cuenca del Zadorra (Fig. 4.16) tiene una extensión de 1365 km^2 y la altitud varía entre 452 y 1548 m. Se sitúa inmediatamente al sur de la línea que conforma la divisoria cantábrico-mediterránea y constituye la zona más occidental de la denominada “Llanada Alavesa”, caracterizada por un corredor de suaves morfologías en dirección E-W y atravesado por el río Zadorra y sus afluentes. Los usos del suelo mayoritarios son el agrícola (tierras de labor en secano, 37 %) y el forestal (bosques de frondosas, 26 %).

La cuenca del Zadorra muestra una importante variabilidad en la precipitación, así, en las zonas de mayor altitud puede variar de 900 a 1500 mm anuales, mientras que en las zonas bajas varía de 500 a 700 mm. Respecto a la temperatura, en las zonas más altas las temperaturas medias anuales son de unos 8-10 ºC, y las zonas bajas rondan los 11-13 ºC (1940-1990; Plan Hidrológico del Ebro, 1995). Este estudio, concretamente, está enfocado a las sub-cuencas

de Otxandio y Audikana (Fig. 4.16), de una extensión aproximada de 36 y 82 km^2, respectivamente, cuencas de cabecera de los embalses Urrunaga y Ulibarri-Ganboa.

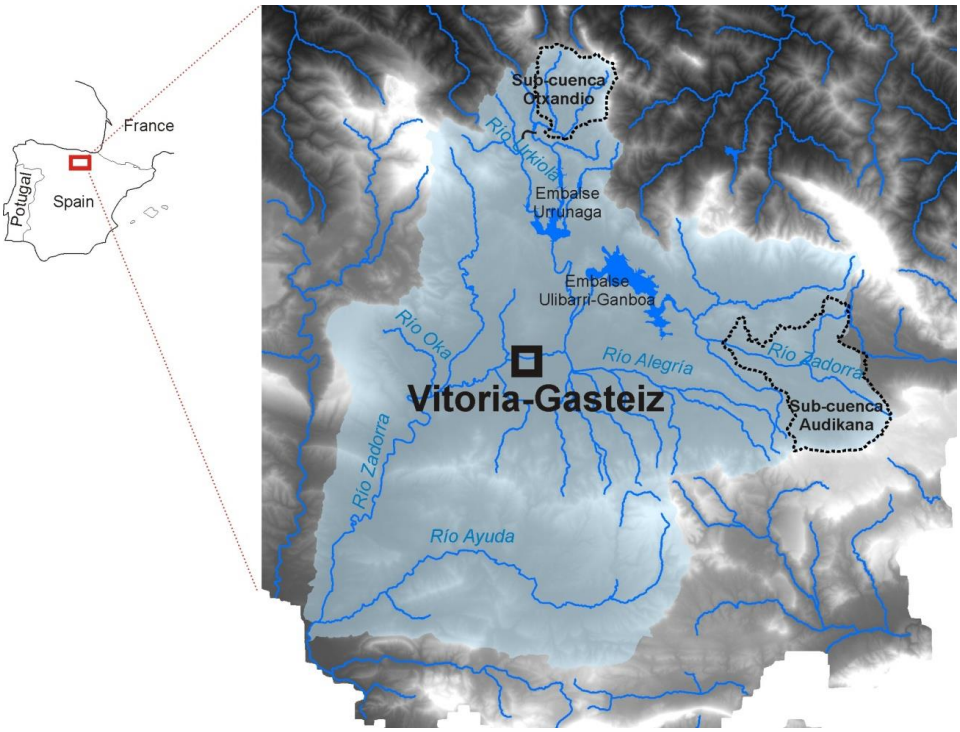

Figura 4.16. *Localización de las sub-cuencas de Otxandio y Audikana en la cuenca del río Zadorra.*

4.4.3 Caracterización física del medio y datos de entrada del modelo hidrológico

La primera etapa en la discretización espacial del modelo consiste en representar la red de drenaje y delimitar tanto la cuenca principal como las sub-cuencas. La delimitación de todos estos aspectos se basa en el Mapa Digital de Elevaciones (MDE). El **MDE** se ha obtenido de datos LIDAR (resolución 5x5 m) descargados de la página web www.geo.euskadi.eus. El presente modelo abarca toda la cuenca del Zadorra hasta su desembocadura en el Ebro (estación de Artze) y consta de un total de 69 sub-cuencas. De ellas, en este trabajo se han considerado las correspondientes a la sub-cuenca de Otxandio (35.7 km^2, sub-cuenca 1 del modelo) y a la de Audikana (81.5 km^2, sub-cuencas 22, 24, 25, 26

y 31 del modelo). El projecto considera toda la cuenca del Zadorra porque en el futuro se procederá a la modelización de toda la cuenca.

Una vez creadas las sub-cuencas, SWAT combina el mapa de suelos, el de usos de suelo y el de pendientes y divide la cuenca en diferentes Unidades de Respuesta Hidrológica (HRU), que representan la discretización de menor tamaño considerada por el código SWAT. En este caso, el modelo se compone de 317 HRUs.

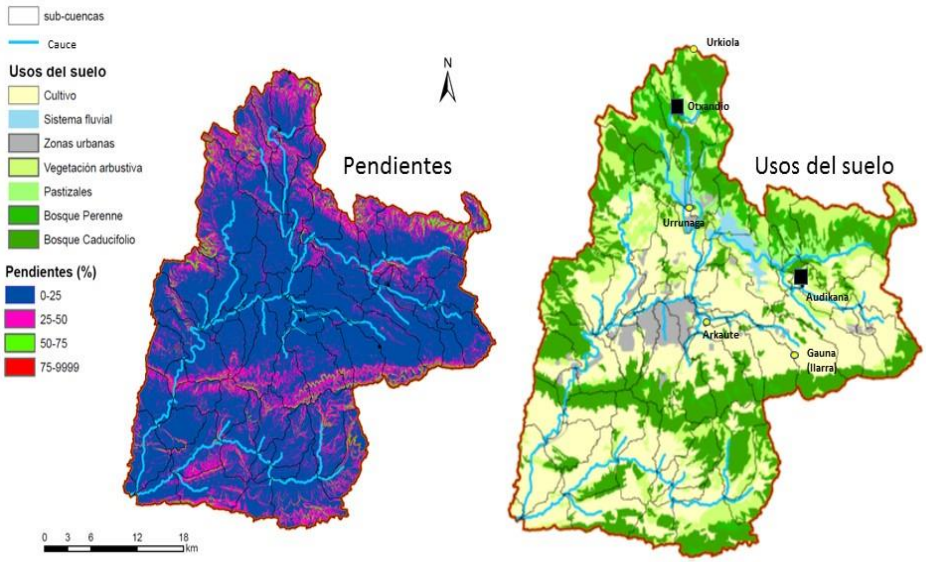

Figura 4.17. *Mapas de pendientes y de usos del suelo de la cuenca del Zadorra. En el mapa de usos se han ubicado las estaciones de aforo y estaciones meteorológicas utilizadas en la modelización.*

SWAT genera el mapa de pendientes a partir del MDE (Fig.4.17). Por su parte, el mapa de **usos del suelo** se ha obtenido del programa de la Unión Europea CORINE (https://www.eea.europa.eu/publications/COR0-landcover)que ofrece una cartografía a escala 1:100.000 que divide la mayor parte de la geografía europea en 44 usos del suelo. El siguiente paso es generar una relación entre los usos del suelo del CORINE y los de la base de datos del SWAT; así, se ha divido la cuenca del Zadorra en 5 usos del suelo mayoritarios (Fig. 4.17). Cabe destacar que SWAT, al ser en su origen un modelo desarrollado para utilizar en cuencas agrícolas, posee una amplia base de datos con usos del suelo y de parámetros relacionados con éstos.

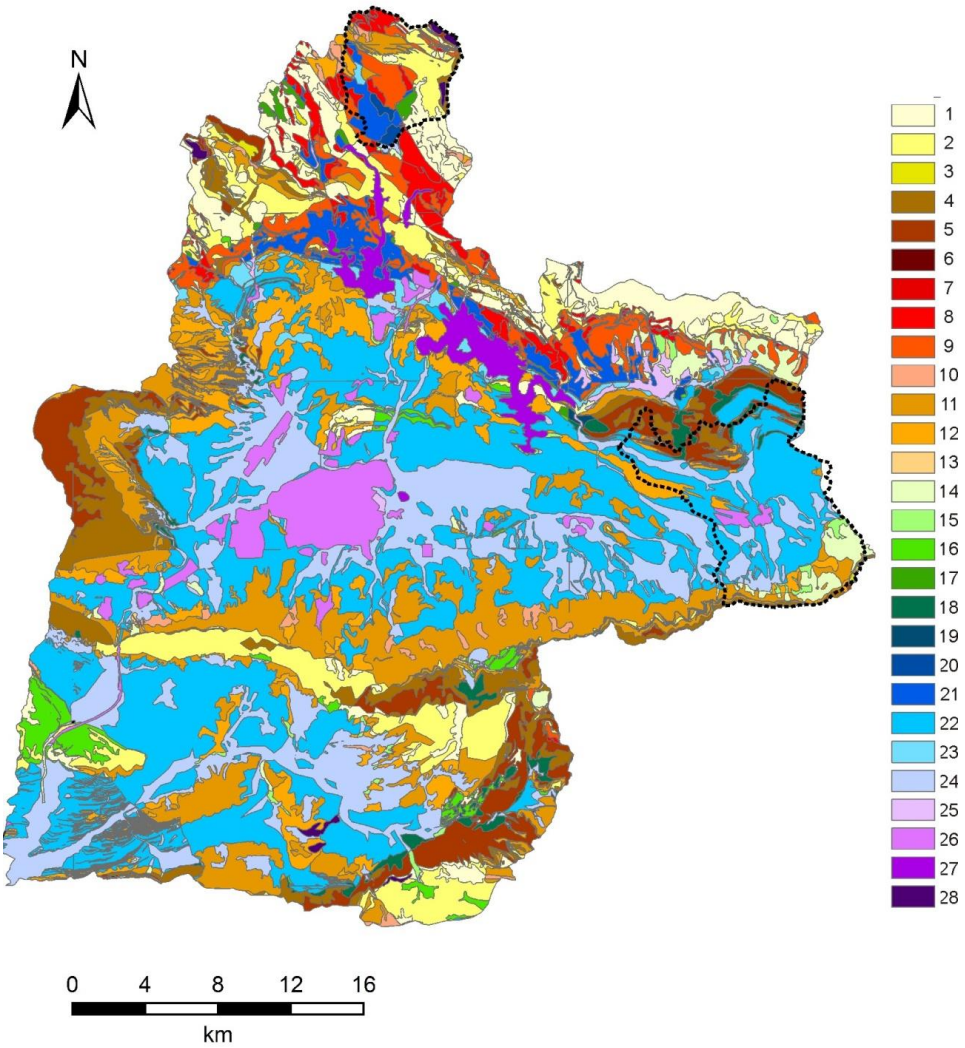

Figura 4.18. *Mapa de suelos de la cuenca del río Zadorra, elaborado mediante la combinación de la litología y la vegetación. Ver tabla 4.9.*

En cuanto al mapa de **suelos** se refiere, debido a la falta de datos, se ha optado por emplear un mapa de suelos elaborado a través de la metodología empleada durante el estudio de la erosión hídrica laminar (Gobierno Vasco, 2005) (Fig. 4.18). De acuerdo con esta metodología, en función de la combinación entre el uso de suelo y la litología se establecen algunos datos físicos de los suelos, como por ejemplo la materia orgánica y la fracción de arcilla, limo y arena. Además de estos parámetros, SWAT necesita otros, como el agua disponible para las plantas (Available Water Content, AWC) y la conductividad hidráulica

(Ks), que se pueden obtener mediante la combinación de la textura y el porcentaje de materia orgánica. En este caso, para el cálculo de dichos parámetros, se ha utilizado el programa de cálculo de propiedades hidráulicas SWC (Soil Water Caracteristics;) (Tabla 4.9). La elección de esta metodología a la hora de establecer las características del suelo facilitará, en cierta medida, que el cambio de las propiedades del suelo al simular los caudales resultantes de cambios en los usos del suelo, se realice con cierta objetividad (no exenta de incertidumbre), y, por lo tanto, los resultados mantengan una misma coherencia (Apartado *4.4.5 Evaluación de la influencia del uso del suelo en los recursos hídricos*).

El modelo requiere que se introduzcan diferentes variables de entrada. Estas son las que establecen el flujo de entrada de agua y energía al sistema modelizado. Considerando la información existente en las estaciones meteorológicas de la zona de estudio, generalmente precipitación y en algunos casos temperatura, se optó por emplear un método que estime la evapotranspiración potencial basado en estas dos variables. Es la selección de este método, Hargreaves en este caso, el factor que limita el tipo de variable de entrada necesario.

Otro aspecto de gran importancia es la selección de las estaciones meteorológicas a considerar por el modelo. En la zona existen diversas estaciones gestionadas tanto por Euskalmet como por AEMET, no obstante, las de Euskalmet han sido descartadas puesto que su puesta en marcha es demasiado reciente (generalmente a partir del año 2000). En cuanto a las de AEMET se refiere, en la zona de estudio existen varias estaciones meteorológicas (Tabla 4.10), pero no todas están en funcionamiento actualmente. En concreto, la de mayor interés es la estación de Urrunaga presa-9080 (en adelante, Urrunaga), puesto que, de todas las estaciones consideradas en la tabla, únicamente para ésta ha elaborado AEMET proyecciones climatológicas, que son las que van a ser empleadas en este estudio. No obstante, la estación no está operativa en la actualidad y, a pesar de que el registro abarque el periodo 1943-2002, aquellos datos registrados durante los últimos 4 años presentan una gran incertidumbre y, además, el registro no es completo.

ID	Litología	Uso	Limo	Arcilla	Arena	Materia orgánica	AWC	Ks	BD
			(%)	(%)	(%)	(%)	(cm^3/cm^3)	(mm/h)	(g/cm^3)
1	Areniscas	Pino albar	24.2	16.9	58.9	8.95	0.14	50.57	1.12
2	Areniscas	Frondosa	25.5	20	54.5	6,025	0.13	30.32	1.26
3	Caliza	Pino albar	16.7	15.8	67.5	7.89	0.12	51.74	1.17
4	Caliza	Frondosa	41.7	23.1	35.2	0.94	0.14	7.57	1.52
5	Caliza	Pasto	30.2	27.2	42.6	9.88	0.15	23.28	1.14
6	Lutitas	Pino albar	25.9	29.2	44.9	8.95	0.14	17.97	1.18
7	Lutitas	Frondosa	46	27	27	5.12	0.17	16.51	1.23
8	Lutitas	Pasto	25.9	29.2	44.9	8.48	0.14	17.97	1.18
9	Lutitas y areniscas	Pino albar	32.8	24	43.2	8.95	0.16	31.13	1.11
10	Marga	Pino albar	21.6	11.6	66.8	10.24	0.13	77.21	1.09
11	Marga	Frondosa	41	32	27	4.4	0.15	8.75	1.3
12	Marga	Pasto	32.2	14.2	53.6	8.48	0.15	67.59	1.05
13	Mixta	Pino albar	26.2	19.8	54	8.95	0.14	39.59	1.13
14	Mixta	Frondosa	19.6	19.8	60.6	0.55	0.09	15.79	1.57
15	Mixta	Pasto	17.6	38.4	44	6.05	0.12	4.17	1.34
16	Areniscas	Cereal	26.6	21.4	52	4.03	0.13	20.63	1.38
17	Areniscas	Prado cultivo	17.8	21.4	60.8	6.41	0.12	27.83	1.28
18	Caliza	Cereal	22.8	20.2	57	6.72	0.13	32.83	1.23
19	Caliza	Prado cultivo	35.6	20.4	44	8.22	0.16	43.77	1.07
20	Lutitas y areniscas	Cereal	14.7	27.7	57.6	3.96	0.11	9.43	1.43
21	Lutitas y areniscas	Prado cultivo	24.8	21.4	53.8	7.4	0.14	33.25	1.18
22	Marga	Cereal	19.8	33.6	46.6	4.55	0.12	5.46	1.38
23	Marga	Prado cultivo	28.4	28	43.6	7.24	0.14	18.17	1.2
24	Mixta	Cereal	20.7	24	55.3	4.24	0.12	15.72	1.39
25	Mixta	Prado cultivo	18	22.8	59.2	3.98	0.11	16.99	1.41
26	Mixta	Cultivo	32.5	32.9	34.6	3.5	0.12	16.99	1.41
27	Superficie artificial	artificial	32.5	32.9	34.6	3.5	0.12	16.99	1.41
28	Zonas húmedas	húmedas	32.5	32.9	34.6	3.5	0.12	16.99	1.41

Tabla 4.9. *Identificación de los suelos de la cuenca del Zadorra. De la combinación de la litología y los usos del suelo se obtienen los distintos tipos de suelo (ID): Los porcentajes de limo, arcilla, arena y materia orgánica se han obtenido del programa elaborado para la creación del Mapa de erosión de suelos de la Comunidad Autónoma de Euskadi (Gobierno Vasco, 2005), mientras que los valores del agua utilizable por las plantas (AWC), la conductividad hidráulica (Ks) y la densidad aparente (BD) se han calculado introduciendo la textura y la materia orgánica en el programa SWC (Soil Water Caracteristics).*

Lo ideal sería emplear los datos meteorológicos, en este caso temperatura y precipitación, de una misma estación tanto para alimentar el modelo durante las fases de calibración y validación del mismo, como durante la fase de aplicación de los escenarios climáticos (o de usos del suelo) que se quieran considerar. En cualquier caso, debe adoptarse una estrategia que permita elaborar las series meteorológicas necesarias durante ambas fases. Fundamentalmente existen dos opciones: por un lado, emplear las series meteorológicas de una estación para alimentar el modelo (para calibrarlo y validarlo) y las de otra estación para

representar las proyecciones climáticas, y, por otro, estudiar las relaciones entre las distintas estaciones y obtener, mediante análisis de correlación, series representativas de la estación de interés.

Estación	Indicativo	Coordenada X	Coordenada Y	Altitud Z	Funciona en la actualidad	Proyecciones climatológicas	Variables disponibles
Albina (Embalse)	9078	530186	4760134	600	Sí	No	Precip.
Gauna (La Ilarra)	9082T	540760	4742305	599	Sí	No	Precip.
Escalmendi	9084U	529288	4747606	515	Sí	No	Precip. & temp.
Arkaute	9086	530662	4744557	515	Sí	No	Precip. & temp.
Urrunaga presa	9080	528481	4756333	540	No	Sí	Precip. & temp.

Tabla 4.10. *Estaciones de AEMET cercanas a la zona de estudio.*

Dado que las de la estación de Urrunaga son las únicas proyecciones climáticas existentes en la zona y teniendo en cuenta la incertidumbre de los datos de los últimos 4 años de registro (1999-2002) en esta estación, así como la ausencia de datos a partir del año 2002, para poder utilizar las series climáticas de Urrunaga en las dos fases mencionadas, se estima necesario completar las series de precipitación y temperatura (máxima y mínima) de forma que abarquen el periodo considerado para la calibración y la validación del modelo. Sin embargo, la zona de estudio presenta una importante variabilidad de precipitación; por ejemplo, la precipitación media anual registrada en la estación de Otxandio entre 2005 y 2015 fue de 1479 mm, mientras que para el mismo periodo en Urkiola (aprox. 2 km al NW) se registraron 1928 mm y 932 mm en Urrunaga (aprox. 9 km al S) (Fig. 4.17). Además, las relaciones existentes entre las variables meteorológicas de distintas estaciones no son buenas, por lo que se optó por no completar la serie de Urrunaga, desechando esta opción.

Así, la primera fase, la calibración y validación del modelo, se ha realizado con datos meteorológicos de las propias sub-cuencas de Otxandio y Audikana. Y, para la segunda fase, aplicación de escenarios, tal y como se explicó en el capítulo *2. Methodology*, sección *2.3 Bias correction*, se ha realizado una corrección de sesgo de las variables meteorológicas para poder utilizar en Otxandio y en Audikana las proyecciones climáticas existentes para Urrunaga. En la Tabla 4.11 se observan las estaciones meteorológicas de las cuales se han obtenido los datos empleados en la calibración y la validación del modelo.

Estación	Indicativo	Coordenada X	Coordenada Y	Altitud Z	Funciona en la actualidad	Proyecciones climatológicas	Variables disponibles
Gauna (La Ilarra)	9082T	540760	4742305	599	Sí	No	Precip.
Urkiola	1069E	529229	4771861	737	Sí	No	Precip.
Arkaute	9086	530662	4744557	515	Sí	No	Temp.
Otxandio	C054	528001	4765557	556	No	Sí	Precip. & temp.

Tabla 4.11. *Estaciones meteorológicas utilizadas en la calibración y en la validación del modelo.*

4.4.4 Calibración, validación y evaluación de la modelización hidrológica

Con el fin de calibrar el modelo, se han utilizado los datos de caudal diario ($m^3 s^{-1}$) de las estaciones de aforo de Otxandio (H153) y Audikana (H152), propiedad de Iberdrola, para calibrar las sub-cuencas de Otxandio y Audikana, respectivamente. Por supuesto, para que la calibración sea satisfactoria la calidad de los datos observados ha de ser buena. En este sentido, es necesario mencionar que, tal y como se expondrá a continuación, los datos registrados muestran incertidumbres.

Estación meteorológica (C054 Euskalmet) y de aforo de Otxandio (H153):

Es sospechoso que el caudal registrado en la estación de Otxandio entre 1985 y 2015 sea mayor que la precipitación registrada en la misma. Además, la diferencia entre ambas variables va aumentando de forma gradual, puesto que el caudal registrado aumenta con el tiempo, aunque sin una tendencia clara que permita corregir los datos de una manera más o menos sencilla. Consideramos que ello es debido al progresivo deterioro que ha sufrido el cauce de la estación de aforo, que con el paso del tiempo se colmata de sedimentos y vegetación. En la Foto 4.1 se observa el estado del cauce de la estación de aforo. No obstante, se realizaron algunos intentos de corregir la serie de caudales, los cuales no dieron resultados satisfactorios.

Además, es necesario tener en cuenta el alto gradiente de precipitación existente en la cuenca y que la estación de Otxandio se encuentra en la zona de menor precipitación dentro de ese gradiente. Por ello, se consideró más correcto utilizar la estación meteorológica de Urkiola (Iberdrola), que estando dentro de la cuenca, se ubica en una zona con precipitaciones considerablemente mayores que las de Otxandio (en el periodo 2005-2015 la precipitación media anual fue

460 mm mayor en Urkiola), quedando mejor reflejadas las precipitaciones en la cuenca.

Foto 4.1. *Estación de aforo de Otxandio, sin fecha conocida (Fuente: Iberdrola).*

Estación de aforo de Audikana (H152):

La forma del hidrograma de esta estación (Fig. 4.19) refleja la incertidumbre existente en los caudales bajos. Como se puede apreciar, en ocasiones el caudal desciende de forma significativa y muestra formas anómalas en el hidrograma (ej. verano de 2003). En diciembre de 2011 la Agencia Vasca del Agua URA comenzó a medir el nivel de agua en una sección del río cercana a la estación de Audikana. Con estos datos, y con los valores de la curva de gastos, se ha estimado el caudal (Fig. 4.19). En verano de 2012, según los datos recogidos en la estación de Audikana, el nivel desciende de forma que el cauce prácticamente se queda seco, sin embargo, los datos de URA muestran que, aunque el descenso es considerable, no es tan extremo. Por otro lado, en general, los datos de URA muestran picos de caudal más altos que los registrados en la estación de Audikana, por lo que también podría existir incertidumbre en los caudales altos. Además, también se en ocasiones las lluvias registradas en la estación meteorológica de Gauna no generan crecidas en Audikana, o su magnitud no es la esperada, y viceversa.

La ejecución del modelo en ambas cuencas se realizó a escala diaria. Se utilizó el periodo 1987-1994 para la calibración y el 2005-2015 para la validación. La interrupción entre los dos periodos es debida a que no hay datos de precipitación de Urkiola entre 1994 y 2005. En cualquier caso, los 18 años de simulación garantizan que existan años húmedos, secos e intermedios, por lo

que la calibración y la validación abarcan todo tipo de condiciones hidro-meteorológicas. Se optó por utilizar los mismos periodos en las dos sub-cuencas para facilitar el procedimiento.

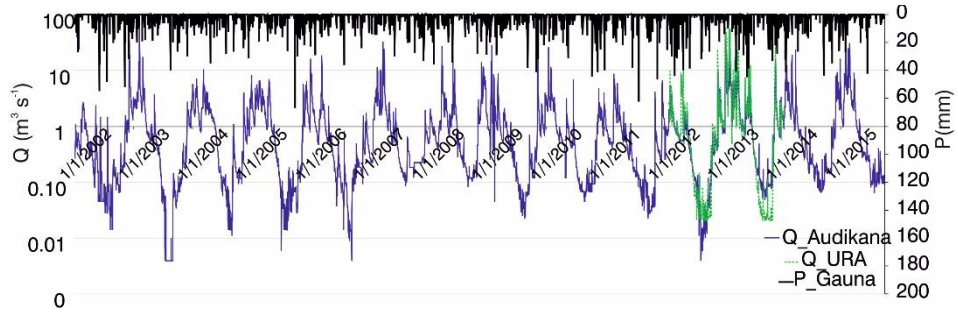

Figura 4.19. *Hidrograma (m^3s^{-1}) de la estación de aforo de Audikana e hidrograma obtenido de los datos de nivel medidos por URA. En la parte superior la precipitación registrada en la estación de Gauna (mm).*

El primer paso en la calibración fue identificar los parámetros más sensibles para el caudal de cada sub-cuenca. Se utilizó el programa de autocalibración SWAT CUP (Abbaspour et al., 2007) para calcular los parámetros más sensibles mediante el método "one at a time" (van Griensven et al., 2006). Este método consiste en evaluar la sensibilidad de cada parámetro mientras el resto se mantienen constantes. Los dos parámetros más sensibles en ambas cuencas son el curve number (CN2), o número de curva, que calcula el valor de la escorrentía superficial y el baseflow alpha factor (Alpha_BF) o constante de recesión. Posteriormente, se realizó una primera calibración manual para ajustar un rango realista para cada uno de los parámetros, y, por último, para concretar los valores óptimos de los parámetros, los rangos establecidos en la calibración manual se introdujeron en el programa SWAT CUP para realizar una autocalibración utilizando el algoritmo SUFI2 (Abbaspour et al., 2004, 2007).

El análisis de los resultados del modelo, tanto en el proceso de calibración como en el de validación, se ha llevado a cabo siguiendo la metodología propuesta por Moriasi et al., 2007. Se han utilizado en todo momento técnicas gráficas que aportan una comparación visual entre los datos simulados y medidos además de una primera perspectiva sobre el funcionamiento del modelo (ASCE, 1993). También se han calculado distintos parámetros estadísticos con el fin de

comprobar la buena correlación entre los datos observados y simulados. En el capítulo *2. Methodology*, apartado *2.4.7. Modelling process and evaluation methods* se explica con más detenimiento todo el proceso de evaluación.

Según Moriasi et al., 2007, se puede dar por satisfactoria una simulación de caudal cuando el índice NSE > 0.5, RSR ≤ 0.7, y PBIAS < 25%. Sin embargo, no se ha considerado la importancia de todos los parámetros por igual. Por ejemplo, los valores altos influyen más en los estadísticos NSE y RSR. Dado que en este estudio se realiza un análisis de caudales bajos y medios, aunque ambos estadísticos se han tenido en cuenta, se ha considerado que tienen menor importancia. Tanto en el proceso de calibración manual como en la autocalibración el parámetro estadístico que se ha tomado como referencia ha sido el PBIAS.

Como el objetivo del estudio es evaluar las afecciones del cambio climático en la hidrología, pero centrándonos sobre todo en los caudales medios (Qm) y bajos (Q20), también se ha realizado un esfuerzo en asegurar que el modelo simula bien las partes bajas del hidrograma. Por un lado, se ha utilizado el programa Base Flow Filter Program-BFP (Arnold et al., 1998) para separar el flujo base de la escorrentía superficial. Así, comparando el flujo base del hidrograma simulado con el observado mediante los métodos estadísticos anteriormente descritos, es posible observar si el modelo simula bien esta parte del hidrograma. Por otro lado, se ha calculado el percentil Q20 y la mediana mensual de los datos simulados y observados y se ha realizado el mismo análisis estadístico. Por último, y teniendo en cuenta que para el norte de la Península Ibérica las proyecciones climáticas futuras a menudo predicen un clima más extremo que el de las últimas décadas (ej. IPCC, 2013), siguiendo la propuesta de Brigode et al. (2013), se eligieron los tres años consecutivos más secos y más húmedos para analizar si el modelo calibrado es capaz de simular correctamente condiciones extremas. Los años más secos y húmedos se seleccionan mediante el cálculo de un "Aridity Index" o índice de aridez (en adelante, AI) para todos los datos disponibles (1987-1994, 2005-2015), siendo AI la relación entre la evapotranspiración potencial y la precipitación (Görgen et al., 2010 Brigode et al., 2013). Los tres años con el AI más bajo son los mismos en ambas sub-

cuencas (2010, 2011 y 2012), mientras que los tres años consecutivos con mayor AI en Audikana son 2007, 2008 y 2009 y en Otxandio son 1991, 1992 y 1993.

4.4.5 Evaluación de la influencia del uso del suelo en los recursos hídricos

El uso del suelo tiene efecto sobre la hidrología por su vinculación con la evapotranspiración (Fohrer et al., 2001), pero también porque afecta a las características de los suelos y a cómo éstos dividen, almacenan y regulan los flujos de agua (Mirus & Loague, 2013). La cuantificación de estos efectos es crucial para muchos problemas ambientales, incluida la predicción de los impactos del cambio climático (Poff et al., 1997).

En este trabajo se realiza una primera aproximación en el estudio de los efectos de los usos del suelo en la hidrología de las sub-cuencas de Otxandio y Audikana. Para ello, se han planteado tres escenarios de cambio posible en cada sub-cuenca teniendo en cuenta factores como la pendiente o los usos de suelo en zonas cercanas. La sub-cuenca de Otxandio es fundamentalmente forestal (Fig. 4.20). Debido a su orografía, en la que aproximadamente la mitad de la sub-cuenca tiene pendientes de entre 25-50 %, no parece probable que en algún momento pudiera predominar el uso del suelo agrícola. Por este motivo, a excepción del primer escenario de cambio de usos del suelo (O1) en el que el 30 % de la cuenca es agrícola (en las zonas de menor pendiente) en los otros dos escenarios (O2 y O3) se plantean distintas posibilidades de cuenca forestal (Fig. 4.20). El uso del suelo en Audikana es mayoritariamente agrícola por lo que se ha optado por aumentar el bosque y la vegetación arbustiva en los distintos escenarios de usos del suelo (Fig. 4.20; A1, A2, A3).

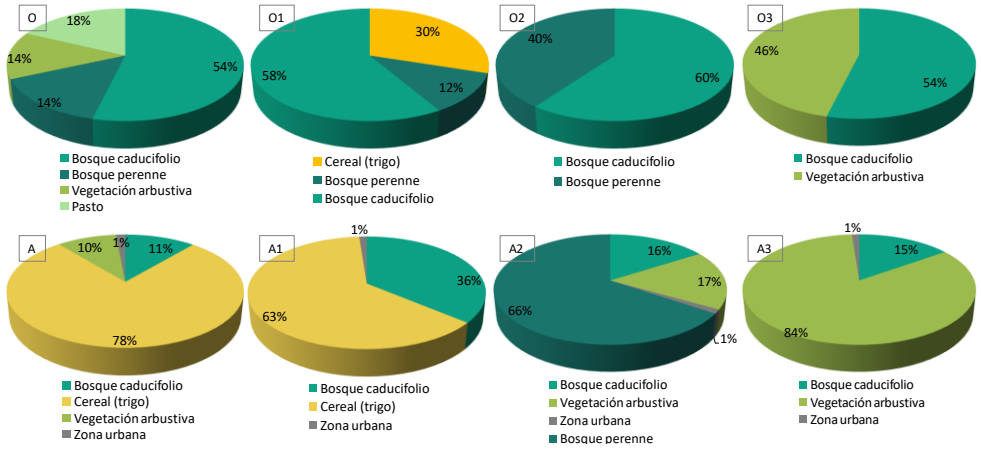

Figura 4.20. *Uso del suelo en las sub-cuencas de Otxandio (O) y Audikana (A). Se incluyen los escenarios de cambio de usos del suelo en Otxandio (O1, O2, O3) y Audikana (A1, A2, A3).*

Los mapas de usos del suelo modificados se han introducido en el modelo SWAT. Es necesario destacar que según el planteamiento explicado en el apartado *4.4.3. Caracterización física del medio* los usos del suelo afectan a las características y, por tanto, a los parámetros hidrológicos del suelo. Por lo tanto, una vez introducido cada uno de los nuevos escenarios de usos del suelo, también se han cambiado las características y los parámetros del suelo en función del nuevo uso. De esta forma no se suponen cambios progresivos en el desarrollo del suelo, sino que consideramos que el nuevo uso del suelo ha tenido el tiempo suficiente para desarrollar el suelo y, por lo tanto, que se consoliden sus características. Por último, se ha realizado la simulación hidrológica sin cambiar los valores del resto de parámetros del modelo obtenidos en la calibración del mismo. Para poder analizar con el menor grado de incertidumbre los posibles efectos de los cambios en los usos del suelo en la respuesta hidrológica, en lugar de incluir estos cambios en las proyecciones climáticas futuras se ha realizado el análisis para el mismo periodo que el de la calibración y la validación (1987-2015), de esta forma es posible aislar la influencia de los usos del suelo en los caudales.

4.4.6 Selección y evaluación de las proyecciones climáticas

Las proyecciones climáticas que se han utilizado en este trabajo corresponden a la quinta fase del Proyecto de comparación de modelos acoplados (CMIP5) a los que AEMET ha realizado dos tipos de downscaling; SDSM y AN.

AEMET suministra las proyecciones de las variables climáticas diarias para varios GCM (previa realización del downscaling) para la estación meteorológica Urrunaga (AEMET 9080) (Fig. 4.17). Para considerar la incertidumbre inherente a las proyecciones climáticas en las proyecciones hidrológicas resultantes, este documento se basa en 5 GCM (ACCESS1-0, BNU-ESM, MPI-ESM-RL, MPI-ESM-MR, CMCC-CESM), 2 RCPs (8,5 y 4.5) y 2 métodos de downscaling (AN y SDSM). Con estas combinaciones, 5 GCM, 2 RCPs y 2 métodos de downscaling, se han simulado con SWAT las proyecciones hidrológicas para 16 proyecciones climáticas. Las proyecciones climáticas utilizadas en este estudio están resumidas en la Tabla 2.3.

Los baseline de los GCM (aplicado el downscaling) se han comparado con los datos registrados en la estación de Urrunaga en el periodo (1961-2000) y se han calculado las diferencias existentes entre el baseline de las proyecciones climáticas y los datos observados para la precipitación y la temperatura media (%) (Fig. 4.21).

Los datos meteorológicos registrados en Urrunaga no son completos y sobre todo en el caso de la temperatura, la falta de datos es importante. Por lo tanto, las diferencias que se calculan en este apartado pueden estar sujetas a errores. Sin embargo, consideramos que sirven para esbozar una idea de las diferencias entre los datos obtenidos de los GCM y los datos registrados. A escala anual el ajuste es mejor que a escala estacional. Las mayores diferencias en temperaturas máximas se registran en verano, y vienen dadas por los GCM a los que se les ha aplicado el método de downscaling de los análogos (AN). En general, tanto a escala estacional, para todas las estaciones, como a escala anual, son estos modelos (a los que se les ha aplicado el método de downscaling AN) los que más se alejan de los datos registrados.

En cuanto a los baseline de precipitación, las proyecciones realizadas con el GCM MPI-ESM-MR son las de mayor incertidumbre puesto que son las que mayores diferencias muestran. Por ejemplo, el modelo MPI-SM-MR_SDSM proyecta casi un 80 % más de precipitación en verano. CMCC-CESM_SDSM también destaca, puesto que, aunque su ajuste es bastante bueno a escala anual y, en general, también estacional, en verano proyecta casi un 60 % más de precipitación que la registrada. Teniendo en cuenta la variabilidad de la precipitación, se puede considerar que, a escala anual, las precipitaciones obtenidas de los GCM y las registradas en Urrunaga se ajustan bastante bien (con excepciones como las ya mencionadas).

Como se ha podido observar, aunque se haya realizado un downscaling de los resultados de los GCM todavía existen diferencias entre los datos registrados y los proyectados. Además, como ya se ha mencionado, en la cuenca del Zadorra la variabilidad de los datos meteorológicos es importante. Por ello, para la simulación de caudales, tanto para el baseline como para las proyecciones futuras, se han corregido los datos de las proyecciones climáticas realizadas para la estación de Urrunaga, teniendo en cuenta los datos de precipitación de la estación de Urkiola (Iberdrola) y la temperatura registrada en Otxandio, para la sub-cuenca de Otxandio, y los datos de precipitación de la estación de Gauna y la temperatura registrada en Arkaute para la sub-cuenca de Audikana.

Para corregir el sesgo de las proyecciones de series climáticas de precipitación y temperatura máxima y mínima (tanto las del baseline como las futuras) se ha utilizado la metodología propuesta por Lenderink et al. (2007) (capítulo *2. Methodology,* apartado *2.3 Bias correction*). Este método utiliza los datos mensuales para corregir la diferencia entre los datos observados y los obtenidos de los GCM. Los valores diarios se ajustan con el mismo factor de corrección cada mes, y este factor no varía en el tiempo. Se ha escogido este método porque no afecta a las posibles tendencias climáticas futuras (se analizarán posteriormente) y a sus proyecciones hidrológicas derivadas.

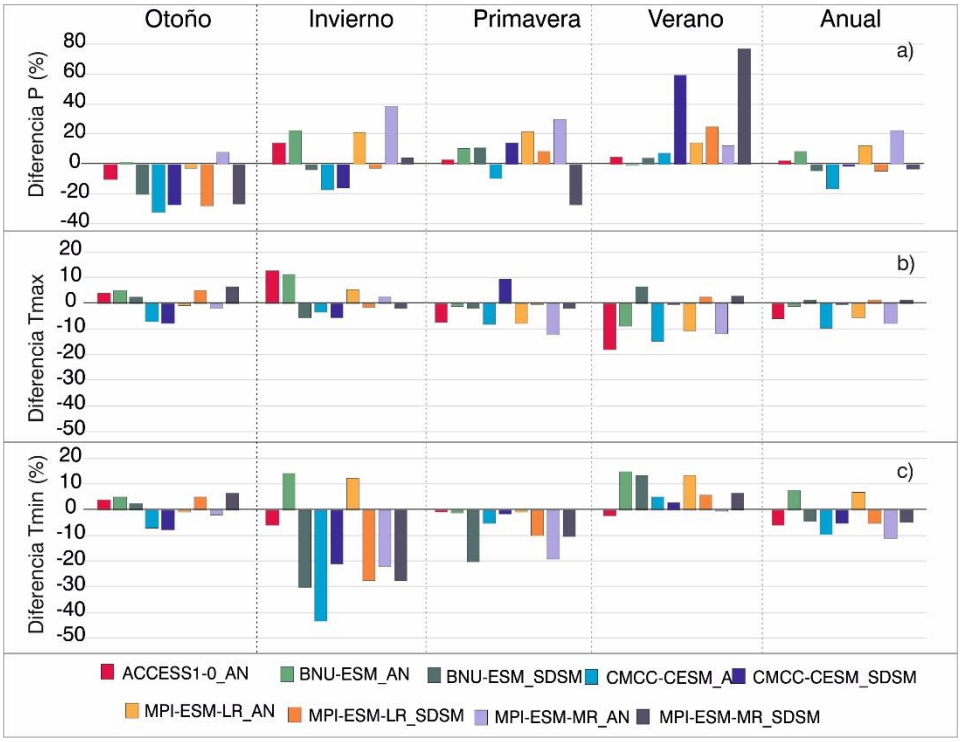

Figura 4.21. *Diferencia entre el promedio anual de la precipitación (a) y el promedio de la temperatura máxima (b) y mínima (c) entre los baseline de las proyecciones climáticas y los datos registrados en Urrunaga. Los datos se presentan en diferencias estacionales y anuales.*

Para corregir el sesgo de las proyecciones climáticas de Otxandio se han utilizado los datos de la estación de Urkiola (1069E) y en el caso de Audikana los de Gauna (9082T). Para la temperatura máxima y mínima en Otxandio se han utilizado los datos de la estación de Otxandio (C054) y en el caso de Audikana los de Arkaute (9086).

4.4.7 Evaluación del impacto de las proyecciones climáticas en los recursos hídricos

Con el objetivo de evaluar su impacto hidrológico, las proyecciones se han dividido en tres horizontes futuros: 2011-2040, 2041-2070 y 2071-2100, que en adelante denominaremos 2030, 2060 y 2090, respectivamente. Las proyecciones hidrológicas futuras (caudales medios) se han comparado con las proyecciones hidrológicas de sus baseline a escala anual y estacional.

Además, también se han estudiado las tendencias que pueden existir en las proyecciones hidrológicas. Para hacer este análisis, se han calculado los caudales medios (Qm) y la duración y la severidad de los caudales bajos (Q20) y posteriormente se han analizado sus tendencias mediante la misma metodología explicada en *2. Methodology*, apartado *2.5 Methodology to evaluate the hydrological impact of climate projections*. Se han tomado en cuenta las duraciones anuales y estacionales (en días). La severidad define el déficit de caudal (volumen), en este caso anual, por debajo de Q20.

4.4.8 Resultados: calibración y validación del modelo

La calibración (1987-1994) y la validación (2005-2015) de las sub-cuencas de Otxandio y Audikana se ha realizado por separado. Como se ha expuesto en el apartado *4.4.4. Calibración, validación y evaluación de la modelización hidrológica*, para realizar este proceso se han utilizado los datos diarios de caudal ($m^3\ s^{-1}$) registrados en las estaciones de aforo de Otxandio y Audikana, y tal y como se ha mencionado, estos datos están sujetos a numerosas incertidumbres, lo cual ha dificultado el proceso.

Los parámetros modificados en cada sub-cuenca y el rango utilizado en el proceso de autocalibración, se pueden observar en la Tabla 4.12. En un principio, la calibración comenzó con unos 15 parámetros relacionados con el caudal, pero debido a su escasa influencia se fueron descartando hasta modificar tan solo los 12 parámetros de la Tabla 4.12. Los parámetros relacionados con las propiedades físicas de los suelos no se han modificado durante la calibración, con el fin de posibilitar una mejor evaluación del impacto de los usos del suelo en los recursos hídricos (Apartado *4.4.10 Influencia de los usos del suelo en los recursos hídricos*).

Los parámetros más sensibles son el número de curva (CN2) y la constante de recesión (Alpha_BF). El primero se ha incrementado en una pequeña proporción para ajustar mejor los picos, mientras que el valor del segundo se ha aumentado de forma considerable para que el flujo base no descienda de forma abrupta. La mayor parte de los parámetros calibrados se han modificado de forma similar en ambas cuencas, sin embargo, a algunos como el LAT_TIME (tiempo de

circulación de flujo lateral) o el CH_K2 (conductividad del canal principal) se les han atribuido valores finales muy distintos. Estas diferencias son producidas por las necesidades de incremento o descenso del caudal en cada sub-cuenca. A la hora de realizar la calibración se ha tenido en cuenta que el rango de valores escogido para los parámetros sea apropiado a las características de la cuenca. Para más información sobre los parámetros calibrados, consultar la documentación del modelo SWAT y el capítulo *2. Methodology*, section *2.4 Hydrological modelling: general descripition of SWAT*.

Tipo de cambio	Nombre del parámetro	Descripción	Caudal		Rango valores de parámetros
			Otxandio	Audikana	
r	CN2.mgt	Número de curva	↑0.9 %	↑0.9 %	↑5-↓5 %
v	CH_K2.rte	Conductividad del canal principal	23.05	175	0.045-200
v	SURLAG.bsn	Coeficiente de retención de la escorrentía superficial	3.64	3.64	0-10
v	ALPHA_BF.gw	Constante de recesión	0.9	0.9	0.5-1
v	ESCO.bsn	Factor de compensación de la evaporación del suelo	0.98	0.98	0.8-1
v	GW_DELAY.gw	Retardo (días) del agua subterránea	10	10	may-25
v	ELEV_FR. sub	Fracción del área de la sub-cuenca con bandas de elevación.	0.2	0.2	-
v	LAT_TTIME.hru	Tiempo de circulación del flujo lateral	4.55	75	0-100
v	OV_N.hru	Valor de *n* (Manning) para la escorrentía superficial	0.075	0.075	0.01-0.3
v	SFTMP.bsn	Temperatura a la que nieva	0.25	0.25	-3
v	SMTMP.bsn	Temperatura base para que la nieve comience a derretirse.	1.65	1.65	0-5
v	RCHR_DP.gw	Factor de percolación al acuífero profundo	0	0	0

Tabla 4.12. *Resumen de los parámetros ajustados en el proceso de calibración, su descripción y rango. *v significa que el valor del parámetro se cambia por el nuevo valor y r significa que el valor del parámetro se cambia de forma relativa.*

Los resultados de la calibración se han comparado de forma gráfica con los datos observados durante todo el proceso. En general se podría decir que en ambas sub-cuencas los caudales pico se han subestimado. Sin embargo, es necesario recordar que, aunque en todo momento se haya intentado que en conjunto la calibración sea satisfactoria, nos hemos centrado fundamentalmente en los caudales medios y bajos. En la sub-cuenca de Otxandio, el caudal simulado tiende a ser menor que el observado. Es necesario tener en cuenta que

la falta de mantenimiento del cauce en la estación de aforos puede dar como resultado el registro de caudales mayores a los reales, sobre todo en aguas bajas, por lo que la subestimación de caudales por parte del modelo quedaría, hasta cierto punto, justificada. Por otro lado, los caudales simulados de la sub-cuenca de Audikana tienden a ser ligeramente mayores que los registrados. Como ya se ha mencionado, los caudales bajos de la estación muestran numerosas incertidumbres, lo que dificulta el proceso de calibración. Los resultados gráficos de la calibración y la validación de estas dos sub-cuencas se puede observar en el Anexo 3.

Una vez calibrado el modelo (1987-1994), se procede a la validación (2005-2015) introduciendo los datos meteorológicos de este periodo, pero sin modificar los parámetros calibrados. Los resultados estadísticos de la calibración y la validación se pueden observar en las Tablas 4.13 y 4.14. En estas tablas además de los resultados estadísticos para los periodos de validado y calibrado en su totalidad, se han incluido los estadísticos para el flujo base de los hidrogramas obtenidos, los de los percentiles Q20 y Qm de los mismos y los de los años de alto AI (años húmedos) y bajo AI (años más secos) por separado. Se puede observar que, a pesar de los problemas de los caudales registrados en ambas cuencas, se ha obtenido una buena calibración que ha podido ser validada, también para los caudales bajos, a los que se presta especial interés en este estudio.

OTXANDIO		Caudal				Flujo base			
		NSE	r2	PBIAS	RSR	NSE	r2	PBIAS	RSR
Calibración	1987-1994	0.69	0.69	9.04	0.56	**0.30**	0.58	-22.91	**0.84**
Validación	2005-2015	0.57	0.58	19.13	0.66	0.67	0.72	12.17	0.57
Años áridos	2010-2012	0.67	0.67	9.94	0.58	0.74	0.79	-6.50	0.51
Años húmedos	1991-1993	0.50	0.51	14.58	**0.71**	0.70	0.73	13.08	0.55
Qm	1987-1994 2005-2015	0.73	0.75	2.01	0.52				
Q20	1987-1994 2005-2015	0.58	0.67	2.16	0.65				

Tabla 4.13. *Resultados estadísticos para la sub-cuenca de Otxandio. Según Moriasi et al., 2007, la calibración se considera satisfactoria cuando NSE> 0.5, R^2 > 0.5, RSR ≤ 0.7, y PBIAS < 25%, los resultados no satisfactorios se han indicado con negrita.*

AUDIKANA		Caudal				Flujo base			
		NSE	r2	PBIAS	RSR	NSE	r2	PBIAS	RSR
Calibración	1987-1994	0.56	0.57	12.61	0.67	0.69	0.73	16.79	0.56
Validación	2005-2015	0.57	0.59	16.29	0.66	0.75	0.79	7.13	0.50
Años áridos	2010-2012	**0.48**	**0.49**	16.95	**0.72**	0.84	0.79	23.59	0.40
Años húmedos	1991-1993	0.65	0.59	12.10	0.60	0.76	0.71	11.81	0.49
Qm	1987-1994 2005-2015	0.77	0.80	2.08	0.48				
Q20	1987-1994 2005-2015	0.69	0.74	10.36	0.55				

Tabla 4.14. *Resultados estadísticos para la sub-cuenca de Audikana. Según Moriasi et al., 2007, la calibración se considera satisfactoria cuando NSE> 0.5, R^2 > 0.5, RSR ≤ 0.7, y PBIAS < 25%, los resultados no satisfactorios se han indicado con negrita.*

Respecto a las incertidumbres asociadas a la modelización hidrológica, por un lado, existen las relacionadas con los caudales registrados en ambas sub-cuencas y que ya se han mencionado con anterioridad. Obviamente, si los caudales con los que se calibra el modelo no son adecuados, independientemente de si la calibración (estadística y gráficamente) es satisfactoria o no, ésta estará sujeta a incertidumbres. En relación con los índices estadísticos obtenidos en la calibración y la validación del modelo, es posible destacar que los valores no satisfactorios que se pueden ver en las Tablas 4.13 y 4.14 están relacionados con índices estadísticos cuyo valor está influenciado por los caudales pico. Centrándonos en el índice RSR, en la sub-cuenca de Otxandio los años húmedos son los que muestran mayor incertidumbre, mientras que en Audikana ocurre al contrario. En ambos casos se considera que la calibración y la validación son lo suficientemente buenas para hacer un análisis de caudales medios (Qm) y bajos (Q20).

4.4.9 Impacto hidrológico de las proyecciones climáticas futuras

Una vez calibrado y validado el modelo hidrológico, se ha procedido a introducir en él las proyecciones climáticas para evaluar su impacto en los recursos hídricos de las cuencas de estudio. Recordemos que AEMET ha realizado downscaling estadístico a los datos obtenidos de los GCM (Modelo General de Circulación) para la estación de Urrunaga. Para poder utilizar estos datos en las sub-cuencas de Otxandio y Audikana y para corregir las diferencias existentes entre los datos históricos y las proyecciones climáticas, a estas últimas se les ha aplicado una corrección de sesgo. Son precisamente estos datos corregidos los que se han introducido en el modelo para obtener los caudales proyectados.

Comenzaremos por analizar las diferencias existentes entre los caudales simulados con a) los datos climáticos históricos y b) los obtenidos de las proyecciones climáticas para el baseline o periodo base. La comparación se realiza entre caudales simulados (y no con los observados) (1987-2000) porque de esta forma no se transfieren las diferencias debidas a la propia modelización. Después, se ha calculado la diferencia (%) existente entre las proyecciones hidrológicas futuras y su proyección del periodo baseline. Este análisis se ha dividido en tres horizontes (2030, 2060 y 2090) y se ha realizado tanto a escala estacional como a escala anual.

Sub-cuenca de Otxandio

La comparación entre el caudal medio simulado para la sub-cuenca de Otxandio (Q_Sim Otxandio) y el obtenido de las proyecciones hidrológicas de los baseline de los escenarios climáticos se pueden observar en la Fig. 4.22.

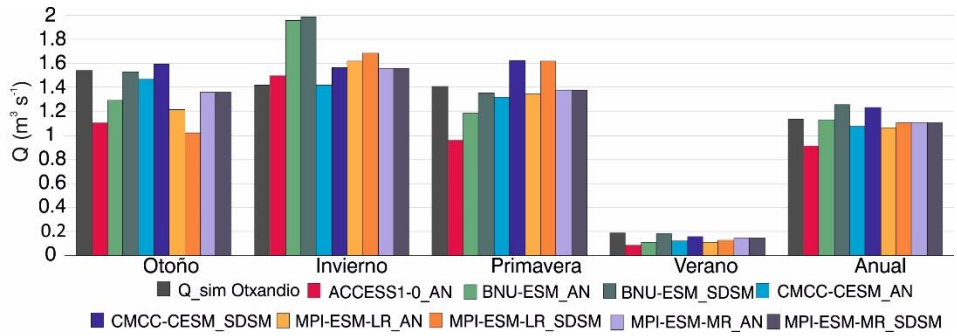

Figura 4.22. *Promedio de caudal (m^3 s^{-1}) para el periodo 1987-2000. Aparece el caudal simulado con los datos climáticos históricos de la estación de Otxandio (Q_Sim Otxandio) y los resultados de los baseline de las proyecciones climáticas.*

En general, a escala anual, el caudal simulado en Otxandio y el obtenido de los baseline de las proyecciones climáticas puede considerarse bastante similar (entre -2.5 % y + 10 %) con excepción de ACCESS1-0_AN que es aproximadamente un 20 % menor que Q_Sim Otxandio. En verano todas las proyecciones subestiman el caudal, mientras que en invierno la sobreestiman. Otoño y primavera muestran resultados variables, pero en general se podría decir que los baseline de las proyecciones subestiman el caudal, sobre todo en otoño.

Para una mejor comprensión de las proyecciones hidrológicas futuras, las diferencias (%) de las proyecciones respecto a su baseline se han agrupado en función del RCP y el método de downscaling, calculando su valor medio. Todos los resultados se pueden observar en el Anexo 4.

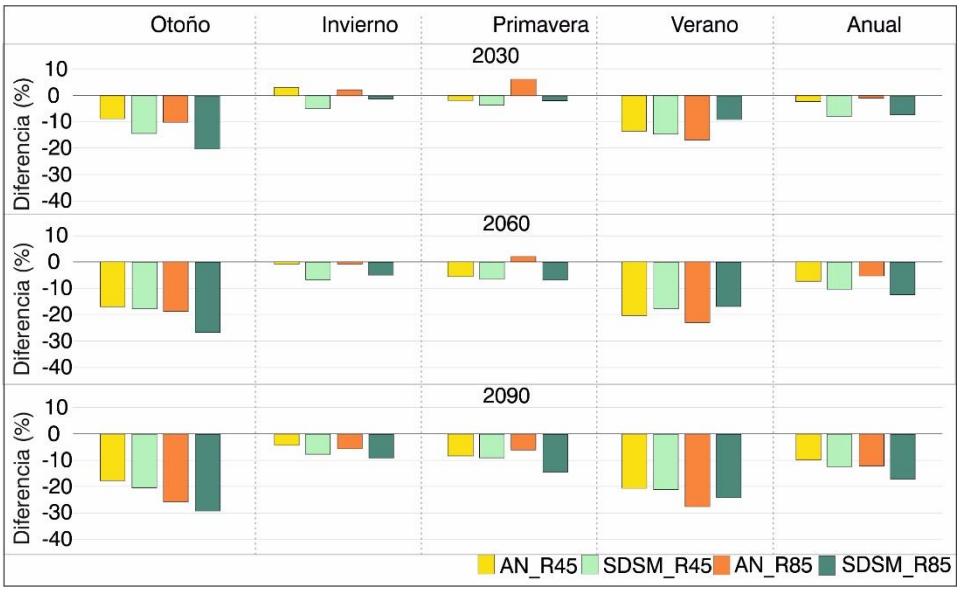

Figura 4.23. *Diferencia (%) entre las proyecciones hidrológicas futuras y su baseline para Otxandio. Para agrupar la diferencia en función del RCP (4.5 y 8.5) y el método de downscaling (SDSM o AN) se ha calculado el valor medio de la diferencia. Los datos aparecen separados en función de los horizontes 2030, 2060 y 2090 y en valores estacionales y anuales.*

Como se puede apreciar en la Fig. 4.23, el descenso del caudal medio va siendo mayor de forma progresiva del horizonte 2030 hasta el 2090, de forma generalizada y en todas las estaciones del año. A finales de siglo, se espera que el caudal medio anual descienda entre un 10 % y un 17 %. Otoño será la estación más afectada, mientras que los menores descensos se darán en invierno. A finales de siglo se espera que el caudal medio de verano descienda entre un 20 y un 27 %. Primavera (abril) es la estación en la que mayores caudales se registran (Fig. 4.24), a lo largo del siglo XXI el caudal en esta estación también descenderá, pero según las proyecciones lo hará en menor medida que en otoño y verano.

Por último, utilizando los valores máximos y mínimos del caudal medio proyectado en cada horizonte, se ha elaborado la Fig. 4.24. De esta forma es

posible evaluar el rango de variación del caudal proyectado. En la figura, al igual que en la Fig. 4.23, se puede observar el descenso progresivo que se da en el caudal a medida que los horizontes proyectados son más lejanos en el tiempo. Los mayores rangos de variación del caudal se dan entre enero y abril, mientras que a medida que el caudal desciende (meses más secos) el rango es más estrecho.

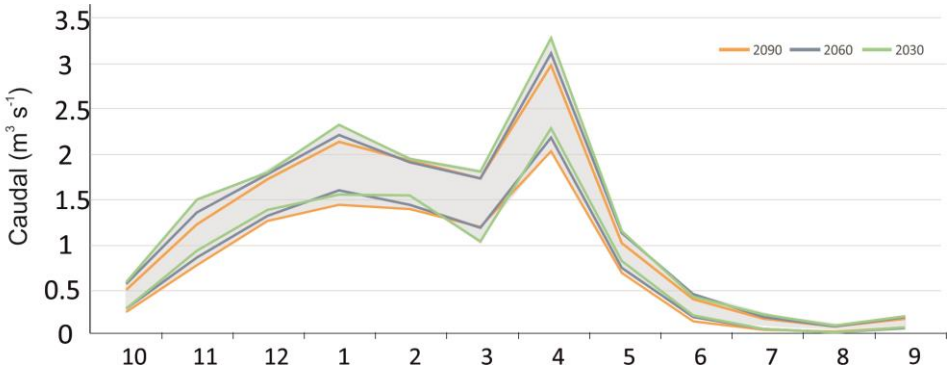

Figura 4.24. *Rango de variación del caudal medio mensual ($m^3 s^{-1}$) simulado con las 16 proyecciones climáticas para los horizontes 2030, 2060 y 2090 en Otxandio. El color gris representa el rango de posibles valores medios de caudal.*

Sub-cuenca de Audikana

En la Fig. 4.25 se puede observar el caudal medio simulado para la estación de Audikana (Q_Sim Audikana) y el baseline de las proyecciones hidrológicas. Tanto a escala anual como en otoño, verano y primavera (excepción de CMCC-CESM_SDSM) los caudales proyectados son menores que los simulados con los datos de precipitación registrados en esta cuenca. Invierno es la única estación en la que algunas de las proyecciones muestran valores de caudal mayores. En caudales bajos, como los de verano, la diferencia existente entre el caudal simulado y el obtenido del baseline de las proyecciones climáticas es considerable, entre un 56 % y un 76 % menor. CMCC-CESM_SDSM muestra las menores diferencias respecto a Q_Sim Audikana; por ejemplo, a escala anual, la diferencia es de tan solo un 0.2 %.

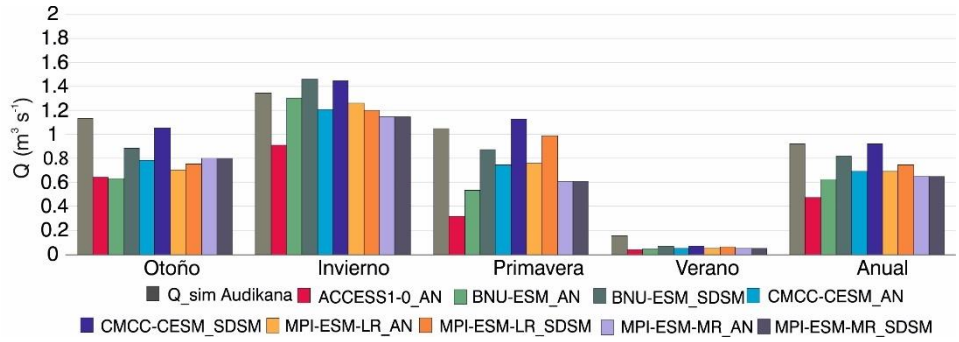

Figura 4.25. *Promedio de caudal (m^3 s^{-1}) para el periodo 1987-2000. Aparece el caudal simulado con los datos climáticos históricos de la estación de Audikana (Q_Sim Audikana) y los resultados de los baseline de las proyecciones climáticas.*

Al igual que para las proyecciones hidrológicas futuras de la estación de Otxandio, las diferencias de caudal existentes entre las proyecciones hidrológicas de los baseline de los escenarios climáticos y sus proyecciones futuras, se han agrupado en función del RCP y el método de downscaling. En el segundo apartado del Anexo 4 se pueden observar las diferencias para cada proyección.

Los resultados, aunque indican que los descensos pueden ser mayores que los de Otxandio, muestran la misma tendencia de descenso del caudal a lo largo del siglo XXI (Fig. 4.26). Para el horizonte 2090 se espera que el caudal anual pueda descender entre un 11 y un 26 %. Otoño es la estación que mayores descensos podrá sufrir (entre un 20 y un 33 %), mientras que en primavera, el caudal podrá descender entre un 10 y un 25 %. En verano e invierno, los caudales proyectados para finales de siglo son bastante similares, en ambos casos los descensos son aproximadamente de entre un 4 y un 14 %.

La Fig. 4.27 muestra el rango de valores de caudal (m^3 s^{-1}) que se podría registrar en la estación de Audikana en función de los resultados de las proyecciones hidrológicas realizadas en este trabajo (valores máximo y mínimo de caudal para cada horizonte). En esta figura, al igual que en la Fig. 4.26, se puede apreciar el descenso de caudal a medida que los horizontes son más lejanos. Donde se aprecia con mayor claridad este descenso es en los caudales máximos y mínimos proyectados entre noviembre y febrero, donde se observa claramente

que el caudal desciende del horizonte 2030 al 2060 y del 2060 al 2090. En verano el rango de caudales posibles es muy estrecho.

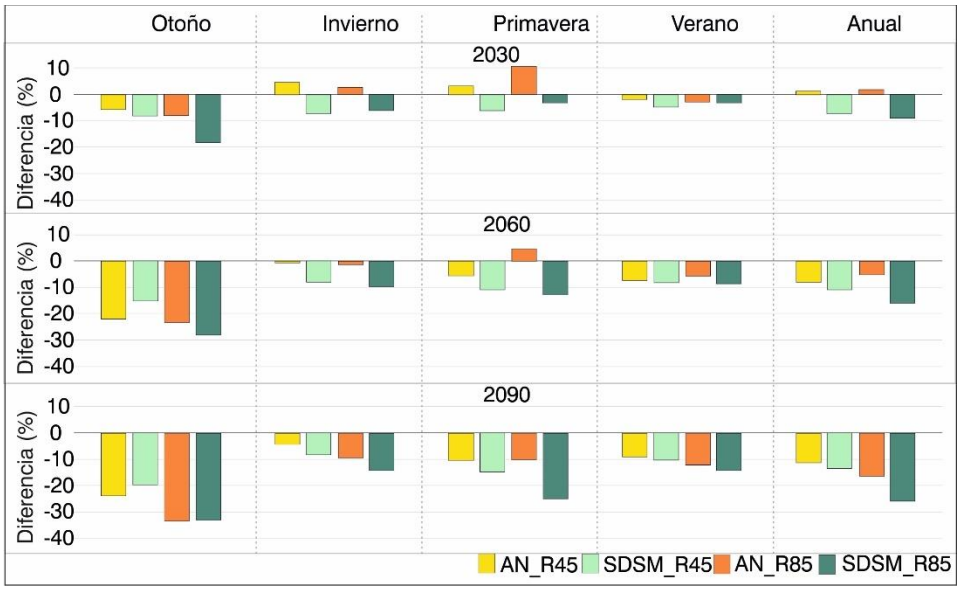

Figura 4.26. *Diferencia (%) entre las proyecciones hidrológicas futuras y su baseline para Audikana. Para agrupar la diferencia en función del RCP (4.5 y 8.5) y el método de downscaling (SDSM o AN) se ha calculado el valor medio de la diferencia. Los datos aparecen separados en función de los horizontes 2030, 2060 y 2090 y en valores estacionales y anuales.*

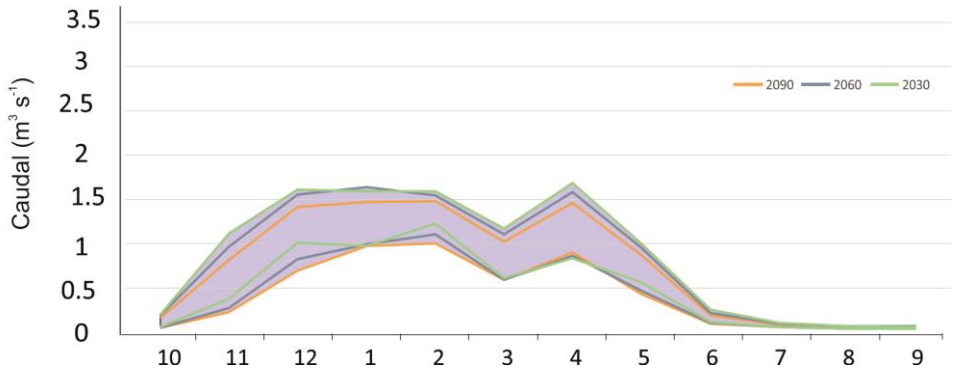

Figura 4.27. *Rango de variación del caudal medio mensual ($m^3 s^{-1}$) simulado con las 16 proyecciones climáticas para los horizontes 2030, 2060 y 2090 en Audikana. El color morado representa el rango de posibles valores medios de caudal.*

4.4.10 Impacto hidrológico de los escenarios climáticos futuros: tendencias de caudales medios (Qm) y bajos (Q20, duración y severidad)

Los resultados obtenidos en los análisis de tendencias realizados para los caudales medios y bajos se muestran en las Fig. 4.30 y 4.31, donde se han considerado las tendencias para el periodo 2011-2100. Las metodologías utilizadas, tanto para el cálculo de los caudales medios (Qm) y bajos (duración y severidad de Q20) como en el cálculo de las tendencias, han sido las mismas que para las tendencias pasadas y han sido descritas en *2.5 Methodology to evaluate the hydrological impact of climate projections.*

A escala anual, en los caudales medios (Qm) y para el RCP 4.5, se observa que, tanto en Otxandio como en Audikana, para la mitad de las proyecciones climáticas la probabilidad de que exista una tendencia no es clara, mientras que para la otra mitad la tendencia es claramente descendente. Para el RCP 8.5, el porcentaje de proyecciones climáticas que provocaría un descenso de los caudales medios aumenta claramente, siendo la mayoría; a escala anual no se observan tendencias ascendentes del Qm para ninguna de las proyecciones. Las tendencias observadas para el Q20 son muy parecidas, con aproximadamente la mitad de las proyecciones mostrando un ascenso de la duración (Fig. 4.30) y la severidad (Tabla 4.15) del periodo de aguas bajas (Q20) para el RCP 4.5, y un mayor porcentaje, con tendencias ascendentes para el RCP 8.5.

Si observamos estas mismas tendencias a escala estacional, veremos que en otoño se repiten las mismas tendencias que a escala anual para los caudales medios (Qm), y que las tendencias de ascenso para la duración de los caudales bajos (Q20) se mantienen en el RCP 8.5, sin embargo, para el RCP 4.5 las tendencias no son tan claras.

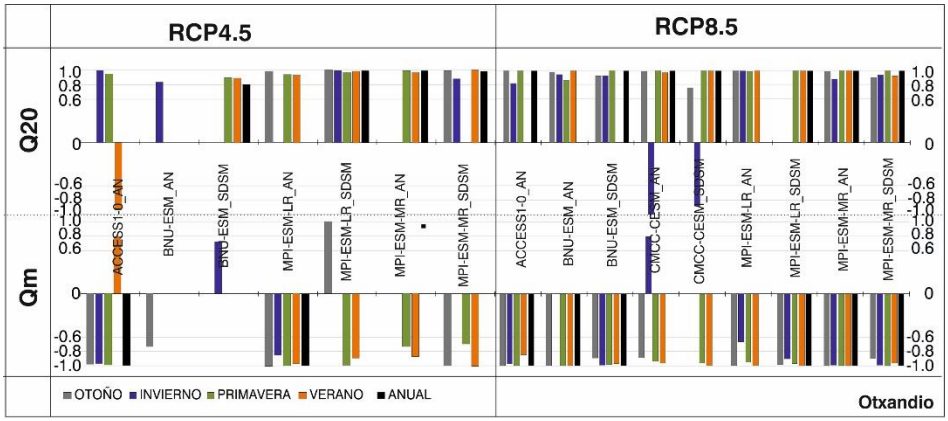

Figura 4.30. *Tendencias para los caudales medios (Qm) y para la duración de los caudales bajos (Q20) de Otxandio representadas a escala anual y estacional para el periodo 2011-2100.Las proyecciones realizadas para los RCP 4.5 (escenario de mitigación) y los RCP 8.5 (escenario de altas emisiones) se muestran separadas. Solo se muestran aquellos valores con una probabilidad de ocurrencia mayor al 66% (0.66).*

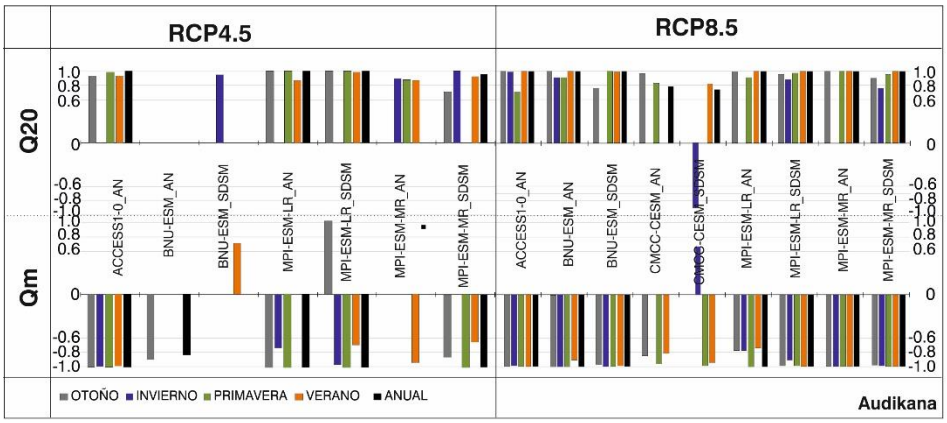

Figura 4.31. *Tendencias para los caudales medios (Qm) y para la duración de los caudales bajos (Q20) de Audikana representadas a escala anual y estacional para el periodo 2011-2100.Las proyecciones realizadas para los RCP 4.5 (escenario de mitigación) y los RCP 8.5 (escenario de altas emisiones) se muestran separadas. Solo se muestran aquellos valores con una probabilidad de ocurrencia mayor al 66% (0.66).*

Invierno es la estación que muestra mayores incertidumbres, sobre todo para los caudales medios en el RCP 4.5 y para los caudales bajos en el RCP 8.5. Las tendencias más claras observadas son, por un lado, el aumento de la duración del periodo de aguas bajas para el RCP 4.5 en Otxandio y, por otro, la disminución de los caudales medios en ambas cuencas para el RCP 8.5. Al contrario que en invierno, en primavera las tendencias son claras con un gran porcentaje de las proyecciones de ambos RCPs mostrando una disminución del

caudal medio y un aumento del periodo de aguas bajas en ambas cuencas. En verano las tendencias son similares a las de primavera con la excepción de que para el RCP 4.5 las incertidumbres son algo mayores.

Tabla 4.15. *Tendencias para la severidad de los caudales bajos (Q20) de Otxandio y Audikana obtenidos a escala anual para el periodo 2011-2100. Se muestran los valores de probabilidad de ocurrencia en %. El signo, ninguno para el ascendente y - para el descendente, se refiere al signo de la tendencia.*

	Audikana	Otxandio
ACCESS1-0-R45	**90**	-47
BNU-ESM_AN_R45	-66	74
CMCC_CESM_SDSM_R45	**100**	**100**
MPI-ESM-LR_AN_R45	**80**	**100**
MPI-ESM-LR_SDSM_R45	**100**	**100**
MPI-ESM-MR_AN_R45	**85**	**100**
MPI-ESM-MR_SDSM_R45	**82**	**100**
ACCESS1-0_AN_R85	-9	19
BNU-ESM_AN_R85	**100**	**100**
BNU-ESM_SDSM_R45	12	**75**
BNU-ESM_SDSM_R85	64	**100**
CMCC-CESM_AN_R85	**100**	**100**
MPI-ESM-LR_AN_R85	**100**	**100**
MPI-ESM-LR_SDSM_R85	**100**	**99**
MPI-ESM-MR_AN_R85	**85**	**100**
MPI-ESM-MR_SDSM_R85	**100**	**100**

Los resultados obtenidos del análisis de tendencias de la severidad del periodo de aguas bajas para el periodo 2011-2100 se pueden observar en la Tabla 4.15. En general, las tendencias obtenidas muestran un ascenso muy probable de la severidad en ambas cuencas. Así, en Audikana 12 de las 16 proyecciones hidrológicas en las que se ha analizado la tendencia de este parámetro muestran tendencias ascendentes probables, siendo en 8 de ellas la tendencia virtualmente cierta. Solamente en uno de los casos, BNU-ESM_AN_R45, la tendencia de la severidad es descendente, con una probabilidad de ocurrencias del 66%. En Otxandio, 14 proyecciones hidrológicas muestran una tendencia ascendente de la severidad, al menos, probable, mostrando 10 de ellas una probabilidad de ocurrencia del 100%. En Otxandio no se observan tendencias probables a la disminución de la severidad del periodo de aguas bajas.

4.4.11 Influencia de los usos del suelo en los recursos hídricos

Para evaluar la influencia que los usos del suelo pueden tener en los caudales, se han planteado diferentes escenarios en las dos sub-cuencas. Se trata, hay que dejarlo claro, de una primera aproximación para conocer mejor los efectos de los cambios en los usos del suelo (y según la metodología empleada también en los parámetros del suelo) sobre los recursos hídricos. Este paso, a modo de ejercicio, es importante realizarlo (habría que jugar con más escenarios "posibles") para conocer mejor esos efectos, y es, además, necesario previamente a una consideración conjunta de los efectos, sobre los caudales, de los cambios de usos del suelo y los climáticos, paso este que habrá que realizar en otros trabajos. En el actual los escenarios tenidos en cuenta se han aplicado para el periodo 1985-2015.

Se han planteado tres escenarios de usos del suelo en cada sub-cuenca (apartado *4.4.5. Evaluación de la influencia del uso del suelo en los recursos hídricos*, Fig. 4.20), en los que la vegetación actual y la superficie que ocupa dentro de la sub-cuenca han sido modificadas. SWAT se basa en el código EPIC (Williams et al., 1990) para simular el crecimiento de la vegetación. Este código asume que el desarrollo de la vegetación puede ser simulado por la teoría de unidades de calor (Boswell, 1926) la cual postula que las plantas tienen una demanda de calor que se puede cuantificar y que está vinculada al tiempo de maduración. Así, cuando la planta alcanza su punto máximo de maduración, es decir, las unidades de calor máximas, su producción de biomasa desciende de forma drástica. En el caso de los bosques, la vegetación arbustiva y el pasto, la producción de biomasa comienza en primavera (entre abril y mayo) y se completa en Invierno (entre diciembre y enero). En el caso del cereal, la producción también comienza en primavera, pero llega al punto máximo de madurez entre los meses de agosto, septiembre u octubre en función de las condiciones que se den ese año para que el cultivo alcance las unidades máximas de calor. Es necesario mencionar que SWAT permite establecer tanto los periodos de siembra y de recogida como las unidades de calor, pero en este caso, al tratarse de una primera aproximación, se ha optado por utilizar las condiciones estándar del modelo.

Otxandio es una sub-cuenca fundamentalmente forestal. Los escenarios de usos del suelo que se han planteado en esta sub-cuenca son:

- O1: Se cambian las zonas de pasto de la parte más llana de la sub-cuenca por cereal.
- O2: La sub-cuenca evoluciona a bosque en toda su extensión.
- O3: Se combinan la vegetación arbustiva y los bosques.

En la Fig. 4.28 están representados los caudales medios mensuales (m^3 s^{-1}) en cada escenario, en líneas continuas, y, las diferencias (%) de caudal generadas por los cambios en los usos del suelo, respecto al uso actual (Q_Sim Otxandio), a escala mensual y anual, mediante barras. A escala anual las diferencias no son importantes, esto es debido a que en los meses de mayor caudal (sobre todo en invierno) los tres escenarios planteados y Q_Sim Otxandio muestran caudales muy similares. Sin embargo, las diferencias observadas en la distribución de los caudales a lo largo del año son más relevantes, sobre todo en los meses de verano y en otoño, cuando los caudales son más bajos.

El escenario O1, en el que las zonas de pasto y vegetación arbustiva de las partes más llanas de la sub-cuenca son cambiadas por cereal, se pueden apreciar cambios considerables en los meses de verano donde, debido a un aumento de la evapotranspiración de los meses previos (junio-julio), el caudal del escenario O1 descendería de forma progresiva entre julio y septiembre (hasta un 14 % en septiembre). En el resto de estaciones del año las diferencias en caudales son poco significativas para este escenario, si bien la simulación refleja un descenso importante de la evapotranspiración en otoño (cerca del 10 % en octubre y noviembre), respecto a la situación actual. Esto indicaría un aumento de la reserva de agua en el suelo que justificaría la mayor evapotranspiración en verano.

Es el escenario O2, en el que se ha considerado que toda la superficie de la sub-cuenca está cubierta por bosque, el que proyectaría mayores descensos de caudales. Aunque, a escala anual el descenso no es considerable (3.5 %), en los meses de verano, e incluso en los de otoño, el caudal descendería por encima

de un 8 % (en septiembre un 27 %, en octubre un 15 %, y cerca de un 10 % en el resto de meses). El principal motivo de este descenso en los caudales puede encontrarse en el importante incremento de la evapotranspiración que supone el bosque, desde mayo a agosto. Esto es así para el verano, pero no para otoño, periodo en el que tanto los caudales como la evapotranspiración disminuyen, lo que hace pensar en un aumento de la reserva de agua regulada en ese momento en el suelo, que justificaría la mayor evapotranspiración en verano. Esta regulación sería ahora mayor que la del escenario O1.

Por tanto, ambos escenarios, O1 y O2, muestran un decremento de los caudales, prácticamente en todos los meses, y de forma muy notable en verano. El aumento de la reserva de agua en el suelo, debida a la menor evapotranspiración que los nuevos escenarios simulan desde septiembre a diciembre, termina favoreciendo el incremento de la evapotranspiración, de mayo a agosto, pero no repercute en un aumento de los caudales. De hecho, en el cómputo anual se observa un aumento de la evapotranspiración (hasta un 5 % en O2) y un descenso, parecido, del caudal.

Por último, el escenario O3 plantea una sub-cuenca cubierta por bosque caducifolio y vegetación arbustiva (casi al 50 %) que, a escala anual, prácticamente no modifica la cantidad de caudal (es ligeramente superior). A escala mensual, sin embargo, se aprecia un claro aumento del caudal en verano (entre 8 y 18 %), y menor en otoño (<5 %), permaneciendo casi sin cambios en los meses más caudalosos (invierno y primavera). En cuanto a la evapotranspiración, a escala anual es algo menor que en la situación actual (2 %), con claro descenso en verano (hasta un 8 % en junio y julio), coincidiendo con el aumento del caudal (entre junio y octubre) llegando a superar el 20 % de aumento en el mes de julio. Sin embargo, la evapotranspiración aumenta en otoño (por debajo del 5 %), época en la que también los caudales aumentan, lo que hace pensar en un consumo de la reserva de agua (en el suelo, alimentando la evapotranspiración, y en el subsuelo, alimentando la escorrentía) que ha podido irse acumulando en las épocas más lluviosas (invierno y primavera).

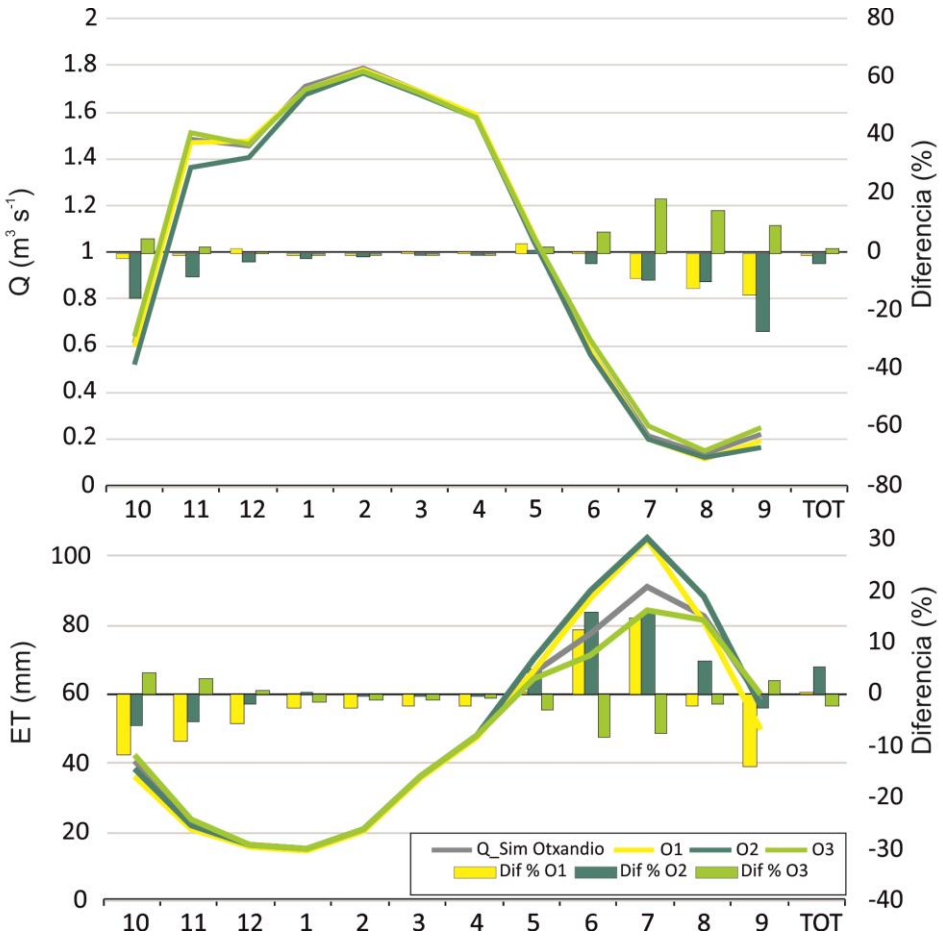

Figura 4.28. *En la parte superior, caudal medio ($m^3 s^{-1}$) y diferencia de caudal medio (%) mensual (octubre a septiembre, 1985-2015), obtenido de la simulación en la sub-cuenca de Otxandio con el uso del suelo actual (Q_Sim_Otxandio) y con los escenarios de usos O1, O2 y O3. En la parte inferior, evapotranspiración media (mm) y diferencia de la evapotranspiración media (%) mensual (octubre a septiembre, 1985-2015), obtenida de la simulación en la sub-cuenca de Otxandio con el uso del suelo actual (Q_Sim_Otxandio) y con los escenarios de usos O1, O2 y O3.*

De este análisis destaca la importancia que tiene la consideración de los cambios, y la variabilidad, en caudales y evapotranspiración a escala mensual, ya que la escala anual enmascara procesos de relevancia para la vegetación y para la escorrentía; normalmente lo que favorece a una perjudica a la otra, ya que la cantidad de agua a repartir viene impuesta. Destaca también la importancia de considerar el papel hidrológico del suelo (variación de humedad), en la medida que su reserva de agua puede favorecer el escalonamiento

temporal de procesos. En resumen, y centrándonos en la evapotranspiración a escala anual, podemos establecer un orden de usos del suelo, de menor a mayor capacidad de evapotranspiración: arbustivo -pasto/cereal - bosque.

En el caso de **Audikana** los escenarios de usos del suelo se han planteado considerando una evolución de la sub-cuenca hacia usos del suelo forestales. Actualmente el uso del suelo en la zona es predominantemente agrícola (cereal) y se han considerado los siguientes cambios:

- A1: El bosque caducifolio aumenta su superficie en la sub-cuenca de un 11 % a un 36 %.
- A2: Fundamentarme el uso del suelo en la sub-cuenca es forestal.
- A3: Es un posible escenario intermedio entre los dos anteriores, planteando que se abandona la actividad agrícola y la vegetación arbustiva ocupa su lugar.

Tal y como se ha mencionado con anterioridad, los escenarios A1, A2 y A3 plantean una evolución de la cuenca de principalmente agrícola a cuenca forestal. Estos escenarios supondrían, a escala anual, menores caudales que los obtenidos con los usos del suelo actuales, pero que en ningún caso superan el 10 % de pérdida de recurso hídrico. Al igual que en la sub-cuenca de Otxandio, es a escala mensual donde mayores diferencias se pueden observar, sobre todo en verano y otoño. En los meses de julio y agosto, en los tres escenarios planteados habría mayor caudal que en el actual, mientras que a partir de septiembre y hasta diciembre, el caudal sería menor. Este descenso de los caudales medios se registraría, incluso, entre enero y abril, aunque las diferencias con respecto a la situación actual serían mínimas.

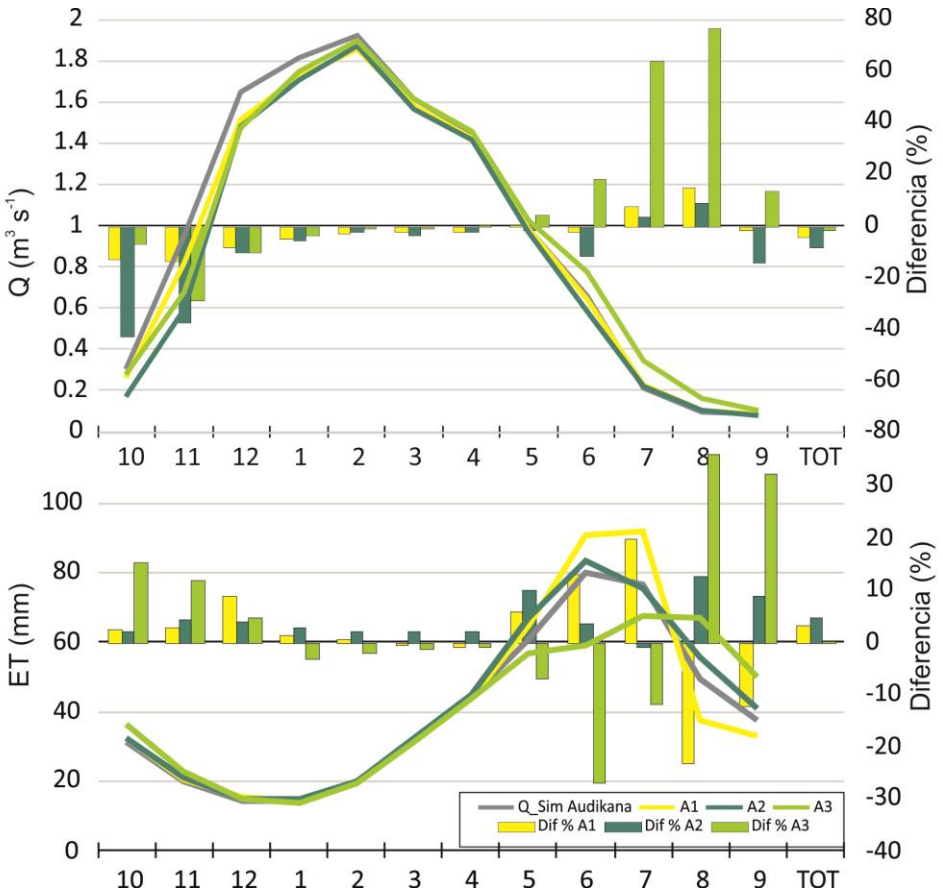

Figura 4.29. *En la parte superior de la figura, caudal medio (m^3 s^{-1}) y diferencia de caudal medio (%) mensual (octubre a septiembre, 1985-2015), obtenido de la simulación en la sub-cuenca de Audikana con el uso del suelo actual (Q_Sim_Audikana) y con los escenarios de usos A1, A2 y A3. En la parte inferior de la figura, evapotranspiración (mm) y diferencia de evapotranspiración media (%) mensual (octubre a septiembre, 1985-2015), obtenida de la simulación en la sub-cuenca de Audikana con el uso del suelo actual (Q_Sim_Audikana) y con los escenarios de usos A1, A2 y A3.*

En el escenario A1 la sub-cuenca sigue siendo fundamentalmente agrícola, aunque la superficie boscosa aumenta en decremento de la vegetación arbustiva. En este escenario se observan pocos cambios en los caudales con respecto a los obtenidos con Q_Sim Audikana. A escala anual, el caudal desciende (<5 %) por un aumento en la evapotranspiración. Debido a que en este escenario la superficie boscosa es mayor, en otoño la evapotranspiración aumenta de forma que los mayores descensos de caudal se registran en esta

estación (<15 %). En invierno, el descenso de caudal es prácticamente inapreciable, mientras que en primavera la evapotranspiración aumenta, lo cual no se traduce en los caudales que sufren descensos mínimos. Este hecho, podría deberse a la capacidad de regulación de agua de los bosques, que en los meses de invierno acumulan más agua que las zonas de cultivo y, por lo tanto, la cantidad de agua disponible en primavera es mayor. En el primer mes de verano, esta tendencia se mantiene, e incluso aumenta el caudal, sin embargo, en agosto, aunque el caudal aumente, la evapotranspiración desciende de forma importante (>20 %). Considerando que en este escenario tanto en primavera (desde mayo) como en julio el aumento de la evapotranspiración es notorio, se podría pensar que en agosto desciende debido a que el agua disponible por las plantas acumulada en el suelo durante el invierno y utilizada en primavera y julio se agota. Así, la evapotranspiración desciende en agosto y septiembre.

Bajo el escenario A2, siendo éste fundamentalmente boscoso, se obtendrían caudales medios anuales menores a los actuales (del orden del 10%). A escala mensual, como consecuencia del aumento de la evapotranspiración, los mayores descensos se observarían entre septiembre y diciembre y en el mes de junio. Por el mismo motivo, en menor medida, el caudal también disminuiría entre enero y mayo. En julio y agosto, aunque la evapotranspiración sea mayor en agosto, los caudales serían algo mayores. Este descenso de los caudales generalizado y el aumento de los mismos en los meses de verano podrían estar relacionados con que el modelo simula, bajo este escenario, un aumento del porcentaje de agua infiltrada en los suelos, y hacia el subsuelo, durante la mayor parte del año y, por lo tanto, un retardo mayor en el tiempo de tránsito de este agua hasta su llegada al río. Así, parte del déficit de caudal en invierno se repondría en verano, a la vez que aumenta la evapotranspiración desde el suelo.

En el escenario A3, donde aproximadamente el 85 % de la sub-cuenca está compuesta por vegetación arbustiva, a escala anual prácticamente no se observan diferencias respecto a Q_Sim Audikana. A escala mensual se registrarían mayores caudales medios en los meses de primavera-verano (de mayo a septiembre), debido a una menor demanda de agua de los arbustos, una

menor evapotranspiración, durante el invierno, y, sobre todo, la primavera y el principio del verano (julio) con respecto a los cultivos. Sin embargo, la diferencia (%) entre la demanda de agua de la vegetación arbustiva y el cultivo aumenta a partir de agosto porque el cereal obtiene su punto máximo de madurez y, por lo tanto, el modelo reduce su producción de biomasa hasta 0, mientras que el arbusto continúa produciendo biomasa y, por tanto, demandando agua. Por ello, a partir de septiembre los caudales medios son menores que los actuales. En resumen, y centrándonos en la evapotranspiración a escala anual, podemos establecer un orden de usos del suelo, de menor a mayor capacidad de evapotranspiración: arbustivo - cereal - bosque, similar al deducido para Otxandio.

A la vista de estos resultados, y con las precauciones debidas a las incertidumbres asociadas (a las propias de modelizar sistemas hidrológicos complejos hay que añadir las debidas a las simplificaciones asumidas en la modelización de estos escenarios, en los que al cambiar los usos del suelo no se han tenido en cuenta todos los aspectos añadidos que tales cambios pueden acarrear), resulta obvio que la ampliación espacial del bosque (escenarios O2 y A2) implica una disminución en los caudales (indicando una mayor evapotranspiración real que la de la actual ocupación de los suelos), lo cual, en principio, parece lógico. Hay que tener en cuenta, sin embargo, varias simplificaciones de partida en la simulación efectuada. Cuando se habla de ampliar el bosque, nos referimos a un bosque en estado ya maduro (sin considerar el propio crecimiento de los árboles), es decir, en una fase de menor consumo de agua que en las fases previas. Por otro lado, respecto a las necesidades hídricas de la vegetación, se han utilizado valores que el propio modelo SWAT proporciona (no hay que olvidar que SWAT es un modelo agro-hidrológico, en origen; pero no necesariamente deben ser los idóneos para las características del medio físico en las cuencas aquí consideradas).

En cualquier caso, insistimos en que el objetivo fundamental de este ejercicio de simulación era plantear la necesidad de considerar los cambios en los usos del suelo, sea cual sea su origen, como causas, añadidas a los cambios en el clima, de modificaciones en el régimen de caudales (estacional y anual),

modificaciones éstas que, incluso, pueden ser de diferente naturaleza en una cuenca y en otra, hasta cercana. De todas maneras, es una línea de investigación que hay que profundizar, tratando de ir aclarando las incertidumbres asociadas.

4.4.12 Conclusiones

En este estudio para evaluar los posibles efectos del cambio climático en la respuesta hidrológica de las sub-cuencas de Otxandio y Audikana (Cuenca del Zadorra) se han utilizado 16 proyecciones climáticas, surgidas de la combinación de 5 Modelos Generales de Circulación -GCM- (ACCESS1-0, BNU-ESM, MPI-ESM-LR, MPI-ESM -MR, CMCC-CESM), 2 métodos de downscaling (análogos AEMET -AN- y el downscaling estadístico -SDSM-) y 2 Trayectorias de Concentración Representativas (RCP 4.5 y RCP 8.5). La simulación hidrológica se ha realizado utilizando el modelo hidrológico numérico SWAT. Aunque exista una importante incertidumbre en los datos disponibles de caudal registrados en ambas sub-cuencas, los resultados de su calibración y validación han sido satisfactorios (1987-1994 y 2005-2015).

Existen numerosas fuentes de incertidumbre relacionadas con las proyecciones hidrológicas (GCM, método de downscaling, RCP, modelo hidrológico). De los resultados obtenidos en este estudio se pueden extraer algunas conclusiones. La diferencia existente entre los baseline de los modelos climáticos (1961-2000) y los datos meteorológicos observados en la estación de Urrunaga (en función de la época del año los modelos simulan más o menos lluvia; en primavera y verano sobreestiman la precipitación, en otoño la subestiman y en Invierno es aleatorio) evidencia la incertidumbre asociada a los GCM en el área de estudio. Además, el método de downscaling también ha resultado ser una importante fuente de incertidumbre. Los resultados de los mismos GCM, a priori, deberían mostrar mayores descensos de caudal al considerar el escenario de altas emisiones (RCP 8.5). Sin embargo, esto no ocurre siempre así puesto que el método de downscaling tiene mucha influencia en los resultados. Al menos a escala anual, en ambas sub-cuencas (Fig. 4.23 y 4.26), las proyecciones climáticas a las que se les ha aplicado el método de downscaling SDSM, simulan mayores descensos de caudal (comparando proyecciones del mismo RCP). Este

hecho es bastante significativo si tenemos en cuenta que el baseline de las proyecciones a las que se les ha aplicado el método SDSM simulan mayores caudales que a los que se les ha aplicado el método AN (Fig. 4.24 y 4.25). Esto quiere decir que las proyecciones futuras realizadas con el método de downscaling AN simulan caudales considerablemente mayores que los calculados mediante SDSM.

De los resultados obtenidos a partir de cinco GCM analizados, se puede decir que, a pesar de la excepción de algunas proyecciones, el caudal descenderá en todas las épocas del año y por consiguiente también lo hará a escala anual. Esta tendencia es más clara en la sub-cuenca de Audikana que en la de Otxandio.

En Otxandio, las proyecciones basadas en el método AN proyectan una diferencia respecto al baseline en los caudales anuales de entre -10 % y -12 % para el horizonte 2090 (Fig. 4.23). En cambio, las proyecciones basadas en el método de downscaling SDSM proyectan mayores descensos (entre -12 % y -17 %). Para el mismo periodo, en Audikana las proyecciones basadas en el método de AN proyectan descensos anuales de entre 12 % y 16 %y los basados en SDSM entre 13 % y 26 % (Fig. 4.26). En ambas sub-cuencas la estación que presenta la mayor disminución del caudal es Otoño (alrededor de -30% para 2090). Estas tendencias a la baja también se detectan en zonas de la región atlántica de Francia y la Península Ibérica, aunque generalmente los estudios de proyecciones hidrológicas realizados en estas áreas muestran descensos más importantes en invierno (Tabla 1.2).

Para el conjunto de las 16 proyecciones hidrológicas analizadas en Otxandio en los tres horizontes, el rango más amplio entre los valores mensuales más altos y más bajos de caudal ocurriría de noviembre a abril (rango de 0.78-1.5 m^3s^{-1} y 2.1-3.2 m^3s^{-1}, respectivamente). El rango más estrecho se daría en Verano (rango de 0.07-0.23 m^3s^{-1}). En Audikana, al igual que en Otxandio, el rango más amplio ocurriría entre noviembre y abril (rango de 0.2-1.1 m^3s^{-1} y 0.8-1.7 m^3s^{-1}, respectivamente) y el más estrecho se proyecta para Verano (entre 0.04-0.1 m^3s^{-1}).

Los resultados obtenidos en los análisis de tendencias realizados para los caudales medios y bajos muestran una alta probabilidad de descenso de los caudales medios (Qm) y aumento de la duración y la severidad de los caudales bajos (Q20) a escala anual, sobre todo para las proyecciones climáticas obtenidas bajo el RCP 8.5. A escala estacional, estas tendencias, disminución de caudal medio y aumento de la duración del periodo de aguas bajas, son muy claras en Primavera para ambos RCPs y en verano y en otoño para el RCP 8.5. Invierno es la estación del año que muestra una mayor incertidumbre en las tendencias observadas. Las mayores diferencias entre cuencas se dan en el otoño para el RCP 4.5, donde la cuenca de Otxandio, más forestada que la de Audikana, muestra una mayor incertidumbre en las tendencias.

El análisis preliminar realizado para estudiar la influencia de los usos del suelo en los recursos hídricos muestra que, aunque a escala anual las diferencias entre distintos escenarios no son grandes, los usos del suelo pueden tener un papel importante en la regulación del agua de la cuenca (variación de la humedad del suelo) sobre todo en caudales bajos. Esto puede ser muy importante desde el punto de vista de la gestión, puesto que tal y como se ha visto con anterioridad, en general las proyecciones hidrológicas futuras muestran tendencias que indican que la duración y sobre todo la severidad de los caudales bajos pueden aumentar.

4.5 REFERENCES

Abbaspour, K.C., Johnson, C.A., van Genuchten, M.T. 2004. Estimating uncertain flow and transport parameters using a sequential uncertainty fitting procedure. Vadose Zone J. 3 (4): 1340–1352. http://dx.doi.org/10.2113/3.4.1340.

Abbaspour, K.C., Vejdani, M., Haghighat, S. 2007a. SWAT CUP calibration and uncertainty programs for SWAT. International Congress on Modelling and Simulation (MODSIM). 7: 1603-1609.

Abbaspour, K.C., Yang, J., Maximov, I., Siber, R., Bogner, K., Mieleitner, J., Zobrist, J., Srinivasan, R. 2007b. Modelling hydrology and water quality in the pre-alpine/alpine Thur watershed using SWAT. Journal of Hydrology 333 (2–4): 413-430. http://dx.doi.org/10.1016/j.jhydrol.2006.09.014.

Abbaspour, K.C., Rouholahnejad, E., Vaghefi, S., Srinivasan, R., Yang, H., Kløve, B. 2015. A continental-scale hydrology and water quality model for Europe: Calibration and uncertainty of a high-resolution large-scale SWAT model. Journal of Hydrology 524 (0): 733-752. http://dx.doi.org/10.1016/j.jhydrol.2015.03.027.

Andréasson, J., Bergström, S., Carlsson, B., Graham, L.P., Lindström, G. 2004. Hydrological change: climate impact simulations for Sweden. A Journal of the Human Environment 33(4–5): 228–234.

Arnell, N.W. 1998. Climate change and water resources in Britain. Climate Change 39: 83–110.

Arnell, N.W. 1999. The effect of climate change on hydrological regimes in Europe: A continental perspective. Global Environmental Change 9 (1): 5-23. http://dx.doi.org/10.1016/S0959-3780(98)00015-6.

Arnell, N.W. 2011. Uncertainty in the relationship between climate forcing and hydrological response in UK catchments. Hydrology and Earth System Sciences 15 (3): 897-912. http://dx.doi.org/10.5194/hess-15-897-2011.

Arnold, J.G., Srinivasan, R., Muttiah, R.S., Williams, J.R. 1998. Large area hydrologic modeling and assessment – Part 1: model development. Journal of American Water Resources. As. 34 (1): 73–89. http://dx.doi.org/10.1111/j.1752-1688.1998.tb05961.x.

Arnold, J.G., Fohrer. N. 2005. SWAT2000: current capabilities and research opportunities in applied watershed modeling. Hydrological Processes 19: 563-572.

Arnold, J.G., Moriasi, D.N., Gassman, P.W., Abbaspour, K.C., White, M.J., Srinivasan, R., Santhi, C., Harmel, R.D., van Griensven, A., van Liew, M.W., Kannan, N., Jha, M.K. 2012. SWAT: Model use, calibration, and validation. Transactions of the ASABE 55 (4): 1491-1508.

ASCE. 1993. Criteria for evaluation of watershed models. J. Irriga- tion Drainage Eng. 119(3) : 429-442.

Ayala-Carcedo, F.J., Iglesias, A. 2000. Impactos del posible cambio climático sobre los recursos hídricos, el diseño y la planificación hidrológica en la España peninsular. El Campo De Las Ciencias y Las Artes 137: 201-222.

Basque Meteorological Agency: EUSKALMET http://www.euskalmet.euskadi.net

Bates, B.C., Kundzewicz, Z.W., Wu, S., Palutikof, J.P. 2008. Climate Change and Water, Technical Paper of the Intergovernmental Panel for Climate Change. IPCC. http://www.ipcc.ch/pdf/technical-papers/climate-change-water-en.pdf. Accessed 5 August 2015.

Bender, E.A., Case, T.J., Gilpin, M.E. 1984. Perturbation Experiments in Community Ecology: Theory and Practice. Ecology 65: 1–13. http://dx.doi.org/10.2307/1939452.

Bergstrom, S., Carlsson, B., Gardelin, M., Lindstro, G., Pettersson, A., Rummukainen, M. 2001. Climate change impacts on runoff in Sweden: assessments by global climate models, dynamical downscaling and hydrological modelling. Climate Research 16: 101–112.

Beven, K. 2011. I believe in climate change but how precautionary do we need to be in planning for the future? Hydrological Processes 25: 1517-1520.

Boorman, D.B., Sefton, C.E.M. 1997. Recognizing the uncertainty in the quantification of the effects of climate change on hydrological response. Climatic Change 35 (4): 415–434.

Boorman, D.B. 2003. Climate, Hydrochemistry and Economics of Surface-water Systems (CHESS): Adding a European dimension to the catchment modelling experience developed under LOIS. Science of the Total Environment. 314–316: 411–437. http://dx.doi.org/10.1016/S0048-9697(03)00066-4

Borah, D.K., Bera, M. 2004. Watershed-scale hydrologic and nonpoint-source pollution models: Review of applications. Trans. ASAE 47(3): 789–803.

Boswell, V.G. 1926. The influence of temperature upon the growth and yield of garden peas. Journal of the American Society for Horticultural Science 23: 162-168.

Bouraoui, F., Galbiati, L., Bidoglio, G. 2002. Climate change impacts on nutrient loads in the Yorkshire Ouse catchment (UK). Hydrology and Earth System Sciences 6(2):197–209. http://dx.doi.org/10.5194/hess-6-197-2002

Boyer, C., Chaumont, D., Chartier, I., Roy, A.G. 2010. Impact of climate change on the hydrology of St. Lawrence tributaries. Journal of Hydrology 384: 65-83. http://dx.doi.org/10.1016/j.jhydrol.2010.01.011.

Brauman, K.A., Daily, G.C., Duarte, T.K., Mooney, H.A. 2007. The Nature and Value of Ecosystem Services: An Overview Highlighting Hydrologic Services. Annual Review of Environment and Resources 32: 67–98. http://dx.doi.org/10.1146/annurev.energy.32.031306.102758.

Brierley, G.J., Fryirs, K. 2000. River style, a geomorphic approach to catchment characterization: implications for river rehabilitation in Bega Catchment, New South Wales, Aust. Environmental Management 25: 661–79.

Brigode, P., Oudin, L., Perrin, C. 2013. Hydrological model parameter instability: A source of additional uncertainty in estimating the hydrological impacts of climate change? Journal of Hydrology 476(0): 410-425. http://dx.doi.org/10.1016/j.jhydrol.2012.11.012.

Chave, P. 2001. The EU Water Framework Directive: An Introduction. IWA Publishing, London, UK.

Chen, J., Brissette, F.P., Leconte, R. 2011. Uncertainty of downscaling method in quantifying the impact of climate change on hydrology. Journal of Hydrology 401(3–4): 190-202. http://dx.doi.org/10.1016/j.jhydrol.2011.02.020.

Chen, H., Xu, C.Y., Guo, S. 2012. Comparison and evaluation of multiple GCMs, statistical downscaling and hydrological models in the study of climate change impacts on runoff. Journal of Hydrology 434-435: 36-45.

Coch, A., Mediero, L. 2015. Trends in low flows in Spain in the period 1949–2009. Hydrological Sciences Journal. 1-17. http://dx.doi.org//10.1080/02626667.2015.1081202.

Coulthard, T.J., Kirkby, M.J., Macklin, M.G. 2000. Modelling geomorphic response to environmental change in an upland catchment. Hydrological Processes 14: 2031–45.

Crane, M. 2003. Proposed development of Sediment Quality Guidelines under the European Water Framework Directive: a critique. Toxicology Letters 142: 195-206

Dibike, Y.B., Coulibaly, P. 2005. Hydrologic impact of climate change in the Saguenay watershed: comparison of downscaling methods and hydrologic models. Journal of Hydrology 307 (1–4): 145-163. http://doi.org/10.1016/j.jhydrol.2004.10.012.

Epelde, A.M., Cerro, I., Sanchez-Perez, J.M., Sauvage, S., Srinivasan, R., Antigueedad, I. 2015. Application of the SWAT model to assess the impact of changes in agricultural management practices on water quality. Hydrological Sciences Journal-Journal Des Sciences Hydrologiques 60: 825-843.

European Commission, 2000. Directive 2000/60/EC of the European Parliament and of the Council of 23 October 2000 establishing a framework for community action in the field of water policy. Official Journal of the European Union L327:1-/72. 22nd December 2000.

FAO, 1977. Guidelines for Soil Profile Description. Rome, Italy.

Farnsworth, K.L., Milliman, J.D. 2003. Effect of climatic and anthropogenic change on small mountainous rivers: the Salinas River example. Global and Planetary Change 39: 53-64.

Flato, G.M., Boer, G.J. 2001. Warming asymmetry in climate change experiments. Geophysics Research. Lett. 28: 195-198.

Fohrer, N., Haverkamp, S., Eckhardt, K., Frede, H. 2001. Hydrologic Response to land use changes on the catchment scale. Physics and Chemistry of the Earth, Part B: Hydrology, Oceans and Atmosphere 26: 577-582.

Fowler, H.J., Blenkinsop, S., Tebaldi, C. 2007. Linking climate change modelling to impacts studies: recent advances in downscaling techniques for hydrological modelling. International Journal of Climatology 27 (12): 1547–1578. http://dx.doi: 10.1002/joc.1556.

Gassman, P.W., Reyes, M.R., Green, C.H., Arnold, J.G. 2007. The Soil and Water Assessment Tool: Historical development, applications, and future research directions. Transactions of the ASABE 50(4): 1211–1250.

Geographical data base of the Basque Government, GEOEUSKADI; http://www.geo.euskadi.net

Giorgi, F., Mearns, L.O. 2002. Calculation of average, uncertainty range, and reliability of regional climate changes from AOGCM simulations via the ''reliability ensemble averaging'' (REA) method. Journal of Climate 15, 1141–1158. http://dx.doi.org/10.1175/1520-0442(2003)016%3C0883:COCOAU%3E2.0.CO;2.

Gobierno Vasco 2005. Mapa de erosión de suelos de la Comunidad Autónoma de Euskadi. Informe realizado por IDER Ingeniería y Desarrollo Rural, S.A. para el Departamento de Medio Ambiente y Ordenación del Territorio. Dirección de Biodiversidad y Participación Ambiental del Gobierno Vasco.

Görgen, K., Beersma, J., Brahmer, G., Buiteveld, H., Carambia, M., de Keizer, O., Krahe, P., Nilson, E., Lammersen, R., Perrin, C., Volken, D. 2010. Assessment of Climate Change Impacts on Discharge in the Rhine River Basin: Results of the RheinBlick2050 Project, CHR Report. 1–23, 229 pp, Lelystad. ISBN 978-90-70980-35-1.

Gosling, S.N., Taylor, R.G., Arnell, N.W., Todd, M.C. 2011. A comparative analysis of projected impacts of climate change on river runoff from global and catchment-scale hydrological models. Hydrology and Earth System Sciences 15: 279-294. http://dx.doi.org/10.5194/hess-15-279-2011.

Goubanova, K., Li, L. 2007. Extremes in temperature and precipitation around the Mediterranean basin in an ensemble of future climate scenario simulations. Global and Planetary Change 57: 27–42.

Gupta, H.V., Sorooshian, S., Yapo, P.C. 1999. Status of automatic calibration for hydrologic models: Comparison with multilevel expert calibration. Journal of Hydrological Engineering 4(2): 135-143.

Habets, F., Boe, J., Deque, M., Ducharne, A., Gascoin, S., Hachour, A., Martin, E., Page, C., Sauquet, E., Terray, L., Thiery, D., Oudin, L., Viennot, P. 2013. Impact of climate change on the hydrogeology of two basins in northern France. Climatic Change 121 (4): 771-785. http://dx.doi.org/10.1007/s10584-013-0934-x.

Hanratty, M.P., Stefan, H.G. 1998. Simulating climate change effects in a Minnesota agricultural watershed. Journal of Environmental Quality 27(6): 1524–1532. http://dx.doi.org/10.2134/jeq1998.00472425002700060032x

http://www.bizkaia.eus

Iñiguez, J., Sánchez-Carpintero, I., Val, R.M., Romeo, A., Basconesm, J.C. 1980. Mapa de suelos de Alava. Vitoria-Gasteiz: Diputación Foral de Alava-Departamento de Edafología de la Universidad de Navarra.

IPCC SRES. 2000. Special Report on Emissions Scenarios [Nebojsa, Nakicenovic, Swart (eds.)]. Cambridge University Press, UK. pp 570.

IPCC. 2001: Climate Change 2001: Synthesis Report. A Contribution of Working Groups I, II, and III to the Third Assessment Report of the Intergovernmental Panel on Climate Change [Watson, R.T. and the Core Writing Team (eds.)]. Cambridge University Press, Cambridge, United Kingdom, and New York, NY, USA, 398 pp.

IPCC. 2007 Climate Change 2007. Contribution of Working Groups I, II and III to the Fourth Assessment Report of the Intergovernmental Panel on Climate Change. [(Pachauri, R.K. and Reisinger, A. (eds.)]. IPCC, Geneva, Switzerland. pp 104

IPCC. 2013. Climate Change 2013: The Physical Science Basis. Contribution of Working Group I to the Fifth Assessment Report of the Intergovernmental Panel on Climate Change. [Stocker TF, D Qin, G-K Plattner, M Tignor, SK Allen, J Boschung, A Nauels, Y Xia, V Bex, PM Midgley (eds.)]. Cambridge University Press, Cambridge, United Kingdom and New York, NY, USA, 1535p.

IPCC. 2014: Climate Change 2014: Synthesis Report. Contribution of Working Groups I, II and III to the Fifth Assessment Report of the Intergovernmental Panel on Climate Change [Core Writing Team, R.K. Pachauri and L.A. Meyer (eds.)]. IPCC, Geneva, Switzerland, 151 pp.

Jha, M., Arnold, J.G., Gassman, P.W., Giorgi, F., Gu, R.R. 2006. Climate change sensitivity assessment on Upper Mississippi River Basin streamflows using SWAT. Journal of the American Water Resources Association 42(4): 997-1016. http://dx.doi.org/10.1111/j.1752-1688.2006.tb04510.x.

Johnson, F., Sharma, A. 2009. Measurement of GCM skill in predicting variables relevant for hydroclimatological assessments. J. Climate 22 (16): 4373-4328. http://doi.org/10.1175/2009JCLI2681.1.

Jothityangkoon, C., Sivapalan, M., Farmer, D.L. 2001. Process controls of water balance variability in a large semi-arid catchment: downward approach to hydrological model development. Journal of Hydrology 254:174–198. http://dx.doiorg/10.1016/S0022-1694(01)00496-6.

JRC (Joint Research Centre). 2004. Climate change and the European water dimension – a report to the European water directors: Chapter V. C. Climate Change, of Ecological Status and the Water Framework Directive.

Kaur, R., Singh, O., Srinivasan, R., Das, S.N., Mishra, K. 2004. Comparison of a subjective and a physical approach for identification of priority areas for soil and water management in a watershed: A case study of Nagwan watershed in Hazaribagh District of Jharkhand, India. Environmental Modelling & Assessment 9(2): 115-127.

Kay, A.L., Davies, H.N., Bell, V.A., Jones, R.G. 2009. Comparison of uncertainty sources for climate change impacts: flood frequency in England. Climatic Change 92: 41-63. http://dx.doi.org/10.1007/s10584-008-9471-4.

Kay, A.L., Jones, R.G., Reynard, N.S. 2006. RCM rainfall for UK flood frequency estimation II. Climate change results. Journal of Hydrology 318: 163-172. http://dx.doi.org/10.1016/j.jhydrol.2005.06.013.

Kendall, M.G. 1975. Rank Correlation Measures. Charles Griffin, London, UK.

Kiely, G. 1999. Climate change in Ireland from precipitation and streamflow observation. Adv. Water Resources Research 23: 141–151.

Lahmer, W., Pfutzner, B., Becker, A. 2001. Assessment of land use and climate change impacts on the mesoscale. Physics and Chemistry of the Earth, Part B. Hydrology, Ocean and Atmosphere 26 (7–8): 565–575. http://dx.doi.org/10.1016/S1464-1909(01)00051-X.

Leavesley, G.H. 1994. Modeling the effects of climate change on water resources – a review. Climatic Change 28: 159–177.

Lenderink, G., Buishand, A., Deursen, W. 2007. Estimates of future discharges of the river Rhine using two scenario methodologies: direct versus delta approach. Hydrology and Earth System Sciences 11 (3): 1145–1159. http://dx.doi.org/10.5194/hess-11-1145-2007.

Lespinas, F., Ludwig, W., Heussner, S. 2014. Hydrological and climatic uncertainties associated with modeling the impact of climate change on water resources of small Mediterranean coastal rivers. Journal of Hydrology 511: 403–422. http://dx.doi.org/10.1016/j.jhydrol.2014.01.033.

Macklin M.G., Lewin J. 2003. River sediments, great floods and centennial-scale Holocene climate change. Journal of Quaternary Science 182: 101–5.

Mann, H.B. 1945. Non-Parametric tests against trend. Econometrica 13: 245–259.

Mearns L.O., Giorgi, F., Whetton, P., Pabon, D., Hulme, M., Whetton, P.H. 2003. Guidelines for use of climate scenarios developed from Regional Climate Model experiments. Data distribution centre of the Intergovernmental Panel on Climate Change.

Meaurio, M., Zabaleta, A., Uriarte, J.A., Srinivasan, R., Antigüedad, I. 2015. Evaluation of SWAT models performance to simulate streamflow spatial origin. The case of a small forested watershed. Journal of Hydrology 525: 326-334. http://dx.doi.org/10.1016/j.jhydrol.2015.03.050.

Mediero, L., Kjeldsen, T.R., Macdonald, N., Kohnova, S., Merz, B., Vorogushyn, S., Wilson, D., Alburquerque, T., Bloeschl, G., Bogdanowicz, E., Castellarin, A., Hall, J., Kobold, M., Kriauciuniene, J., Lang, M., Madsen, H., Gul, G.O., Perdigao, R.A.P., Roald, L.A., Salinas, J.L., Toumazis, A.D., Veijalainen, N., Porarinsson, O. 2015. Identification of coherent flood regions across Europe by using the longest streamflow records. Journal of Hydrology 528: 341-360. http://.dx.doi.org/10.1016/j.jhydrol.2015.06.016.

Menzel, L., Burger, G. 2002. Climate change Scenarios and runoff response in the Mulde catchment (Southern Elbe, Germany). Journal of Hydrology 267(1-2): 53-64.

Merritt, W.S., Letcher, R.A., Jakeman, A.J. 2003. A review of erosion and sediment transport models. Environ. Modell. Softw. 18(8–9): 761–799.

Meybeck, M. 2005. Looking for water quality. Hydrological Processes 19: 331-338.

Michael, A., Schmidt. J., Enke, W., Deutschlander, T., Malitz, G. 2005. Impact of expected increase in precipitation intensities on soil-loss results of comparative model simulations. Catena 61(2-3): 155-164.

Milliman, J.D., Syvitski, J.P.M. 1992. Geomorphic/tectonic control of sediment transport to the ocean: the importance of small mountainous rivers. Journal of Geology 100: 525-544.

Mimikou, M.A., Baltas, E., Varanou, E., Pantazis, K. 2000. Regional impacts of climate change on water resources quantity and quality indicators. Journal of Hydrology 234: 95–109.

Mirus, B.B., Loague, K. 2013. How runoff begins (and ends): characterizing hydrologic response at the catchment scale. Water Resources Research 49: 2987–3006. DOI: 10.1002/wrcr.20218

Moriasi, D.N., Arnold, J.G., Van Liew, M.W., Bingner, R.L., Harmel, R.D., Veith, T.L. 2007. Model evaluation guidelines for systematic quantification of accuracy in watershed simulations RID H-4911-2011. Transactions of the ASABE 50(3): 885-900.

Murphy, J. 1999. An evaluation of statistical and dynamical techniques for downscaling local climate. Journal of Climate 12: 2256-2284.

Murphy, J. 2000. Predictions of climate change over Europe using statistical and dynamical downscaling techniques. Int. Journal of Climatology 20: 489-501.

Murphy, J.M., Sexton, D.M.H., Barnett, D.N., Jones, G.S., Webb, M.J., Stainforth, D.A. 2004. Quantification of modelling uncertainties in a large ensemble of climate change simulations. Nature 430 : 768–772. http://dx.doi.org/10.1038/nature02771.

Nash, J.E., Sutcliffe, J.V. 1970. River flow forecasting through conceptual models: Part 1. A discussion of principles. Journal of Hydrology 10(3): 282-290. http://dx.doi.org/10.1016/0022-1694(70)90255-6.

Nearing, M.A., Jetten, V., Baffaut, C., Cerdan, O., Couturier, A., Hernandez, M., Le Bissonnais, Y., Nichols, M.H., Nunes, J.P., Renschler, C.S., Souchère, V., van Ost., K. 2005. Modeling response of soil erosion and runoff to changes in precipitation and cover. Catena 61(2–3): 131–154. http://dx.doi.org/10.1016/j.catena.2005.03.007

Nijssen, B., O'donnell, G.M., Hamlet, A.F., Lettenmaier, D.P. 2001. Hydrologic sensitivity of global rivers to climate change. Climate Change 50: 143–175.

Peraza-Castro, M., Ruiz-Romera, E., Montoya-Armenta, L.H., Sanchez-Perez, J.M., Sauvage, S. 2015. Evaluation of hydrology, suspended sediment and Nickel loads in a small watershed in Basque Country (Northern Spain) using eco-hydrological SWAT model. Annales De Limnologie-International Journal of Limnology 51: 59-70.

Phan, D.B., Wu, C.C., Hsieh, S.C. 2011. Impact of climate change on stream discharge and sediment yield in Northern Vietnam. Water Resources Research 38(6): 827– 836. http://dx.doi.org/10.1134/S0097807811060133

Plan Hidrológico del Ebro. 1995. Ministerio de Agricultura, Alimentación y Medio Ambiente. Confederación Hidrográfica del Ebro. http://www.chebro.es/contenido.visualizar.do?idContenido=14093&idMenu=3048

Poff, N.L., Allan, J.D., Bain, M.B., Karr, J.R., Prestegaard, K.L., Richter, B.D., Sparks, R.E., Stromberg, J.C. 1997. The natural flow regime. BioScience 47: 769–784.

Qiu, L.-j., Zheng, F-l., Yin, R.S. 2012. SWAT-based runoff and sediment simulation in a small watershed, the loessial hilly-gullied region of China: capabilities and challenges. Int. Journal of Sedimentary Research 27: 226-234.

Ribalaygua, J., Pino, M.R., Pórtoles, J., Roldán, E., Gaitán, E., Chinarro, D., Torres, L. 2013. Climate change scenarios for temperature and precipitation in Aragón (Spain). Science of Total Environment 463–464: 1015-1030. http://dx.doi.org/10.1016/j.scitotenv.2013.06.089.

Roeckner, E., Oberhuber, J.M., Bacher, A., Christoph, M., Kirchner, I. 1996. ENSO variability and atmospheric response in a global coupled atmosphere–ocean GCM. Climate Dynamics 12: 737–754. http://dx.doi.org/10.1007/s003820050140.

Schmidli, J., Goodess, C.M., Frei, C., Haylock, M.R., Hundecha,Y., Ribalaygua, J., Schmith, T. 2007. Statistical and dynamical downscaling of precipitation: An evaluation and comparison of scenarios for the European Alps. Journal of Geophysical Research 112: D04105.

Sheshukov, A.Y., Siebenmorgen, C.B., Douglas-Mankin, K.R. 2011. Seasonal and annual impacts of climate change on watershed response using an ensemble of global climate models. Trans ASABE 54(6): 2209-2219.

Shorthouse, C., Arnell, N. 1999. The effects of climate variability on spatial characteristics of European river flows. Physics and Chemistry of the Earth 24 (1–2): 7–13.

Sivitsky, J.P.M., Kettner, A.J., Peckham, S.D., Kao, S-J. 2005. Predicting the flux of sediment to the coastal zone: application to the Langyang watershed, Northern Taiwan. Journal of Coastal Research 21(3): 580-587.

Stahl, K., Tallaksen, L.M., Gudmundsson, L., Christensen, J.H. 2011. Streamflow data from small basins: a challenging test to high resolution regional climate modeling, Journal of Hydrometeorology 12: 900–912.

SWC, Soil Water Characteristics; https://hrsl.ba.ars.usda.gov/soilwater/Index.htm

Takle, E.S., Jha, M., Anderson, C.J. 2005. Hydrological cycle in the Upper Mississippi River basin: 20th century simulations ny multiple GCMs. Geophysical Research Letters 32, L18407: 1-5. http://dx.doi.org/10.1029/2005GL023630.

Teng, J., Vaze, J., Chiew, F.H.S., Wang, B., Perraud, J.M. 2012. Estimating the relative uncertainties sourced from GCMs and hydrological models in modeling climate change impact on runoff. Journal of Hydrometeorology 13 (1): 122–139. http://dx.doi.org/10.1175/JHM-D-11-058.1.

Todd, M.C., Taylor, R.G., Osborn, T.J., Kingston, D.G., Arnell, N.W., Gosling, S.N. 2011. Uncertainty in climate change impacts on basin-scale freshwater resources – preface to the special issue: the Quest-GSI methodology and synthesis of results. Hydrology and Earth System Sciences 15: 1035-1046.

Touhami, I., Chirino, E., Andreu, J.M., Sánchez, J.R., Moutahir, H., Bellot, J. 2015. Assessment of climate change impacts on soil water balance and aquifer recharge in

a semiarid region in south east Spain. Journal of Hydrology 527 (0): 619-629. http://dx.doi.org/10.1016/j.jhydrol.2015.05.012.

Valverde, P., Serralheiro, R., de Carvalho, M., Maia, R., Oliveira, B., Ramos, V. 2015. Climate change impacts on irrigated agriculture in the Guadiana river basin (Portugal). Agricultural Water Management 152 (0): 17-30. http://dx.doi.org/10.1016/j.agwat.2014.12.012.

van Griensven, A., Meixner, T., Grunwald. S. 2006.A global sensitivity analysis tool for the parameters of multi-variable catchment models. Journal of Hydrology 324: 10-23. http://dx.doi.org/10.1016/j.jhydrol.2005.09.008.

Varanou, E., E. Gkouvatsou, E. Baltas, and M. Mimikou. 2002. Quantity and quality integrated catchment modelling under climatic change with use of Soil and Water Assessment Tool model. Journal of Hydrologic Engineering. 7(3): 228–244. doi:10.1061/ (ASCE)1084-0699(2002)7:3(228)

Veith, T.L., Sharpley, A.N., Weld, J.L. Gburek, W.J. 2005. Comparison of measured and simulated phosphorus losses with indexed site vulnerability. Trans. ASAE 48(2): 557-565.

Viles, H.A., Goudie, A.S. 2003. Interannual, decadal and multidecadal scale climatic variability and geomorphology. Earth-Science Reviews 61: 105–31.

von Storch H., Zorita, E, Cubasch, U. 1993. Downscaling of global climate change estimates to regional scales: an application to Iberian Rainfall in wintertime. Journal of Climate 6: 1161-1171.

Vörösmarty, C.J., McIntyre, P.B., Gessner, M.O., Dudgeon, D., Prusevich, A., Green, P., Glidden, S., Bunn, S.E., Sullivan, C.A., Liermann, C.R., Davies, P.M. 2010. Global threats to human water security and river biodiversity. Nature 467 (7315): 555-561. http://dx.doi.org/10.1038/nature09440.

Werritty A. 2002. Living with uncertainty: climate change, river flows and water resource management in Scotland. Science of the Total Environment 294: 29–40.

Wilby, R.L., Orr, H.G., Hedger, M., Forrow, D., Blackmore, M. 2006. Risk posed by climate change to the delivery of Water Framework Directive objectives in the UK. Environment International 32: 1043-1055. http://doi.org.10.1016/j.envint.2006.06.017.

Wilby, R.L., Charles, S.P., Zorita, E., Timbal, B., Whetton, P., Mearns, L.O. 2004. Guidelines for use of climate scenarios developed from statistical downscaling methods. Supporting material of the Intergovernmental Panel on Climate Change, available from the DDC of IPCC TGCIA, 27.

Wilby, R.L. 2005. Uncertainty in water resource model parameters used for climate change impact assessment. Hydrological Processes 19 (16): 3201–3219. http://doi.org/10.1002/hyp.5819.

Wilby, R.L., Harris, I. 2006. A framework for assessing uncertainties in climate change impacts: low-flow scenarios for the River Thames, UK. Water Resources Research 42 (2), W02419. http://dx.doi.org/10.1029/2005WR004065.

Willems, P., Vrac, M. 2011. Statistical precipitation downscaling for small-scale hydrological impact investigations of climate change. Journal of Hydrology 402: 193-205.

Williams, J.R. 1990. The erosion productivity impact calculator (EPIC) model: A case history. Philosophical Transactions of the Royal Society of London 329: 421-428.

www.geo.euskadi.eus

https://www.eea.europa.eu/publications/COR0-landcover

Xu, C.Y., Halldin, S. 1997. The effect of climate change on river flow and snow cover in the NOPEX area simulated by a single water balance model. Nordic Hydrology 28: 273–282.

Xu, J.X. 2003. Sediment flux to the sea as influenced by changing human activities and precipitation: Example of the Yellow River. China. Environmental Management 31(3): 328-341.

Zabaleta, A., Martínez, M., Uriarte, J.A., Antigüedad, I. 2007. Factors controlling suspended sediment yield during runoff events in small headwater catchments of the Basque Country. Catena 71: 179-190.

Zabaleta, A., Meaurio, M., Ruiz, E., Antigüedad, I., 2014. Simulation climate change impact on runoff and sediment yield in a small watershed in the Basque Country, northern Spain. Journal of Environmental Quality 43: 235–245. http://dx.doi.org/10.2134/jeq2012.0209.

Zabaleta, A., Meaurio, M., Morales, T., Epelde, A., Uriarte, J., Antiguedad, I (coord.). 2017. Vulnerabilidad hídrica: de las tendencias del pasado reciente a las del futuro. Adaptación a nuevos escenarios hidrológicos (EGHILUR). En: Colección KLIMATEK. Ed.: Ihobe, Sociedad Pública de Gestión Ambiental, Departamento de Medio Ambiente, Planificación Territorial y Vivienda, Gobierno Vasco. Bilbao, 125 pp..http://www.ingurumena.ejgv.euskadi.eus/contenidos/informacion/cclimatico_investigacion/es_def/adjuntos/02KLIMATEK.pdf

Zhu, Y.M., Lue, X.X., Zhou, Y. 2008. Sediment flux sensitivity to climate change: A case study in the Longchuanjiang catchment of the upper Yangtze River, China. Global and Planetary Change 60: 429-442.

5.

DISCUSSION AND CONCLUSIONS

5. DISCUSSION AND CONCLUSIONS

5.1 DISCUSSION AND CONCLUSIONS

The climate change has effects in hydrological systems and therefore, has influence in the quantity and quality of water, and sediments, which involves ecological, social and economic impacts. In this Thesis, the climate change effects in hydrological systems of four mountain headwater gauged catchments (from 4.6 km^2 to 185 km^2) located in the Atlantic region (Bay of Biscay) were evaluated.

To evaluate the climate change impacts on hydrological systems, the most common method is to introduce the climate projections derived from General Circulation Models (GCMs) into hydrological models. In this Thesis, the Soil and Water Assessment Tool (SWAT) was selected to perform the discharge and

sediments projections. Nevertheless, before using the model to perform the future projections, an **evaluation of its performance to model hydrological systems** (chapter *3. Evaluation of the performance of the hydrological model*) in a Cantabrian-type catchment (Aixola) was carried out. The catchment is characterized by being small (4.6 km^2) and forested. The results show that although not having an in depth knowledge on catchment characteristics, it is possible to obtain *satisfactory* discharge and sediment yield daily simulation for the outlet, although the peaks were underestimated.

To obtain better results, with the electrical conductivity (EC) registered in Aixola stream a conductivity-based mass balance (CMB) approach was applied and, with this methodology, the discharge in different sub-basins of the catchment and the baseflow/surface runoff rate were calculated. Thus, when CMB based discharge data were used in the calibration, the streamflow spatial distribution was simulated accurately and the results for the outlet were *very good*, obtaining a good fit between the observed and simulated discharge for high and low flows, also in driest seasons. In addition, the simulated baseflow/surface runoff rate was similar to the calculated with the CMB approach, and, as a result, hydrological processes seemed to be well simulated.

Therefore, field data (soil physical characteristics and water physico-chemical characteristics) helps achieving better and more reliable results. This demonstrates that it is possible to obtain good daily simulation results with SWAT model in small and forested catchments.

These catchments (small and forested), typical in the Cantabrian Watershed (Bay of Biscay), usually show a quick response to precipitation. A sub-daily modelling could take into account the precipitation intensity and better simulate the rapid response of these small catchments to precipitation. For that reason, an evaluation of **hourly simulation of discharge and sediments** (chapter *3*, section *3.6 Sub-daily streamflow and sediment load simulation*) in Aixola catchment was carried out. The hourly discharge simulation results are *very good*. Considering the suspended sediments simulation, the amount of sediment transported by water in a day is simulated *very good* but the timing of sediment transport needs

to be improved. It is not easy to obtain clear conclusions from the analysis made to the performance of the model **in different types of storm events**. However, it seems that the antecedent saturation (soil moisture conditions) of the catchment plays an important role; when the saturation is high the discharge simulation performance is better.

Zabaleta & Antiguedad (2013) observed in Aixola catchment that runoff coefficients tended to be significantly higher in winter than in summer, with efficiency of the precipitation to generate runoff becoming lower in dryer conditions. Therefore, it could be interpreted that the sub-daily simulation performed with SWAT does not simulate well soil moisture recharge and evapotranspiration processes, probably because soil water and evapotranspiration estimation routines are performed by SWAT at daily time-step. To obtain more definitive conclusions, it would be advisable to compare these results with other studies and observe if they achieve good discharge simulation in low soil moisture conditions. However, there are not many research works where SWAT is run on a sub-daily time-step, specially over long periods, and its performance in different types of events is evaluated.

To evaluate the impacts of climate change in hydrological systems of the Bay of Biscay, climate projections derived from an ensemble of General Circulation Models (GCMs) from different climate modelling projects (PRUDENCE, ENSEMBLES and CMIP5), downscaled with different methods (regional and statistical) and considering various emission scenarios or Regional Concentration Pathways (RCPs) were used. For the purpose of studying these impacts, the results of the projections (discharge and sediments) were grouped into three consecutive 30-year horizons: 2030s, 2060s and 2090s. The future **hydrological projections indicate that the discharge would decrease with respect to the baseline** (1961-2000) (chapter *4. Evaluation of climate change impacts on water resources and sediment yield*). The difference between the baseline and future projections is higher when the century draws on. Thus, considering the general results, annually the discharge is expected to decrease, on average, 6% for 2030s, 11 % for 2060s and 18 % for 2090s. Seasonally, the lowest decrease, as it happens in other zones of the Atlantic region, is projected

for winter and it is followed by spring, and summer (Table 5.1). **Autumn is the season that projects the highest decrease** which is a fairly consistent result, because it is possible to observe it in all the studied catchments and in discharge projections performed with different climate modelling projects. These annual and seasonal results are slightly different from previous studies undertaken in the Atlantic region of France and the north of the Iberian Peninsula (Table 1.2), where most of the research works show that the highest discharge decreases occur in summer, followed, depending on the study area, by autumn or spring. In any case, an extension of the driest season can be expected (from summer to autumn), with lower discharges and higher duration of the low flow period.

	AUTUMN	WINTER	SPRING	SUMMER	YEAR
2030s	-14	-1	-2	-5	-6
2060s	-21	-6	-8	-13	-11
2090s	-25	-12	-18	-20	-18

Table 5.1. *Summary of the discharge differences (%) in mean values, between baseline and future projections. The values have been calculated using all the discharge projections for all the analysed catchments, except for those that project more discharge than the baseline.*

From the analysis performed to the high (>Q80), mean (Qm) and low (<Q20) flows, broadly it seems that, considering all the century (2011-2100), the high and mean flow duration (days) would decrease annually, in autumn, winter and spring and low flow duration would increase annually, in autumn, summer and probably in spring, which is indicating a trend of greater influence of the low part of the hydrograph. Using the historical discharge series registered in 117 gauging stations located in the Atlantic region (Bay of Biscay), a recent research to identify hydrological signs of changes in climate (Zabaleta et al., 2017) was carried out. The research was focused in mean and low flows. For the period between 1955-1956 and 2014-2015 the results showed a decrease in Qm and an increase of the duration of Q20 annually and in practically all the seasons. Thus, it seems that, although not in all the seasons, these trends would continue in the future.

The **future projections** on **suspended sediment yield are highly uncertain** (chapter *4*, section *4.2 simulation climate change impact on streamflow and sediment yield in Aixola catchment*). Most of the analysed projections indicate that

the sediment would decrease with respect to the baseline, on average 11 % for 2030s, 21 % for 2060s and 32 % for 2090s.

In this Thesis, during hydrological projections performance, it was assumed that there will be no **changes in land use** and management conditions. The land use has influence on the soil characteristics and, consequently, on the hydrological response and, therefore, it has an impact on the predictions of the effects of climate change. That is why, in this research a first approximation to the study of the effects of the land use in the hydrology of some catchments of the study area was made. In order to perform this study with less uncertainty, instead of including land use changes in future climate projections, the analysis was performed for the past; in this way, it is possible to isolate the influence of land uses on discharge. The results show that although on an annual scale the differences between different land use scenarios (forest, pasture, exotic plantations) are not high, land use may play an important role in the water regulation capacity of the catchment, especially in the low flow period (summer and the beginning of autumn). This should be considered in territorial and hydrological planning since, as it has been seen above, in general, future hydrological projections show that the highest discharge decreases would occur, precisely, in autumn, when the duration of the low flow period may also increase.

Previous studies have highlighted the degree of **uncertainty** involved in different climate-change scenarios and the use of different methodological approaches to assess potential impacts (e.g. IPCC, 2013). Uncertainties that accompany the evaluation of climate change impacts on hydrology can be found at all levels of the process, that is, 1) in the emission scenarios or Regional Concentration Pathways (RCPs), 2) global climatic projections, 3) downscaling methods and 4) hydrological simulations. The quantitative assessment of the uncertainties associated with future hydrological projections is complicated and this lies outside the scope of this Thesis, nevertheless it is possible to perform a qualitative evaluation.

The highest sources of uncertainty come from the emission scenarios/RCPs and the climate models. In this sense, the results of this Thesis are subject to

the information provided by the corresponding meteorological agencies. As far as it was possible, an attempt has been made to select the GCMs that best fit with the climate conditions of the study area. Nevertheless, it is important to have in mind that the Bay of Biscay is a complex climate zone due to the influence of the Cantabrian sea and the proximity of the Pyrenees, besides, it is located in the transition zone of the climate projections from GCMs for the Atlantic region. Thus, in addition to the uncertainty inherent to the GCMs it is necessary to consider the high uncertainty associated to the specific location of the study area.

The hydrological projections performed in this Thesis also show **the high source of uncertainty of the downscaling methods**. On the one hand, the precipitation projections (baseline, 1961-2000) from ENSEMBLES project, which were regionalized (RCMs), fit better with the observed precipitation than those derived from CMIP5 project. Nevertheless, as a consequence of the bias-correction (linear-scaling approach) applied to the climate projections, the hydrological projections performed with both sources of data are similar on average values. Hence, when linear-scaling approach is applied, there are not high differences between the baseline discharge projections obtained from regionalized climate projections and non-regionalized ones. But as the linear-scaling approach do not modify the daily distribution of climate variables, the regionalization or the non-regionalization of the climate projections will affect to the high and low flows study.

On the other hand, in addition to the eventual regionalizations, all the climate projections used in this Thesis have been statistically downscaled by the Spanish Meteorological Agency (AEMET) using two methods, the AEMET analogues (AN) and the Statistical Downscaling Method (SDSM). In general, the climate projections downscaled with SDSM method fit better with the observed climate variables and practically always predict a higher discharge decrease than AN method in future hydrological projections. Consequently, the statistical downscaling method used is a high source of uncertainty.

The hydrological modelling, although to a lesser extent, is another source of uncertainty. The methodology used in this Thesis to calibrate and validate the

model was stricter than in conventional modelling. Thus, it is intended to reduce, as far as possible, the uncertainty associated to the hydrological modelling. The steps carried out were: 1) the hydrological model performance was evaluated, 2) considering the objectives, the best statistical indices to evaluate the performance of the simulation were selected, 3) the simulation results were evaluated for all the period and also for the driest (high "aridity index") and wettest years (low "aridity index") and 4) the simulation performance was evaluated not only for total discharge but also for base flow and surface runoff.

All the aforementioned uncertainties have important implications for decisions to be taken in terms of adaptation. Nevertheless, as Beven (2011) suggests, adaptation strategies should be adopted despite uncertainties, taking into account what level of risk we are prepared to accept and how expensive the adaptation to different scenarios might be. Moreover, as many of the impacts of the climate change would not be noticeable in the near future (Wilby et al., 2006), decision tools should be improved in order to more robustly capture future uncertainties.

This Thesis was focused in a **transition area where climate projections have a high associated uncertainty** and the number of research works on hydrological impacts of climate change is scarce (Table 1.2). The results obtained show the need to consider a wide range of climate projections focusing not only on annual values but also on seasonal variation of discharge. This enables a better approximation of future distribution of freshwater resources. This approximation, together with the consideration of the extremes of the hydrograph in the analysis, highlighted **the need to understand better the lower part of the hydrograph, where the related uncertainties are high and where the land use can play and important role**. This would allow a better planning of future measures in terms of water quantity and quality in catchments of the Atlantic region (Bay of Biscay).

5.2 PERSPECTIVE WORK AND RECOMMENDATIONS

Taking into account that in the Atlantic region (Bay of Biscay) the small catchments with quick response to precipitation are predominant, the sub-daily time-step modelling could be a good option. Nevertheless, usually it is difficult to obtain sub-daily field data (with enough quality) to perform the modelling. In addition, the calibration process is longer and more complicated than at daily time-step. Even so, the capability of SWAT to simulate individual storm events and perform continuous simulations is very useful because it is possible to capture processes that occur in short time intervals while investigating long term impacts. Therefore, **continuing with sub-daily simulation performance in different storm events could help in the identification simulation processes that need to be improved**.

Considering the climate change effects on the hydrological systems of the Atlantic region (Bay of Biscay), being this a high uncertainty region where there is a scarcity in research works of this type, it is necessary to continue with this type of studies in more catchments, prioritizing those that have long series of discharge and sediment measurements with enough data quality. To do so, **more accurate climate projections are needed**. In this sense, the administration and meteorology agencies should take the responsibility to perform the regionalization of as much GCMs as possible considering the climate variability of the Bay of Biscay.

The methodology used to obtain the hydrological projections in this Thesis was established to reduce the uncertainty as far as possible. Nevertheless, it is **necessary to gradually reduce the existing uncertainties**. For example, working with more climate projections (GCMs, RCPs, downscaling methods) than those used in this Thesis. It would also be recommendable the use of more models to perform the hydrological projections. Note, that as it was demonstrated in this Thesis, **field data are necessary to achieve more reliable simulations** and consequently, to reduce the uncertainties related to the hydrological modelling. Therefore, the use of field data allows a better understanding of

hydrological processes that occur in the catchment and thus, performing hydrological projections with less uncertainty.

Additionally, to study the affection of climate change in the ecological status of water bodies and evaluate if they will meet the environmental quality standards, the investigation of future suspended sediment transport is essential. In this regard, it would be convenient to continue with the first attempt presented in this Thesis to estimate future changes in sediment yields. Therefore, to evaluate the climate change impacts on hydrological systems, a more integrated research should be done, focusing not only on water quantity but also on its quality.

In this Thesis, a first approximation of the land use influence on the hydrology of catchments of the study area was performed. The results pointed out the important role of the land use in the soil water regulation, specially at low flow periods. Hence, it is necessary to simulate different land use scenarios, and consider them back in time (to separate the hydrological effect of the land use from future climate projections) and forward (considering the effect of both changes: land use and climate), with all the uncertainties involved in the projection of future territorial planning decisions. However, when considering land use changes, changes on soil properties, and hence, on the hydrological functions of soils, should also be taken into account. In this sense, more research is needed on the land use/land management-soil properties relations and on the application of that knowledge to hydrological modelling. Advances on that direction would improve the results of hydrological modelling and, undoubtedly, would help establishing measures on a territorial scale to mitigate adverse hydrological effects that may occur in the future.

5.3 REFERENCES

Beven, K.J. 2001. How far can we go in distributed hydrological modeling? Hydrology and Earth System Sciences. 5: 1-12.

IPCC, 2013: Climate Change 2013: The Physical Science Basis. Contribution of Working Group I to the Fifth Assessment Report of the Intergovernmental Panel on Climate Change [Stocker, T.F., D. Qin, G.-K. Plattner, M. Tignor, S.K. Allen, J. Boschung, A. Nauels, Y. Xia, V. Bex and P.M. Midgley (eds.)]. Cambridge University Press, Cambridge, United Kingdom and New York, NY, USA, 1535 pp. doi:10.1017/CBO9781107415324.

Wilby, R.L., Harris, I. 2006. A framework for assessing uncertainties in climate change impacts: low-flow scenarios for the River Thames, UK. Water Resources Research. 42 (2), W02419. http://dx.doi.org/10.1029/2005WR004065.

Zabaleta, A., Antiguedad, I. 2013. Streamflow response of a small forested catchment on different timescales. Hydrology and Earth System Sciences. 17(1): 211-223.

Zabaleta, A., Meaurio, M., Morales, T., Epelde, A., Uriarte, J., Antiguedad, I (coord.). 2017. Vulnerabilidad hídrica: de las tendencias del pasado reciente a las del futuro. Adaptación a nuevos escenarios hidrológicos (EGHILUR). En: Colección KLIMATEK. Ed.: Ihobe, Sociedad Pública de Gestión Ambiental, Departamento de Medio Ambiente, Planificación Territorial y Vivienda, Gobierno Vasco. Bilbao, 125 pp..http://www.ingurumena.ejgv.euskadi.eus/contenidos/informacion/cclimatico_investigacion/es_def/adjuntos/02KLIMATEK.pdf

APPENDIX

APPENDIX 1

Results of the analysis performed to the soils of Aixola catchment

Identif_Cliente	Arena gruesa, %	Arena Fina, %	Limo, %	Arcilla, %	Clasificación	% elementos gruesos	pH 1:2.5	Materia Orgánica, %
018	-	-	-	-	-	-	6.88	1.74
019	-	-	-	-	-	-	5.85	0.95
020	-	-	-	-	-	-	7.24	0.31
004	-	-	-	-	-	-	8.26	0.69
006	-	-	-	-	-	-	6.36	0.43
007	-	-	-	-	-	-	5.57	0.21
008	-	-	-	-	-	-	6.44	0.17
012	-	-	-	-	-	-	6.49	1.25
013	-	-	-	-	-	-	7.48	0.20
014	-	-	-	-	-	-	7.69	0.20
016	-	-	-	-	-	-	7.15	1.53
017	-	-	-	-	-	-	8.00	1.38
003	-	-	-	-	-	-	8.40	-
005	-	-	-	-	-	-	5.44	-
015	-	-	-	-	-	-	7.54	-
B8	8,93	31,51	38,54	21,02	Franca	7,10	4.71	2.34
TDR4	1,94	27,17	45,12	25,77	Franca	0,86	5.75	5.15
B16	6,84	25,87	42,36	24,93	Franca	3,84	6.49	3.09
B17	6,93	13,63	34,00	45,44	Arcillosa	2,68	5.14	2.07
TDR6	7,55	36,44	36,67	19,34	Franca	2,54	4.35	5.12
TDR2	3,69	14,89	46,70	34,72	Franco-arcillo-limosa	1,15	5.14	3.09

Identif_Cliente	Materia Orgánica, %	N, %	Relación C/N	P, ppm	Carbonatos, %	Caliza, %	Aluminio, me1/100g	Sat. Al %	mg N-NO3/kg	mg N-NH4/kg	M.S. %
018	1.74	0.11	9.20	6.83	-	-	-	-	-	-	-
019	0.95	0.08	6.90	3.83	-	-	-	-	-	-	-
020	0.31	0.05	3.60	2.48	-	-	-	-	-	-	-
004	0.69	0.03	13.37	3.79	50.70	8.71	-	-	-	-	-
006	0.43	0.05	5.00	1.05	-	-	-	-	-	-	-
007	0.21	0.03	4.07	0.63	-	-	1.31	40.07	-	-	-
008	0.17	0.04	2.47	6.66	-	-	-	-	-	-	-
012	1.25	0.12	6.06	5.96	-	-	-	-	-	-	-
013	0.20	0.06	1.94	5.49	-	-	-	-	-	-	-
014	0.20	0.05	2.33	12.96	0.81	-	-	-	-	-	-
016	1.53	0.10	8.90	8.18	-	-	-	-	-	-	-
017	1.38	0.07	11.46	4.01	17.08	-	-	-	-	-	-
003	-	0.08	-	1.59	2.32	-	-	-	-	-	-
005	-	0.08	-	1.18	-	-	0.62	12.42	-	-	-
015	-	0.08	-	3.00	1.62	-	-	-	-	-	-
B8	2.34	0.13	10.47	< 0,2	-	-	5.68	79.89	< 1,5 *	0.68	81.85
TDR4	5.15	0.39	7.68	14.89	-	-	0.53	4.70	3.84	4.91	71.71
B16	3.09	0.23	7.81	37.29	-	-	-	-	1.61	3.02	79.42
B17	2.07	0.15	8.02	<0,2	-	-	6.99	64.65	< 1,5 *	0.80	73.68
TDR6	5.12	0.25	11.91	1.27	-	-	8.05	81.66	20.13	0.17	79.81
TDR2	3.09	0.17	10.57	< 0,2	-	-	4.54	57.43	< 1,5 *	0.29	79.71

APPENDIX 2

Annual and seasonal trends detected for the duration (days) of the period below Q20 and above Q80:

2011-2040:

		RCP 4.5						
		ACCESS 1-0_AN	BNU-ESM_AN	BNU-ESM_SDSM	MPI-ESM-RL_AN	MPI-ESM-RL_SDSM	MPI-ESM-MR_AN	MPI-ESM-MR_SDSM
Q20	YEAR	-0.31	-0.36	0.07	-0.54	-0.44	0.96	0.88
	AUTUMN	-0.48	0.58	-0.78	0.87	0.58	0.77	0.95
	WINTER							
	SPRING	0.86	-0.16	0.31	-0.41	-0.78	0.48	0.49
	SUMMER	-0.22	-0.64	0.16	-0.66	-0.70	0.66	0.76
Q80	YEAR	-0.72		0.25		0.41	0.10	-0.66
	AUTUMN	-0.54	-0.39	-0.41	0.51	0.16	-0.68	-0.88
	WINTER	-0.46	0.00	0.22	0.19	0.31	0.60	-0.01
	SPRING		0.25	0.79		-0.39	-0.04	-0.90
	SUMMER	-0.70						

2011-2060:

		RCP 4.5						
		ACCESS1-0_AN	BNU-ESM_AN	BNU-ESM_SDSM	MPI-ESM-RL_AN	MPI-ESM-RL_SDSM	MPI-ESM-MR_AN	MPI-ESM-MR_SDSM
Q20	YEAR	-0.39	0.02	-0.99	0.43	-0.20	0.93	0.99
	AUTUMN	0.26	0.25	-0.73	0.98	0.33	0.65	0.83
	WINTER							
	SPRING	0.25	-0.87	-0.74	-0.29	-0.38	0.96	0.61
	SUMMER	-0.96	0.47	-0.99	0.15	-0.23	0.65	0.96
Q80	YEAR	-0.93	-0.81	0.97	-0.91	-0.59	-0.67	-1.00
	AUTUMN	-0.79	-0.90	0.54	-0.01	0.14	0.04	-0.98
	WINTER	-0.64	-0.65	0.57	-0.72		-0.66	-0.68
	SPRING		0.80	0.81	-0.97	0.08	-0.73	-1.00
	SUMMER	-0.39			-0.10	-0.93		

		RCP 8.5								
		ACCESS 1-0_AN	BNU-ESM_AN	BNU-ESM_SDSM	MPI-ESM-RL_AN	MPI-ESM-RL_SDSM	MPI-ESM-MR_AN	MPI-ESM-MR_SDSM	CMCC-CESM_AN	CMCC-CESM_SDSM
Q20	**YEAR**	-0.84	-0.56	0.60	-0.41	0.56	1.00	1.00	-0.58	-0.64
	AUTUMN	0.54	-0.51	0.71	-0.28	0.83	0.97	0.98	0.08	-0.18
	WINTER									
	SPRING	-0.37	-0.05	0.72	0.53	0.86	0.30	0.29	-0.51	-0.33
	SUMMER	-0.87	-0.31	0.31	-0.77	0.07	0.75	0.82	-0.33	-0.54
Q80	**YEAR**	0.41	0.00	-0.39	-0.41	-0.72	-0.97	-0.97	0.99	0.98
	AUTUMN	0.00	0.28	0.22	0.10	-0.79	-0.99	-1.00	0.73	0.86
	WINTER	0.39	-0.31	-0.31	-0.46	-0.60	-0.84	-0.82	0.90	0.72
	SPRING	0.96	0.25	-0.09	0.51	0.13	0.22	0.13	0.96	0.98
	SUMMER	-0.62								

		RCP 8.5								
		ACCESS1-0_AN	BNU-ESM_AN	BNU-ESM_SDSM	MPI-ESM-RL_AN	MPI-ESM-RL_SDSM	MPI-ESM-MR_AN	MPI-ESM-MR_SDSM	CMCC-CESM_AN	CMCC-CESM_SDSM
Q20	YEAR	-0.99	-0.92	-0.08	0.27	0.97	0.99	0.99	-0.79	-0.63
	AUTUMN	0.26	-0.68	-0.30	0.40	0.08	0.20	0.22	-0.02	0.19
	WINTER		0.99	-0.56	-0.56					
	SPRING	0.00	0.77	0.91	-0.65	0.40	0.85	0.95	-0.32	0.02
	SUMMER	-1.00	-0.95	-0.74	-0.07	0.98	0.93	0.96	-0.80	-0.70
Q80	YEAR	-0.25	-0.65	-0.97		0.00	-0.99	-0.98		0.81
	AUTUMN	0.17	0.52	-0.17	0.22	-0.50	-0.83	-0.99	0.86	0.81
	WINTER	0.83	-0.92	-0.72	-0.32	0.26	-1.00	-0.79	0.62	0.78
	SPRING	-0.65	-0.07	-0.98		0.18	-0.70	-0.82	-0.79	-0.79
	SUMMER									

Annual and seasonal trends detected for the duration (days) of the period below Q20 and above Q80, in the top for the period 2011-2040 and in the bottom for 2011-2060.

APPENDIX 3

The calibration and validation hydrological simulation (m^3 s^{-1}) results for Otxandio and Audikana catchments.

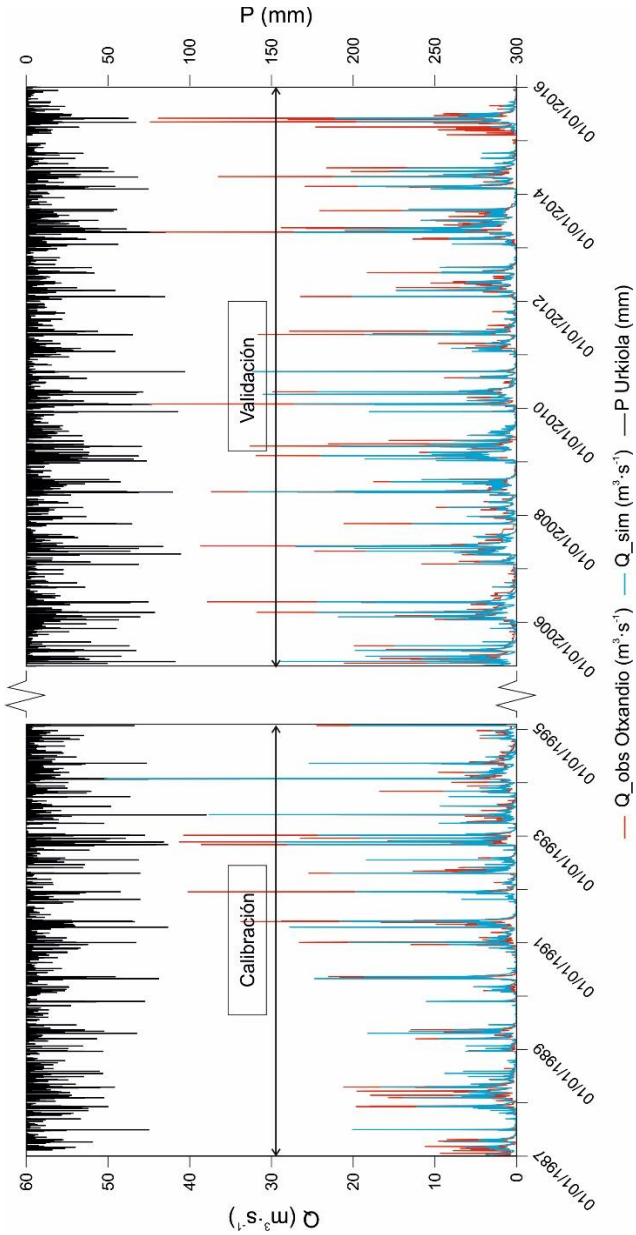

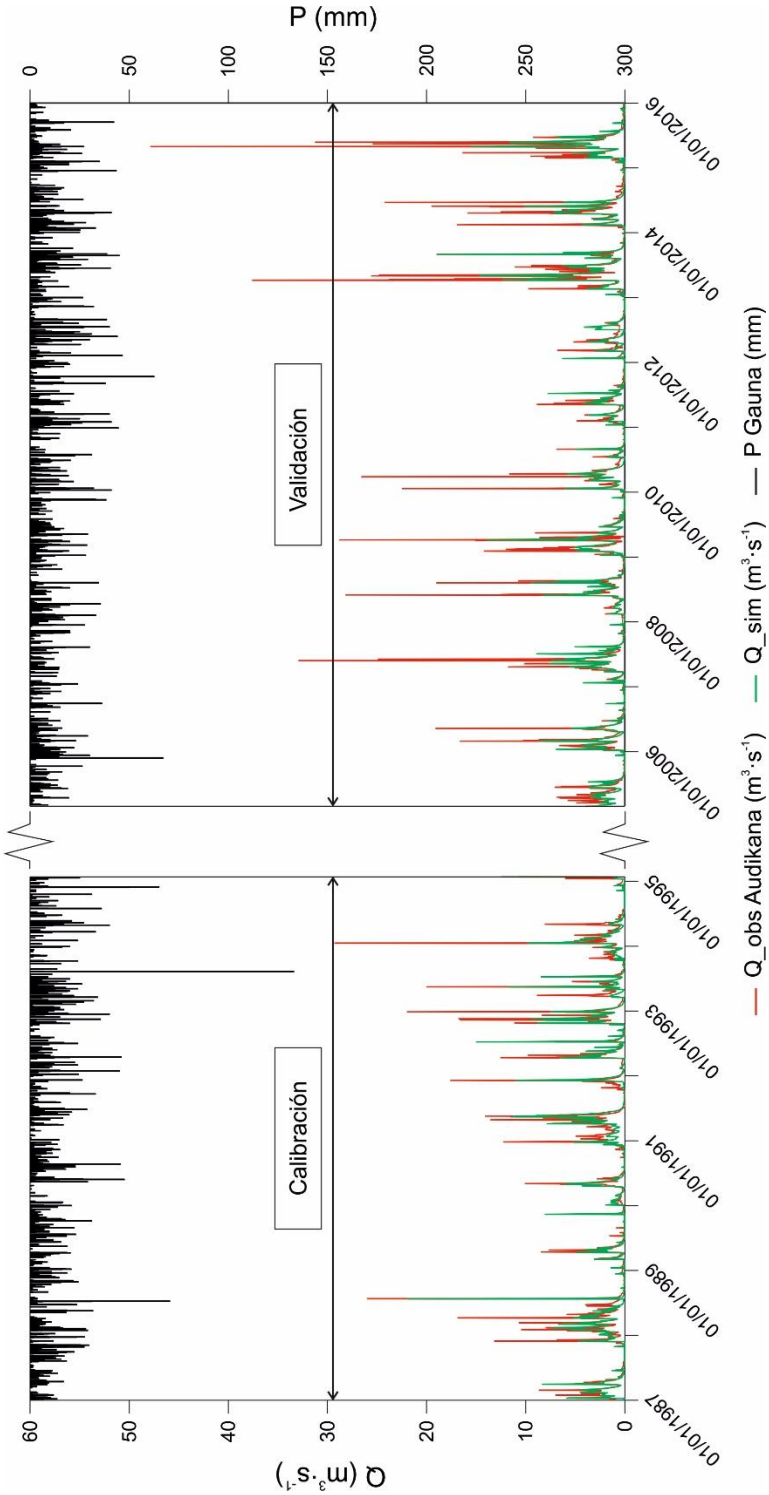
P (mm)
0
50
100
150
200
250
300
Validación
Calibración
Q (m³·s⁻¹)
60
50
40
30
20
10
0
01/01/1987
01/01/1989
01/01/1991
01/01/1993
01/01/1995
01/01/2006
01/01/2008
01/01/2010
01/01/2012
01/01/2014
01/01/2016
Q_obs Audikana (m³·s⁻¹)
Q_sim (m³·s⁻¹)
P Gauna (mm)

APPENDIX 4

Discharge difference (%) between the 16 hydrological projections (CMIP5) and its respective baseline simulations, divided into three 30-year horizons (2030s, 2060s, 2090s).

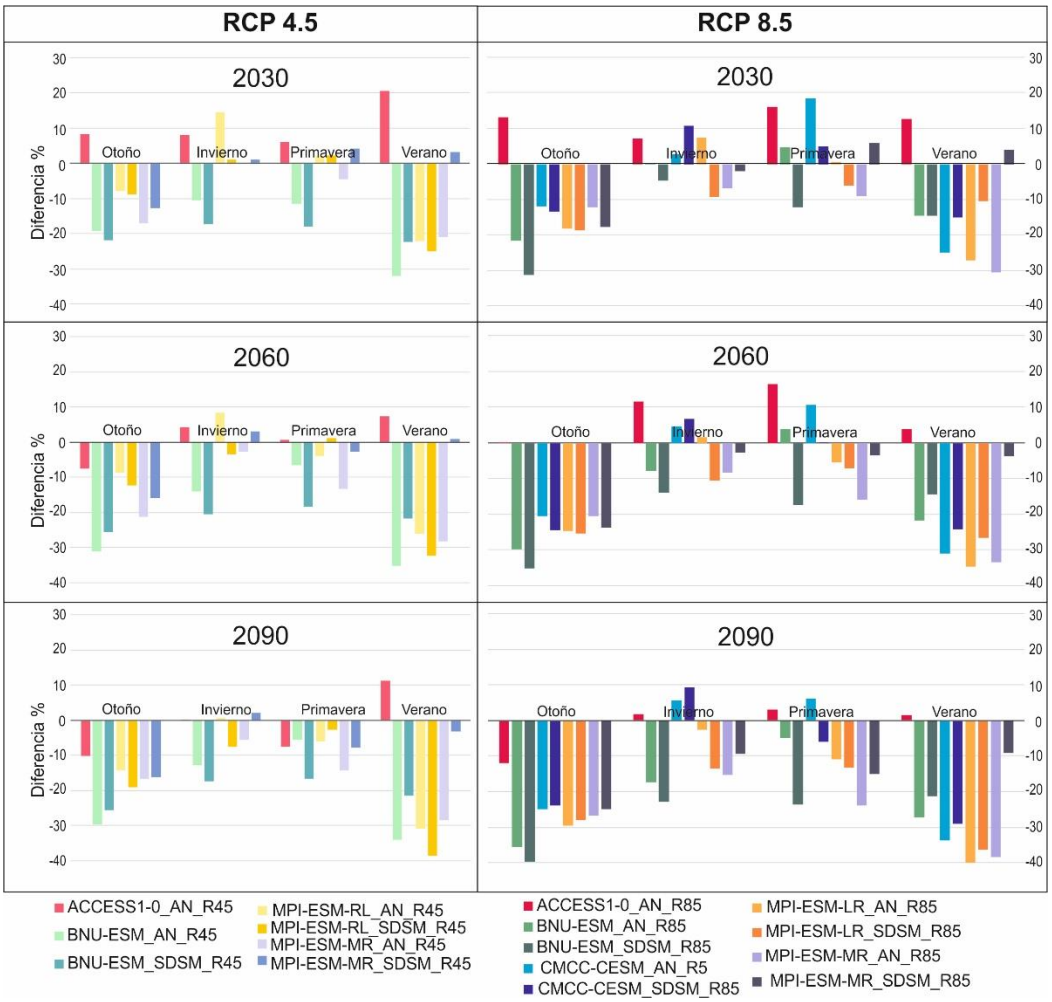

OTXANDIO

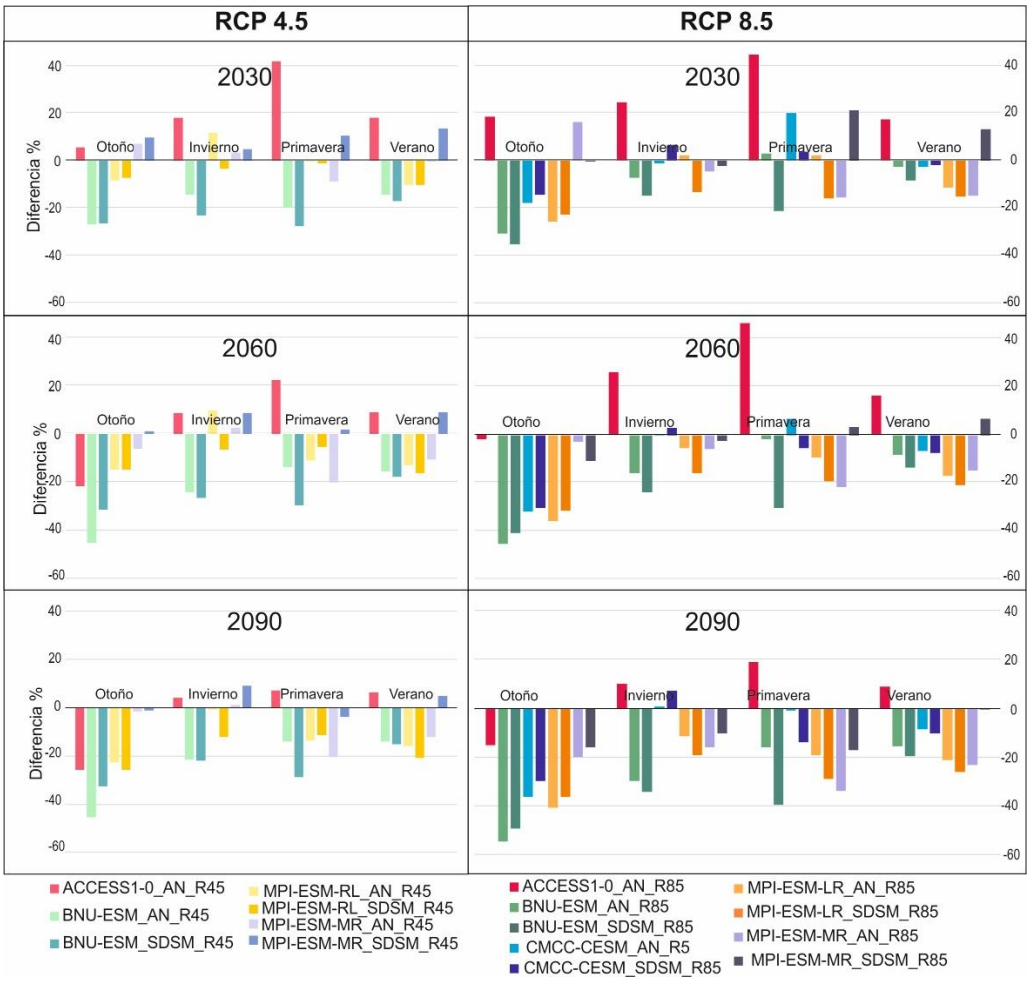
RCP 4.5
RCP 8.5
2030
2060
2090
Diferencia %
Otoño
Invierno
Primavera
Verano
ACCESS1-0_AN_R45
BNU-ESM_AN_R45
BNU-ESM_SDSM_R45
MPI-ESM-RL_AN_R45
MPI-ESM-RL_SDSM_R45
MPI-ESM-MR_AN_R45
MPI-ESM-MR_SDSM_R45
ACCESS1-0_AN_R85
BNU-ESM_AN_R85
BNU-ESM_SDSM_R85
CMCC-CESM_AN_R5
CMCC-CESM_SDSM_R85
MPI-ESM-LR_AN_R85
MPI-ESM-LR_SDSM_R85
MPI-ESM-MR_AN_R85
MPI-ESM-MR_SDSM_R85

AUDIKANA